EVALUATION OF STEAM TURBINES TRIANGULAR TOOTH ON STATOR LABYRINTH SEAL

A Thesis

by

HOSSAIN AHMED TANVIR

Submitted to the Office of Graduate Studies of
Texas A&M University
in partial fulfillment of the requirements for the degree of

MASTER OF SCIENCE

May 2012

Major Subject: Mechanical Engineering

EVALUATION OF STEAM TURBINES TRIANGULAR TOOTH ON STATOR LABYRINTH SEAL

A Thesis

by

HOSSAIN AHMED TANVIR

Submitted to the Office of Graduate Studies of
Texas A&M University
in partial fulfillment of the requirements for the degree of

MASTER OF SCIENCE

Approved by:

Chair of Committee,	Gerald L. Morrison
Committee Members,	Eric Petersen
	Ding Zhu
Head of Department,	Jerald A. Caton

May 2012

Major Subject: Mechanical Engineering

ABSTRACT

Evaluation of Steam Turbines Triangular Tooth on Stator Labyrinth Seal . (May 2012)

Hossain Ahmed Tanvir, B.S., Bangladesh University of Engineering and Technology

Chair of Advisory Committee: Dr. Gerald L. Morrison

Labyrinth seals are often utilized in locations where contact seals cannot be utilized due to the large displacements of the rotating shaft. The performance evaluation of a labyrinth seal is very important to make sure that optimum performance of turbomachinery is attained. Performance parameters such as carryover coefficient, discharge coefficient were evaluated for a see through triangular tooth on stator labyrinth seal. This computational study investigates how flow conditions and seal parameter variations for see through tooth on stator triangular cavity labyrinth seals affect the value of the carryover coefficient and discharge coefficient. A Finite volume CFD commercial code was used to accomplish the above study. The influence of Reynolds number, rotational speed, seal radial clearance, pitch, tooth angle, tooth width are considered using the finite volume method of computational fluid dynamics. It was found that Reynolds number, high shaft speed and clearance have a significant effect on the carryover coefficient and the discharge coefficient. Clearance is the major influential parameter to be considered among all seal geometric parameters to optimize an ideal seal.

DEDICATION

To my beautiful wife.

ACKNOWLEDGEMENTS

I would like to express my deepest gratitude to my advisor, Dr. Gerald L. Morrison, and my committee members for their excellent guidance and constant support, throughout the course of this research.. I express my deepest and sincere thanks to Dr. Eric Petersen, and Dr. Ding Zhu for accepting to serve on my advisory committee. This report has been improved by their comments and valuable discussions.

I would like to thank my parents Mr. Asghar Ahmed and Mrs. Nasima Akhter for their constant love, caring and motivation throughout my academic pursuit. Also I would like to thank Mr. Dawood Al Asaad and Mrs. Sonia Islam for their unconditional love and support throughout my academic tenure. As a former aggie, their valuable suggestions helped me to complete my academic career at TAMU successfully. I would like to thank my friend Mr. Pratanu Roy for his support throughout my academic tenure at Texas A & M University.

I would like to especially thank my beloved wife, Jinia Islam, for her constant patience and love. This wouldn't have been possible without her support.

NOMENCLATURE

A -	Clearance area , πDc
D -	Shaft diameter, mm
W_{sh} -	Shaft rotational speed, rad/sec
c -	Clearance, mm
h -	Tooth height, mm
L -	Axial length of the seal, mm
$\dot{m}$ -	Leakage mass flow rate , kg/s
P_{in} -	Seal inlet pressure , Pa
P_{out} -	Seal outlet pressure, Pa
s -	Tooth pitch, mm
B -	Tooth angle
w -	Tooth width, mm
β -	Divergence angle
γ -	Kinetic energy carryover coefficient
χ -	Fraction of kinetic energy carried over
φ-	Expansion coefficient
Re -	Reynolds number based on clearance, $\frac{\dot{m}}{\pi D \mu}$
μ -	Dynamic viscosity, Pa/s
C_D -	Discharge coefficient
pr -	Pressure ratio, P_{out}/P_{in}

T1 -	First tooth
T2 -	Second tooth
T3 -	Third tooth
T4 -	Fourth tooth
ρ	Fluid density at upstream

TABLE OF CONTENTS

Page

LIST OF FIGURES

Page

LIST OF TABLES

Page

1 INTRODUCTION

1.1. General Background

Labyrinth seals are widely used in turbomachinery to block high pressure gas from flowing into a region of low pressure. Labyrinth seals are contactless type. Main objective of labyrinth seals are to prevent leakage of working fluid between rotating and stationary part of turbomachinery devices. A labyrinth seal consists of several cavities connected with small radial clearances. Fluid flow passes through small clearances of the seal and experiences large total pressure drop from upstream to downstream. Flow accelerates under each tooth due to the contraction then the kinetic energy is dissipated in the cavity.

Correct prediction of leakage rate and control is very important for the economic operation of turbomachinery. This leakage rate is highly dependent on a wide variety of parameters such as geometry of the teeth, number of cavities, absolute pressure differences across the seal, temperature and type of fluid flow. To increase the flow resistance optimization of the above parameters is very important to obtain a good seal design.Stator and rotor are the main mounting location of labyrinth seal in a turbomachinery device.

This thesis follows the style of *Journal of Applied Mechanics.*

On the basis of tooth location they are called tooth on stator or tooth on rotor labyrinth seals. Labyrinth seals can be classified into three main categories according to the arrangement of the teeth. See through labyrinth seals are simple in arrangement, the stepped labyrinth seal creates maze like channel, and finally the staggered labyrinth seal orientation maintain same seal clearances by introducing alternate teeth arrangement in rotor and stator. Schematic diagram of see through, stepped, staggered labyrinth seals are shown in Fig. 1.1, Fig. 1.2 and Fig. 1.3.

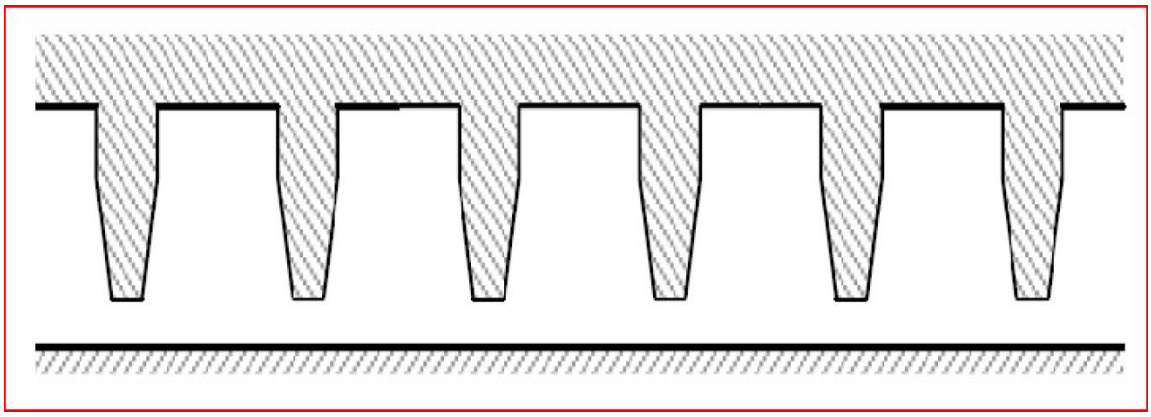

Fig. 1.1. See through labyrinth seal [1].

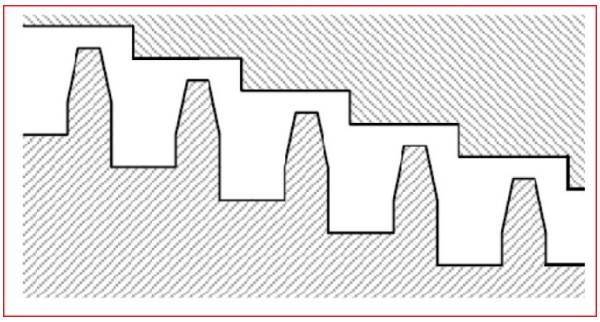

Fig. 1.2. Stepped labyrinth seal [1].

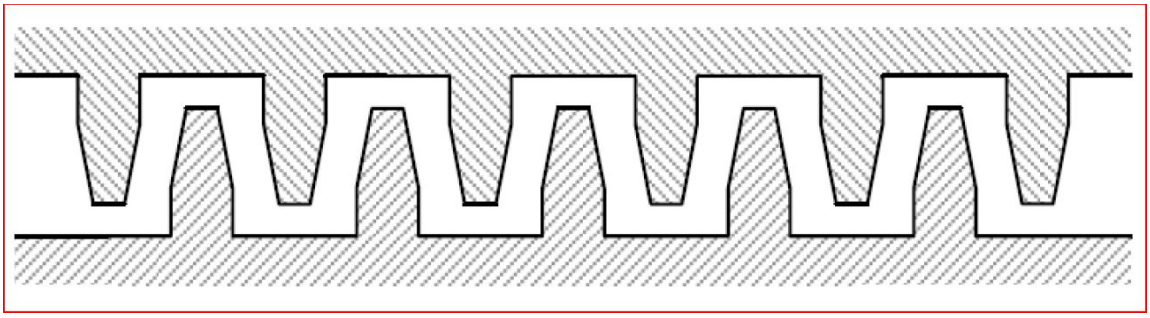

Fig. 1.3. Staggered labyrinth seal configuration [1].

See through isosceles triangle and right angle tooth shapes labyrinth seals are commonly used in steam turbines. A generic schematic of the above two see through triangular shape tooth on stator labyrinth seal is given in Fig. 1.4 and Fig. 1.5.

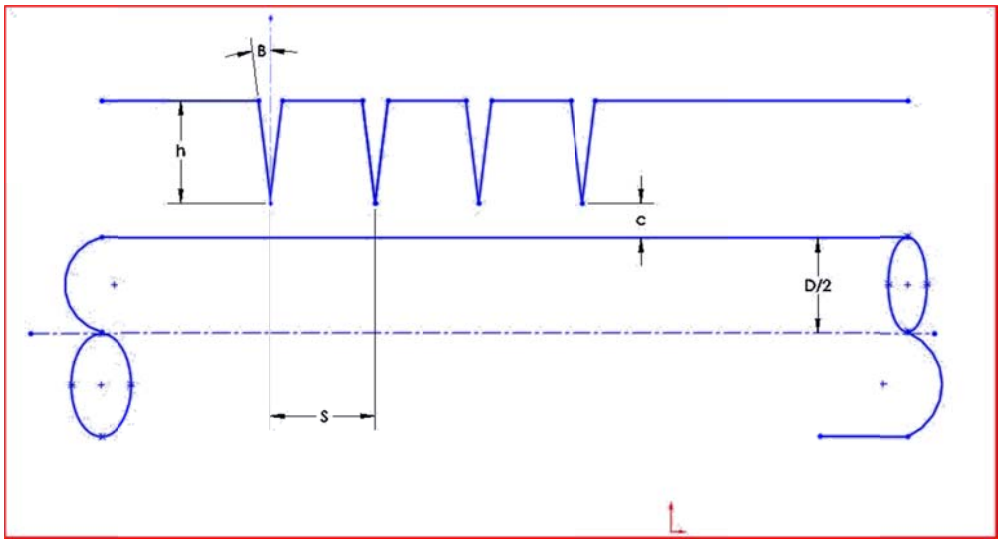

Fig. 1.4. See through isosceles triangle tooth on stator labyrinth seal (h= height, c= radial clearance, D= shaft diameter, B= tooth angle).

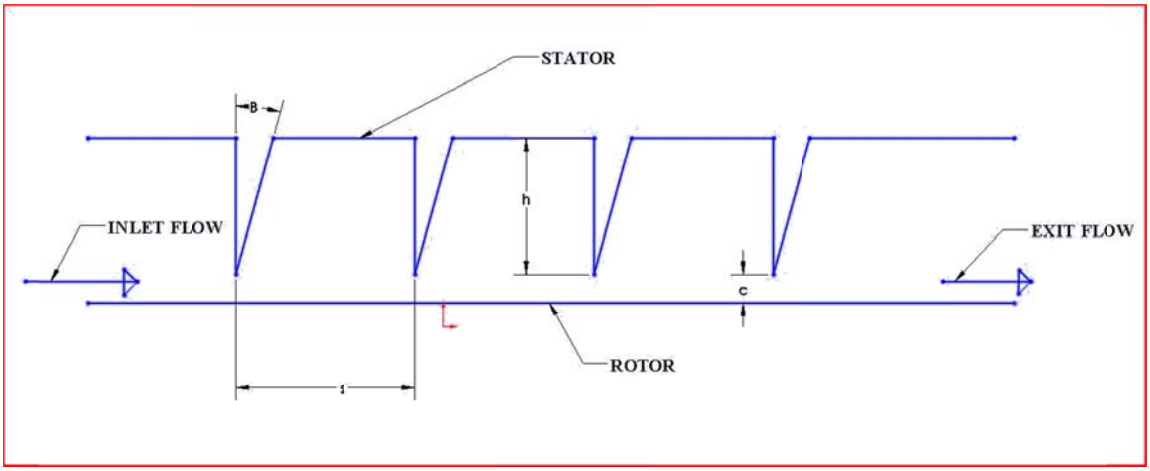

(a)

Fig. 1.5. Schematic of see through right angle shape tooth labyrinth seal (w = tooth width), (a) with tooth width, (b) without tooth width.

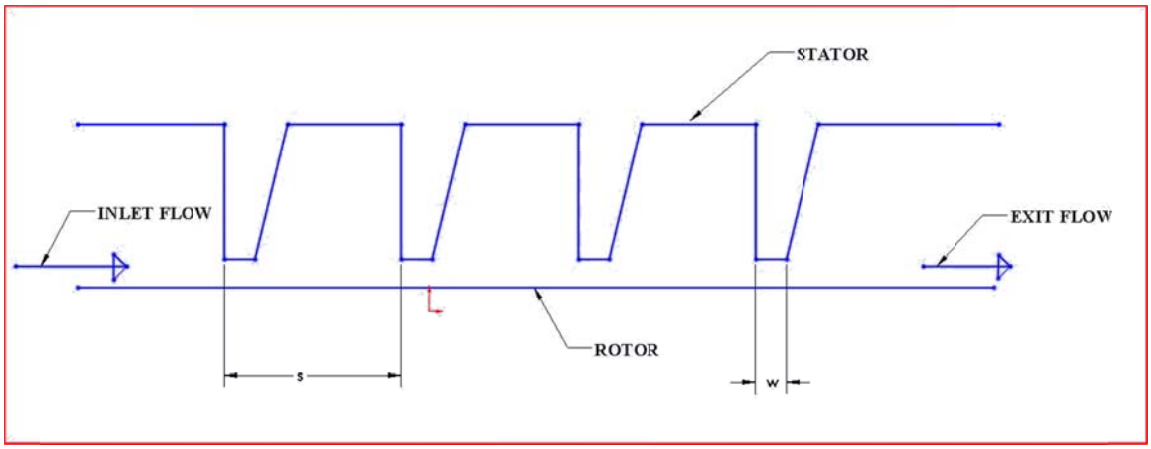

(b)

"Figure 1.5 Continued"

1.2. Objective

The primary objective of this study is to evaluate see through triangular shape tooth on stator labyrinth seals used in steam turbines for both incompressible and compressible flows Different geometric configurations (angle, pitch, clearance, height, width) are applied to determine the effect on three major seal performance parameters including carryover coefficient, discharge coefficient and expansion coefficient in order to predict the leakage flow. This objective is accomplished through applying Finite Volume CFD technique. A commercial CFD software, Fluent version 12.0.16 is used to simulate the working fluid flow characteristics inside the proposed labyrinth seal.

1.3. Research Methodology

This study is completely based on computational results. The Step by step approach including geometry creation, mesh generation, definition of boundary conditions, execution of simulation is presented to complete one geometrical configuration for incompressible and compressible flows. In the following context, a brief chronological order of research methodology are given to understand how evaluation are done for one seal geometry using CFD technique.

A. Gambit software version 2.4.6 is used to generate the seal domain grid.
B. CFD commercial software Fluent version 12.0.16 is used perform the simulation at different mass flow rate for a constant exit pressure of 1 atm.
C. Tecplot 360 version 2009 is employed as a post processing tool to extract all the results from the executed simulation
D. Discharge and carry over coefficient and compressibility factor are calculated for three cavities and four tooth respectively. Microsoft Excel is used to plot the above parameters as functions of shaft speed, axial Reynolds number and pressure ratio to evaluate the effect of different geometrical parameters.

1.4. Computational Technique

A finite volume computational fluid dynamics technique is adapted to perform simulation using Fluent version 12.0.16. This computer code is able to handle both structured and unstructured grid domains using pressure gradient adaptation for different flow and geometric conditions. Fluent uses the averaged Navier-Stokes and conservation of mass equations of fluid dynamics to simulate internal flow. Reynolds average energy equation and the ideal gas law equation are incorporated to consider the effect of compressibility in this study. Morrison and Ghasem [2] showed the k-ε model is the effective one among available turbulence model to avoid convergence problem. Enhanced wall treatment function is used under the k-ε model to obtain better convergence. Morrison and Ghasem [2] found that Y^+ value below 10 yield good results and properly determine the flow field. Due to high sheared flow, wall treatment is a crucial factor to obtain accurate results. As a result, throughout this study, Y^+ values are kept below 5 to obtain better result.

1.5. Seal Mesh

Gambit version 2.4.6 is used to generate the grid domain of the labyrinth seal. In the entire study, seal is meshed using quad elements. For most of the cases, the initial mesh is generated with 50000 elements and later on pressure gradient adaptation technique is applied to obtain a grid independent result. The maximum number of nodes used is

1000000 by keeping refined threshold minimum as 1 for highest pressure differentials and rotational speed Near the wall, the mesh grid is kept tight to resolve the effect of the boundary layer formation. A typical mesh grid used in this study is given in Fig. 1.6.

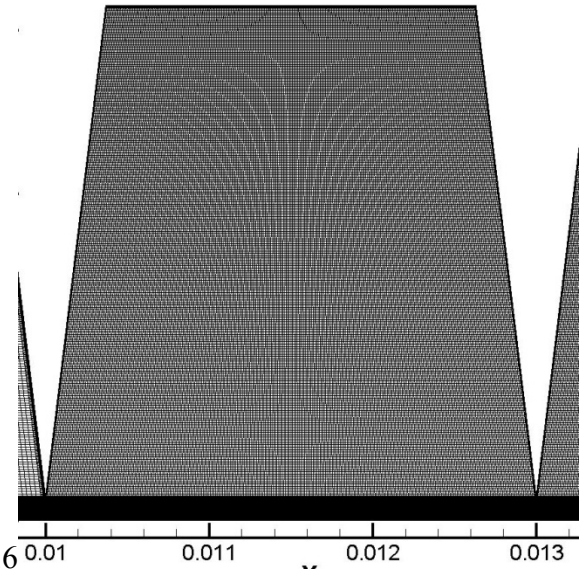

Fig. 1.6

Fig. 1.6. Mesh structure of seal geometry.

A grid independency study is conducted to make sure that the results are independent of the mesh after certain mesh gridding. This study is performed by recording the absolute pressure differences across the seal for a given Reynolds number for various level of grid refinement. In this study, near wall treatment is very important because of the high sheared flow. Initially most of the cases are started with 60000 nodes. Y+ adaptation is used to refine the wall and the value kept below 5 to obtain accurate results. Pressure gradient based adaptation is used to refine the flow and Y+

adaptation is used to refine the wall. After several thousand iterations and the number of nodes, the pressure differences across the seal are recorded. Finally the recorded pressure differences are plotted as a function of Re which is shown in the Fig. 1.7. From the above plot, it is observed that the change in pressure difference (P_{in}-P_{out}) is less than 0.5% when more than 100000 nodes are employed.

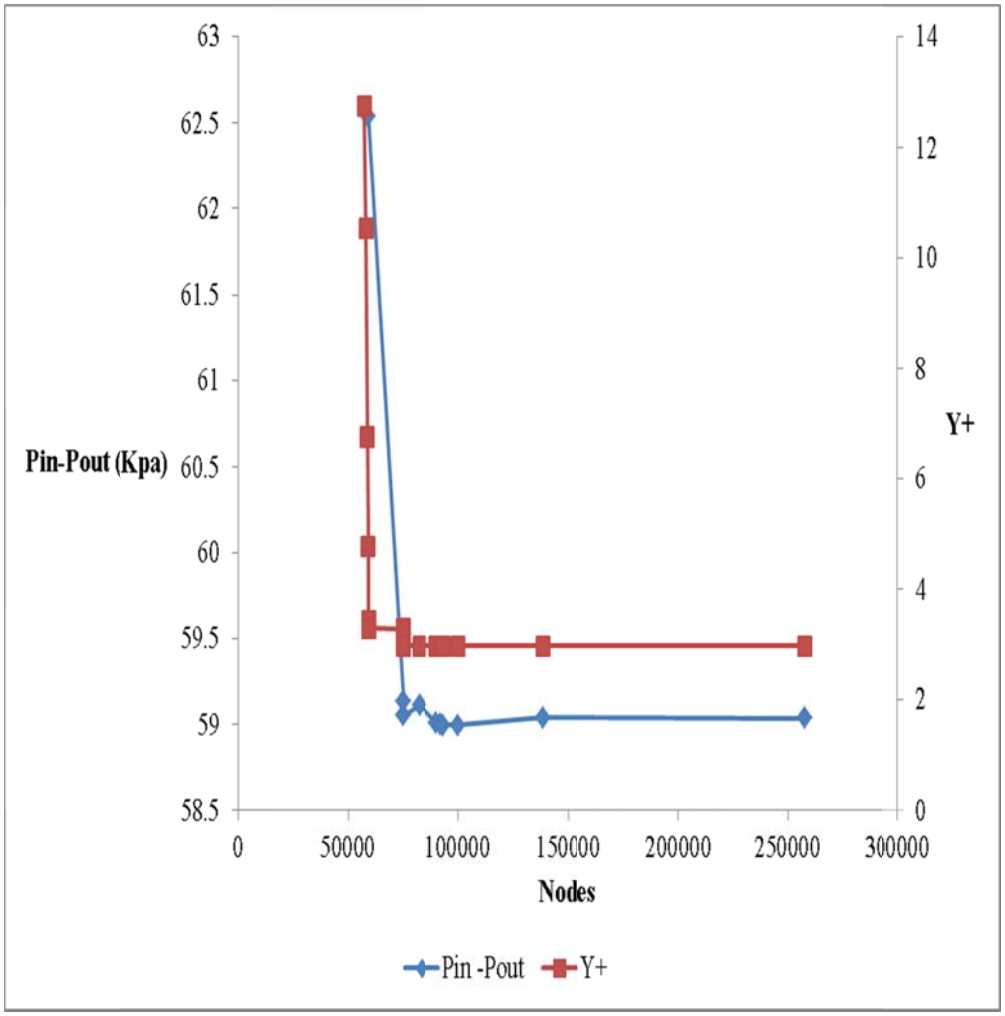

Fig. 1.7. Grid Independence study.

1.6. Seal Geometry

Different seal geometries are investigated to evaluate the labyrinth seal performance for different geometric parameters such as pitch, width, angle, and clearances. A matrix of different geometries considered in this entire study is given in the Table 1.1

Table 1.1. Labyrinth seal geometries.

#Case	Radial Clearance (c) (mm)	Pitch (s) (mm)	Tooth Height (h) (mm)	Tooth Width (w) (mm)	c/s	w/s	s/h	Upstream Tooth Forward Angle (B)	Tooth shape
1	0.05	3	3	0	0.0167	0	1	7	ISOSCELES TRIANGLE
2	0.05	3	3	0	0.0167	0	1	14	
3	0.1	3	3	0	0.0333	0	1	7	
4	0.15	3	3	0	0.0500	0	1	7	
5	0.15	3	3	0	0.0500	0	1	14	
6	0.2	3	3	0	0.0667	0	1	7	
7	0.05	4	4	0	0.0125	0	1	7	
8	0.05	3	3	1	0.0167	0.333	1	7	
9	0.05	3	3	0.5	0.0167	0.167	1	7	
10	0.05	5	5	0	0.0100	0.000	1	7	
11	0.05	3	3	0	0.0167	0.000	1	7	RIGHT ANGLE
12	0.1	3	3	0	0.0333	0.000	1	7	
13	0.05	3	3	0.5	0.0167	0.167	1	7	
14	0.05	3	3	0	0.0167	0.000	1	14	
15	0.05	4	4	0	0.0125	0.000	1	7	
16	0.05	3	3	1	0.0167	0.333	1	7	
17	0.05	5	5	1	0.0100	0.200	1	7	

1.7. Flow Pattern in Labyrinth Seals

It is very important to visualize the flow pattern inside of a labyrinth seal to understand the evaluation of the seal in terms of carryover coefficient, discharge coefficient and expansion factor. So in this section, details flow pattern of the labyrinth seal including isosceles and right angle tooth shape are shown for the different seal flow (Re, Shaft speed) and geometrical parameters (c, s, w, h, B).

Fig. 1.8 shows the flow pattern for incompressible flow for case 1. This plot is showing the flow pattern inside the first cavity. Flow pattern inside the first cavity is shown in Fig. 1.9 for compressible flow. This flow is generated for case 1.

For compressible flow, the Fig. 1.10 shows the primary vortex pattern inside the first cavity of a isosceles tooth shape labyrinth seal. There are no secondary recirculation zone observed at high shaft speed inside the cavity for both of the cases.

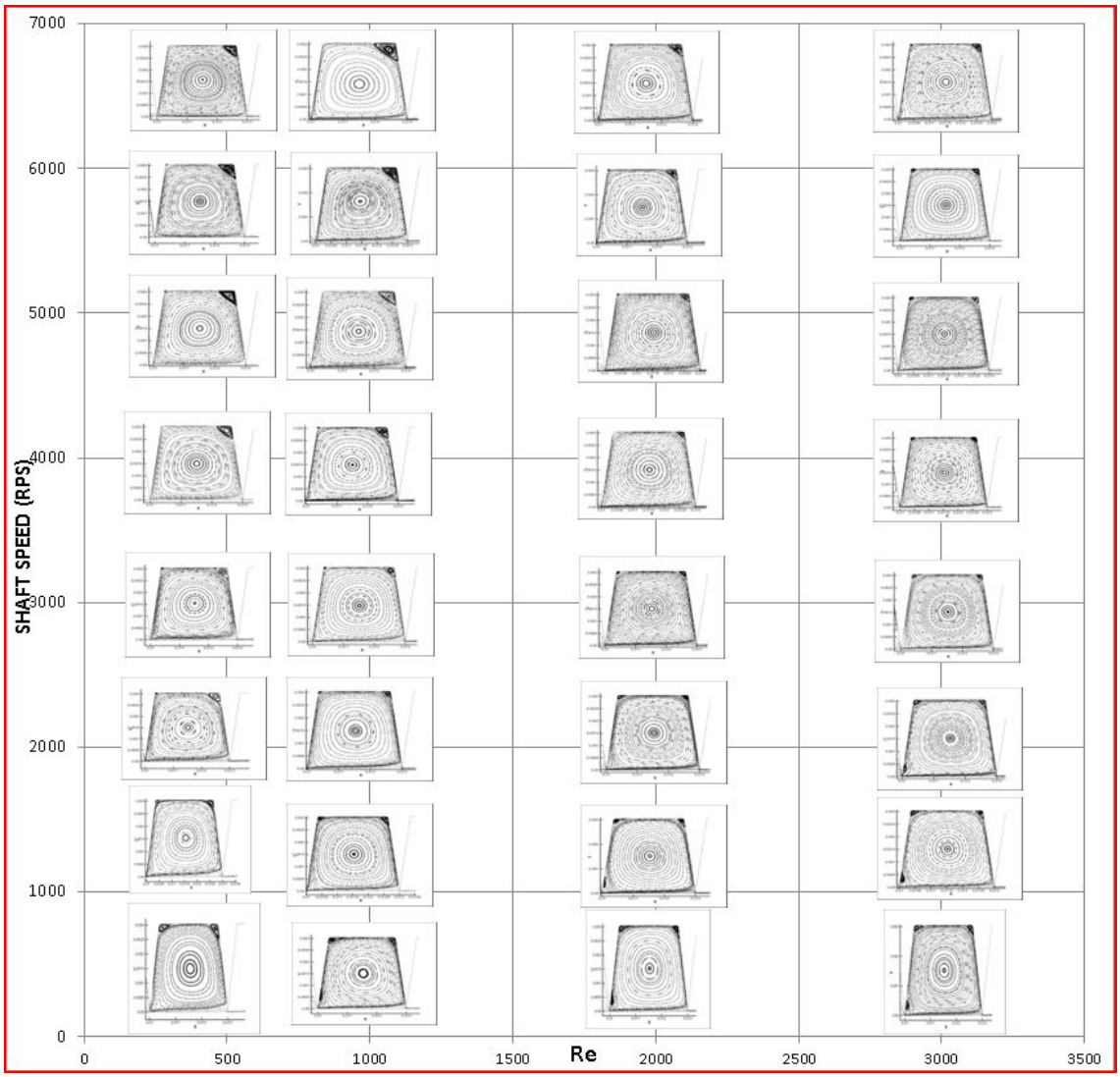

Fig. 1.8. Flow pattern inside the labyrinth seal cavities for incompressible flow (case 1, c=0.05, s=3, B=7°, w=0, cavity 1).

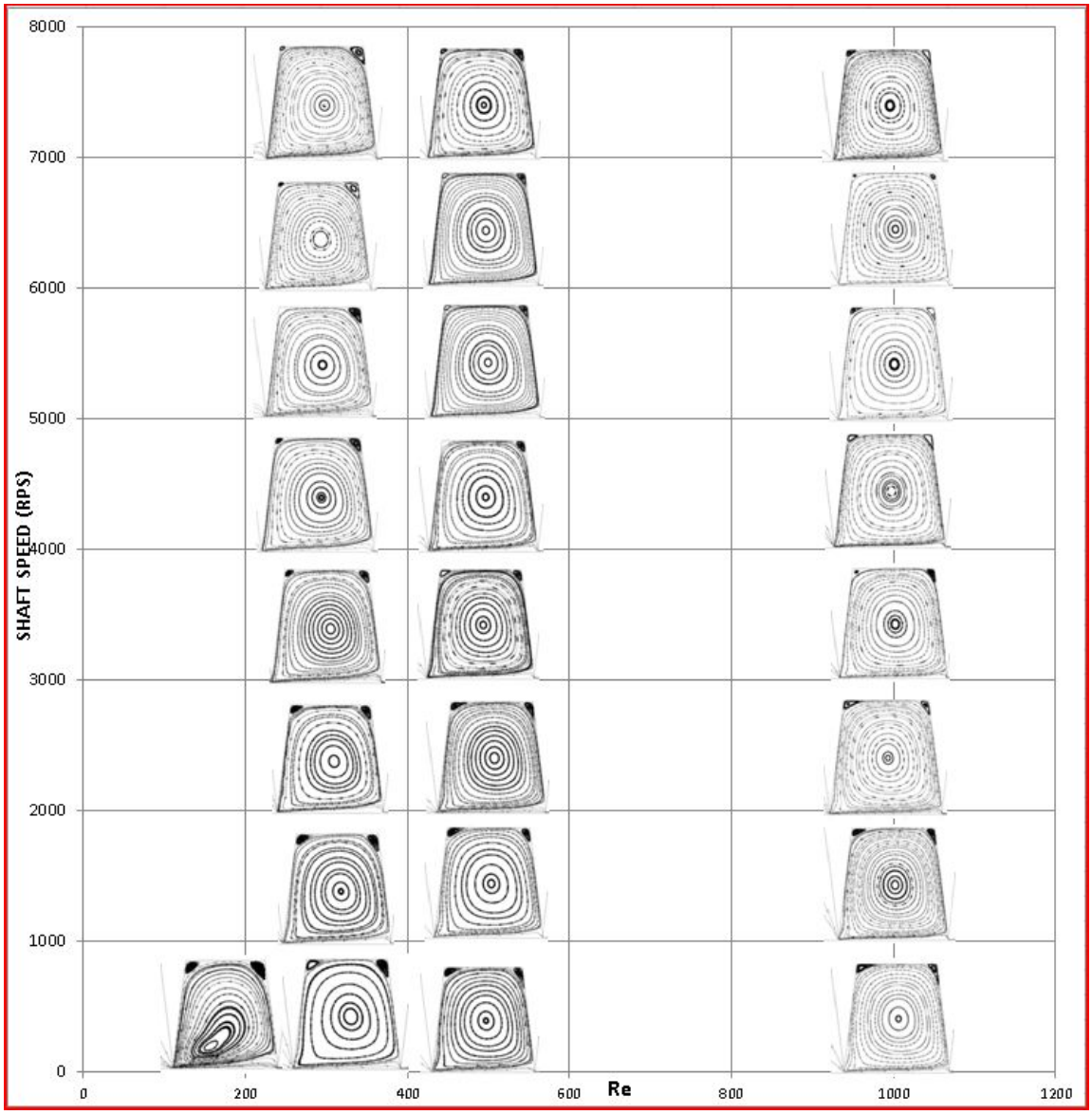

Fig. 1.9. Flow pattern inside the labyrinth seal cavities for compressible flow (case 1, c=0.05, s=3, b=7°, w=0, cavity 1).

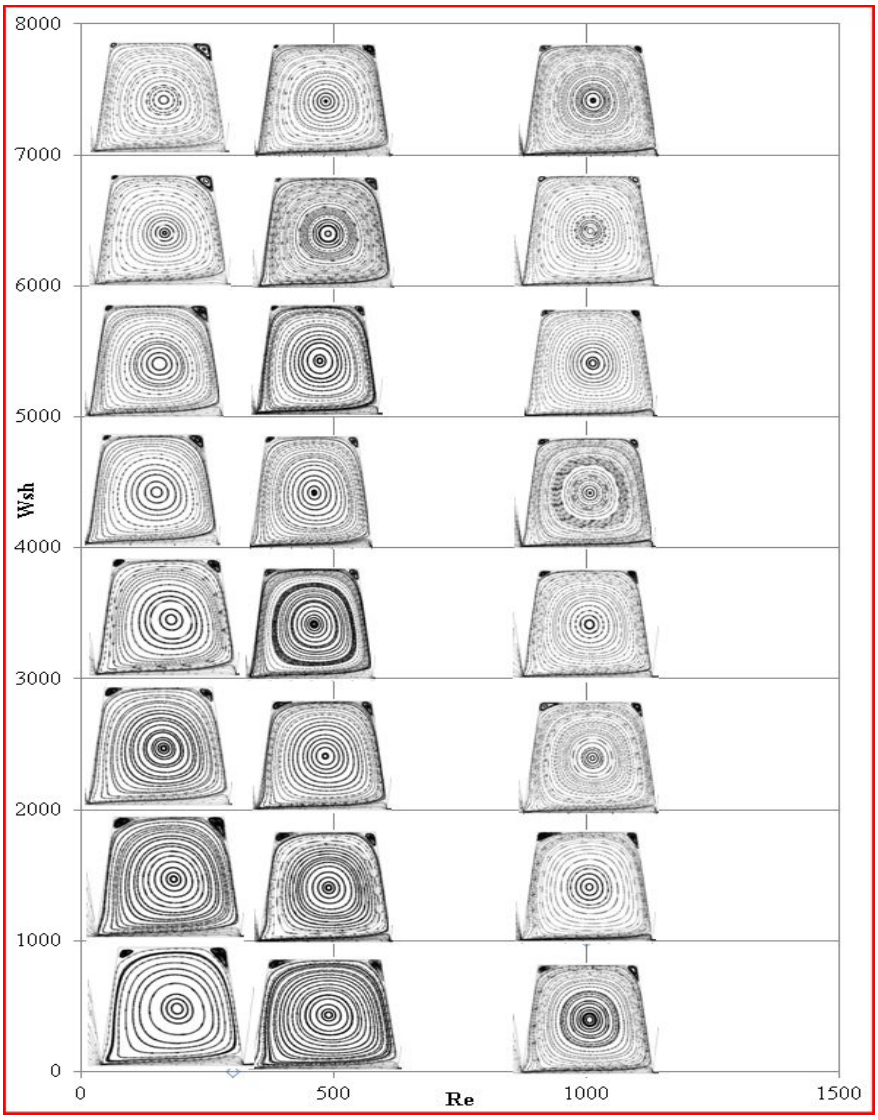

Fig. 1.10. Stream traces inside the labyrinth seal cavities for compressible flow (case 3, c=0.05, s=3, b=7°, cavity 1).

The figure shown in Fig. 1.11 represents a general view of fluid flow inside the cavity of the right angle tooth shape labyrinth seal at different Reynolds number. This figure is representing case 11.

In this study secondary recirculation zone inception is observed inside the cavity at low Reynolds number and maximum shaft speed for the incompressible flow and wider tooth seal geometry. The figure shown in Fig. 1.12 represent the recirculation zone for incompressible flow for wider tooth. This figure is generated for case 8.

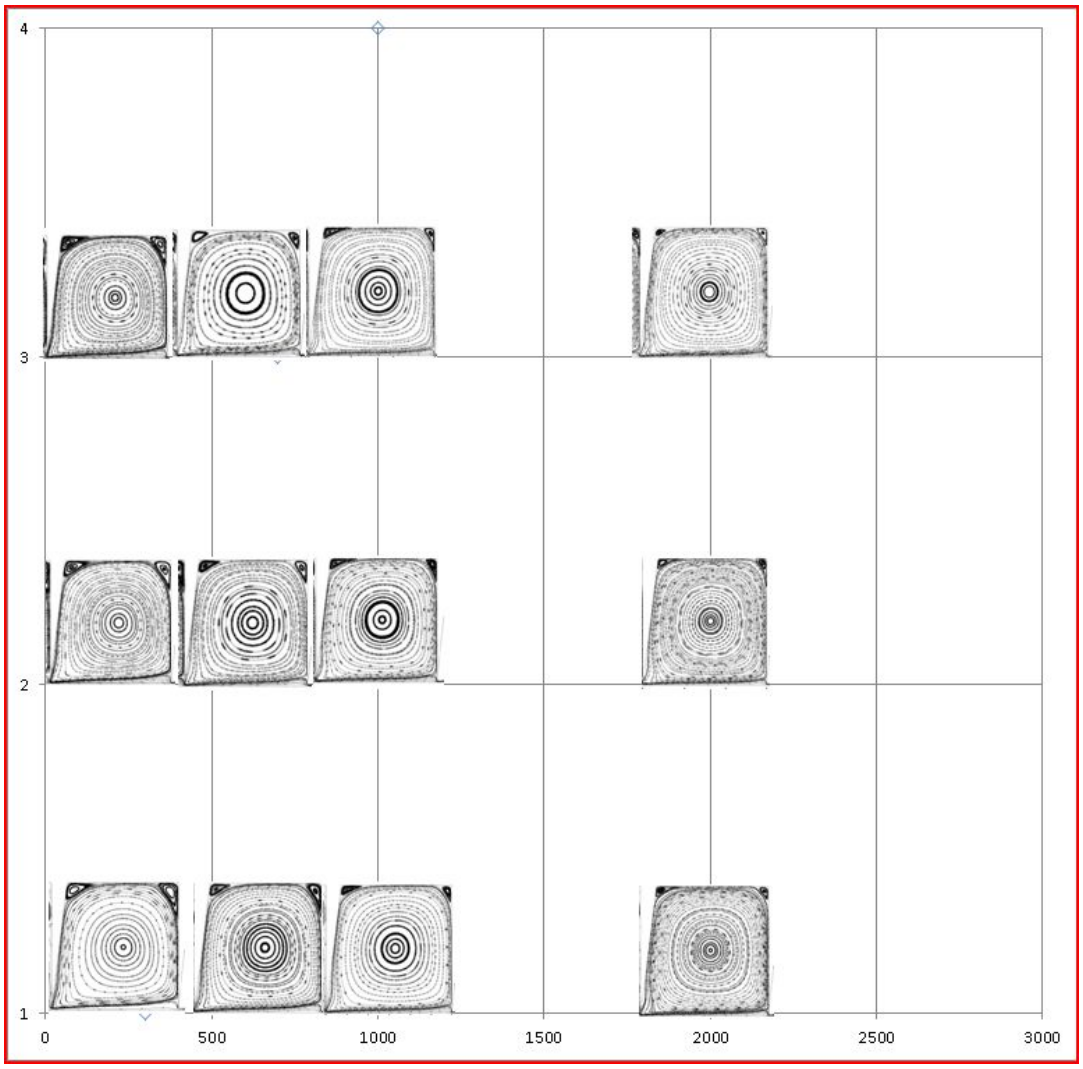

Fig. 1.11. Stream traces in different cavities at zero shaft speed (case 11, right angle tooth, incompressible flow).

The result in Fig. 1.13 shown that there is no recirculation zone present at low Reynolds number and maximum shaft speed for compressible flow and wider tooth seal geometry. Secondary recirculation zone was observed only in incompressible flow cases.

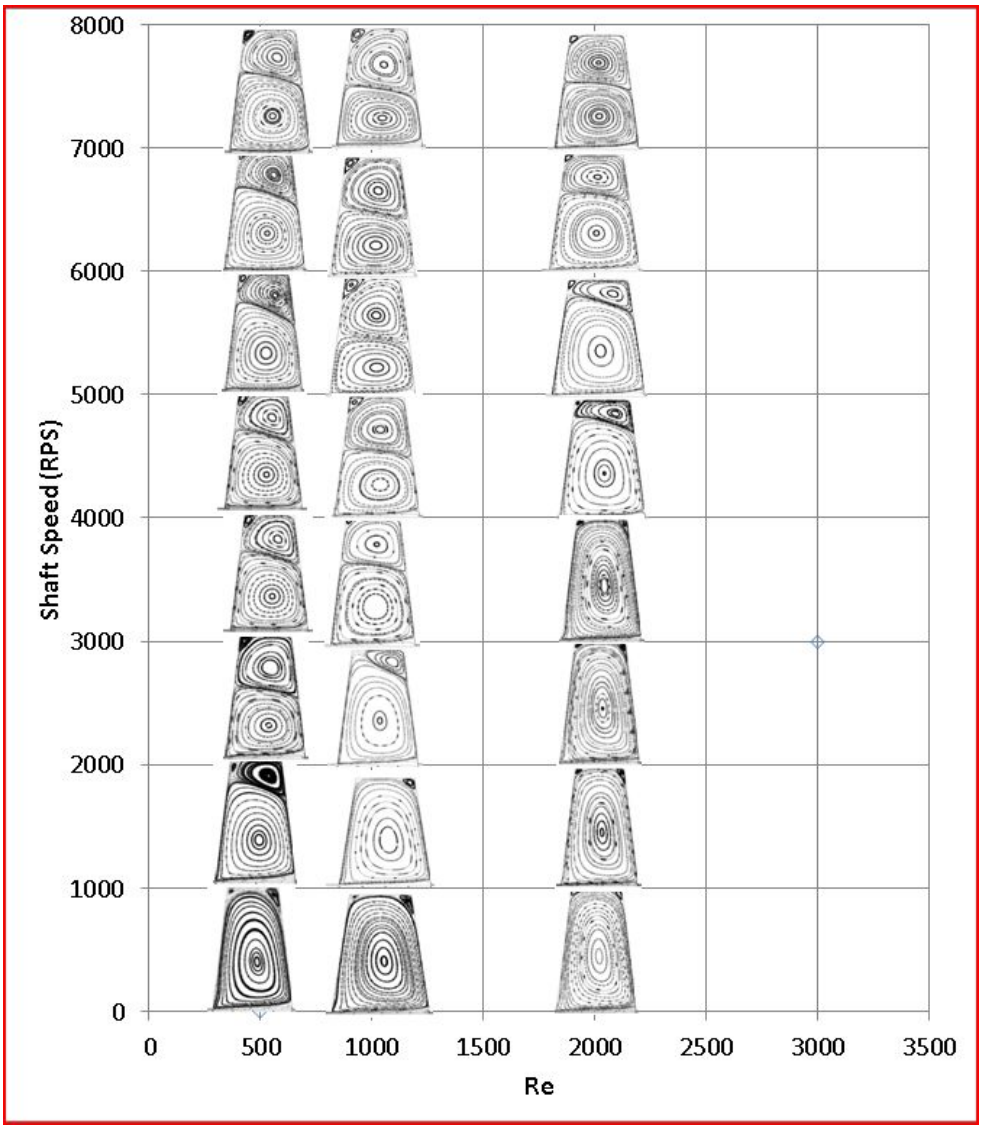

Fig. 1.12. Flow pattern for wider tooth (case 8 , w=1, incompressible flow).

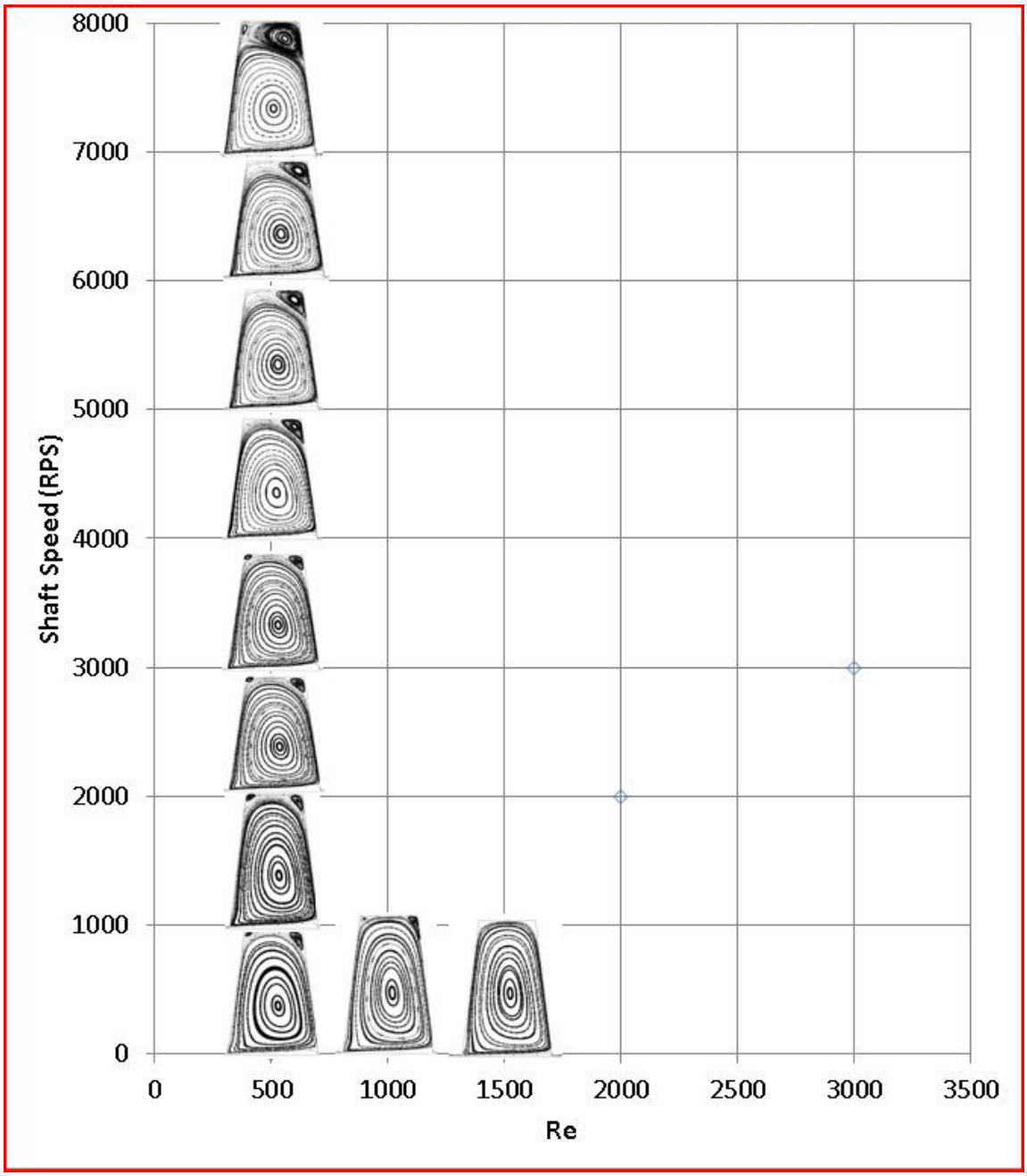

Fig. 1.13. Flow pattern for wider tooth (case 8 , w=1, compressible flow)

Fluid flow pattern inside the cavity of the case 9 is shown in Fig. 1.14. Secondary recirculation zone is not present in this case. Finally it can be said that after a critical w/s ratio, inception of secondary recirculation is observed at low Reynolds number with shaft speed for incompressible flow.

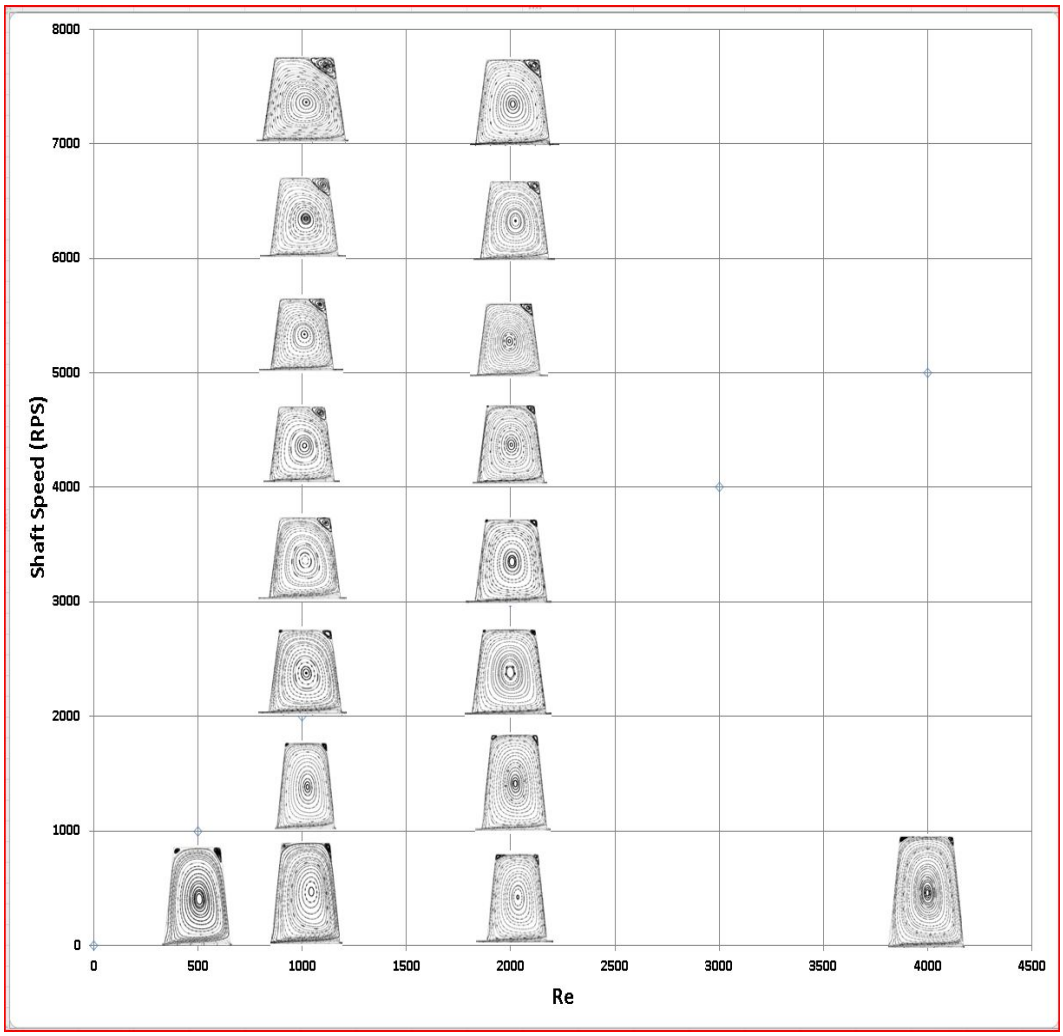

Fig. 1.14. Stream traces pattern inside the seal cavity (for case 9, w=0.5, incompressible flow).

2 LITERATURE REVIEW

The main purpose of designing any seal is to minimize leakage of the working fluid used in the system. Therefore, understanding the seals working principle is a very important issue. A seal has different geometrical parameters and these parameters play a vital role for the efficient and economic operations of turbomachinery devices. See through isosceles triangular tooth labyrinth seal is the seal type under study. This is a modern seal type used in steam turbine Very few data are available regarding leakage rate and design parameters in the open literature.

Sneck [3] 1974 generated a background of the labyrinth seal theory and design from the thermodynamic and fluid mechanics point of view. In 1939 C.A.Parsons [4] first introduced the labyrinth seal along with his development of the steam turbine. Later on, staggered and step labyrinth seals were proposed on the basis Parson's design as a modification. Becker [5] developed a model to analyze the flow through labyrinth seal as Poiseuille flow and calculated the friction coefficient. Martin [6], using, the for an ideal gas for an isothermal flow neglected the energy carryover from one orifice to another. Martin [6] demonstrated fluid flow through labyrinth seal using the concept of flow through series of orifices. Stodola [7] compared his data with Martin's work using experimental data and 14% leakage different was found. The following equation was developed by Martin using the above assumptions.

$$m = \frac{A P_i}{\sqrt{RT_i}} \sqrt{\frac{1 - (\frac{P_e}{P_i})^2}{n - ln(\frac{P_e}{P_i})}} \quad (2\text{-}1)$$

The importance of the kinetic energy carryover between orifices was first demonstrated by Grecke [8]. He considered the effect of kinetic energy carryover in his study between orifices whereas Martin didn't consider the above effect in his study. Egli [9] performed an analytical and empirical modified method to analyze labyrinth leakage which is still a very effective way to predict leakage using kinetic energy carryover. He generated a leakage equation for straight through and staggered type labyrinth seals. He added two factor in his approximate equation, one for carryover energy and the other flow coefficient to compensate for the fluid flow friction effect due to orifice as a function of throttle number, clearance to pitch ratio, tooth thickness and pressure ratio. His leakage equation is given by:

$$\dot{m} = A\alpha\psi\gamma\sqrt{\rho_i P_i} \quad (2\text{-}2)$$

$$\psi = \sqrt{\frac{1 - (\frac{P_e}{P_i})^2}{n - ln(\frac{P_e}{P_i})}} \quad (2\text{-}3)$$

Hodkinson [10] developed a formula to calculate energy carryover fraction and carryover coefficient using the flows divergence angle. His equation is given by:

$$x = \left(\frac{c}{c + s\tan\theta}\right) \quad (2\text{-}4)$$

$$\gamma^2 = \left(\frac{1}{1-x}\right) \tag{2-5}$$

Hodkinson [10] assumed that the stream spreads uniformly at an angle θ to a total width $(c + s\tan\theta)$ as in Fig. 2.1, and neglected the effect of any vena contracta. In the current study radial clearance defined as c instead of δ which is shown in Fig. 2.1.

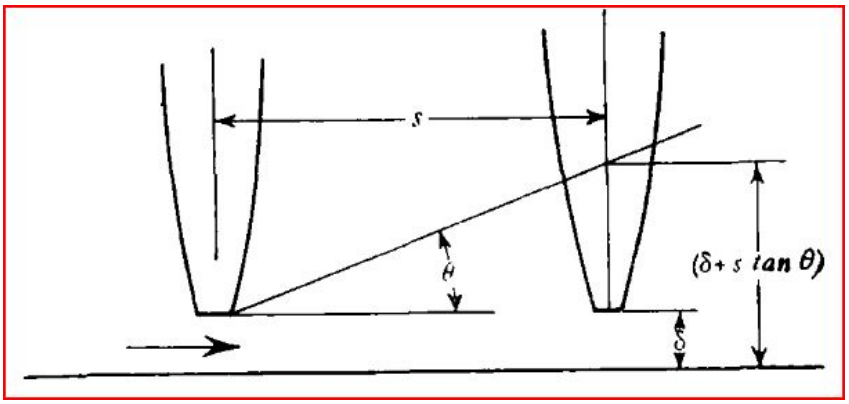

Fig. 2.1. Energy carryover fraction [10]

Zabriskie and Sternlicht [11] developed a general leakage equation considering seal geometrical parameters (tooth width, upstream angle, cavity size and clearance). They concluded that the leakage rate can be minimized by optimizing the tooth depth to pitch ratio, tooth width to clearance ratio and upstream angle of tooth with respect to flow direction. Heffner [12] developed a correlation using experimental data to predict the leakage rate of straight through labyrinth seal excluding rotational effect. A contraction coefficient was calculated using experimental data and is a function of seal geometry and pressure ratio. Later he modeled the leakage phenomena for the entire seal

with a specific number of teeth and clearances as a function of expansion factor described by Egli [9].

Prasad [13] et al. performed an experimental investigation using straight tooth labyrinth seal excluding rotation for different pressure ratio and radial clearances. They compared their results with a finite volume commercial code using standard k-ε model A variation of 8.6% was observed between experimental and CFD results. This finding is very important for the current study as in this study a similar analysis approach is adapted. Rhode and Hibbs [14] developed a finite difference code by solving the Reynolds Averaged Navier Stokes equations using a k-ε model to predict leakage phenomena for both annular and straight through rectangular labyrinth seal. They defined the inlet and outlet pressure condition in the simulated flow. Their prediction was in line with Prasad et al. in terms of an 8% difference between experimental and CFD values. Rhodes and Hibbs [14] also concluded with an important finding that labyrinth seal leakage rate is 20% less than annular seals. Witting [15] et al investigated pressure ratio and Reynolds number effects on straight–through labyrinth seals. He plotted the nondimensional discharge coefficient against the overall pressure ratio in different scales and concluded that this effect is more acute for small clearances. Willenborg [16] investigated the effect of pressure ratio and Reynolds number using stepped labyrinth seal for different seal parameters such as radial clearances, tooth tip. He mentioned that the above parameters are a governing factor of leakage rate. Finally he made a conclusion that the pressure ratio and seal clearance are proportional with flow coefficient.

Some researchers have studied the effect of shaft rotation in addition to varying geometrical parameters. Komotori and Miyake [17] investigated a straight through labyrinth seal tooth on rotor to develop a theoretical model to predict leakage rate. In this study they considered seal clearances (0.2-0.36mm), tooth number (1-12), tooth thickness (1-6mm) and performed the test for 250 m/s shaft speed along with different pressure ratios Finally they compared tooth on stator and tooth on rotor and concluded that rotation has minimal effect on tooth on stator case. Stocker investigated a staggered labyrinth seal with different clearance, tooth width, pitch in order to minimize leakage rate by incorporating more turbulence inside the cavities. He generated a plot of non-dimensional flow coefficient against different pressure ratio. In the boundary conditions he used a maximum inlet pressure of 2.5 atm and considered rotational maximum speed of 240 m/s. His advanced design ended up with 10-25% less leakage reduction. Finally he concluded that rotational speed had less effect in leakage rate which is approximately 0-3%.

Waschka [18] et al. investigated leakage rate rpm effect up to 10000 for tooth on rotor for a straight see through labyrinth seal for different radial clearances and pressure ratios. In their study they concluded rotation effect is acute when Ta/Re >0.2. The Taylor number, Ta and the Reynolds number, Re definition are shown in eqn. (2-7) and (2-8) Beyond this ratio discharge coefficient decrease with increasing rotational speed. In this study discharge coefficient is given:

$$\dot{C_d} = \frac{\dot{m}_{meas}}{\dot{m}_{ideal}} \qquad (2\text{-}6)$$

$$\mathrm{Ta} = \frac{u_w * 2 * s}{\nu} \sqrt{\frac{s}{r_w}} \qquad (2\text{-}7)$$

$$Re = \frac{\dot{m}_{meas}}{\overline{\mu} * \pi * r_w} \qquad (2\text{-}8)$$

Zimmerman and Wolff's [19] concluded in their study with different seal geometries for straight through and stepped labyrinth seal that beyond Re>10000 point rotation effect is negligible. They defined discharge coefficient as a function of axial Reynolds number.

Demko [20] et al. studied the incompressible flow for straight through labyrinth seal including rotating effect at very low leakage rates. This study showed secondary recirculation zone formed when Taylor number increased beyond the ratio Ta/Re>0.45. This finding is very important for effective seal design. Secondary recirculation zone formation increase the seal performance by introducing more pressure drop and frictional losses.

Saikishan [21] investigated the see through rectangular tooth on stator labyrinth seal. In his study, he showed that carryover coefficient is a function of Re and seal geometries. His study was based on incompressible flows. Saikishan [22] also showed that flow pattern and carryover over coefficient is similar within all cavities of multiple cavities labyrinth seals. Also he identified that carry over coefficient is independent of shaft rotation. He developed a model for thin tooth to show the relationship between carryover coefficient and Re which is given in eq. (2-9)

$$\gamma = C1\left(\dot{Re} + (C1)^{\frac{-1}{C2}}\right)^{C2} \quad (2\text{-}9)$$

Later on Saikishan [23] modified his earlier model of the carryover coefficient which is shown in eq. (2-9) and his modified model is given in eq.

$$\gamma = \left(1 - 6.5\left(\frac{C}{S}\right)\dot{} - 8.638\left(\frac{C}{S}\right)\left(\frac{W}{S}\right)\right)(Re + R_0)^{\left(2.454\left(\frac{C}{S}\right)+2.268\left(\frac{C}{S}\right)\left(\left(\frac{W}{S}\right)^{1.673}\right)\right)} \quad (2\text{-}10)$$

where

$$R_0 = \left(1 - 6.5\left(\frac{C}{S}\right) - 8.638\left(\frac{C}{S}\right)\left(\frac{W}{S}\right)\right)^{\left(\frac{-1}{2.454\left(\frac{C}{S}\right)+2.268\left(\frac{C}{S}\right)\left(\left(\frac{W}{S}\right)^{1.673}\right)}\right)} \quad (2\text{-}11)$$

3 CARRYOVER COEFFICIENT

3.1. Definition of Carryover Coefficient

The main objective of the labyrinth seal is to dissipate kinetic energy in the cavities using the concept of fluid flow through orifices. Carryover coefficient is the standard non dimensional parameter to evaluate the energy dissipation in cavities. This non dimensional parameter value should be 1 for any ideal seal. This value indicate that the kinetic energy of the working fluid is dissipated completely inside the cavity by vortices. Carryover coefficients above 1 indicate a larger fraction of energy is carried over to the next cavity without being dissipated. So this is a very crucial parameter to evaluate seal design and performance.

3.2. Carryover Coefficient Calculation

The carryover coefficient in this study is calculated according to the method described by Hodkinson [10]. According to his study, the carryover coefficient is a function of the divergence angle, β. The following two empirical relations are used to the calculate the carryover over coefficient throughout the entire study.

$$\gamma^2 = \frac{1}{1-\chi} \qquad (3\text{-}1)$$

$$tan\beta = c\left(\frac{1-\chi}{\chi * s}\right) \qquad (3\text{-}2)$$

The divergence angle is calculated on the basis of the streamline that separates the main recirculating vortex flow region and the main streamline escaping under the orifice. This streamline pattern for zero shaft speed is illustrated in Fig. 3.1 for cavity 1.

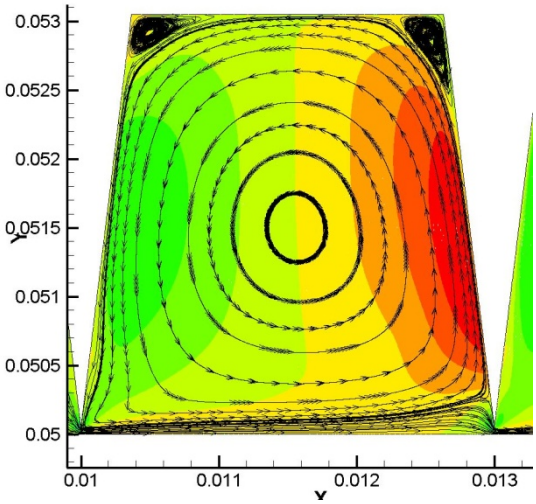

Fig. 3.1. Stream traces in cavity 1 (case 1, re 500, c/s=0.0167, s=3, w_{sh}=0, s/h=1, incompressible flow).

The separating stream line is shown more closely in Fig. 3.2

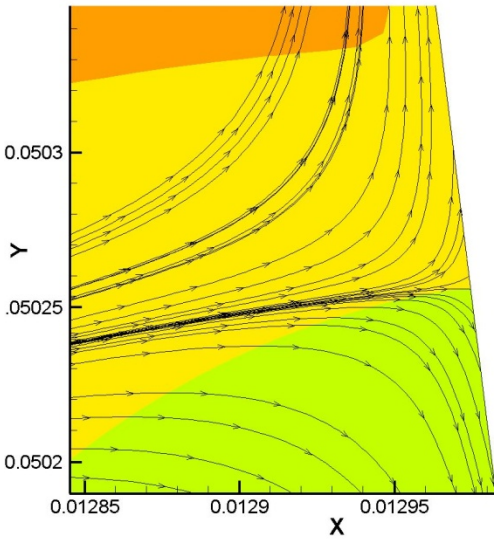

Fig. 3.2. Separating Stream traces enlarged view for Fig. 3.1.

The divergence angle, β, is formed by constructing a line from upstream tooth lip to the stagnation point on downstream tooth. Identification of this stagnation point is the main key feature to calculate the divergence angle. This point is found on the downstream tooth by identifying the location of zero radial velocity in the Y direction. For better understanding a schematic diagram is shown in Fig. 3.3. Point B in Fig. 3.3 is the stagnation point where the radial velocity contour is zero at intersection point on the downstream tooth. Tecplot 360 post processing commercial tool is used for this analysis. After picking all the three points (A, B, C), the trigonometric relation in Eq. (3-3) is used to obtain the divergence angle, β.

$$tan\dot{\beta} = \frac{Y2 - Y3}{X3 - X1} \qquad (3\text{-}3)$$

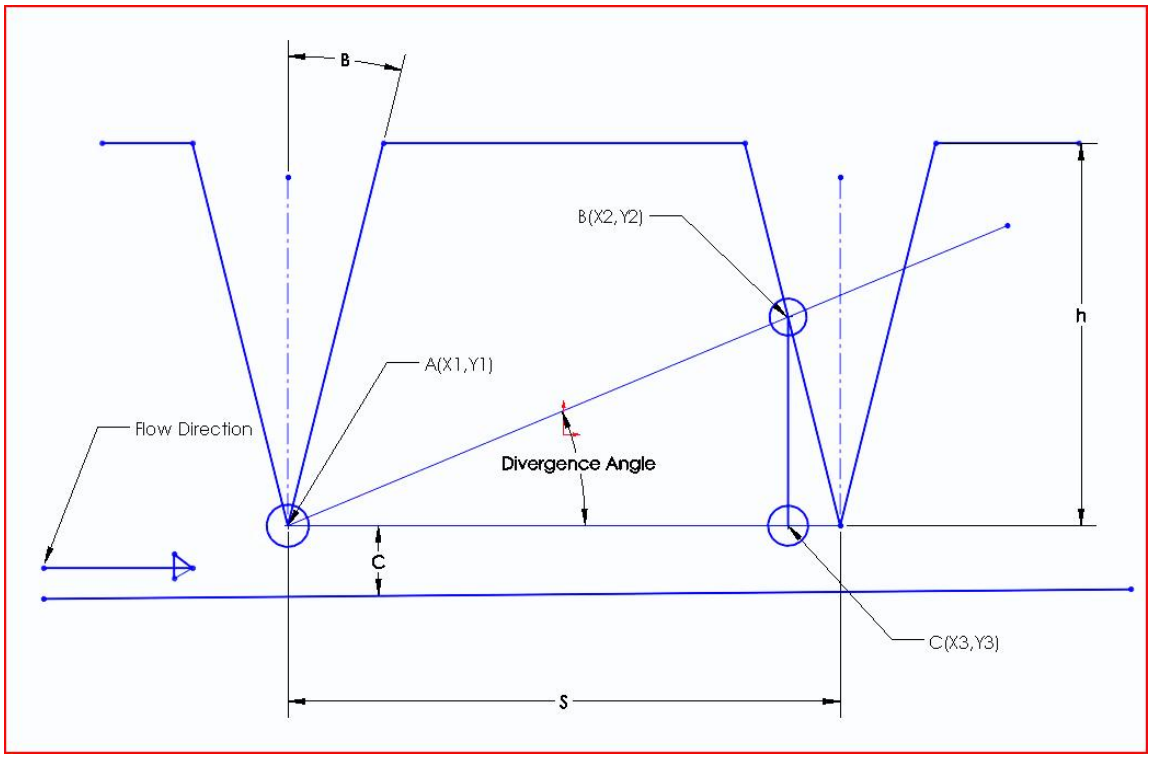

Fig. 3.3. Divergence angle calculation schematic.

In section (3-1) it is mentioned that for an ideal seal carryover coefficient should be 1. Equation (3-1) shows, the relation between kinetic energy carryover, χ, and carryover coefficient, γ. This relation is given in Fig. 3.4. The higher carryover coefficient, γ, means less effective cavity design in terms of the kinetic energy dissipation.

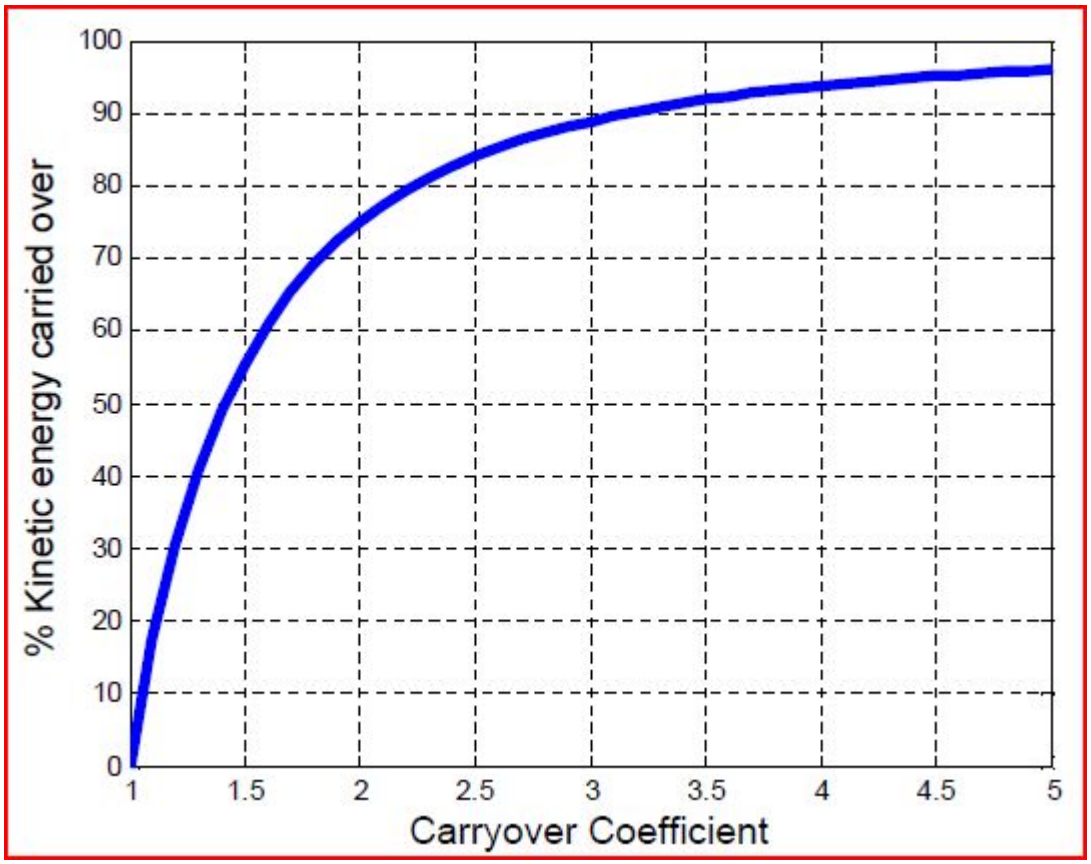

Fig. 3.4. Relationship between γ and χ [24].

3.3. Evaluation of Carryover Coefficient

In this study, the carryover coefficient is evaluated for the isosceles and right angle tooth on stator labyrinth seal. The carryover coefficient is investigated in this study for different tooth geometries such as radial clearance, pitch, clearance over pitch ratio, tooth tip width, width over pitch ratio and flow parameters such as different mass flow rates. Also this study investigated the effect of shaft speed on the carryover coefficient, γ at different Reynolds numbers. In the following sections, the effect of the above parameters on the carryover coefficient is described with visuals and proper reasoning.

3.3.1. Effect of Reynolds Number

The influence of mass flow rate on the carryover coefficient is described using the non dimensional parameter Reynolds number for both compressible and incompressible flow. To investigate the carryover coefficient for the isosceles triangle tooth, case 1 and case 4 geometries are considered for the Reynolds number range of 500 to 10000. In this study, Reynolds number is the ratio of jet inertia force approaching under tooth to the viscous force of flow under the same tooth. So the inertia force is larger compare to the viscous force in the labyrinth seal at higher Reynolds number. The Fig. 3.5 shows that the association between the carryover coefficient of air and water as a function of Re for the same geometric configurations. The results show that at higher Reynolds numbers the carryover coefficient, γ, increases up to 1.7 for case 4. For the lower Reynolds number this value is close to 1 for both air and water in Case 1. It can be concluded easily that at higher Reynolds number working fluid dissipate less kinetic energy inside the cavity and carries more energy to the next one. This is a notification of less effectiveness of seal at the higher Reynolds number. Also from Fig. 3.5, it is obvious from the plot that isosceles triangle can be utilized for both incompressible and compressible working fluid as the carryover coefficient value is almost identical as a function of Re.

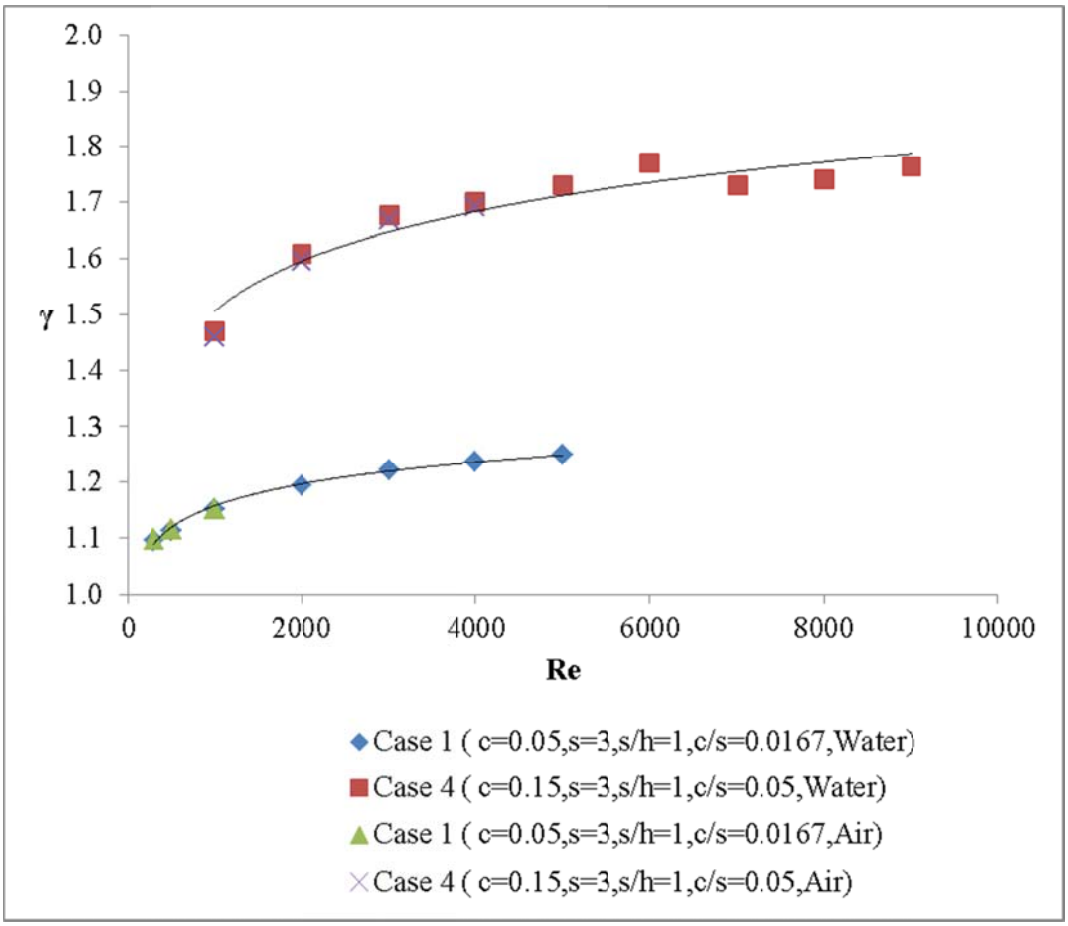

Fig. 3.5. Connection between γ and Re for both air and water.

These results are in well agreement with Saikishan's [22] findings. He found that the kinetic energy is completely dissipated inside the cavities at low Reynolds number and increasing with further increment of the Reynolds number. He concluded that the labyrinth seal lost its effectiveness at higher Reynolds number.

The radial velocity contours of cavity 1 for both of the cases are displayed in Fig. 3.6 and Fig. 3.7. The carryover coefficient evaluation as a function of Re number is also investigated for right angle tooth and association between γ as a function of Re is shown

in the Fig. 3.8. For instance of case 1 and case 11 at Re of 1000, it is found that the carryover coefficient is 2.54 % less for isosceles triangle tooth over right angle tooth labyrinth seal for the both compressible and incompressible fluid. This deviation is attributed relatively large radial velocity for the isosceles triangle tooth..

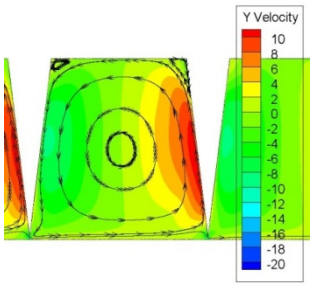

Fig. 3.6. Radial velocity contour for Isosceles triangle for Re 1000 (case 1, water)

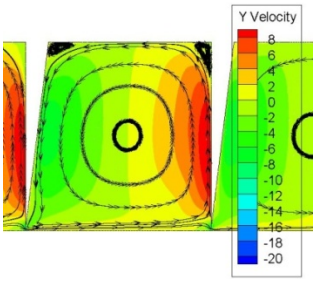

Fig. 3.7. Radial velocity contour of Right angle tooth for Re 1000 (case 11, water).

The relationship of the carryover coefficient with Reynolds number can also be explained using divergence angle, β. At the higher Reynolds number working fluid has high inertia force and escaping under the tooth without being dissipated into the cavity

by turbulence viscosity interactions. As a result, the main jet creates less divergence angle. This scenario is vice versa at low Reynolds number.

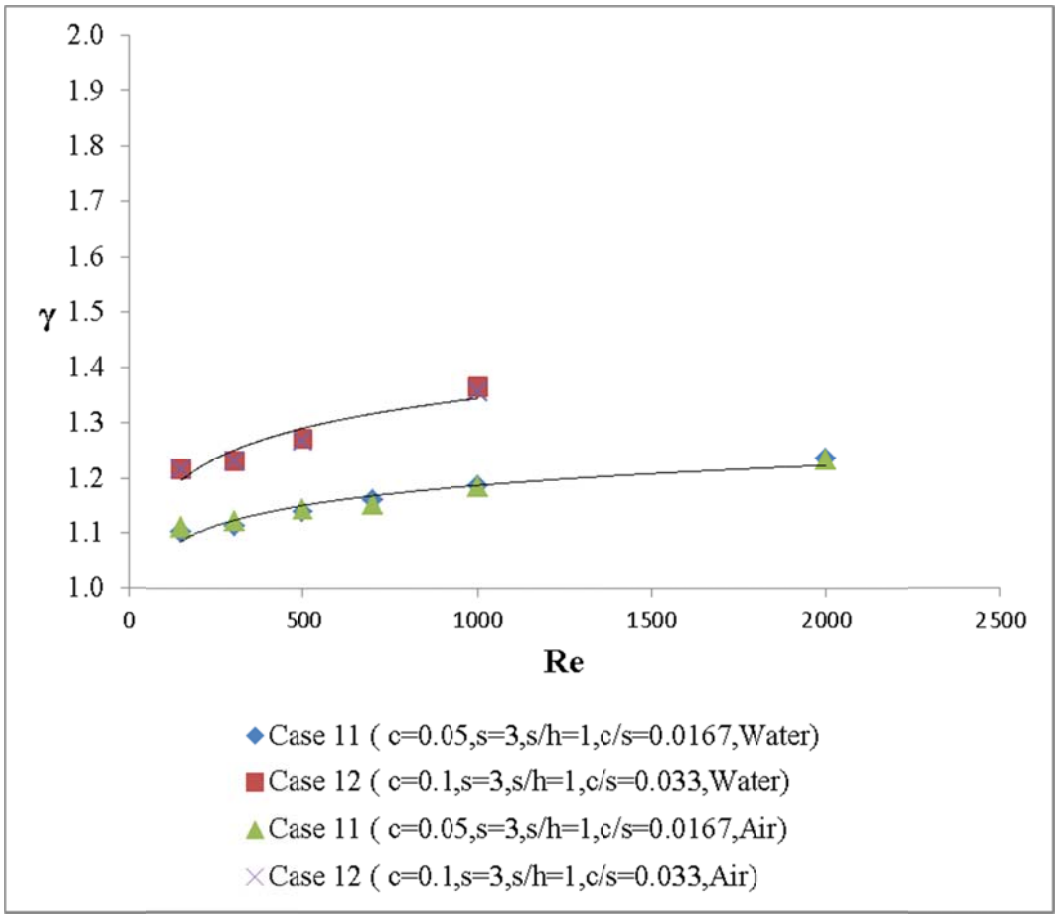

Fig. 3.8. Association between γ and Re for both air and water (Right angle tooth).

3.3.2. Effect of Clearances

Clearance is a vital parameter in labyrinth seal design as it has a significant impact on the carryover coefficient for both incompressible and compressible fluid. Hodkinson

[10] used the dimensionless parameter c/s in his study to show the effect of clearance in labyrinth seal performance investigation. Different c/s ratio applied for constant pitch, height and tooth angle are used to explore the effect of clearances for both incompressible and compressible fluid.

The result shows in Fig. 3.9 demonstrate the evaluation of carryover coefficient, γ, for incompressible flow as a function of Re for different c/s ratio such as 0.0167 (Case 1), 0.033 (Case 3), 0.05 (Case 4), 0.066 (Case 6) where the other parameters like pitch, angle, height, are kept constant. This plot is generated for the isosceles triangle tooth shape labyrinth seal. It can be concluded from the Fig. 3.9 that the carryover coefficient is strongly dependent on the clearance over pitch ratio. The carryover coefficient increase rapidly for the higher c/s ratio. It is observed that lowering the c/s from 0.0333 to 0.0167 (factor of 2) reduces the carryover coefficient, γ, by 10% at Re 1000 This observation agrees with Saikishan's [22] results for the rectangular tooth. At Re = 3000, the carryover coefficient increases by 58% as of c/s increases from 0.0167 to 0.066.

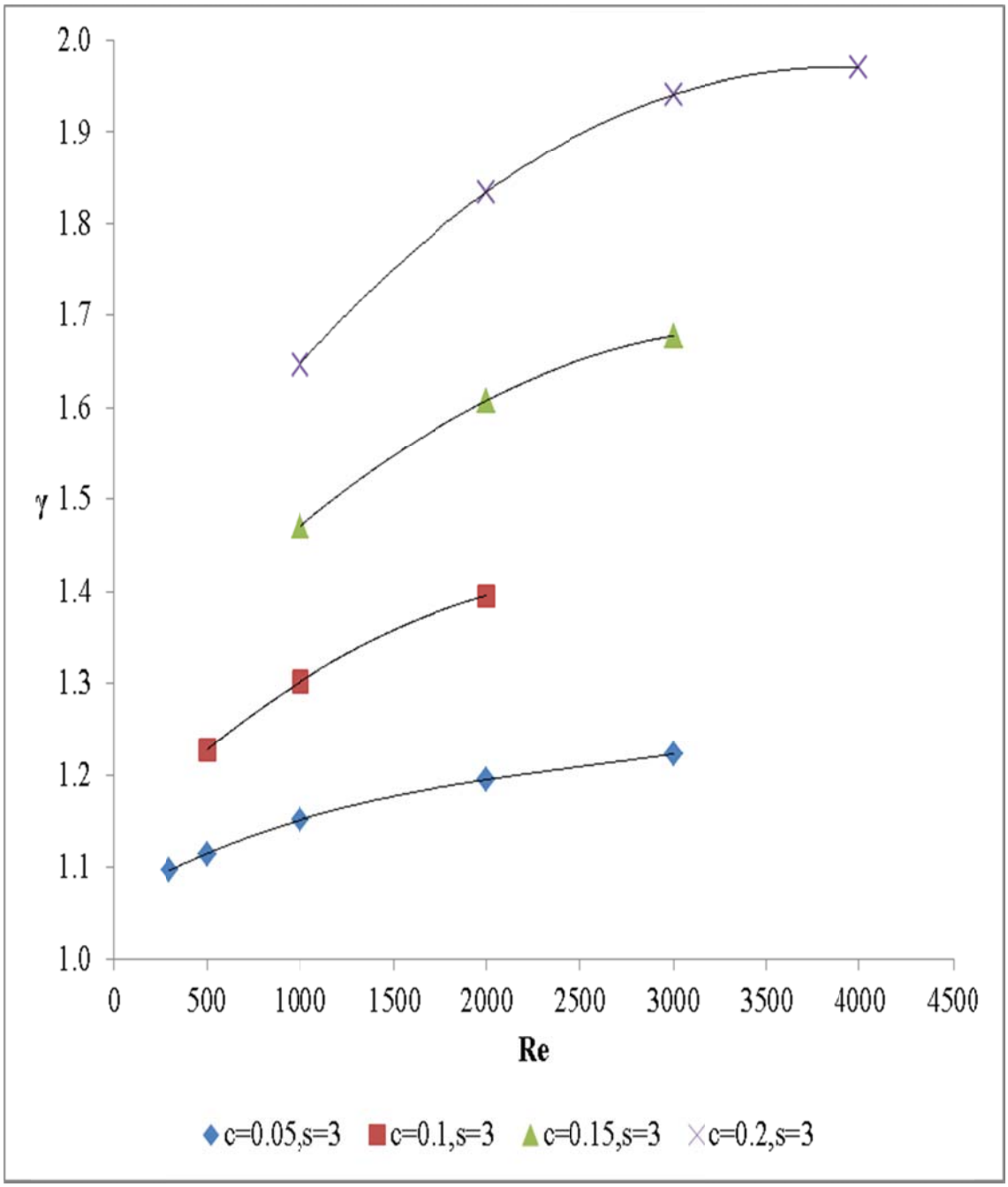

Fig. 3.9. Deviation of γ as a function of Re for different c/s ratio (water , isosceles, case 1, case 3, case 4, case 6).

In the previous paragraph, carryover coefficient dependence on c/s ratio is described for the isosceles triangle tooth. For the right angle tooth, the carryover coefficient dependence on c/s ratio is evaluated in Fig. 3.10 for the case 11 and case 12. The two c/s ratios (0.0166 , 0.033) are considered for this investigation. The Right angle tooth posseses similar behavior like the isosceles triangle tooth which is shown in the Fig. 3.10. At low Reynolds number, Re 300, a 9% reduction of carryover coefficient was obtained with the clearance value from 0.1 to 0.05 mm. Both type of the tooth show similar dependency for the carryover coefficient as a function Re for different c/s ratios.

This phenomenon can be described alternatively by using the velocity components and divergence angle. The radial velocity contour and stream traces of case 1 are shown in Fig. 3.11 for the isosceles triangle tooth at Re 3000 (Incompressible fluid). The streamlines presented in Fig. 3.11 and Fig. 3.12 help to explain the affect. The higher clearance causes larger amounts of mass flow rate to pass under the tooth compared to smaller clearance. From the simulation results, large differences are observed in the radial velocity between case 1 and case 6. Case 1 shows the radial velocity contour near the downstream tooth of value 30 m/s whereas 10 m/s observed for case 6. This velocity difference causes the divergence angle deviation between two cases. Divergence angle is found 1.92° and 1.38° for case 1 and case 6 respectively. This deviation can also be explained by considering the vena contracta effect. For the higher clearances, less vena contracta effect is observed compare to the smaller clearances.

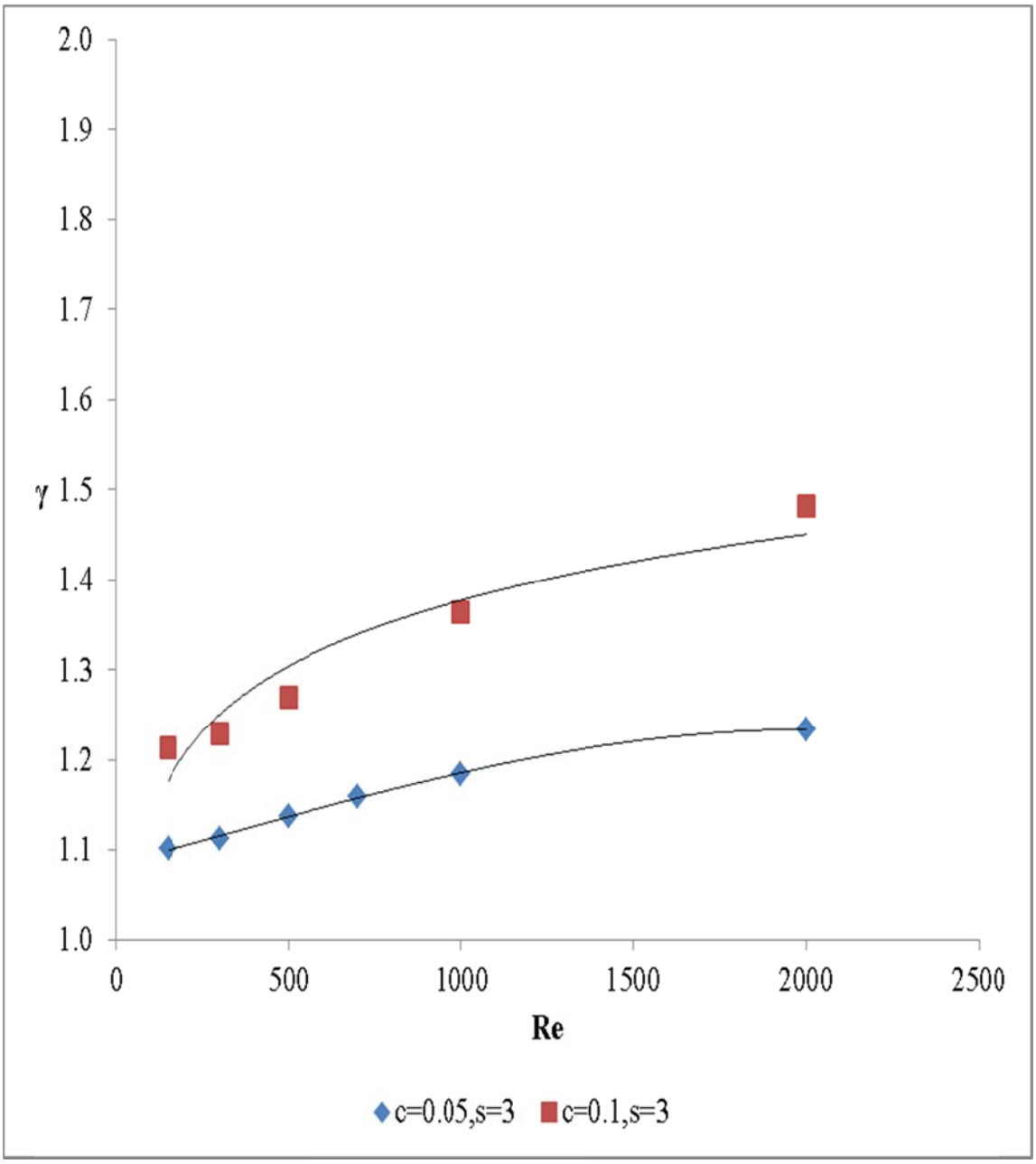

Fig. 3.10. Deviation of γ as a function of Re for different c/s ratio (water, right angle tooth, case 11, case 12).

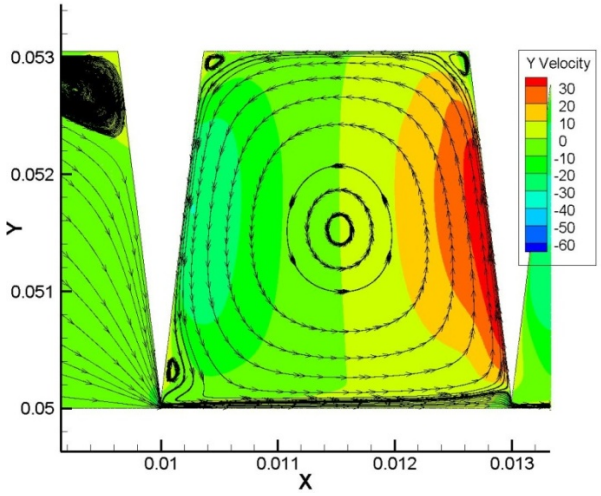

Fig. 3.11. Radial velocity contour and stream traces for case 1 (water, re 3000, c/s = 0.0167).

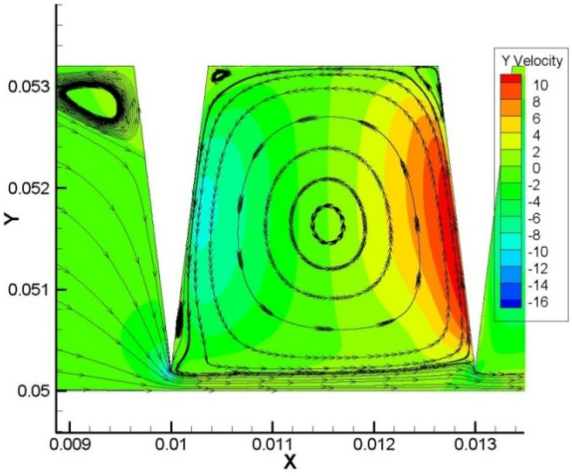

Fig. 3.12. Radial velocity contour and stream traces for case 6 (water, re 3000, c/s=0.066).

It is obvious from the above results that carryover coefficient is a strong function of c/s ratio. It is also concluded that the small clearances are effective for both isosceles and right angle tooth labyrinth seal at constant pitch

3.3.3. Effect of Tooth Width

The evaluation of carryover coefficient for different tooth width is investigated for case 1, 8, 9, 11, 13, 16. These cases are listed in Table 1.1. Both the isosceles and right angle tooth shapes are considered in this investigation. In the above cases, w/s ratios of as 0.16, and 0.33 are considered for constant clearance, c, of 0.05 mm and pitch, s, of 3 mm.

This study considered Reynolds number 500,1000,2000,3000 to investigate the behavior of the carryover efficient, γ, as a function of w/s for the isosceles triangular tooth for incompressible flow. From the results shown in Fig. 3.13, it is observed that the carryover coefficient association with the w/s ratio is insignificant up to Reynolds number 2000. Higher tooth width, w, increases the carryover coefficients slightly beyond Re = 2000. At Re = 4000, the carryover coefficient increased by 2.5% for the 100% increment of the w/s ratio. This can be attributed to the divergence angle of the flow. At Re = 4000, the difference between the divergence angle of w=1 & w=0.5 is 0.145°. Higher divergence angle is observed for the case with lower tooth width. As a result the geometry with the lower tooth width gives slightly lower carryover coefficient.

For the case of compressible flow, a similar behavior to the incompressible flow case is observed. The compressible flow carryover coefficient plot as a function of Re for different tooth widths is shown in the Fig. 3.14

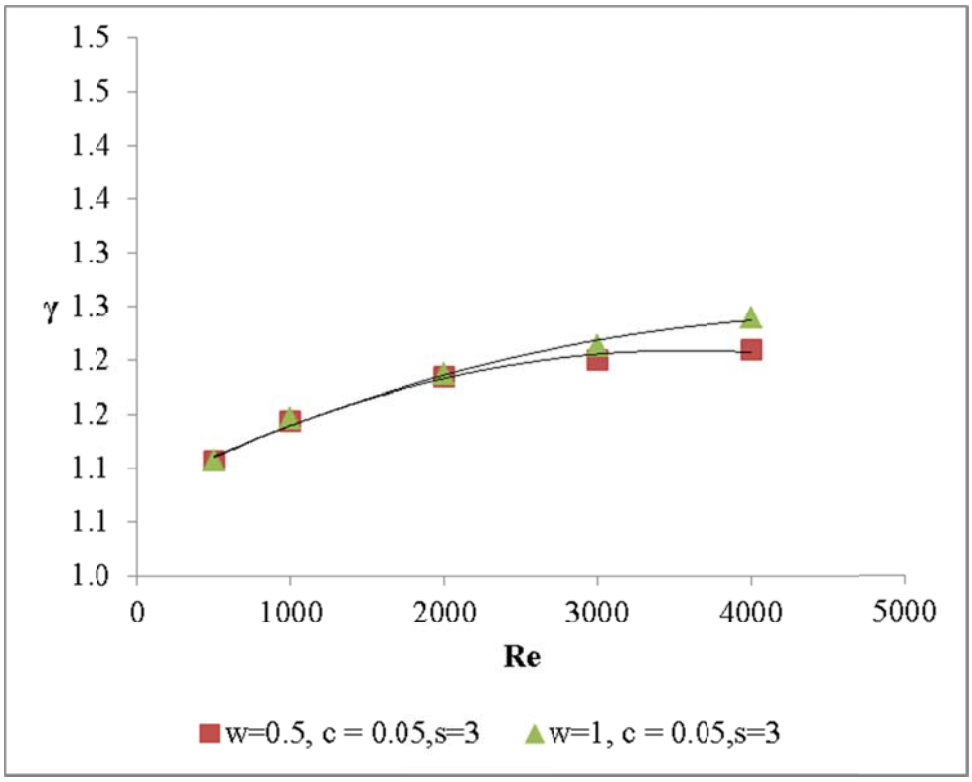

Fig. 3.13. Association of γ as a function of Re for different tooth width (water, case 8, case 9).

Cases 13 and 16 in Table 1.1 possesses similar association of the carryover coefficient as a function of Re for w/s ratios of 0.17 and 0.33 for constant pitch, s =3 and clearance, c =0.05 for both the compressible and incompressible flow. Association of γ

as a function of flow parameter (Re) and geometrical parameters (w=0.5,1 & s=3,c=0.05) for incompressible flow is shown in the Fig. 3.15.

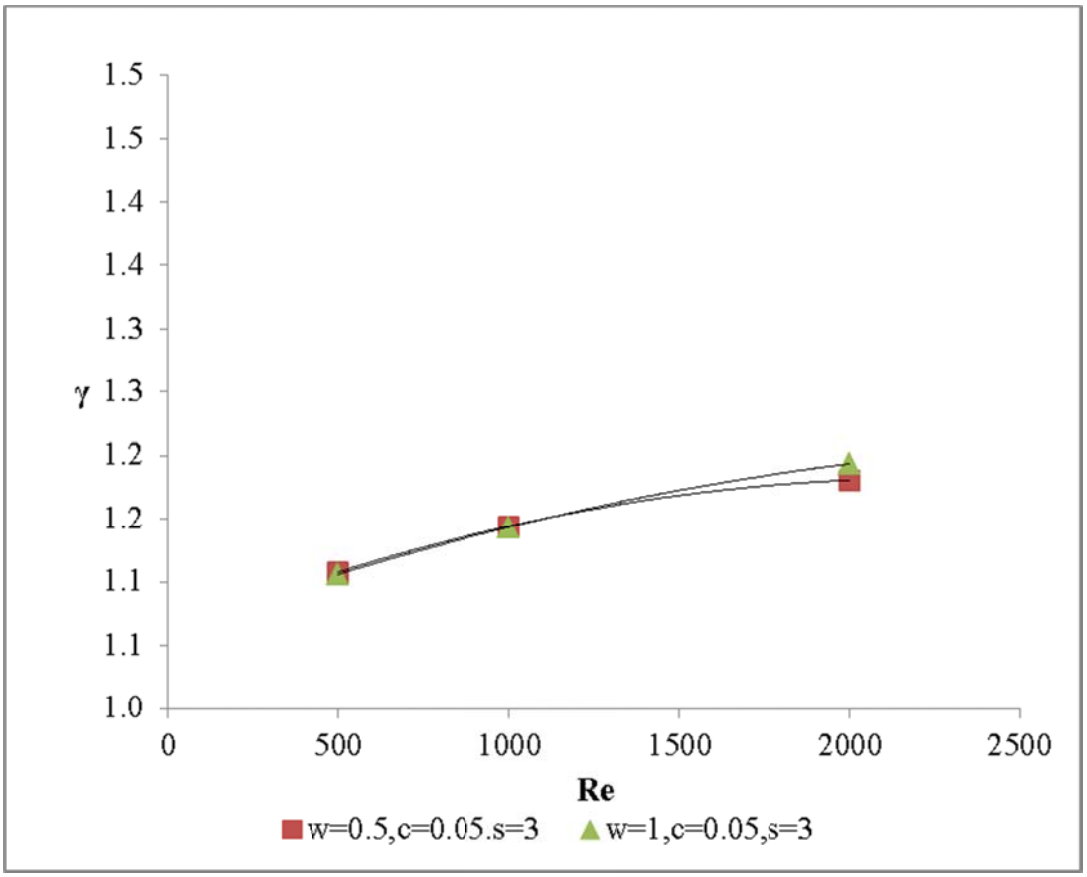

Fig. 3.14. Association of γ as a function of Re for different tooth width (compressible flow, case 8, case 9).

From the above discussions, it is observed that the tooth width has less effect on the carryover coefficient for both compressible and incompressible flow. This can be explained in another way by observing the radial velocity contour. For the above cases,

the radial velocity contour is similar. This is shown in the Fig. 3.16 for cases 8,9,13,16 for Re = 2000 and incompressible flow.

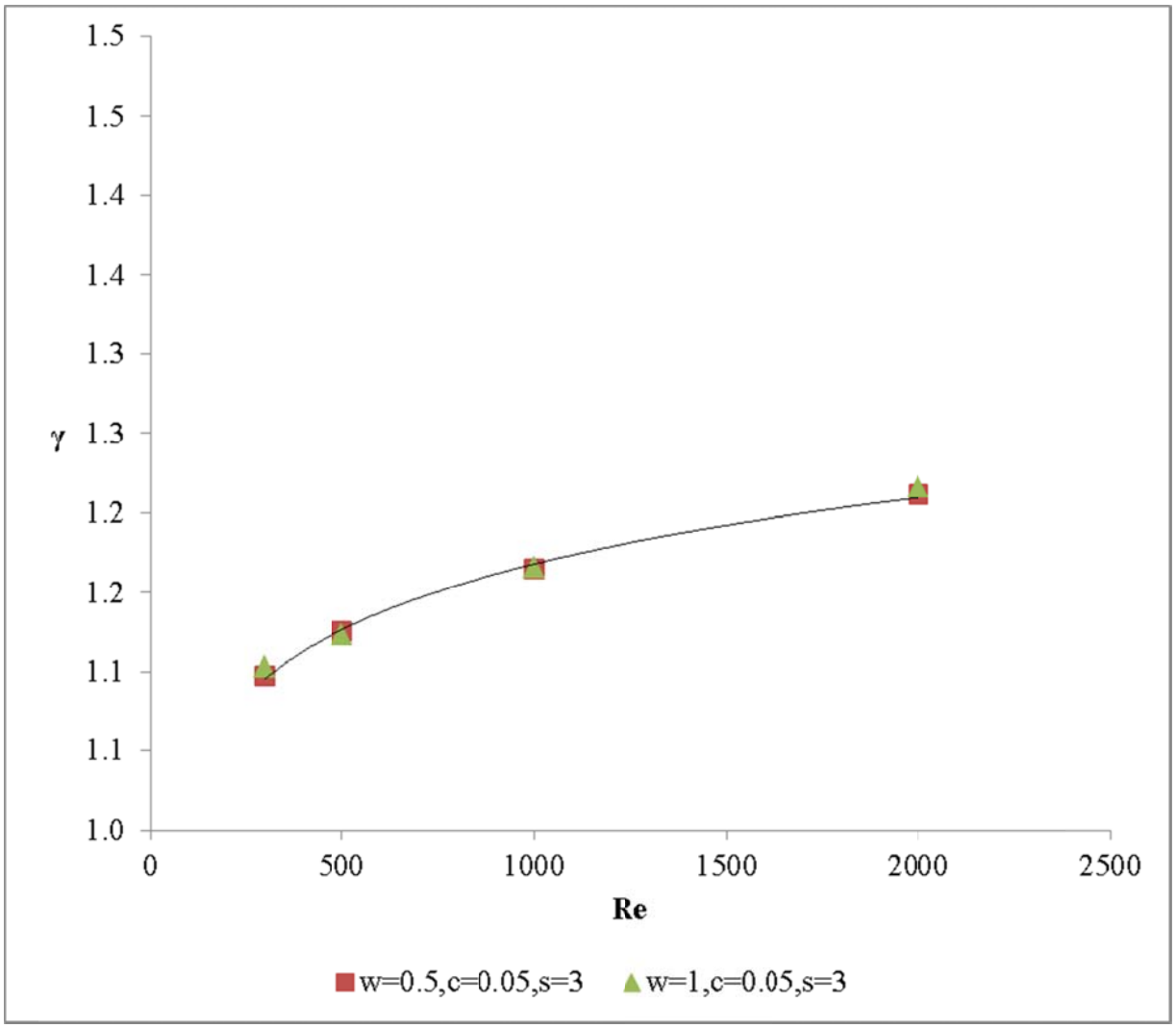

Fig. 3.15. Association of γ as a function of Re for different tooth width (case 13, case 16, incompressible , right angle tooth).

3.3.4. Effect of Pitch

The effect of pitch on the carryover coefficient, γ, is investigated by simulating case 1, 7, 10, 11, 15. The details of the cases are given in Table 1.1. Both the isosceles (Case 1, 7, 10) and right angle tooth (Case 11, 15) shape are considered to compare the effect of pitch, s, on the carryover coefficient, γ, for different tooth shape. In the entire study, the pitch over tooth height ratio is considered 1. Saikishan [23] showed that tooth height, h, has no effect on kinetic carryover coefficient, γ, and this assumption is valid when h/s value of the cavity is close to or greater than 1.

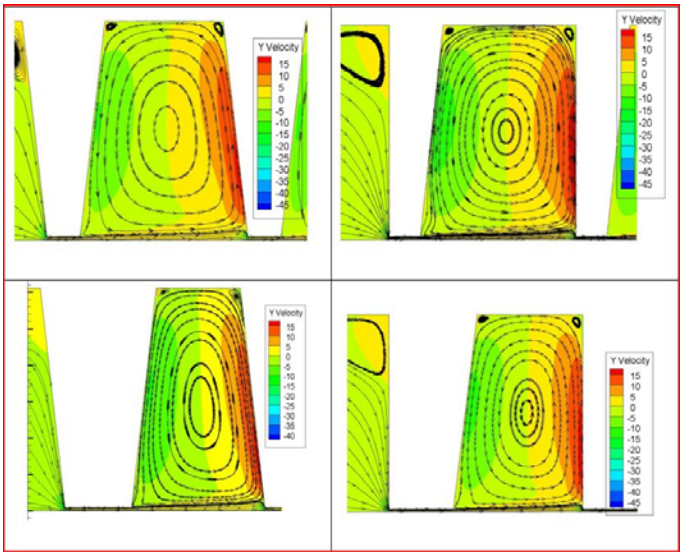

Fig. 3.16. Distribution of stream traces and radial velocity contour for incompressible flow at Re2000 (clockwise case 9, 13, 16, 8).

The results shown in Fig. 3.17 illustrate that the kinetic energy carryover coefficient, γ, decreases as the pitch increases for the incompressible flow. The result shown in Fig. 3.17 is for the isosceles triangle shape tooth.

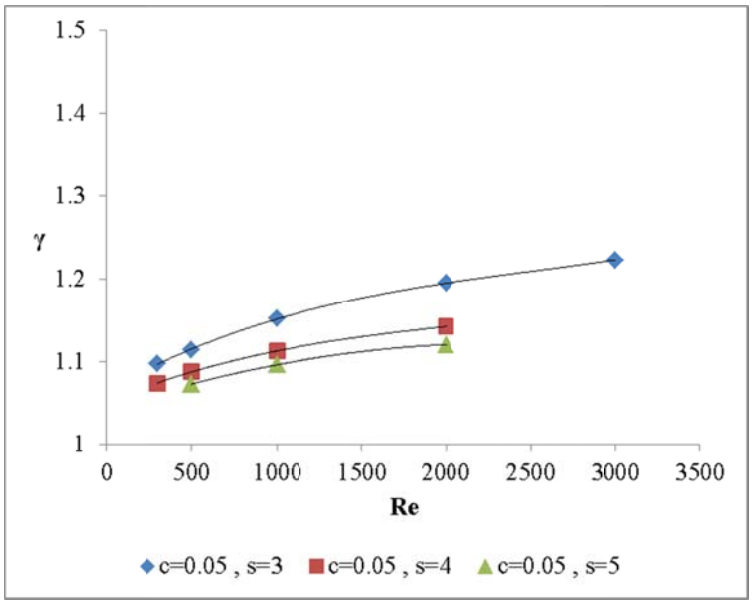

Fig. 3.17. Association of γ as a function of Re for different pitch, s (for incompressible, isosceles, case 1, case 7, case 10).

The result shown in the Fig. 3.18 illustrates that the axial velocity is higher for the lower pitch. This can be attributed that the larger pitch create more viscous effect near wall which allows more time to the fluid particle to circulate inside the cavity due to pressure difference . This viscous force is responsible for reducing the axial velocity as a result the divergence angle at downstream tooth wall goes up. The carryover coefficient is low for the higher divergence angle that what is explained in section 3.3.2. The pitch effect is also evaluated for the right angle tooth seal.

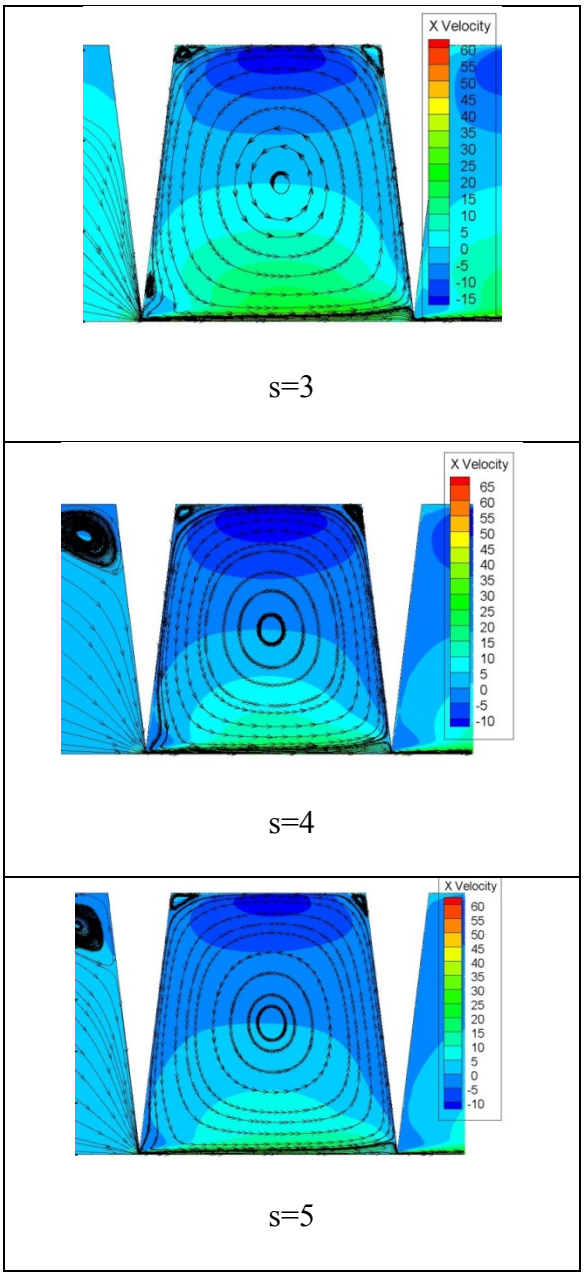

Fig. 3.18. Axial velocity contour and stream traces distribution for s=3, 4, 5 at Re 2000 (incompressible flow, cavity 1, case 1, case 7, case 10).

A comparison between the carryover coefficient of isosceles and right angle tooth is shown in Fig. 3.19. It is observed from the Fig. 3.19 that for lower Re, the difference of the carryover coefficient value for both cases are low for s =3,4. At Re 2000 and s =4, the value of the γ for the isosceles triangle tooth shape is 2.56% less than that of the right angle tooth shape.

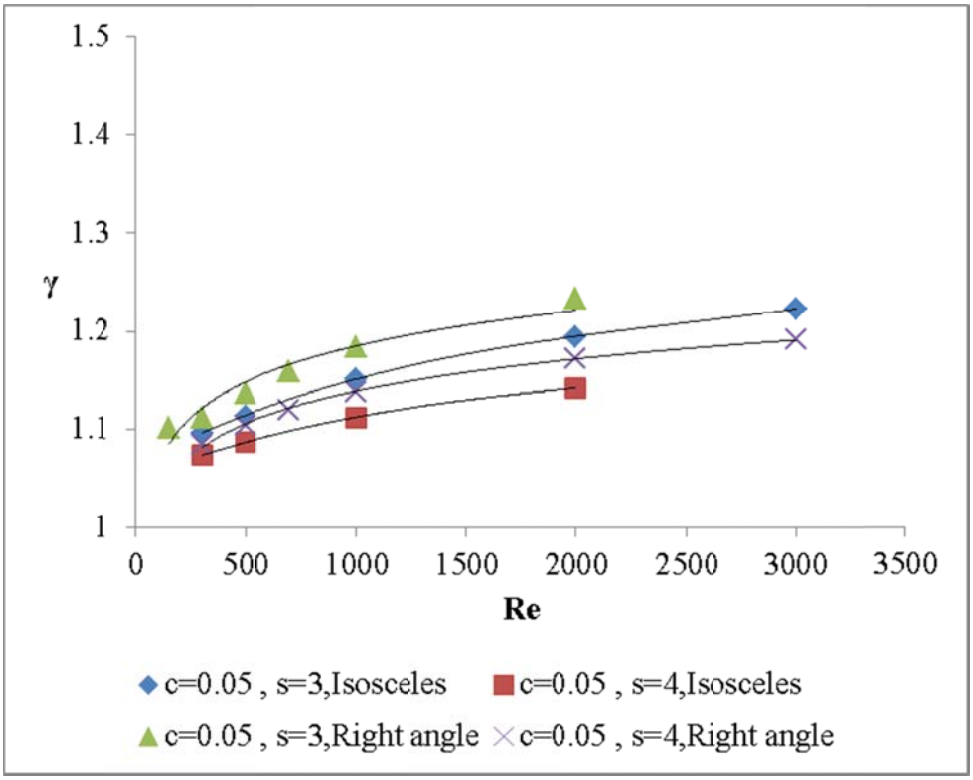

Fig. 3.19. Comparison between the γ of isosceles and right angle shape tooth seal for different pitch (incompressible flow, case 1, case 7, case 11, case 15).

The radial velocity contours in Fig. 3.20 illustrates that the radial velocity has higher ranges for isosceles at the near wall of downstream tooth. The divergence angle is higher for the higher radial velocity contour near the downstream tooth wall. This is the reason for the lower carryover coefficient value for the isosceles triangle compare to right angle tooth.

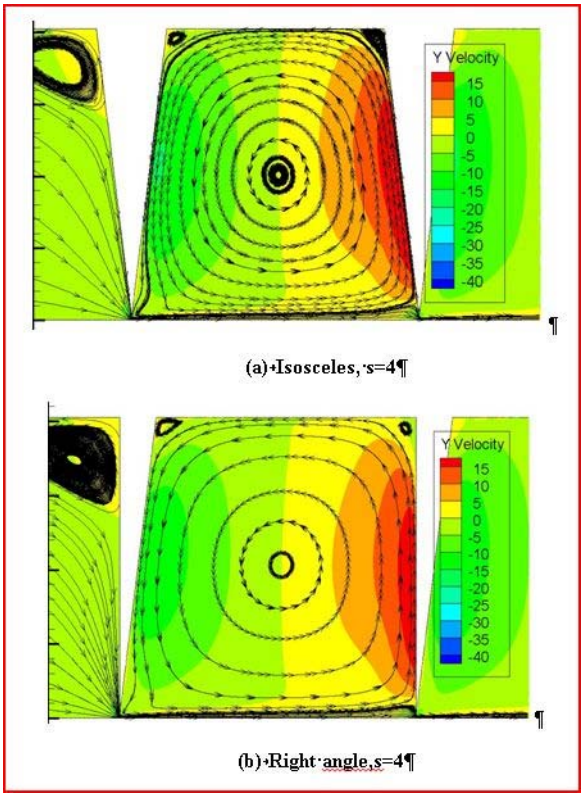

Fig. 3.20. Stream traces and radial velocity contour at Re 2000 (incompressible flow, case 7, case 15).

Fig. 3.21 shows that for a constant clearance, c =0.05, the carryover coefficient is higher for right angle tooth for same pitch compare to isosceles triangle for compressible flow.

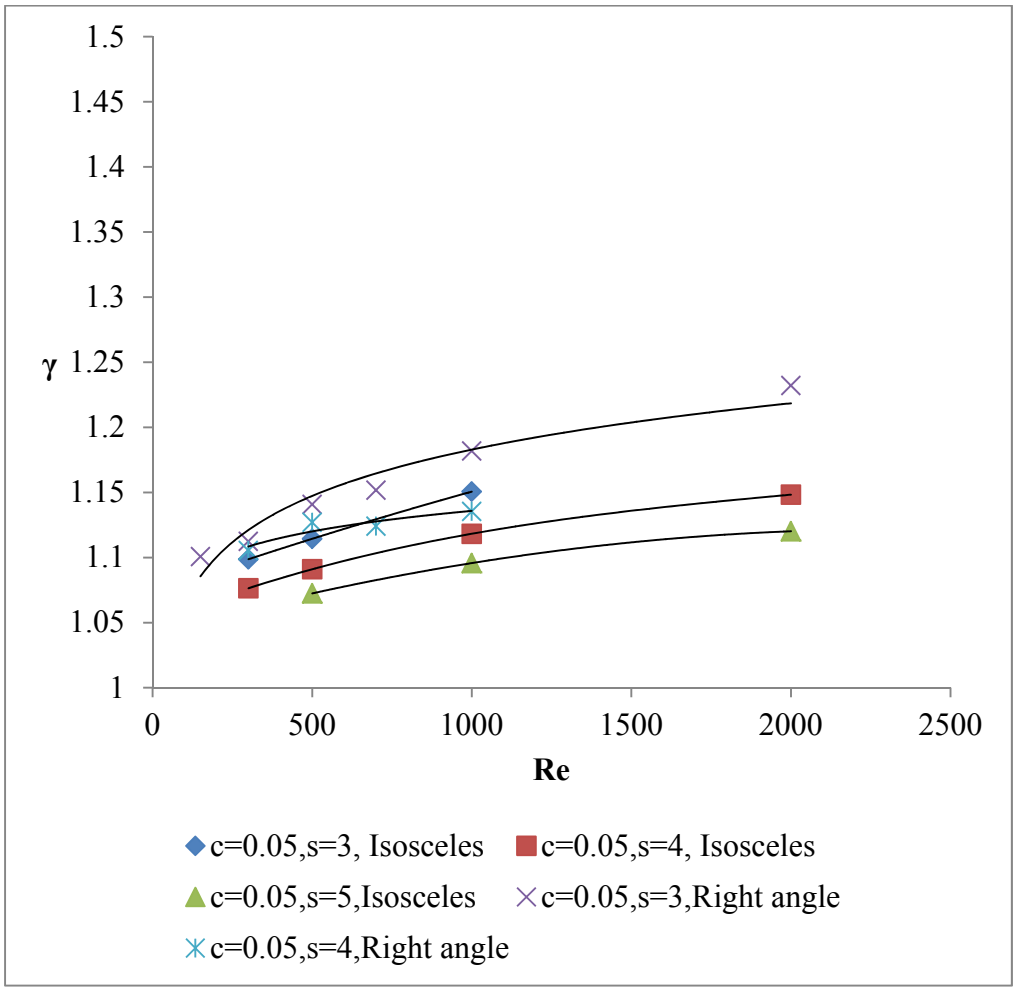

Fig. 3.21. Comparison of pitch effect on the γ (for compressible flow, isosceles and right angle tooth, case 1, case 7, case 10, case 11, case 15).

3.3.5. Effect of Tooth Angle

The tooth upstream angle effect on the carryover coefficient, γ, is evaluated on the basis of cases 1, 2, 13, 14. Fig. 3.22 shows the tooth angle, B, arrangement for both the isosceles and right angle tooth. The tooth angle effect is investigated for both the compressible and incompressible flow.

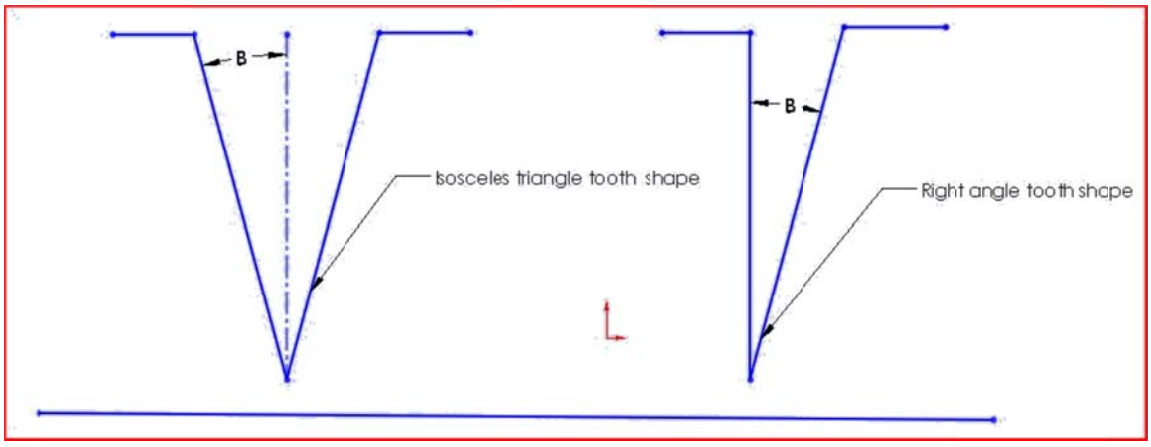

Fig. 3.22. Configurations of tooth with tooth angle, B.

Fig. 3.23 illustrates that the tooth angle effect is insignificant for compressible flow where as for the incompressible flow the effect is significant.

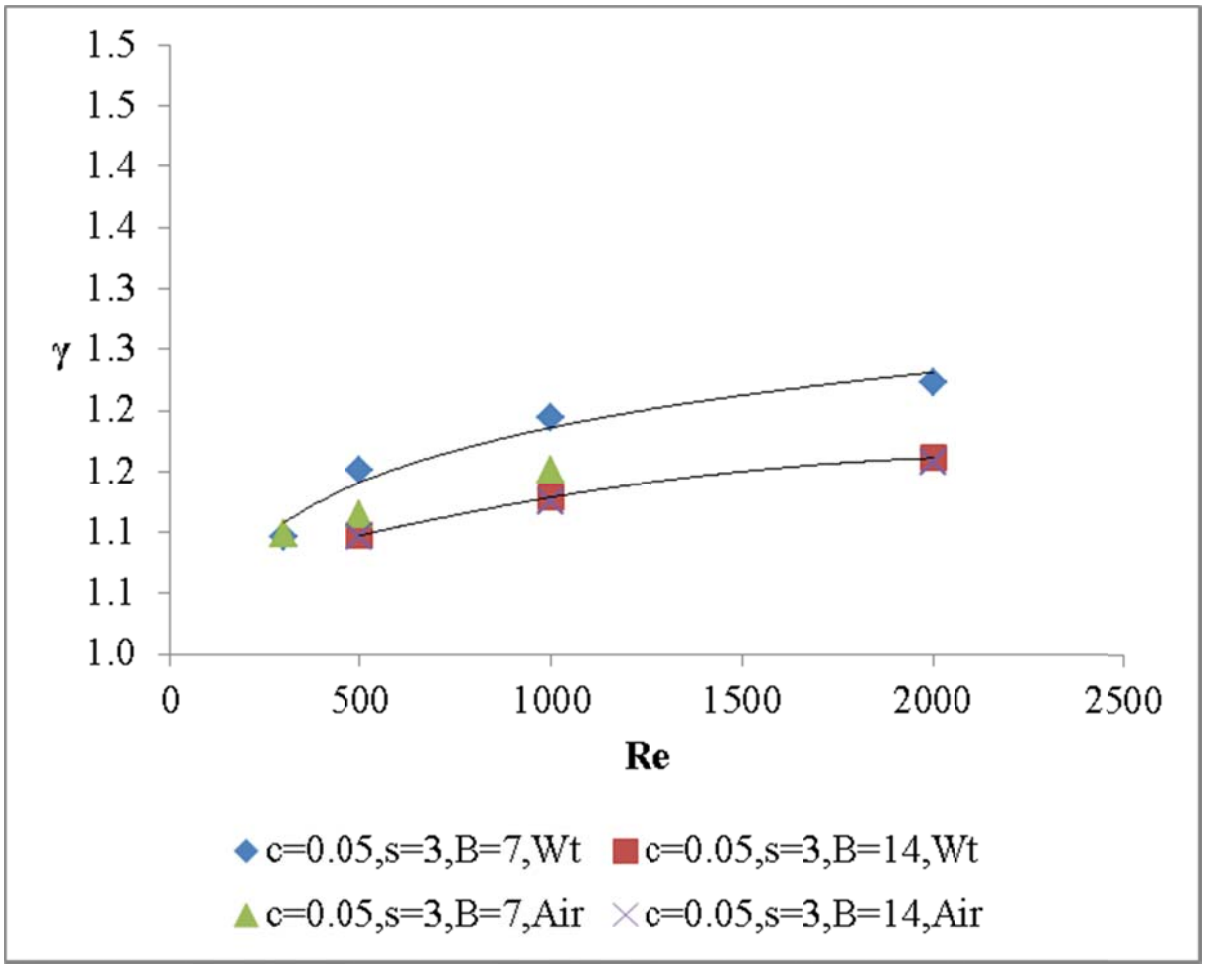

Fig. 3.23. Association of γ as a function of Re for B=7, 14 degree (case 1, case 2).

The results in the Fig. 3.24 shown the carryover coefficient evaluation comparison between the isosceles and right angle tooth It can be concluded that the upstream angle has significant effect on the isosceles triangle tooth shape. On the other hand the effect of the upstream angle is insignificant for the right angle shape.

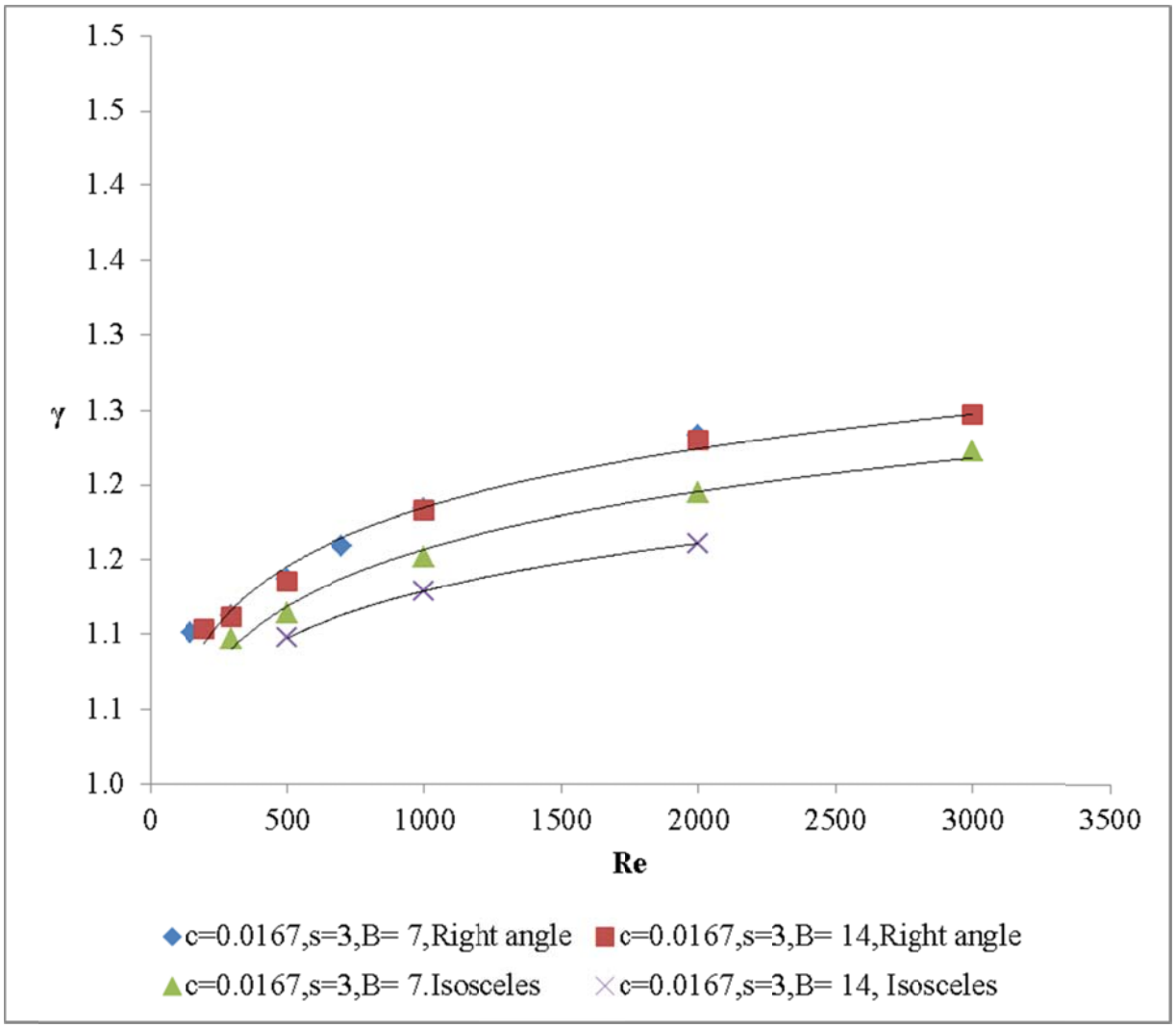

Fig. 3.24. Comparison of the γ for B = 7 and 14 degree tooth angle between the isosceles and right angle tooth shape (incompressible, case 1, case 2, case 11, case 14).

It is observed from the Fig. 3.25 that the approach upstream streamline angle is higher when B=7 compare to B =14 for the isosceles triangle tooth. This lower approach angle helps the flow to recover from the vena contracta effect and as a consequence the divergence angle is higher. The higher divergence angle is causes the lower carryover

coefficient. For the right angle tooth, increasing the tooth angle has no effect on approach angle of stream line as a result divergence angle remains same for both of the cases in Fig. 3.25 (c) & (d).

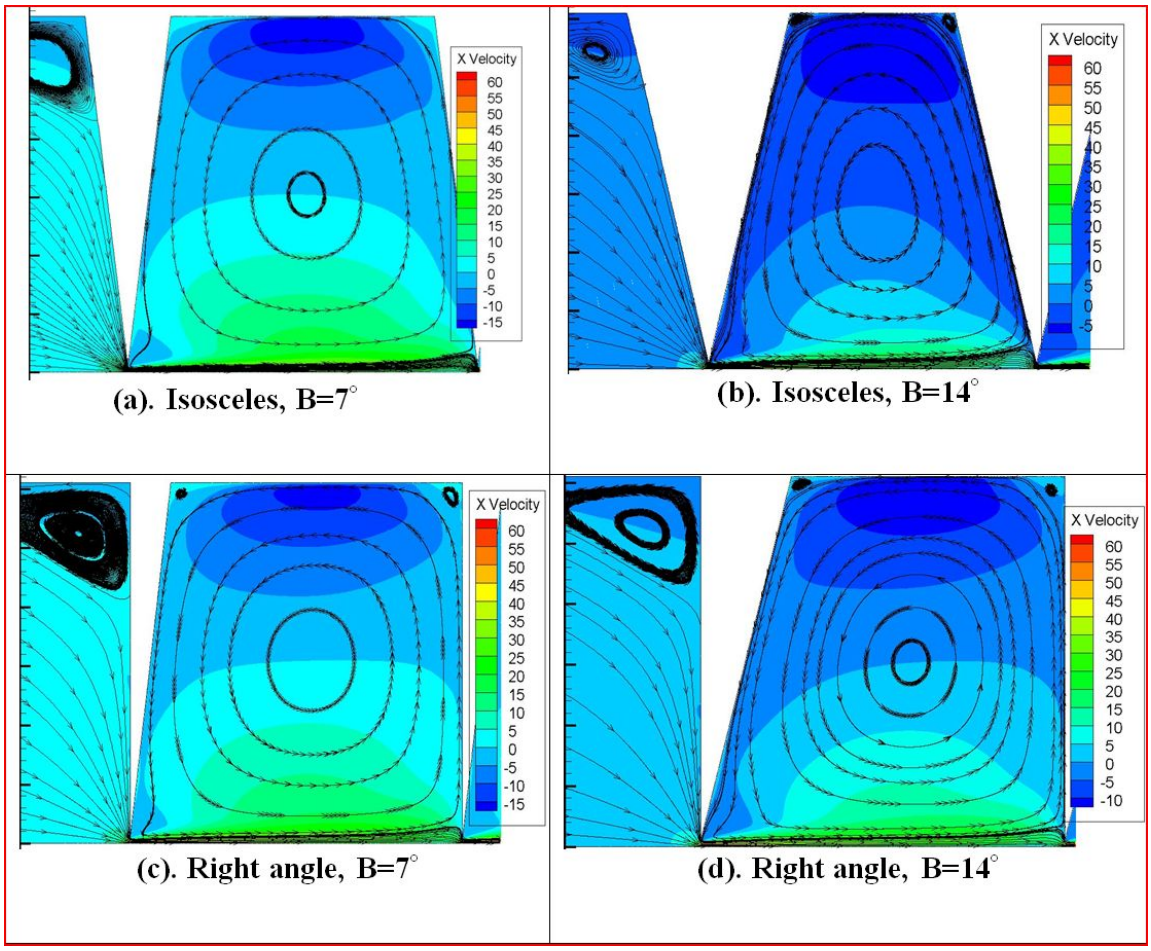

Fig. 3.25. Stream traces and axial velocity distribution of isosceles and right angle tooth for B=7, 14 degree tooth angle , Re 2000, incompressible flow (case 1, case 2, case 11, case 14).

Fig. 3.26 shows the comparison of angle effect between isosceles and right angle tooth shape on the carryover coefficient for compressible flow.

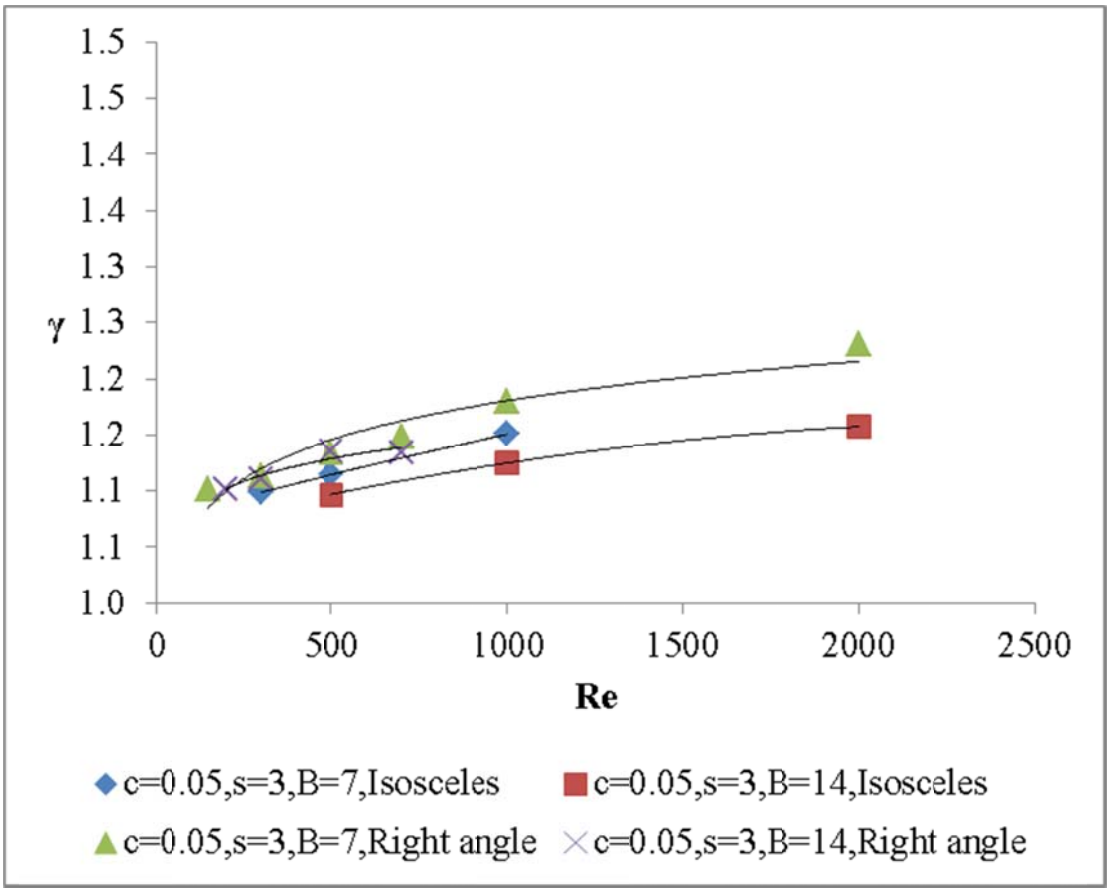

Fig. 3.26. Comparison of upstream angle on the γ for isosceles and right angle tooth (for compressible flow, case 1, case 2, case 11, case 14).

3.3.6. Effect of Shaft Speed

Introducing rotation in the shaft may change the flow behavior within the seal due to the presence of swirl velocity. This swirl velocity might influence the carryover coefficient. Simulations are performed for a given flow and seal geometry at different shaft speeds such as 1000, 2000, 3000, 4000, 5000, 6000, 7000 rad/sec. Both incompressible and compressible flow are considered to analyze this effect. Shaft rotation is applied to different seal geometries including c, s, w, B. In this section, association of the carryover coefficient and shaft speed is analyzed for different seal geometries.

3.3.6.1 Effect of Shaft Speed on γ for Different Clearances

In the earlier section, 3.3.2. , it is shown that the clearance pitch ratio, c/s, has a significant effect on the carryover coefficient, γ, at zero shaft rotation. To analyze the effect of shaft rotation, swirl velocity is applied on the isosceles triangle tooth shape labyrinth seal. In the simulation, the moving wall boundary condition is applied in the rotor.

The results, as seen from Fig. 3.27 , shows that the carryover coefficient is not strongly dependent of shaft rotation for compressible flow. This study is performed for different Reynolds numbers and c/s ratios (0.0167, 0.033, 0.05, 0.066) with the rotational speed of shaft varies from 1000 to 7000 rad/sec. It has to be noted that this study deals with tooth on stator labyrinth seals.

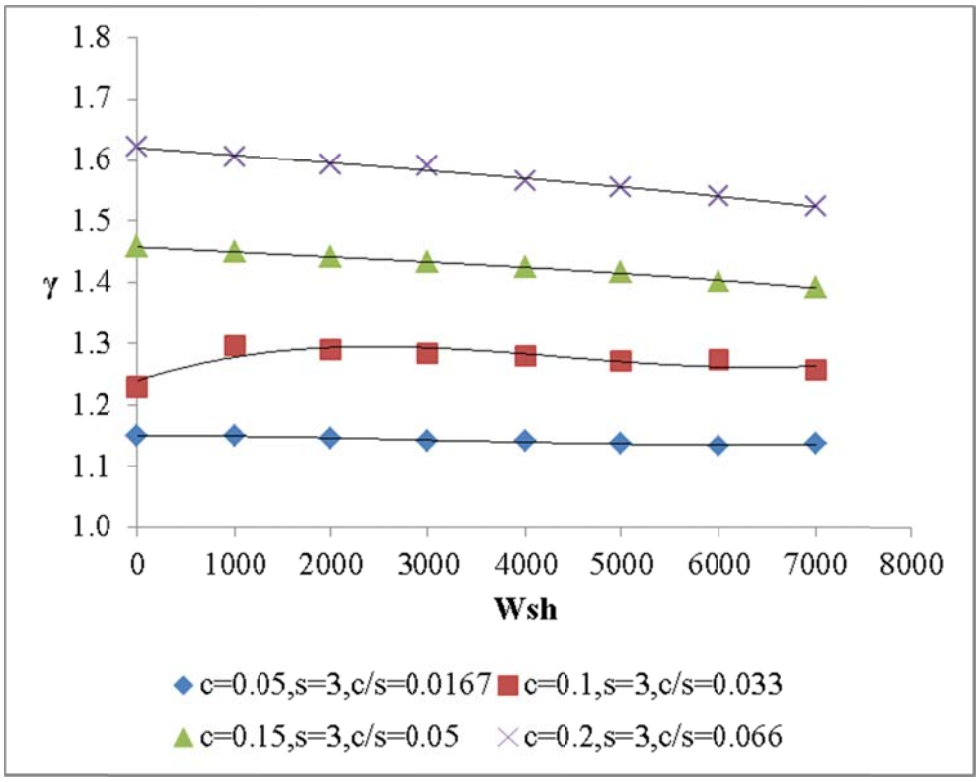

Fig. 3.27. Variation of γ with shaft speed (Re 1000, cavity 1, case 1, case 4, compressible flow).

From the Fig. 3.27, it is observed that for the clearance 0.1, the deviation of carryover coefficient is 3% for the 600% increment of shaft speed. And similarly 0.87% change is observed in carryover coefficient for the 600% increment of shaft rotation.. The Fig. 3.28 illustrates the association of carryover coefficient with Re and shaft rotation, W_{sh}, for two c/s ratios (0.05, 0.1). This three dimensional plot is used to visualize the effect of shaft rotation on carryover coefficient, γ, for different clearances, c, and Reynolds number, Re. Fig. 3.28 shows that the carryover coefficient is less dependent of shaft rotation for compressible flow. Fig. 3.29 illustrates the effect of shaft

rotation on the carryover coefficient for incompressible flow at Re 1000 and c/s ratios of 0.0167, 0.033, 0.05.

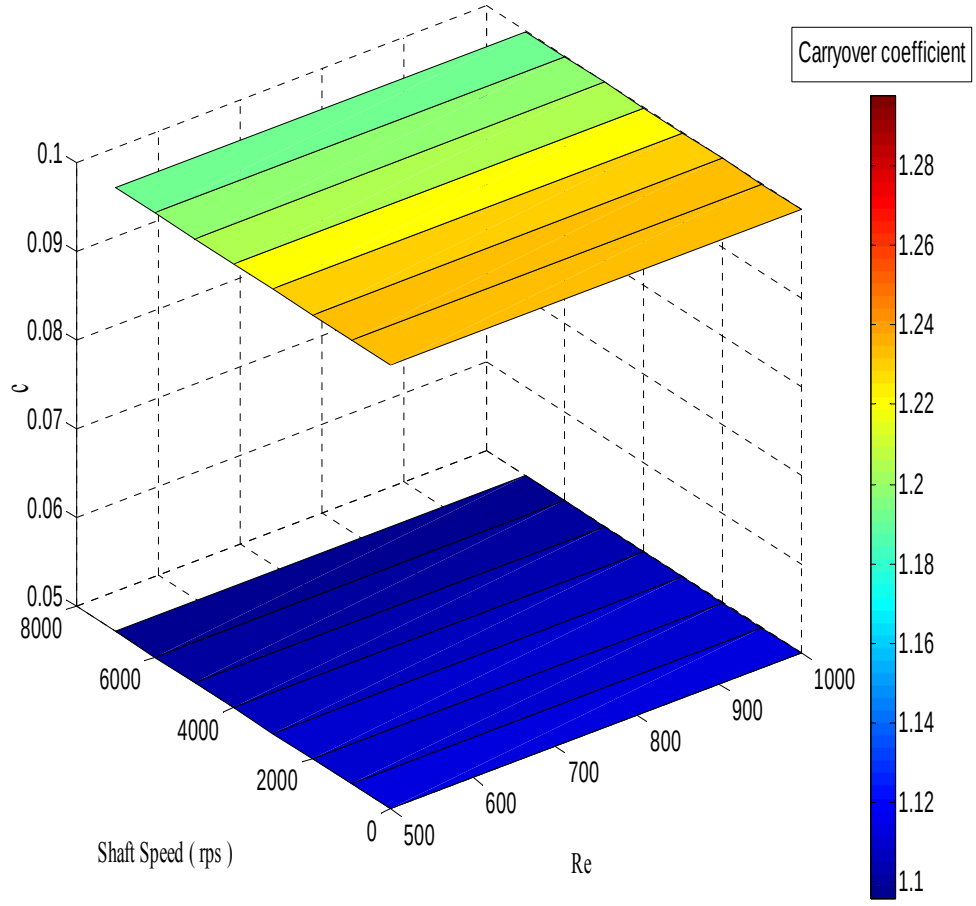

Fig. 3.28. Association of γ with Wsh for different clearances (compressible flow, c= 0.05 and 0.1 mm, cavity 1, case 1, case 3).

The combined effect of the shaft speed and clearance on the carryover coefficient as a 3D plot in the Fig. 3.30. It is also evident from the Fig. 3.30 that for c=0.05 the effect is insignificant but for higher clearance, c=0.1 the carryover coefficient, γ, varies from 1.3 to 1.18. This variation is 10% which is larger for higher Reynolds number.

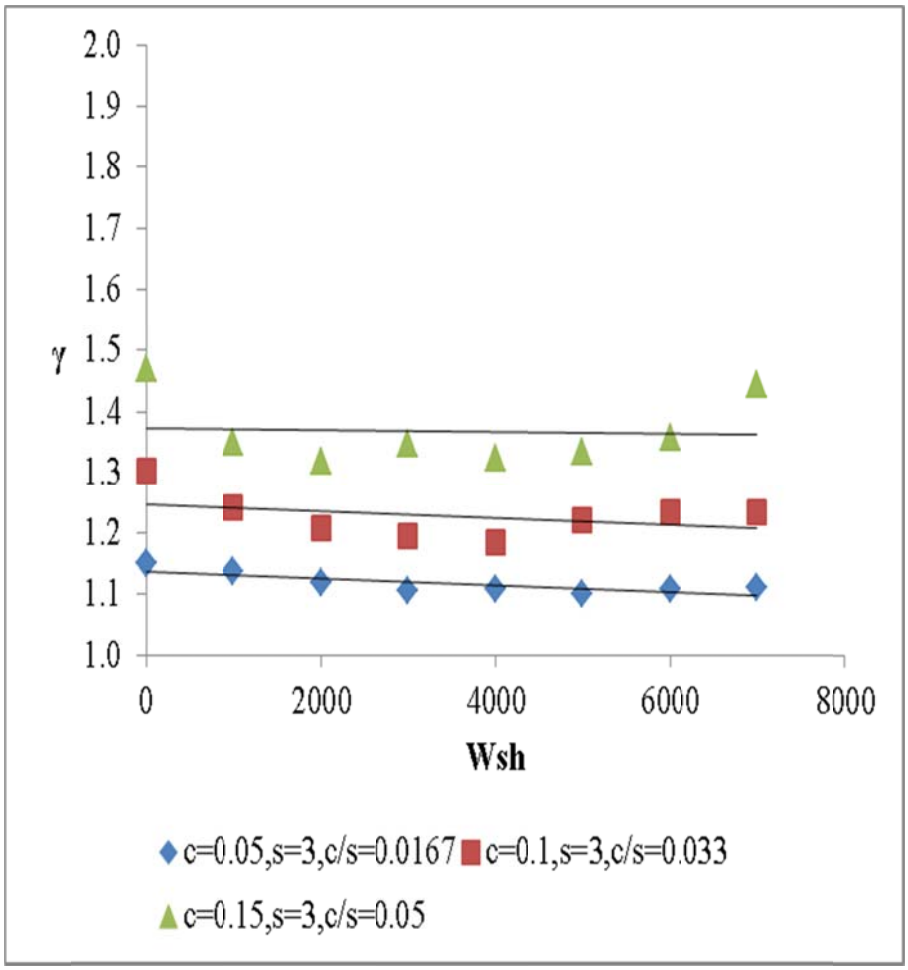

Fig. 3.29. Variation of γ with shaft speed (Re 1000, case 1, case 3, case 4, cavity 1, incompressible flow).

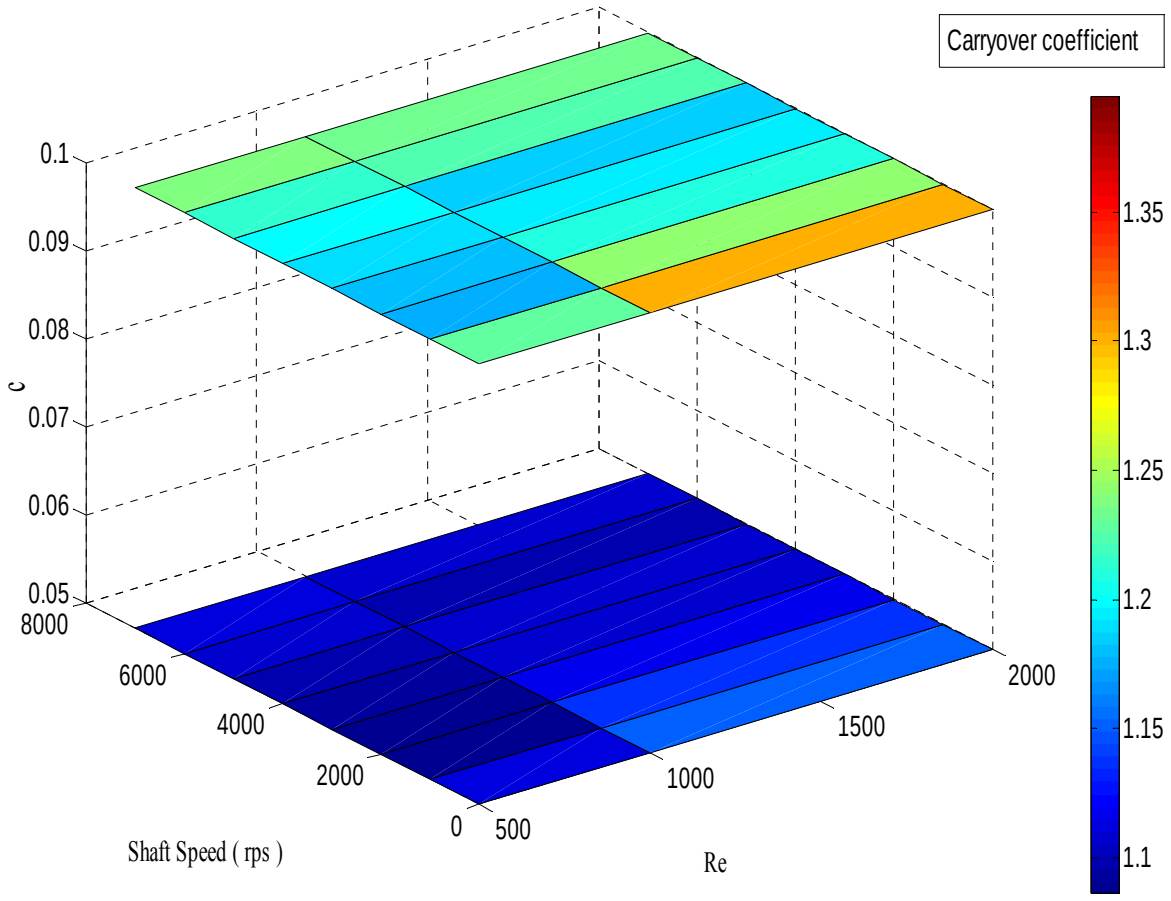

Fig. 3.30. Association of γ with Wsh for different clearances (incompressible flow, cavity 1, case 1, case 3).

Fig. 3.31 shows the effect of the shaft speed on the carryover coefficient on the 3 cavities for case 1. The results shows that variations of the carryover coefficient for shaft speed as a function of Re are similar for all 3 cavities.

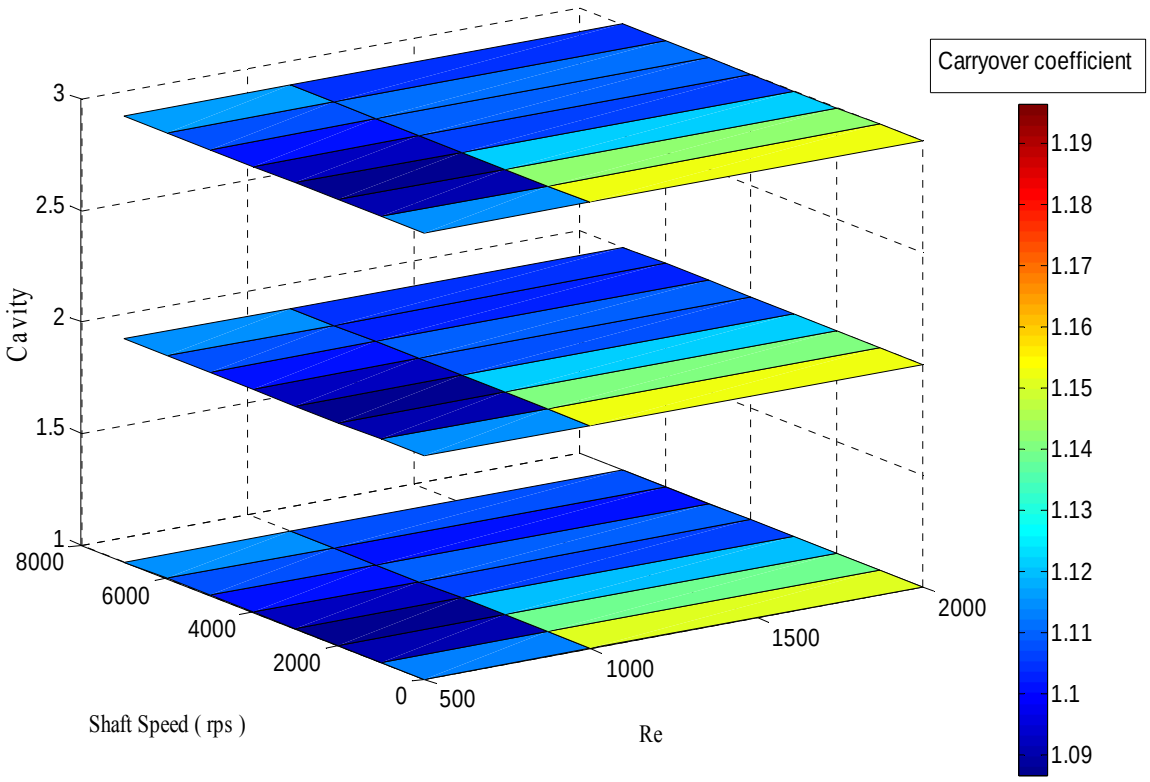

Fig. 3.31. Carryover coefficient distribution in different cavities(incompressible flow, case 1).

It seems from the Fig. 3.32 at Re 1000 that axial velocity is decreasing while shaft speed is increasing. And reverse phenomenon is observed for the case of radial velocity. Swirl effect near the wall of rotor is the reason which reducing the axial velocity.

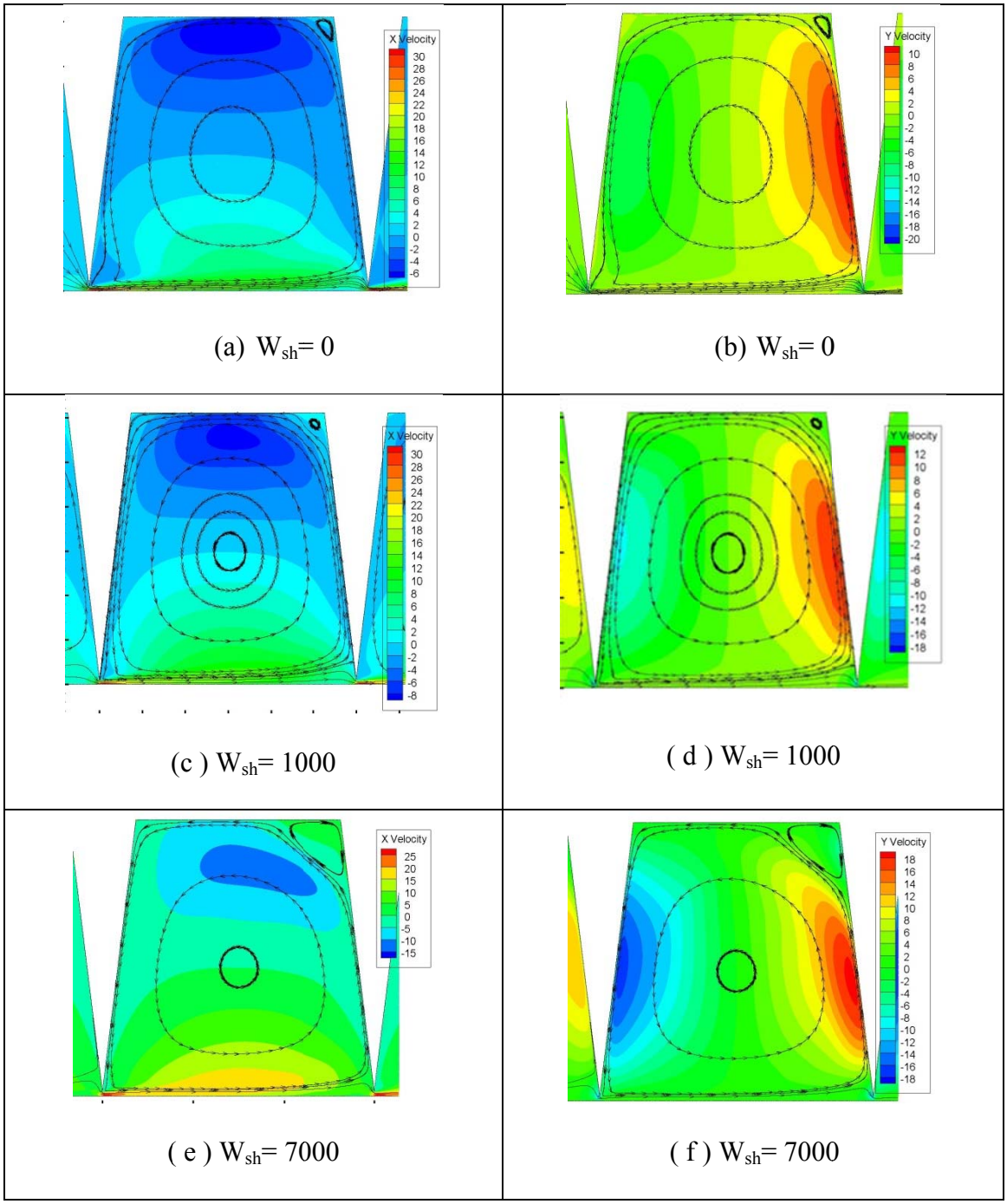

(a) W_{sh}= 0

(b) W_{sh}= 0

(c) W_{sh}= 1000

(d) W_{sh}= 1000

(e) W_{sh}= 7000

(f) W_{sh}= 7000

Fig. 3.32. Axial and radial velocity distribution for different shaft speed (Re 1000, c=0.05, s=3, incompressible flow, case 1).

So far the shaft speed effect on the carryover coefficient is discussed only for the first cavity. It is important to show the variation of carryover coefficient for different shaft speed in the 2nd and 3rd cavity of the labyrinth seal. It is observed from Fig. 3.33 that the carryover coefficient, γ, changes are almost constant in all cavities for different shaft speed for both compressible and incompressible flow at Re = 1000.

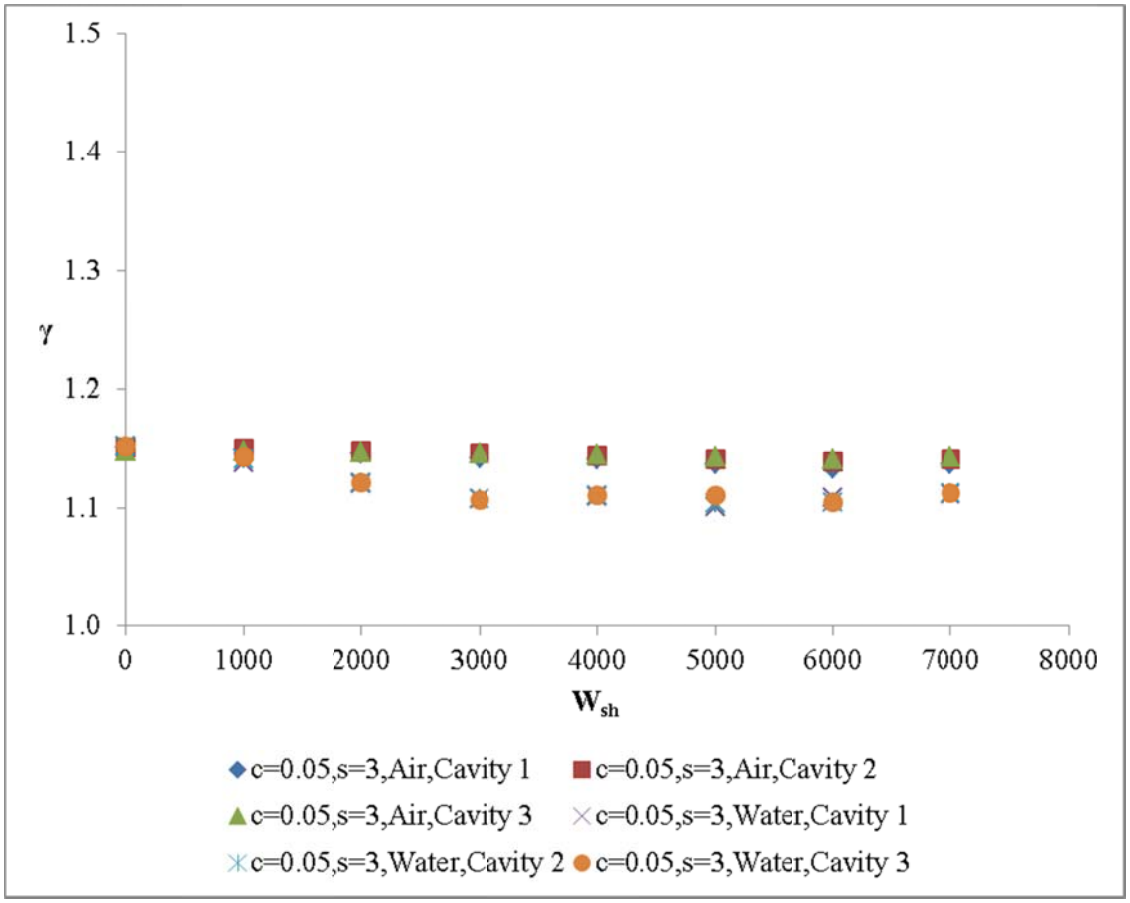

Fig. 3.33. Association of γ with shaft rotation in 3 cavities (for Re 1000, c=0.05, s=3, incompressible and compressible flow).

3.3.6.2 Effect of Shaft Speed on γ for Different Re

In the section 3.3.1. , it is shown that the carryover coefficient is a strong function of Reynolds number at zero shaft speed. The results in Fig. 3.34 show that the carryover coefficient variation as a function of Re is insignificant for different shaft speed. This plot is limited to Re 300 to 1000 for compressible flow. For the incompressible flow, the Fig. 3.35 show that at higher Reynolds number (Re 3000) and maximum shaft speed (W_{sh} = 7000) , a 6% reduction of the discharge coefficient was obtained.

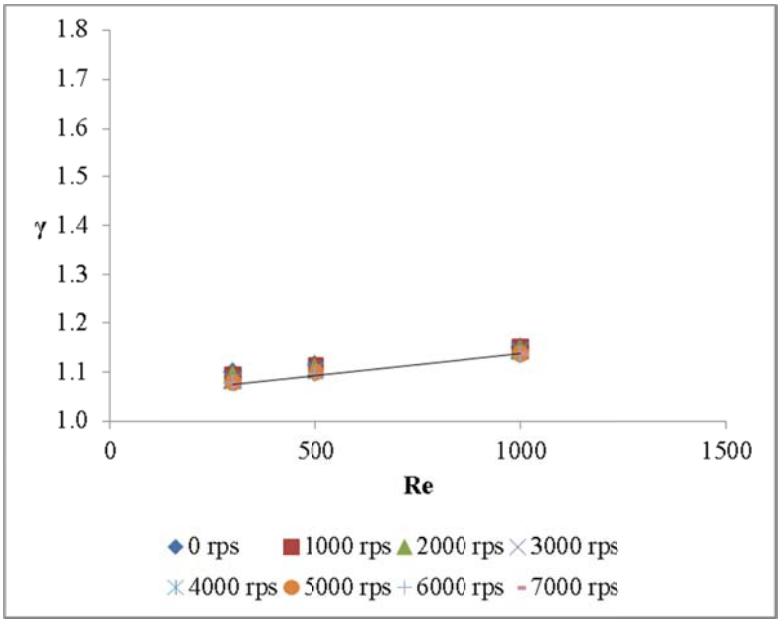

Fig. 3.34. Shaft speed effect on γ for different Re (compressible flow , c=0.05, s=3, case 1).

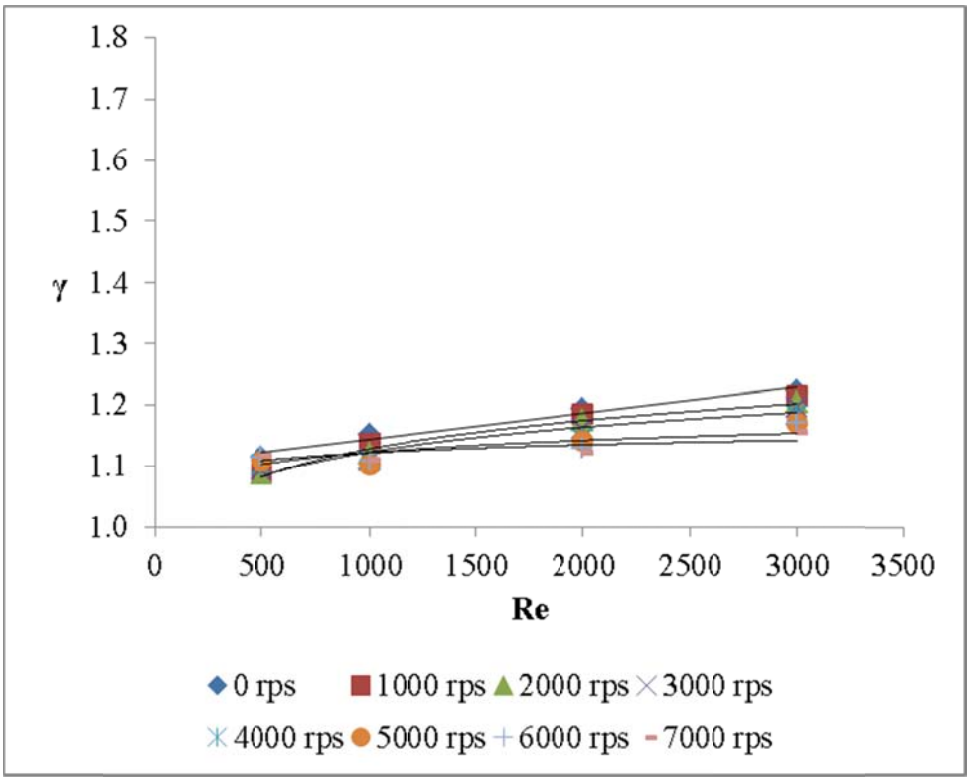

Fig. 3.35. Shaft speed effect on γ for different Re (incompressible flow , c=0.05, s=3, case 1).

So far from the above discussion it is observed that shaft rotation has an effect at high Reynolds number for incompressible flow. So it is very important to determine the physics behind this behavior. At low Reynolds number, Re 500, there is very little change in divergence angle between 0 and 7000 rps as a result the effect of shaft speed is insignificant. Also it has noticed from the Fig. 3.36 that the divergence angle is affected more for shaft rotation at higher Reynolds number.

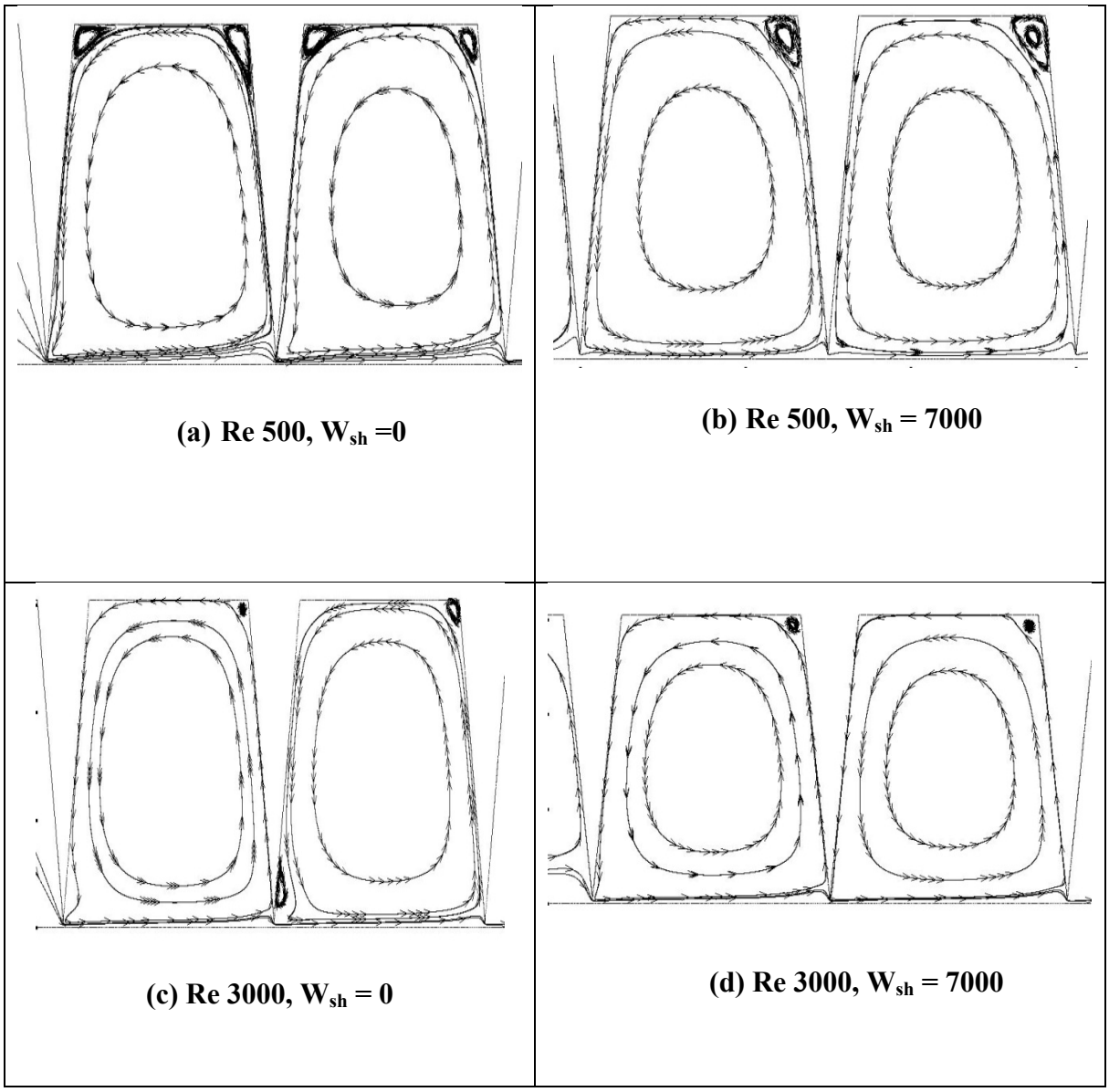

(a) Re 500, W_{sh} =0

(b) Re 500, W_{sh} = 7000

(c) Re 3000, W_{sh} = 0

(d) Re 3000, W_{sh} = 7000

Fig. 3.36. Flow pattern inside cavity at lowest and highest shaft speed (for incompressible flow, Re 500 and 3000, c =0.05, s=3, case 1).

3.3.6.3 Shaft Rotation Effect on γ for Pitch

The result in Fig. 3.37 shows that the effect of shaft rotation as a function of pitch on carry over coefficient, γ, is insignificant. At higher shaft speed and higher Reynolds number for higher pitch seal, it is observed that the divergence angle is a little lower as a result higher carryover coefficient was obtained. This is explained in Fig. 3.38. At higher Reynolds number, Re 1000, for the longer tooth, 1% increment in divergence angle was obtained at 7000 rps shaft speed. So it is valid to say that rotation effect is insignificant on the carryover coefficient as a function of pitch. and

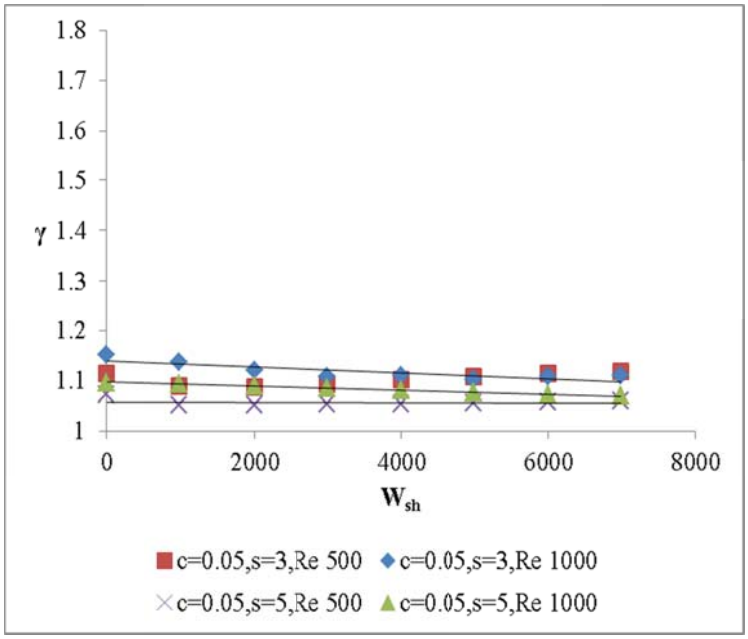

Fig. 3.37. Effect of shaft rotation as a function of pitch (for incompressible flow, case 1, case 10).

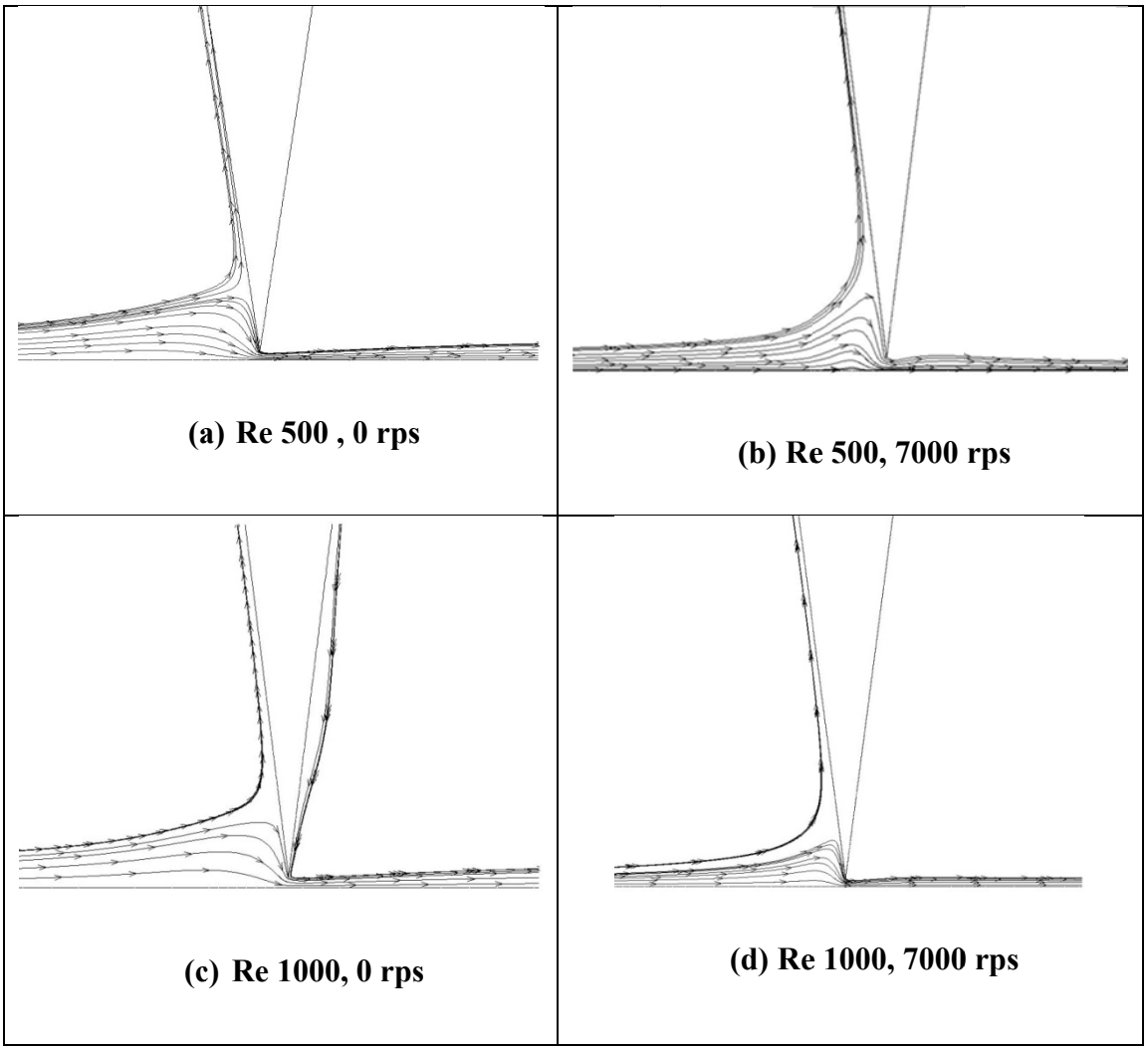

Fig. 3.38. Variation of fluid flow under 2nd tooth for minimum and maximum shaft speed at Re 500 and 1000 (for incompressible flow, s=5, case 10).

The combined effect of Reynolds number, shaft speed and pitch on the carryover coefficient is shown in Fig. 3.39. It is evident that at maximum shaft speed and Reynolds number, Re = 500, higher pitch value provides lower carryover coefficient compare to lower pitch value.

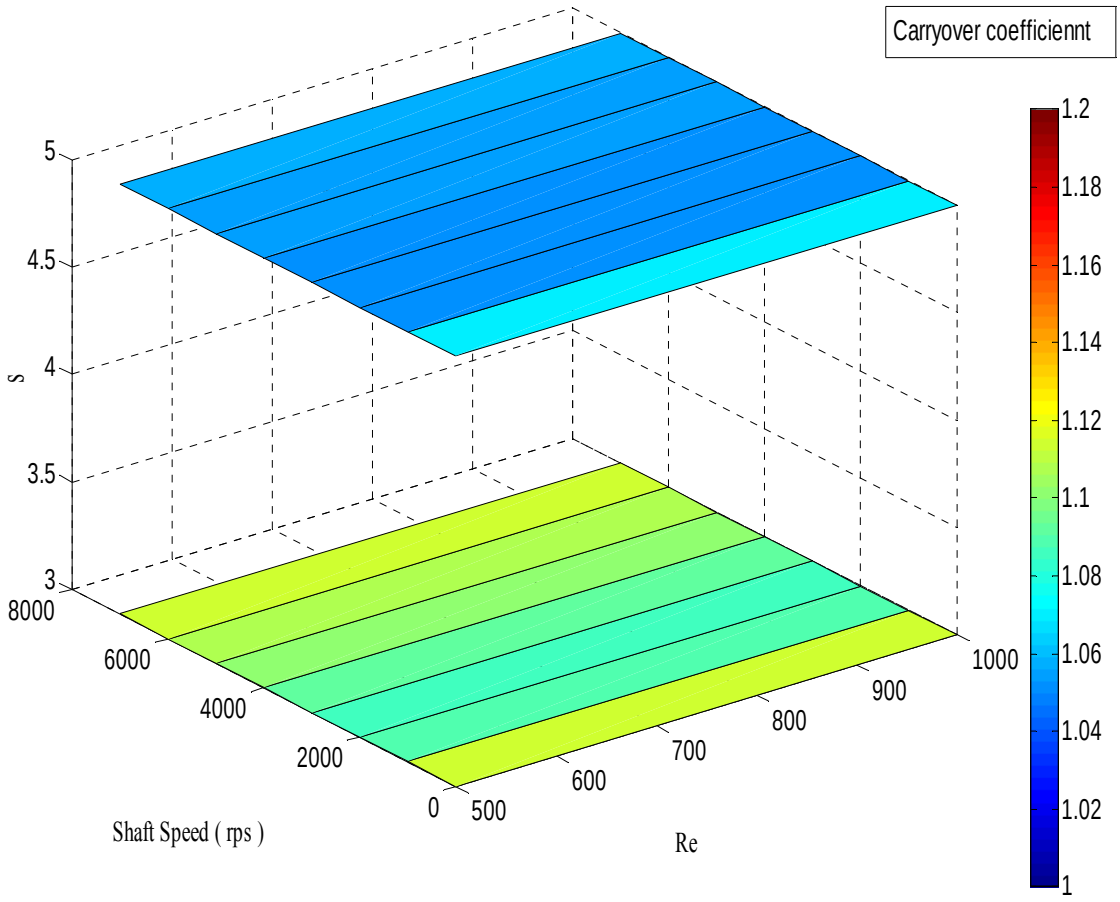

Fig. 3.39. Combined effect of s, Re and W_{sh} on γ (cavity 1, incompressible flow , case 1, case 10).

Fig. 3.40 shows the combined effect of $W_{sh,}$ Re, s on the carryover coefficient for incompressible flow. From the 3D plot it is observed that at higher pitch, lower carryover coefficient values were obtained at higher shaft speed compare to lower pitch. But this effect is not very intense.

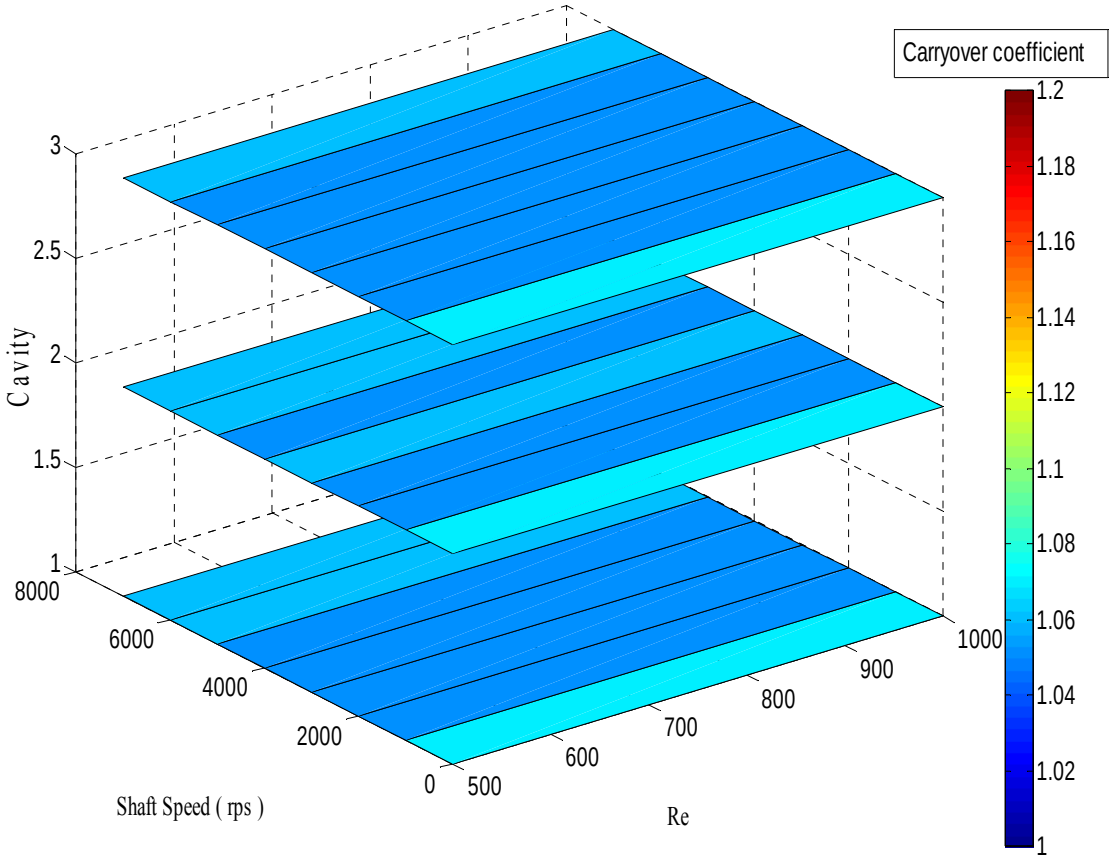

Fig. 3.40. Combined effect of s, Re and W_{sh} on γ(for all cavities, incompressible flow , case 10, s=5).

For the compressible flow, a similar investigation is performed. Shaft rotation effect is evaluated only at Reynolds number, Re 1000. From the Fig. 3.41, it is observed that shaft rotation effect as a function of pitch is slight, 5% different.

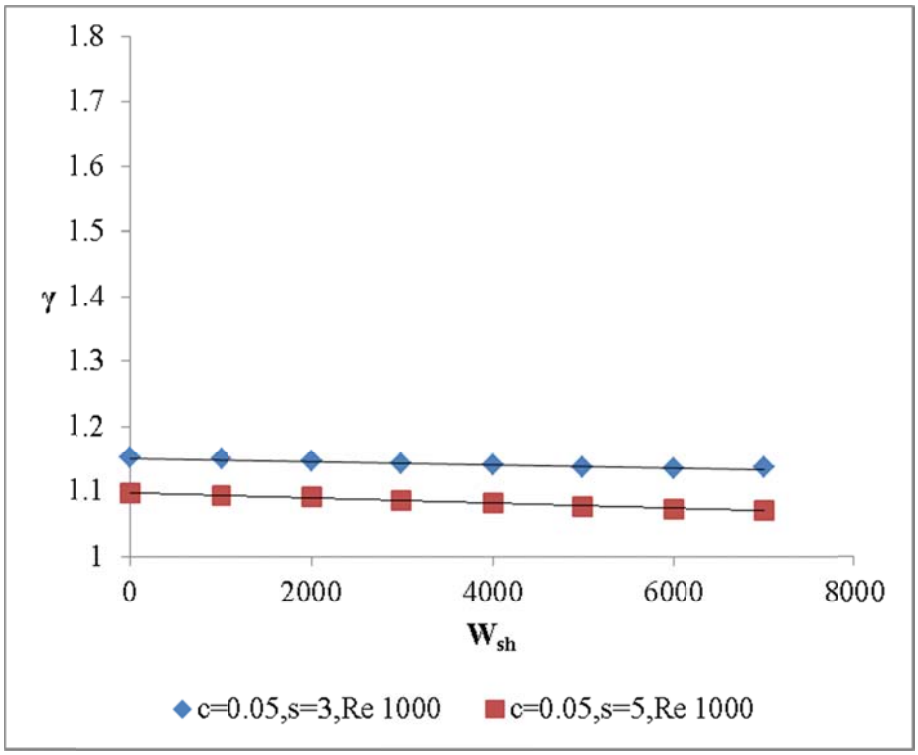

Fig. 3.41. Shaft speed effect on carry over coefficient as a function of pitch (for compressible flow , case 1, case 10).

3.3.6.4 Effect of Shaft Speed on γ for Tooth Width

It is found that shaft rotation affects are a function of tooth width and has a significant effect on the carryover coefficient. At high Reynolds number (Re 2000) for both of the tooth widths (w = 0.5, 1) shaft rotation has less effect at high W_{sh} = 7000 rps. Fig. 3.42 shows that at lower Reynolds number (Re 500) the shaft rotation rate has significant effect on the carryover coefficient.

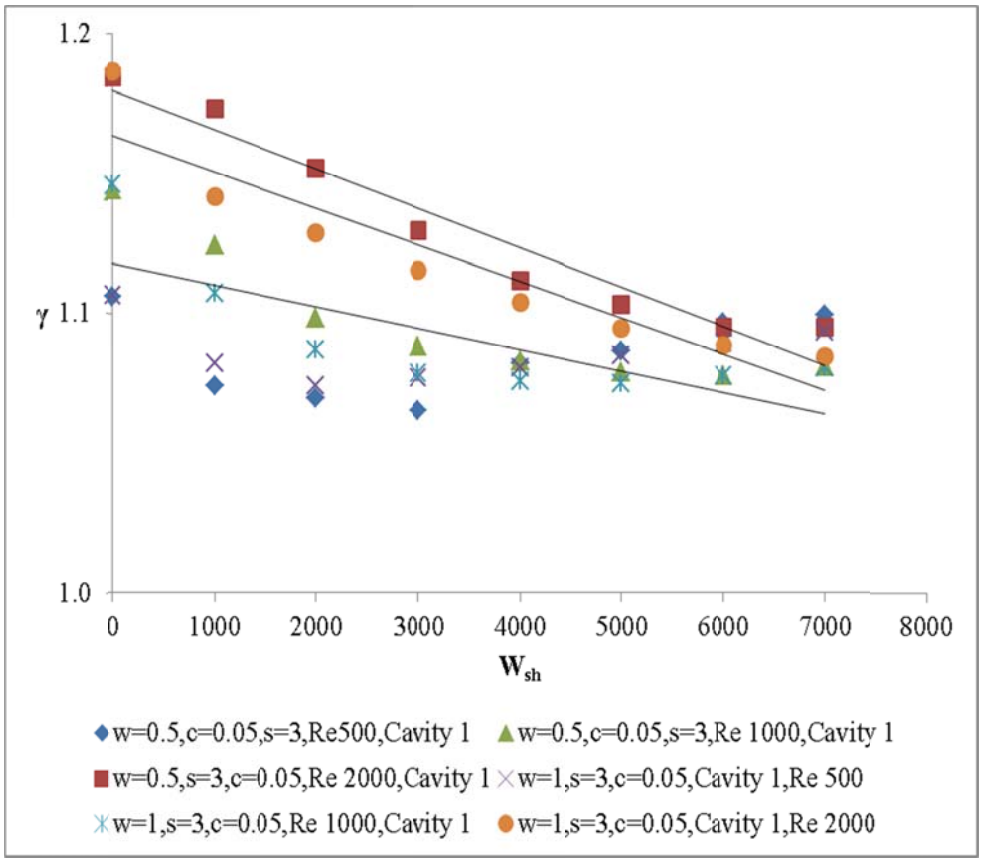

Fig. 3.42. Effect of shaft speed as a function of tooth width on γ (incompressible flow , case 9, case 8).

Fig. 3.43 and Fig. 3.44show the flow pattern in the cavity as a function of shaft speed for two different tooth widths with constant clearance.. For both of the tooth width (w =0.5, 1) it is found that inception of the secondary vortices is observed at higher shaft speed. For the case of large tooth width, large secondary vortices is observed compare to lower tooth width with same clearance. From the seal point of view secondary recirculation zone is preferable as it reduces the carryover coefficient and the discharge coefficient as well by increasing the peripheral momentum fluid in the cavity.

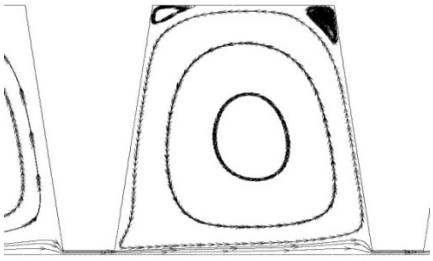

(a) Re 500, W_{sh} = 0 rps

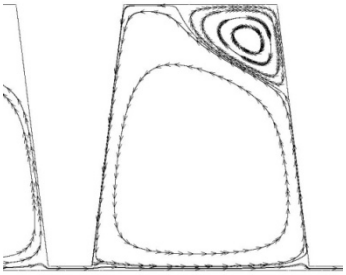

(b) Re 500, W_{sh} = 7000 rps

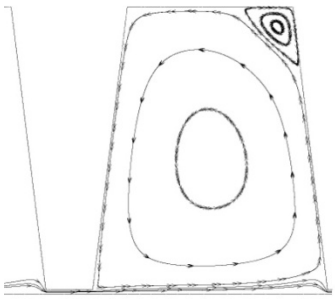

(c) Re 2000, W_{sh} = 7000 rps

Fig. 3.43. Flow pattern for shaft speed at W=0.5 (for incompressible flow, case 9).

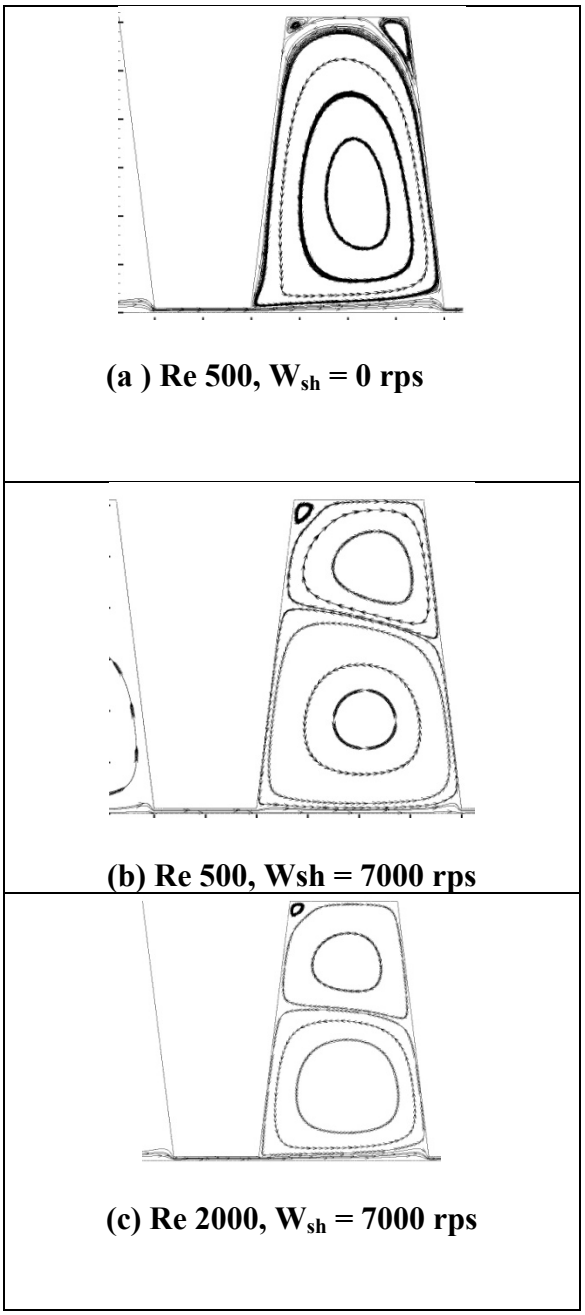

(a) Re 500, W_{sh} = 0 rps

(b) Re 500, Wsh = 7000 rps

(c) Re 2000, W_{sh} = 7000 rps

Fig. 3.44. Shaft speed effect on flow pattern for w =1 (incompressible, case 8).

Fig. 3.45 shows the combined effect of shaft speed, flow parameter, and tooth width on the carryover coefficient. This 3D plot is for second cavity. For water, Fig. 3.45 shows that for larger tooth width at maximum shaft speed (W_{sh} = 7000 rps), γ decrease as Re increase. Again for short tooth, γ increase as Re increase at maximum shaft speed.

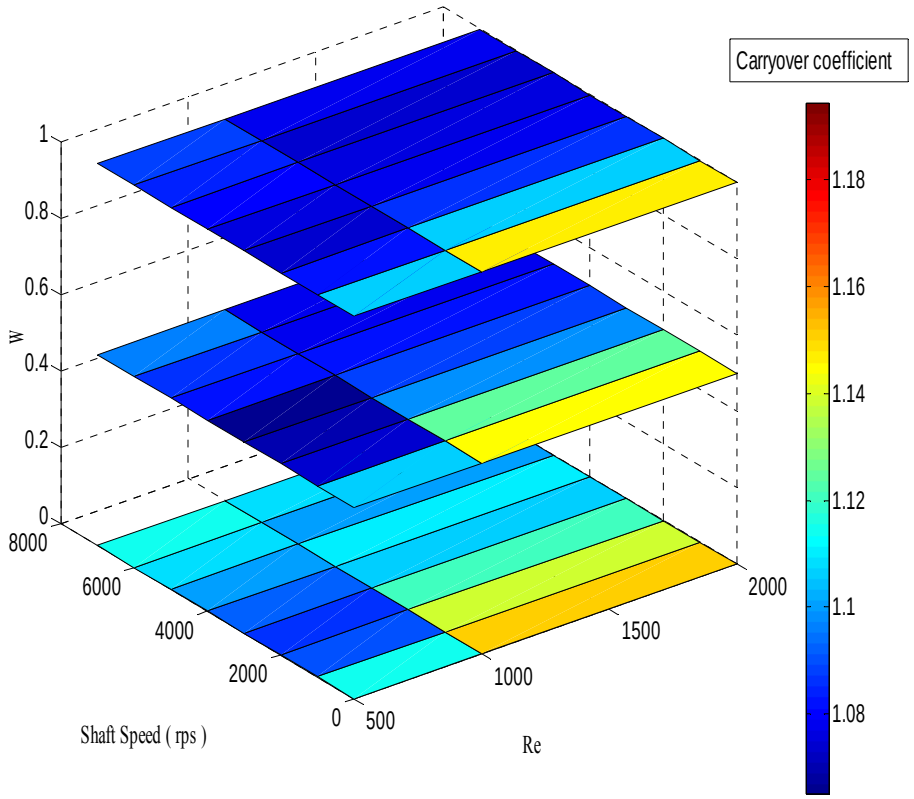

Fig. 3.45. Combined effect of Re, W_{sh}, w, on the carryover coefficient (for incompressible flow, case 1, case 8, case 9).

For air, Fig. 3.46 shows that at Re = 500, the carryover coefficient decreases as W_{sh} increases for large tooth width. So it can be concluded that for compressible flow, the large tooth width gives low carryover coefficient compare to small tooth width when

shaft speed is introduced. Secondary recirculation zone is large at maximum shaft speed for large tooth width whereas less presence of secondary flow zone is observed for small tooth width. This secondary flow zone is more visible in low Reynolds number and at shaft speed is reducing axial flow under the tooth as a result high tangential radial velocity increase in the cavity due to centrifugal acceleration. This is the reason to obtain low carryover coefficient in the cavity for large tooth width.

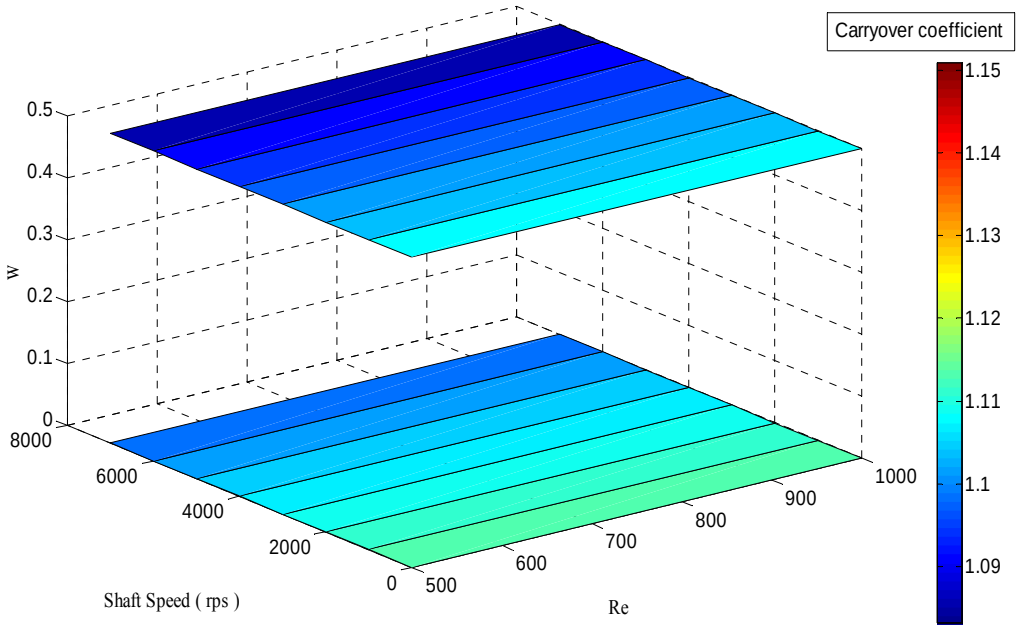

Fig. 3.46. Combined effect of Re, W_{sh}, w on the carryover coefficient. (air, case 1, case 9).

3.3.6.5 Effect of Shaft Speed on γ for Tooth Angle

The 3D plot shown in Fig. 3.47 illustrates that at low Reynolds number (Re = 500) and maximum shaft speed (w_{sh} = 7000 rps), large tooth angle (B= 14 degree) provides low carryover coefficient compare to tooth angle B = 7 degree for compressible flow.

For the incompressible flow, Fig. 3.48 show that at maximum shaft speed w_{sh} = 7000 rps, the carryover coefficient decreases with increasing Reynolds number for both tooth angle, B =7 and 14 degree. It is also evident from the Fig. 3.48 that at maximum shaft speed large tooth angle provide low carryover coefficient at maximum shaft speed.

At maximum shaft speed and low Reynolds number, higher tooth angle creates secondary recirculation zone inside the cavities. This secondary recirculation zone provides additional flow resistance results in higher divergence angle. This higher divergence angle r4esults in low carryover coefficient.

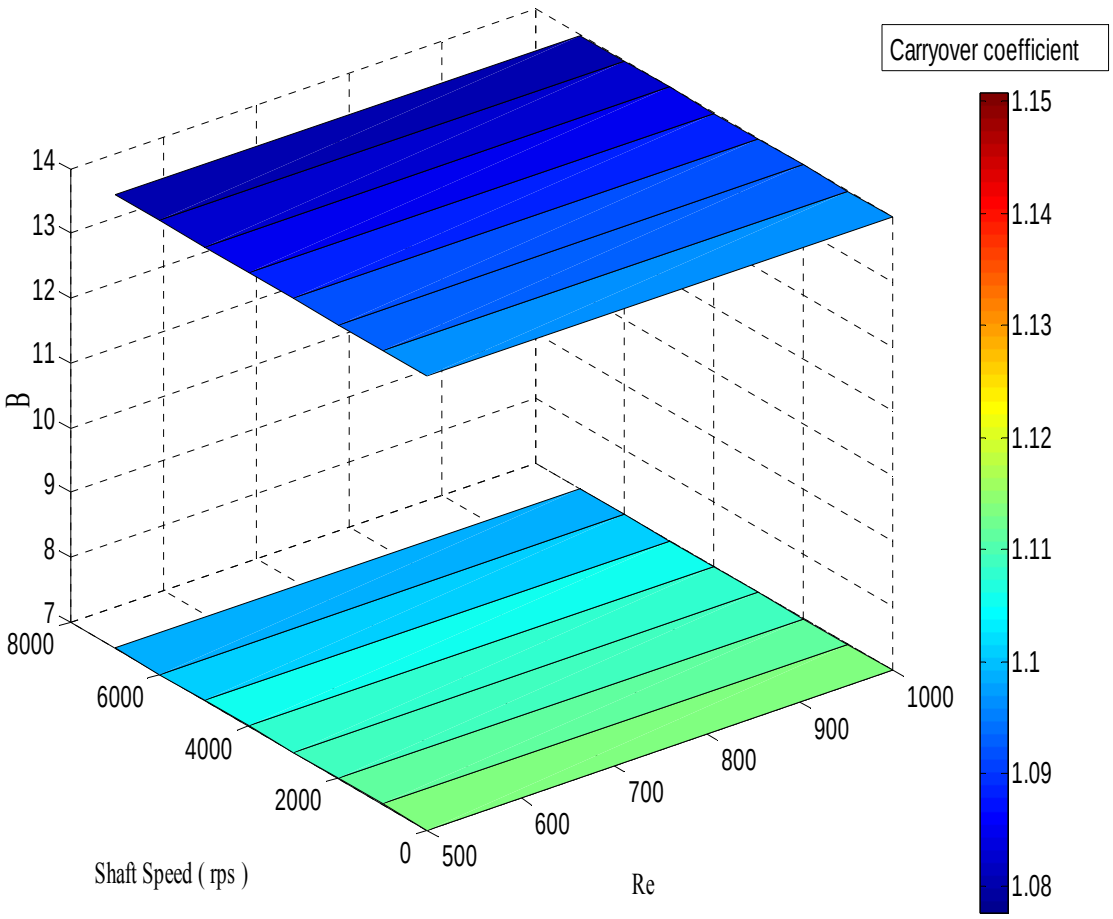

Fig. 3.47. Combined effect of Re, W_{sh}, B, on the carryover coefficient. (air, case 1, case 2).

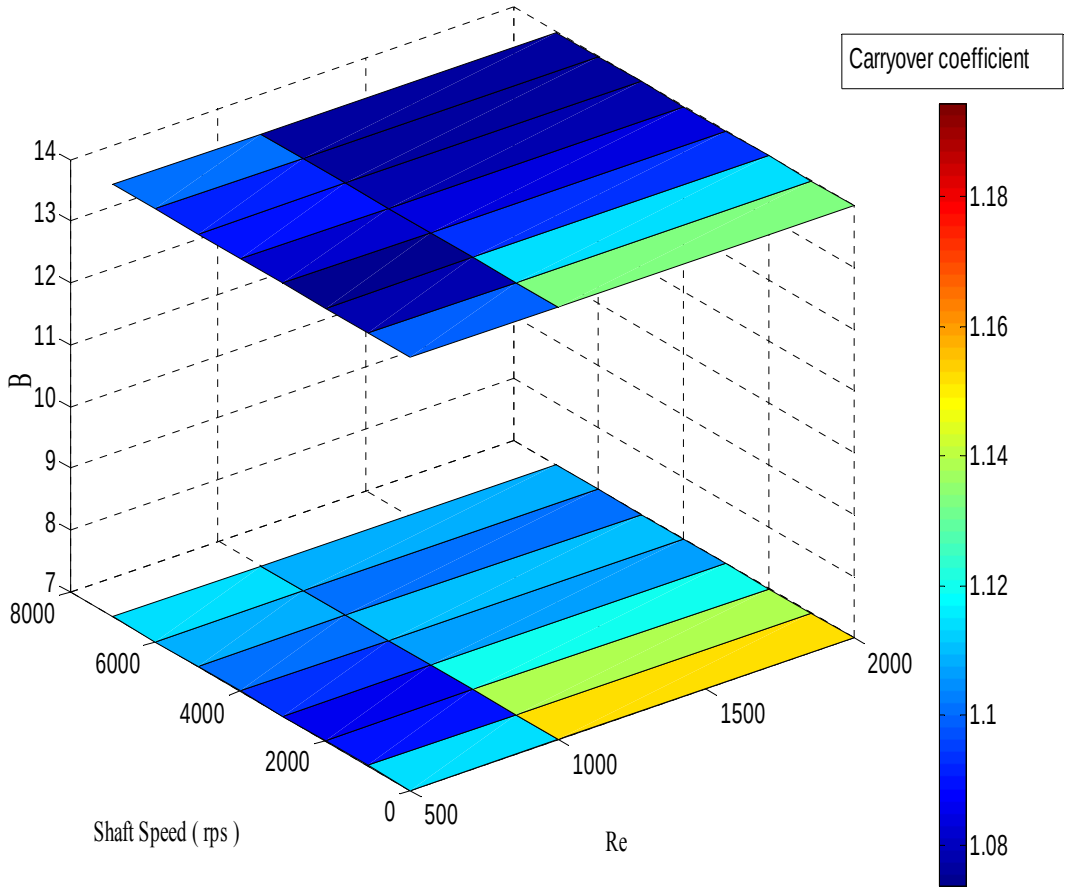

Fig. 3.48. Combined effect of Re, $W_{sh,}$ B, on the carryover coefficient. (water, case 1, case 2).

4 DISCHARGE COEFFICIENT

4.1. Definition of Discharge Coefficient

Discharge coefficient, C_d, is a dimensionless parameter. Throughout this study, the "discharge coefficient" term means the total absolute pressure losses that occur due to the fluid flows through the labyrinth seal cavity and under the tooth. Discharge coefficient is a term that explains the effect of energy dissipation in the labyrinth seal cavity and the frictional losses that occur at the tooth. The discharge coefficient is defined as

$$C_d = \frac{\dot{m}}{A\sqrt{2\rho(P_i - P_e)}} \qquad (4\text{-}1)$$

It is possible to calculate the overall leakage mass flow rate based on the overall pressure difference across the seal if the discharge coefficient, C_d, is known for the entire labyrinth seal. In the above equation (4-1), P_i and P_e are the inlet and exit pressures across a tooth and ρ is the density of upstream of the tooth so C_d is for a single tooth used in this study.

4.2. Discharge Coefficient Calculation

The computational results used to analyze the carryover coefficient are used here to analyze the discharge coefficient. The discharge coefficient is a very important

parameter to evaluate the labyrinth seal performance. From equation (4-1), four parameters (P_i, P_e, ρ, $\dot{m}$) are required to calculate the discharge coefficient. To obtain a consistent value for discharge coefficient, it is very important to define specific locations where the pressures P_i and P_e are measured. A commercial post processing tool, Tecplot 360 version 2009, is used to obtain the thermodynamic properties from the executed simulations. For the better understanding of the reader, a graphical presentation is given in Fig. 4.1 to show the pressure and density measurement locations across the length of the labyrinth seal.

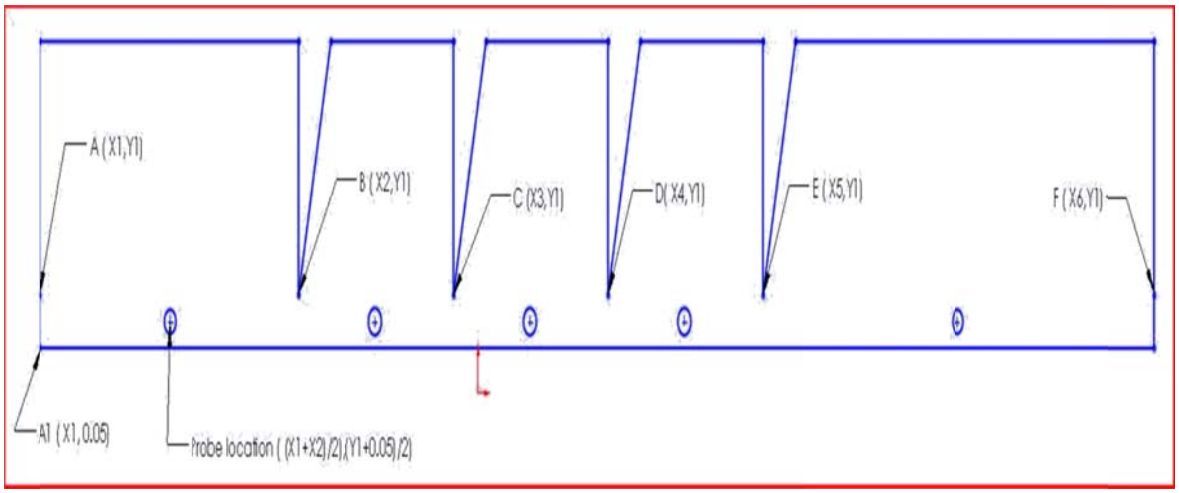

Fig. 4.1. Probe location to pick pressure and density to calculate discharge coefficient.

4.3. Evaluation of Discharge Coefficient

The discharge coefficient is evaluated on the basis of the flow and geometric parameters. Throughout the study Reynolds number, Re, and shaft speed, W_{sh}, are defined as flow parameters. The geometric parameters are defined as clearance, c, pitch, s, tooth angle, B, and tooth width, w. The effect of geometric and flow parameters upon the discharge coefficient, C_d, is evaluated in the same manner as the carryover coefficient. This evaluation is performed on the isosceles and right tooth shape labyrinth seal for both incompressible and compressible flow.

4.3.1. Effect of Reynolds Number

The effect of Reynolds number upon the discharge coefficient is investigated for a given geometry for both compressible and incompressible flow. The effect of Reynolds number is analyzed for both isosceles and right angle tooth shape.

The result shown in Fig. 4.2 illustrate that the discharge coefficient variation with Re for compressible flow is insignificant except for the fourth tooth. The discharge coefficient value at four teeth locations is almost similar for increasing Reynolds number. For this study, Re 300, 500, 1000 are applied to evaluate the effect of flow parameter on Reynolds number.

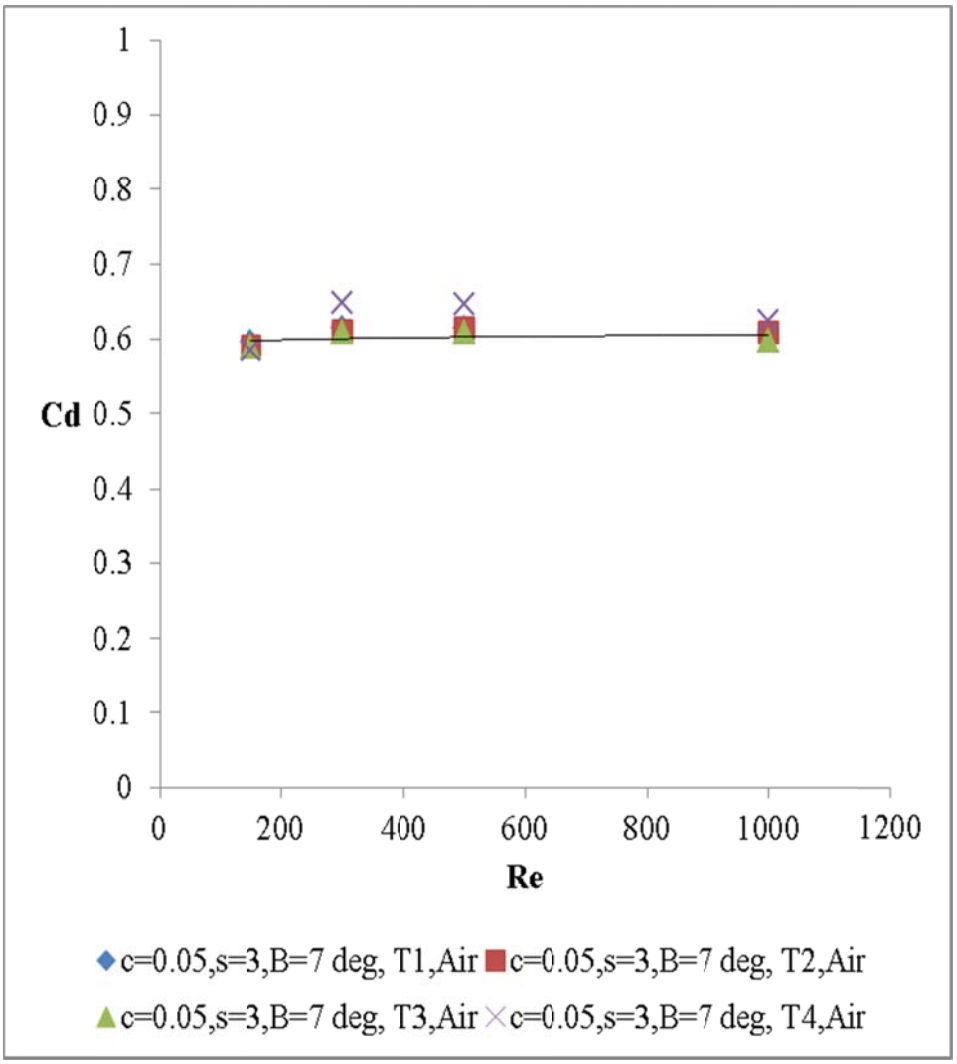

Fig. 4.2. Variation of discharge coefficient with Re at different tooth position (isosceles triangle tooth, compressible flow, case 1).

Fig. 4.3 shows the discharge coefficient variation at four tooth locations for case 1. It can be concluded that for a small clearance the flow parameter, Re effect on the discharge coefficient is small for compressible flow

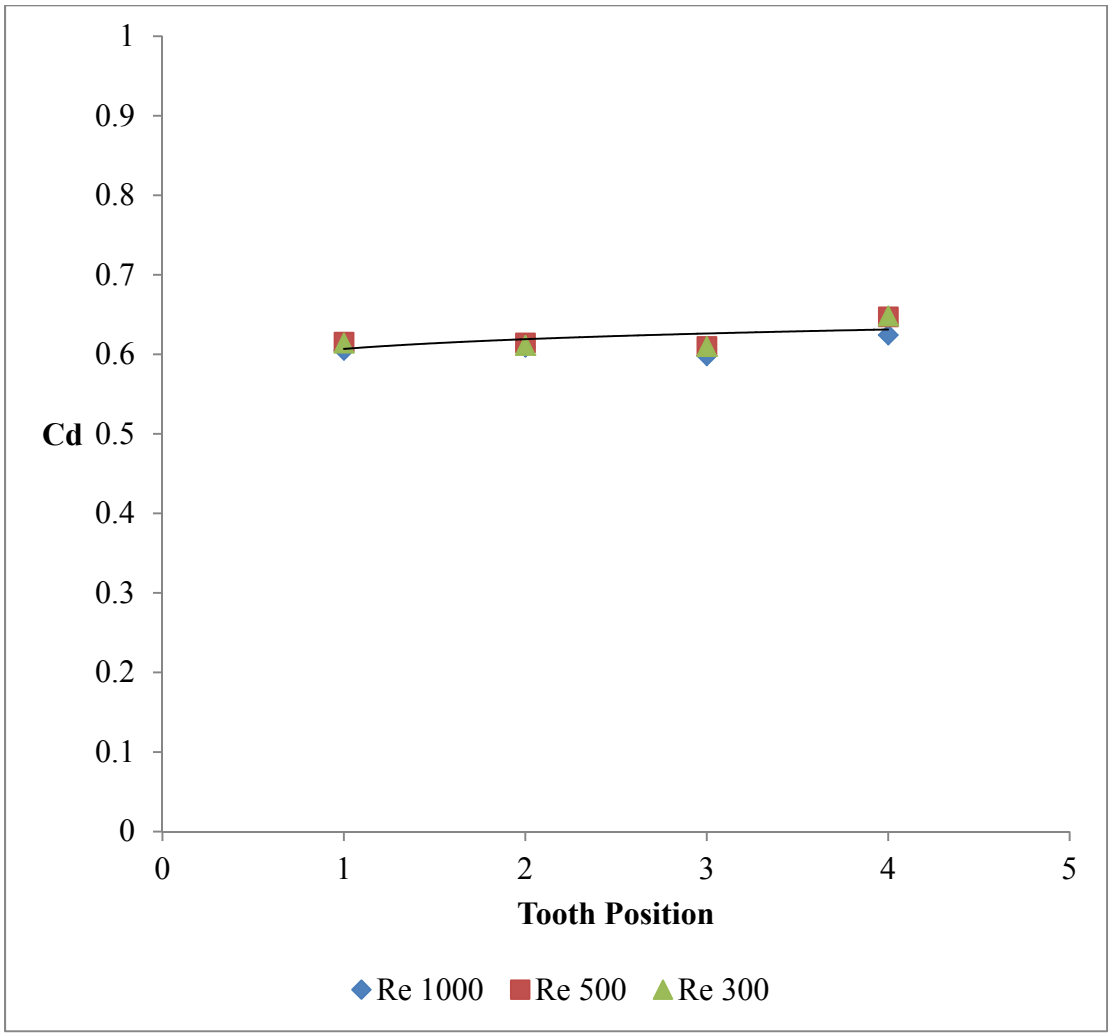

Fig. 4.3. Discharge coefficient at different tooth position for different Re (c=0.05,s=3,compressibile flow, isosceles triangle tooth, case 1).

The discharge coefficient dependence on Reynolds number for a given geometry with four right angle teeth is shown in Fig. 4.4 for compressible flow. The discharge coefficient for this case is not a strong function of the flow parameter, Re.

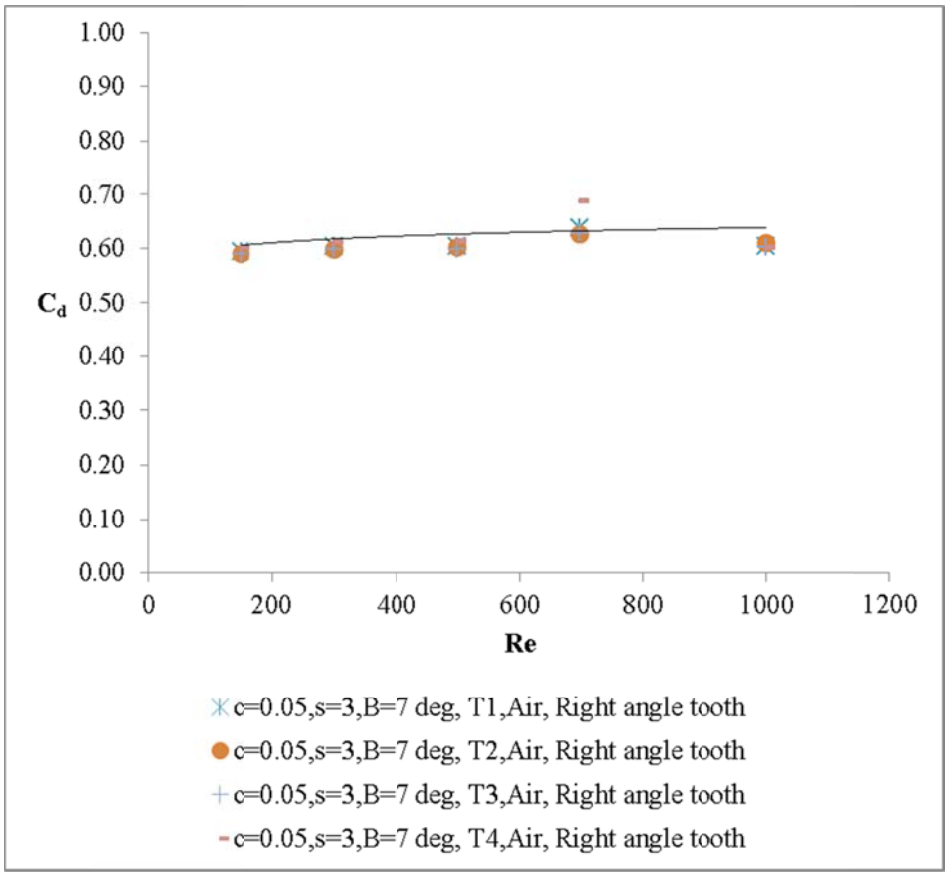

Fig. 4.4. Association of discharge coefficient with Re at different tooth location (compressible flow, case 11).

Fig. 4.5 show the streamlines and axial velocity contour for both isosceles and right angle tooth shape labyrinth seal at Re 150 for both compressible and incompressible flow. Finally results confirm that isosceles shape has more vena contracta effect and this effect reduced the effective clearance in the 1st, 2nd and 3rd tooth. But in the last tooth less vena contracta effect reduces axial velocity as a result less pressure drop was found across the tooth.

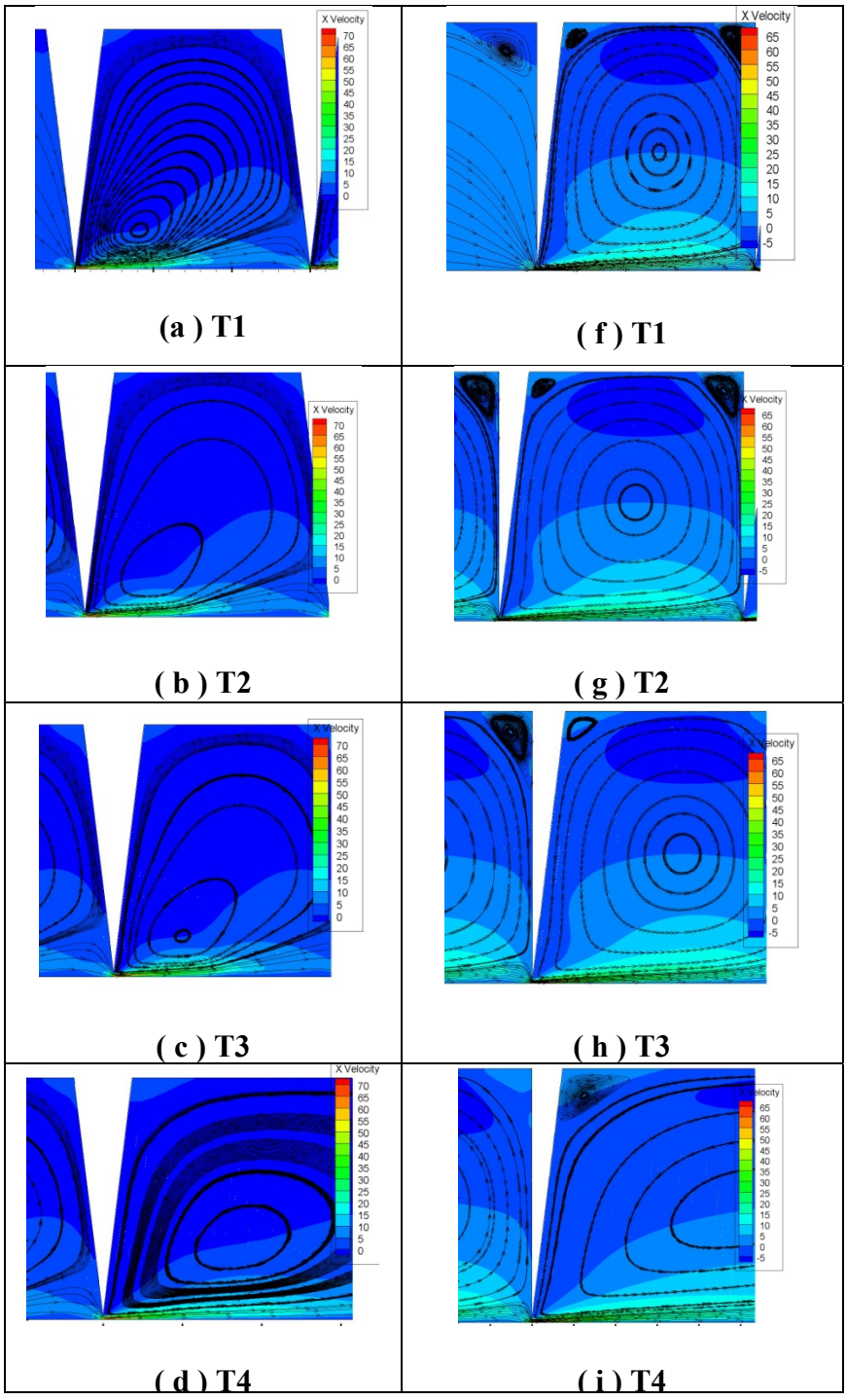

Fig. 4.5. Streamlines and axial velocity distribution in four teeth (for 1st column isosceles, 2nd column right angle, Re 150, compressible flow).

So far, the effect of Reynolds number upon discharge coefficient is discussed for the compressible flow for both isosceles and right angle tooth. In the following context similar effect is discussed for the incompressible flow. This study includes both isosceles and right angle tooth shape to analyze the effect. Fig. 4.6 presents the discharge coefficient values of the four isosceles triangle tooth labyrinth seal for different Reynolds numbers for incompressible flow. It is observed from the Fig. 4.6 that the discharge coefficient for first tooth is independent of flow parameter whereas the rest of the teeth the discharge coefficient is a strong function of flow parameter.

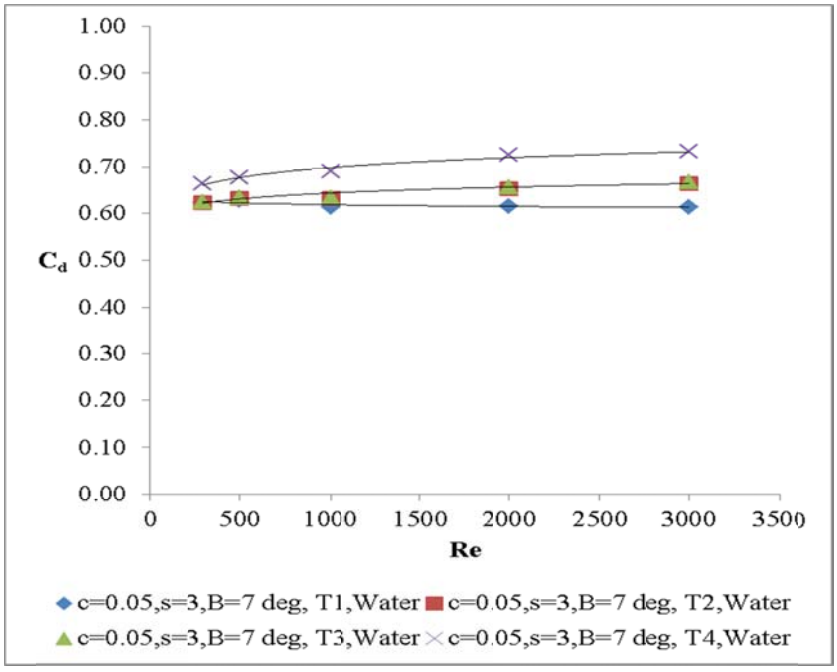

Fig. 4.6. Discharge coefficient of the seal with four teeth (isosceles triangle tooth, incompressible flow, case 1).

It can be concluded from the Fig. 4.6 and Fig. 4.7 that the discharge coefficient of 2^{nd},3^{rd} and 4^{th} tooth location is a strong function of Reynolds number. The main reason is due to the flow deformation taking place inside the seal cavity upstream of the subsequent teeth. The first tooth generates a wall jet along the shaft. This jet concentrates the fluid flow in the clearance area of the downstream tooth resulting in a smaller pressure drop since the flow is already partially contracted to pass under the tooth.

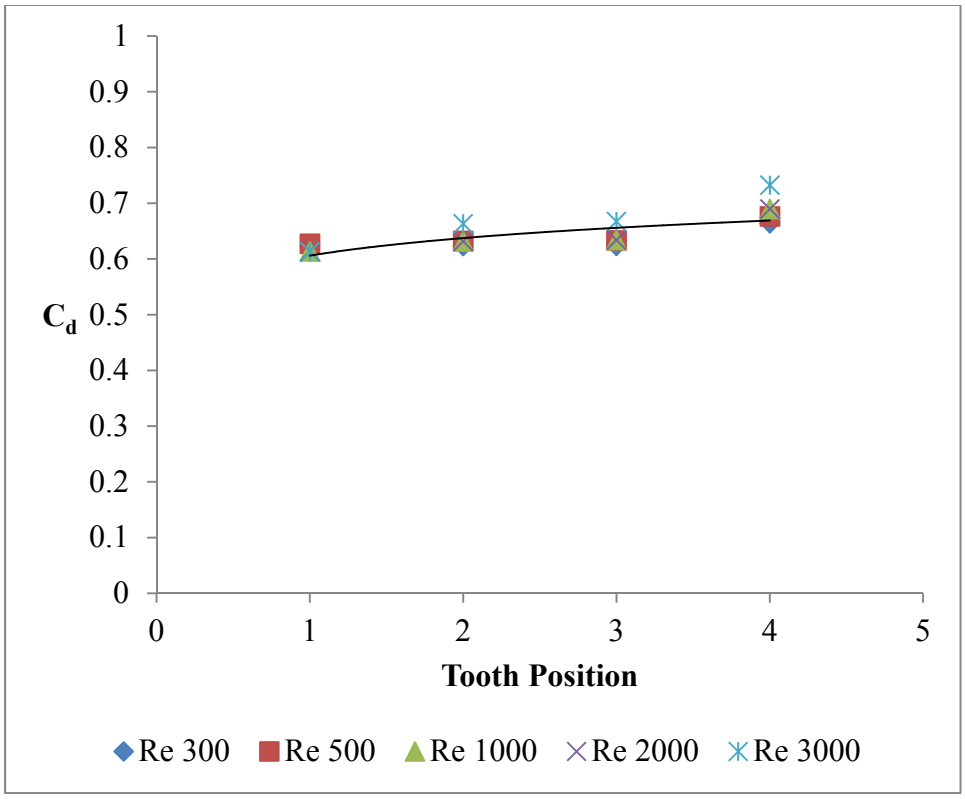

Fig. 4.7. Deviation of Cd values at different tooth position for Re (incompressible flow , isosceles triangle shape, case1).

It has to be noted that for the right angle tooth shape seal, the discharge coefficient value is increasing as Reynolds number increasing. This result is shown in Fig. 4.8. Also less fluctuation of the discharge coefficient is observed in different tooth position compare to isosceles triangle tooth seal.

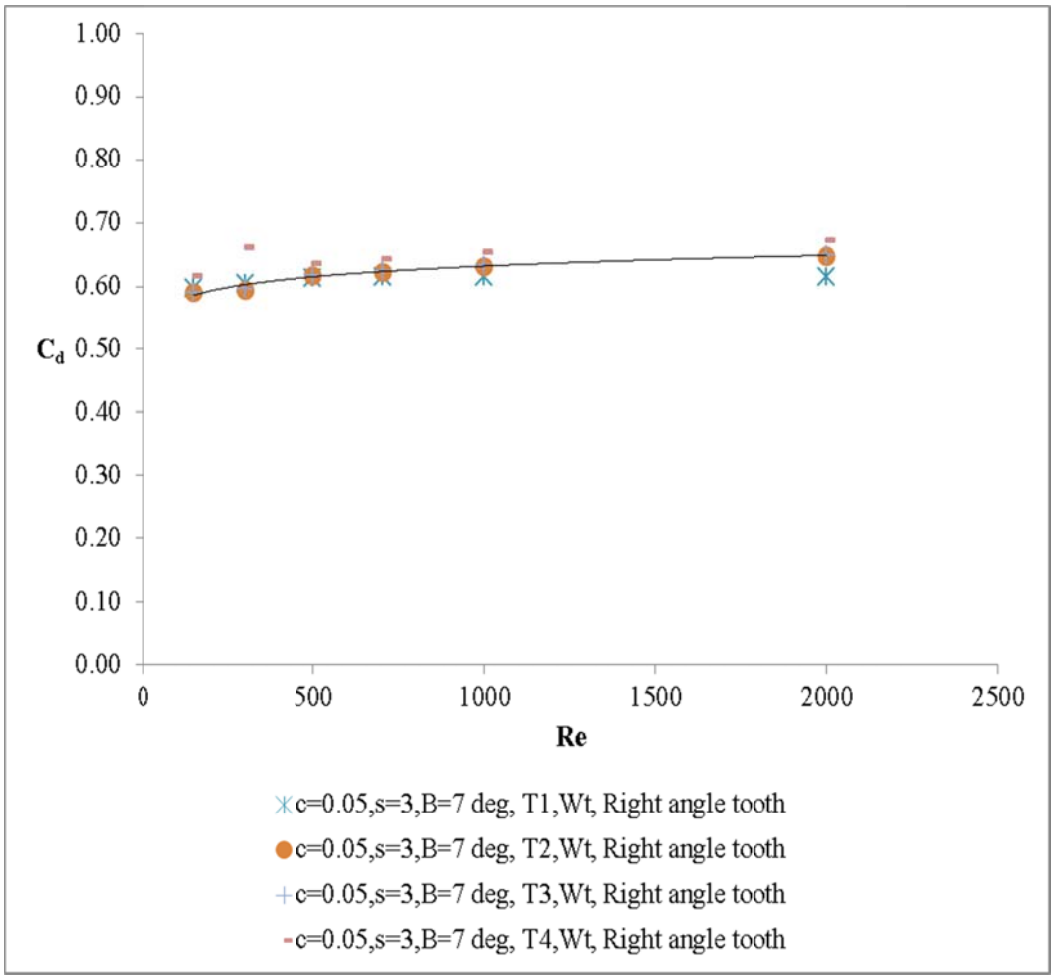

Fig. 4.8. Association of C_d with Re for different tooth position (incompressible flow, case 11).

4.3.2. Effect of Clearances

To analyze the effect of clearances, simulations were performed for different radial clearances such as 0.05, 0.1, 0.15, 0.2 mm. In this study, the effect of clearance on discharge coefficient is investigated for isosceles and right angle tooth shape labyrinth seal for both compressible and incompressible flow.

First in this section, the effect of clearance on discharge coefficient is discussed for compressible flow. Result in Fig. 4.9 shows the association of discharge coefficient with the Reynolds number for different clearances. The results as seen in the Fig. 4.9 shows that the discharge coefficient variation with Re for different clearance is insignificant for 1st tooth whereas it is increasing for 2^{nd}, 3^{rd}, 4^{th} tooth of the seal. C_d increases more rapidly as c increases. Dependence on Re about the same for all c. Therefore should be able to compensate for c as Saikishan's [22] showed c/s important.

For the case of right angle tooth shape, the clearance has similar effect on the discharge coefficient as the isosceles triangle. The results are shown in Fig. 4.10. The investigation on right angle tooth is done for two clearances (c=0.05, 0.1 mm).

It can be concluded from the above figures that at different clearances, the flow parameter has no effect on the discharge coefficient of first tooth of the seal for both isosceles and right angle shape

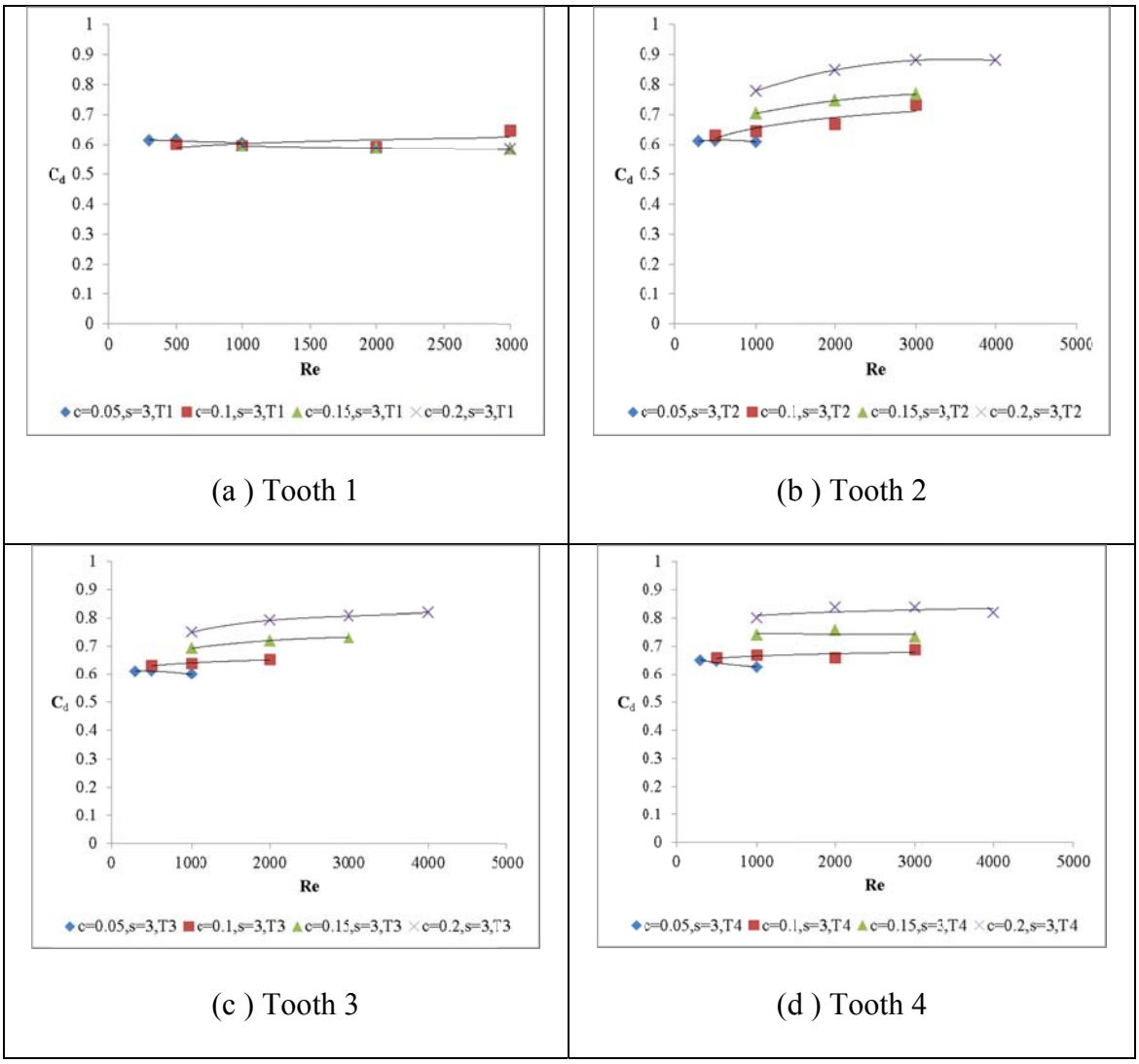

Fig. 4.9. Association of C_d with Re for different clearances at different tooth positions (for compressible flow, isosceles triangle tooth, case 1, case 3, case 4, case 6).

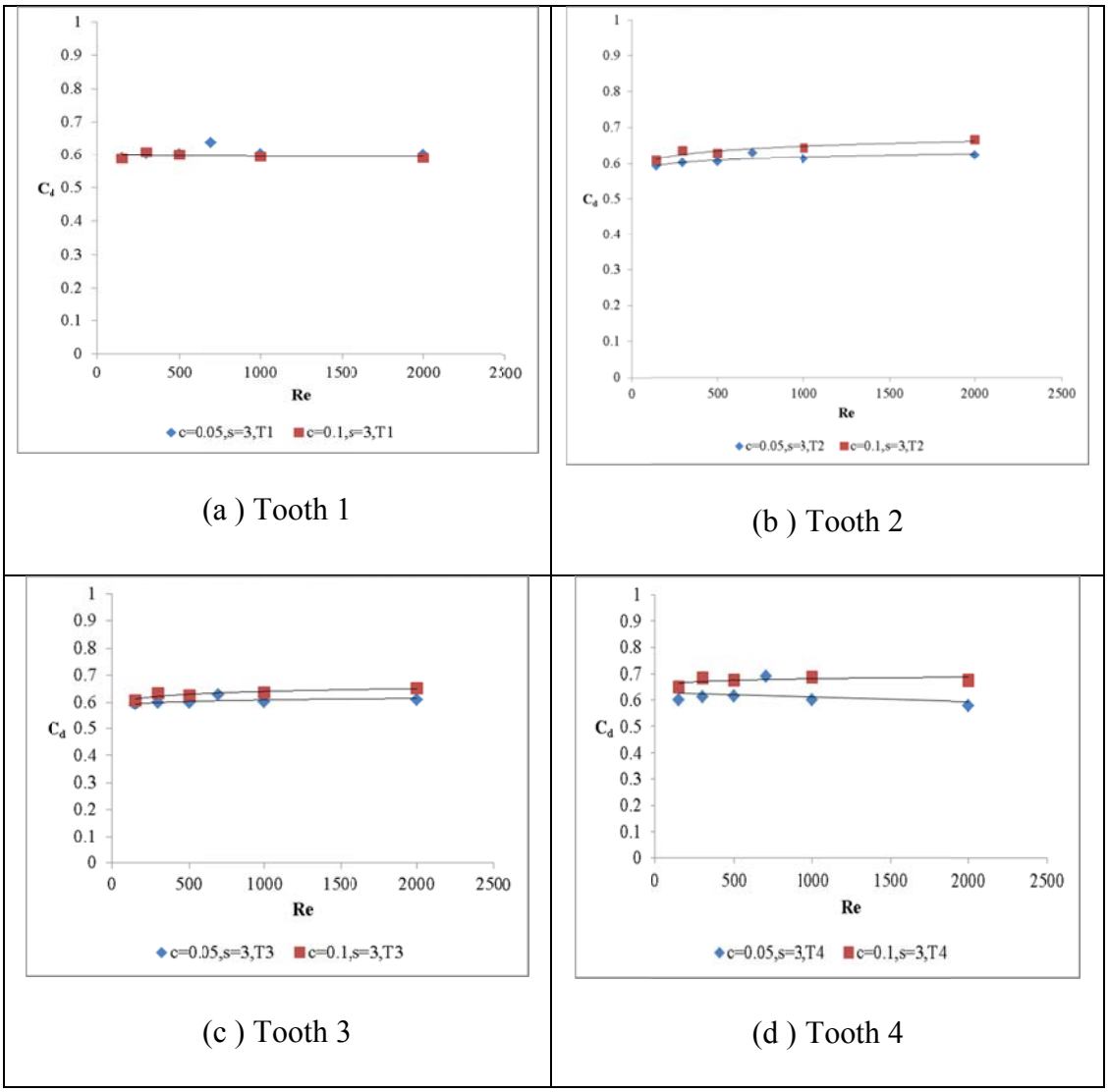

Fig. 4.10. Association of C_d with Re for different clearances at different tooth positions (for compressible flow, right angle tooth, case 1, case 3).

For the incompressible flow and isosceles triangle shape tooth, it is observed from the result of Fig. 4.11 that variation of the discharge coefficient is significant in 2^{nd},3^{rd} and 4^{th} tooth at different clearances with the Reynolds number. For the incompressible flow and isosceles tooth shape the discharge coefficient variation at different clearances with Re is significant for 2^{nd},3^{rd} and 4^{th} tooth. The change of the C_d at 1^{st} tooth position is insignificant with Re at different clearances. The results obtained in Fig. 4.11 shows that at Re 1000 and 2^{nd} tooth, 6% higher change in C_d for air compare to water is found with an increment of clearance from 0.05 t0 0.15 mm. Similar investigation shows that for 3^{rd} tooth, this change was obtained 5%. At higher Reynolds number (Re 2000), the discharge coefficient change with Re is insignificant. So it can be concluded that less compressibility effect was observed when clearance increase up to a certain limit.Similar result is shown in Fig. 4.12 for incompressible flow for right angle tooth shape.

It is found in the result that C_d increases more rapidly as c increases. Dependence on Reynolds number is same for all c. Therefore should be able to compensate for c as Saikishan showed c/s important.

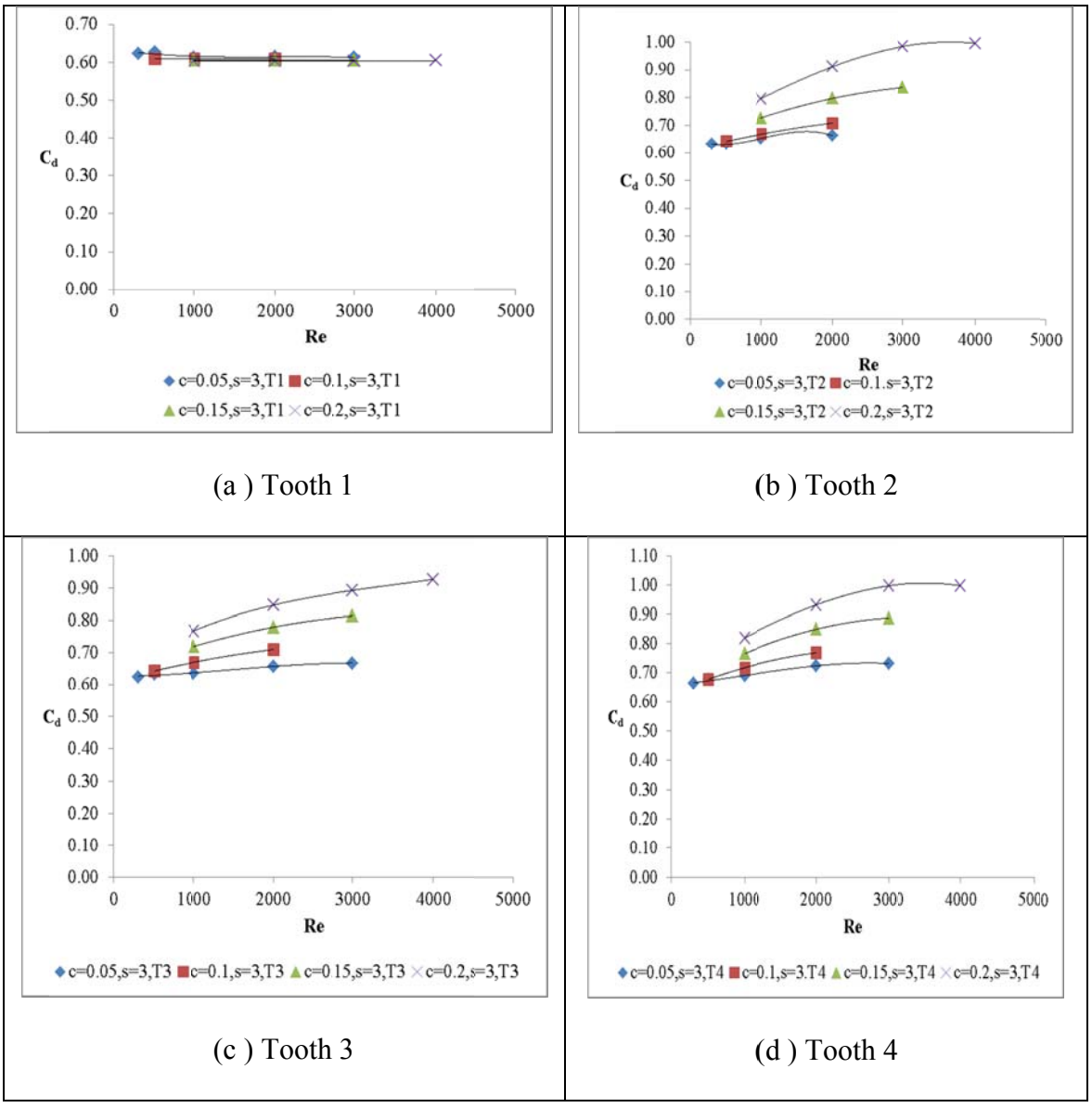

(a) Tooth 1

(b) Tooth 2

(c) Tooth 3

(d) Tooth 4

Fig. 4.11. Association of C_d with Re for different clearances at four teeth positions (for incompressible flow, isosceles triangle tooth, case 1, case 3, case 4, case 6).

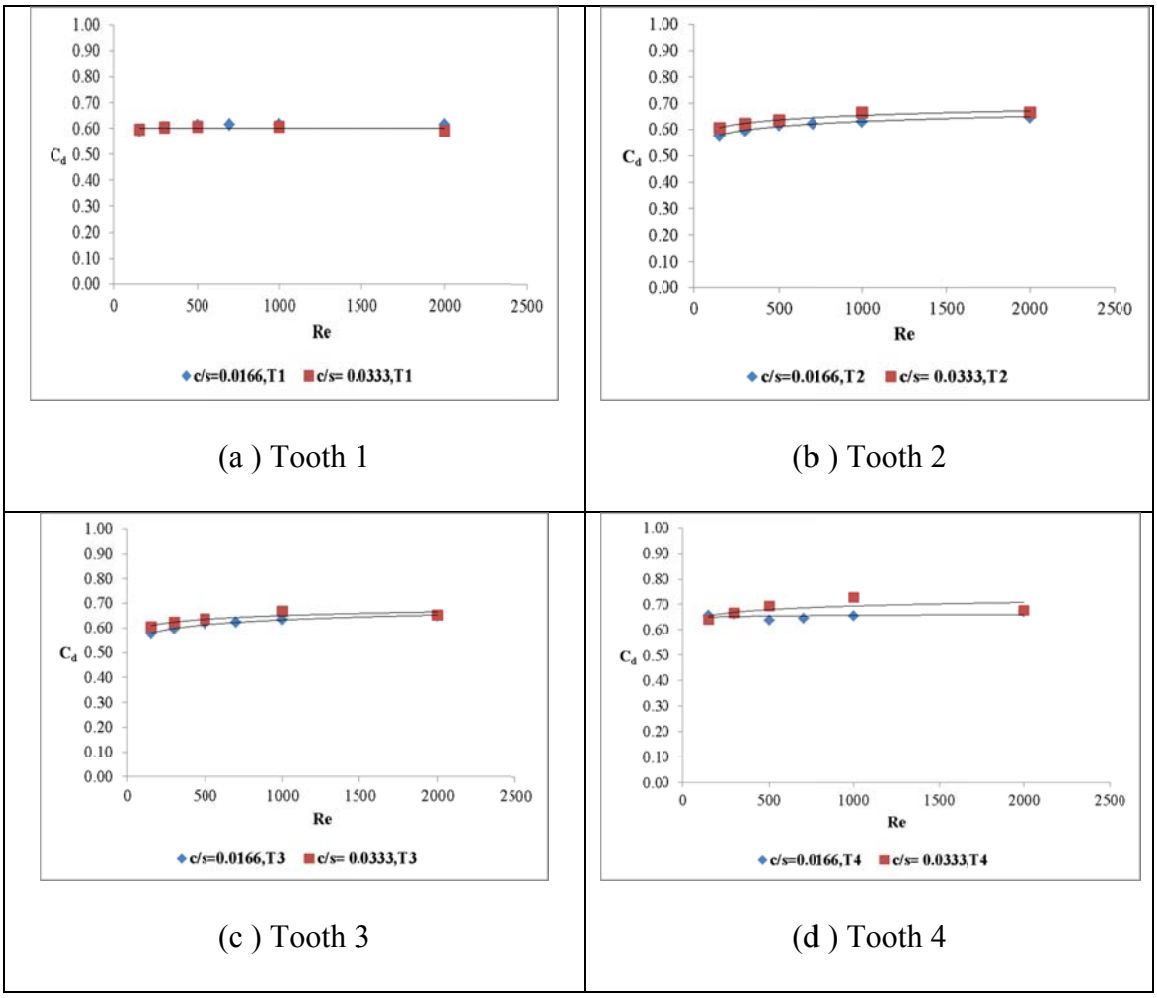

(a) Tooth 1

(b) Tooth 2

(c) Tooth 3

(d) Tooth 4

Fig. 4.12. Association of C_d with Re for different clearances at different teeth locations (for incompressible flow, right angle tooth , case 11, case 12).

From the above discussion it is determined that clearance has a significant effect on the discharge coefficient. The discharge coefficient increases with the increase of the radial clearance for both compressible and incompressible flow. The reason for this increase can be explained in terms of axial velocity and pressure distribution across the teeth of the labyrinth seal. The results are shown in Fig. 4.13 and Fig. 4.14.

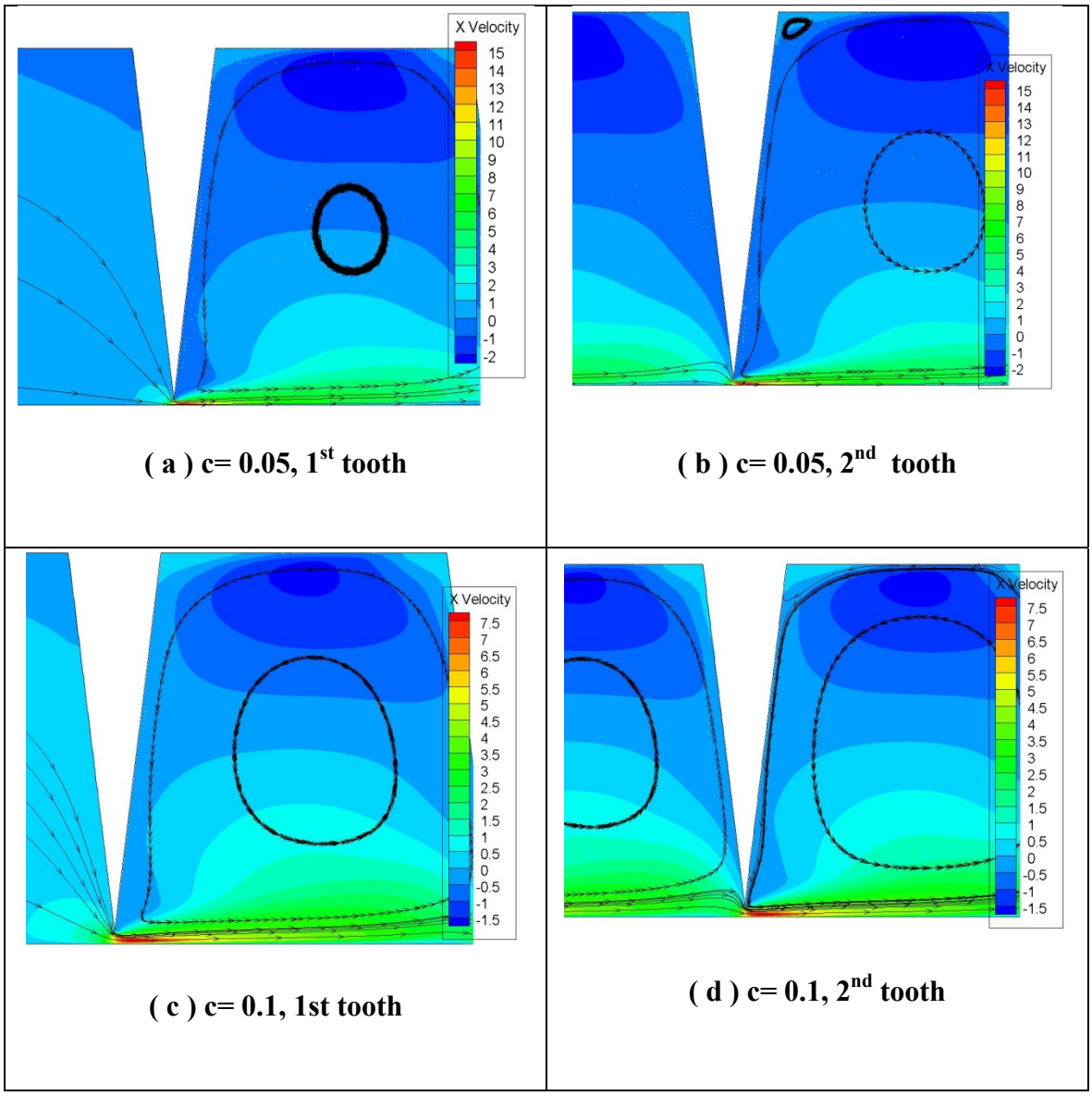

(a) c= 0.05, 1st tooth

(b) c= 0.05, 2nd tooth

(c) c= 0.1, 1st tooth

(d) c= 0.1, 2nd tooth

Fig. 4.13. Axial velocity contour variation with clearance at Re 500 (for incompressible flow, case 1, case 3).

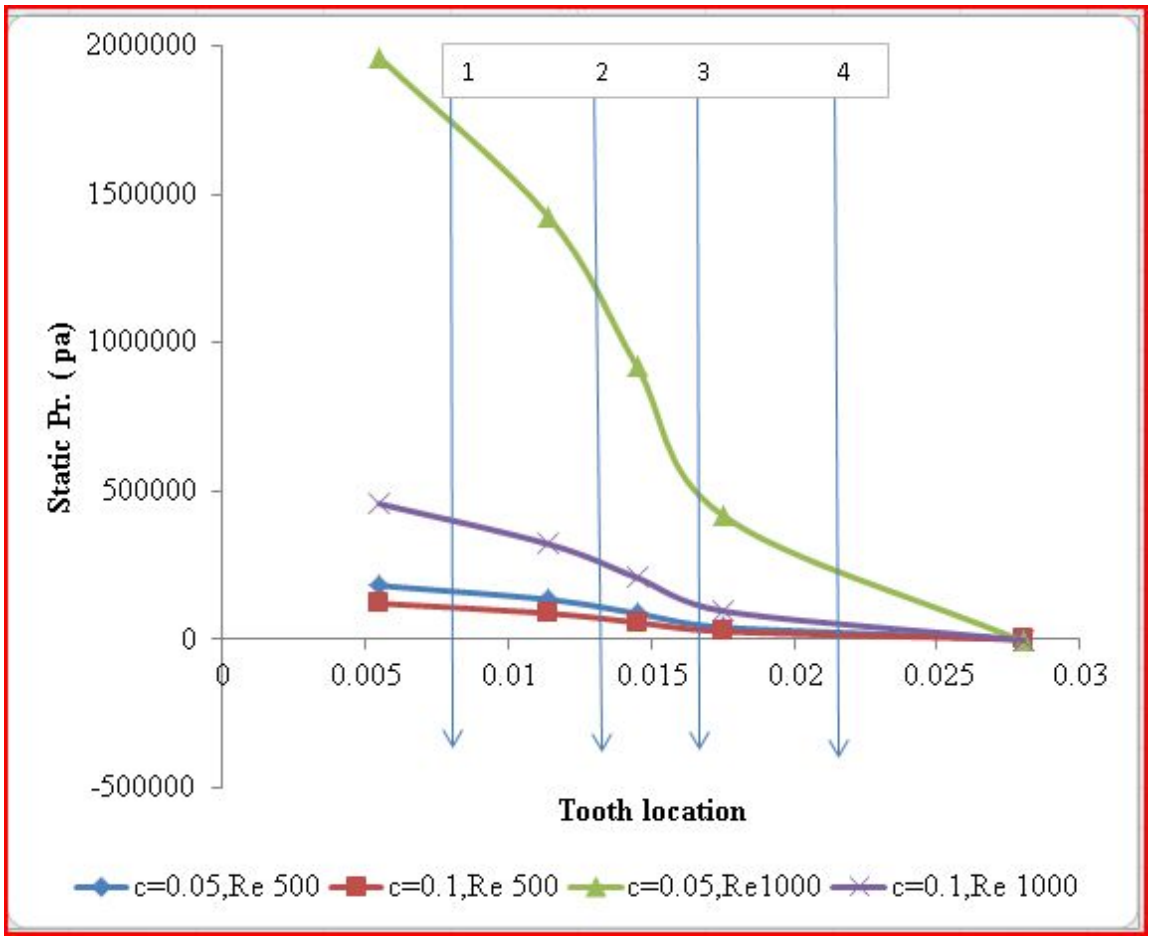

Fig. 4.14. Pressure drop across the tooth of the seal (incompressible flow, case 1, case 3).

For the higher clearance, the axial velocity decreases for a given Reynolds number compared to a small clearance. From the Fig. 4.14, it is observed that at lower clearances the pressure drop is higher for a given Reynolds number. As a result, the discharge coefficient value decreases whereas for the higher clearance, it is vice versa.

4.3.3. Effect of Tooth Width

The effect of tooth width on the discharge coefficient is investigated for w=0.5 and 0 1 mm at zero shaft speed This study is performed for the isosceles and right angle tooth shapes for both compressible and incompressible flow. The results in the Fig. 4.15 show that the discharge coefficient is lower at higher tooth width, w=1 compare to lower tooth width, w=0.05 at given Reynolds number. This graph is plotted for only the 1st tooth of isosceles triangle tooth considering the incompressible flow. Also it is observed that at w =0 , the C_d has insignificant change with Re compare to large tooth width at zero shaft speed. It can be concluded that at zero shaft speed, zero tooth width provides lower discharge coefficient compare flat tooth.

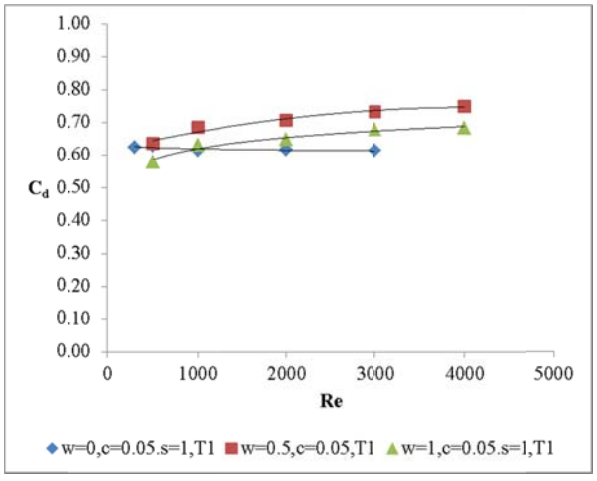

Fig. 4.15. Variation of discharge coefficient with Re for tooth width 0, 0.5 and 1 mm (isosceles triangle tooth, 1st tooth, incompressible flow , case 1, case 8 and case 9).

So far in the previous section all the analysis are executed for zero tooth width. From the Fig. 4.15, it is evident that tooth width has significant effect on discharge coefficient at first tooth. So it is very important to see the effect on tooth on the rest of the seal teeth.

Fig. 4.16 shows the association of the discharge coefficient with Re for different tooth width (w=0, 0.5, 1) at four teeth locations. This graph is plotted includes all four tooth to provide information on the effect of tooth width at each tooth location. The results show w=0 gives the lower C_d value compare to w=0.5, 1 at higher Reynolds number for zero shaft speed. This result is true for all of the isosceles teeth in the labyrinth seal. Fig. 4.16 show, at smaller Reynolds number (Re 500), larger tooth width (w =1) provides low discharge coefficient compare to zero tooth width.

For the right angle tooth shape seal, similar dependence of C_d is found at the same geometric and flow parameters for the incompressible flow. Fig. 4.17 shows the effect of tooth width on discharge coefficient for all four teeth of the seal. For the right angle tooth, the tooth width has significant effect on discharge coefficient.

Finally it can be concluded from the above investigation that for a given Reynolds number, the zero tooth width produces a lower discharge coefficient for both isosceles and right angle tooth shape seal for the incompressible flow without shaft rotation.

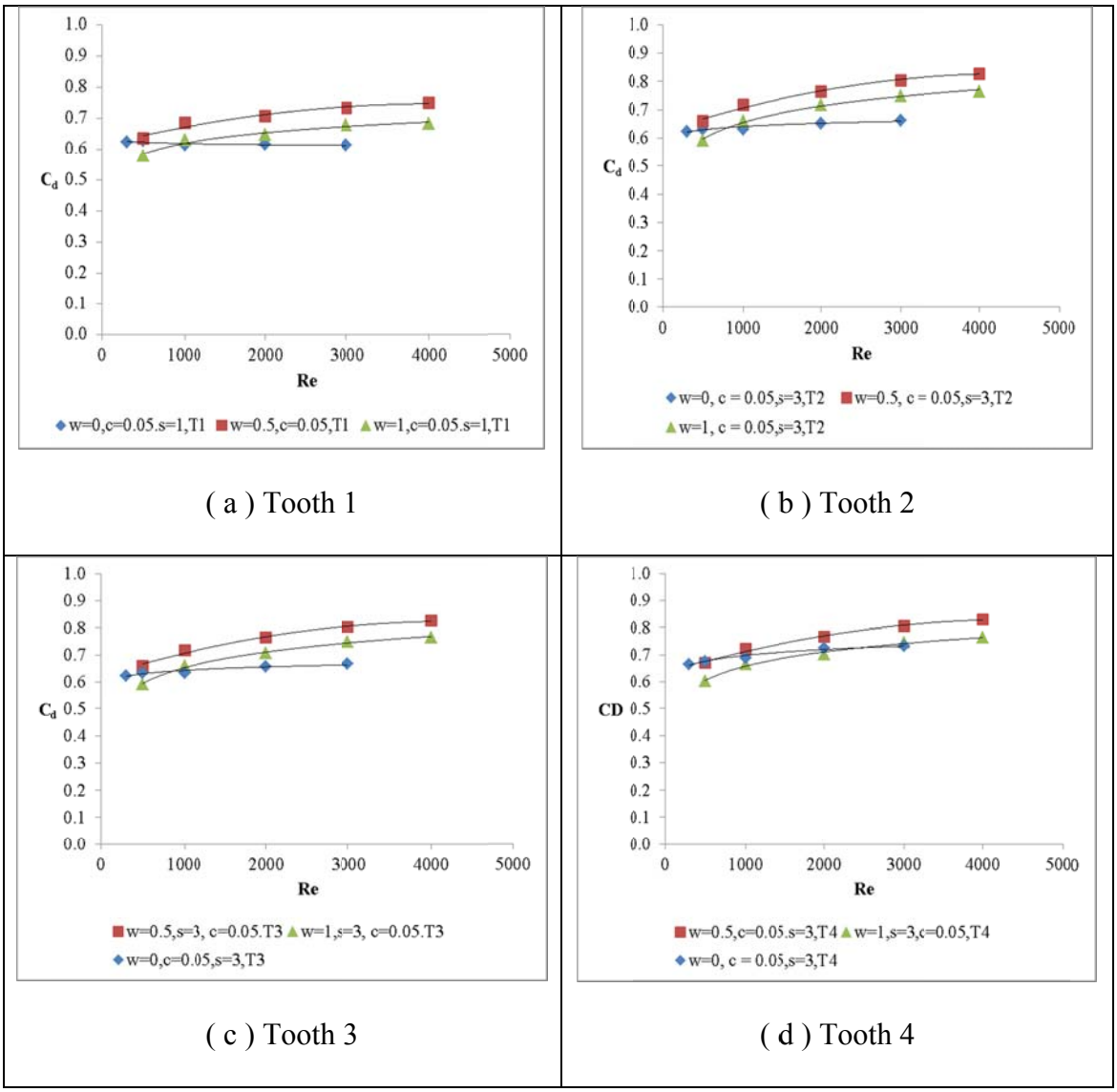

Fig. 4.16. Comparison of discharge coefficient variation with Re at different tooth location for w=0, 1 and 0.5 (incompressible flow, isosceles triangle tooth , case 1, case 8, case 9).

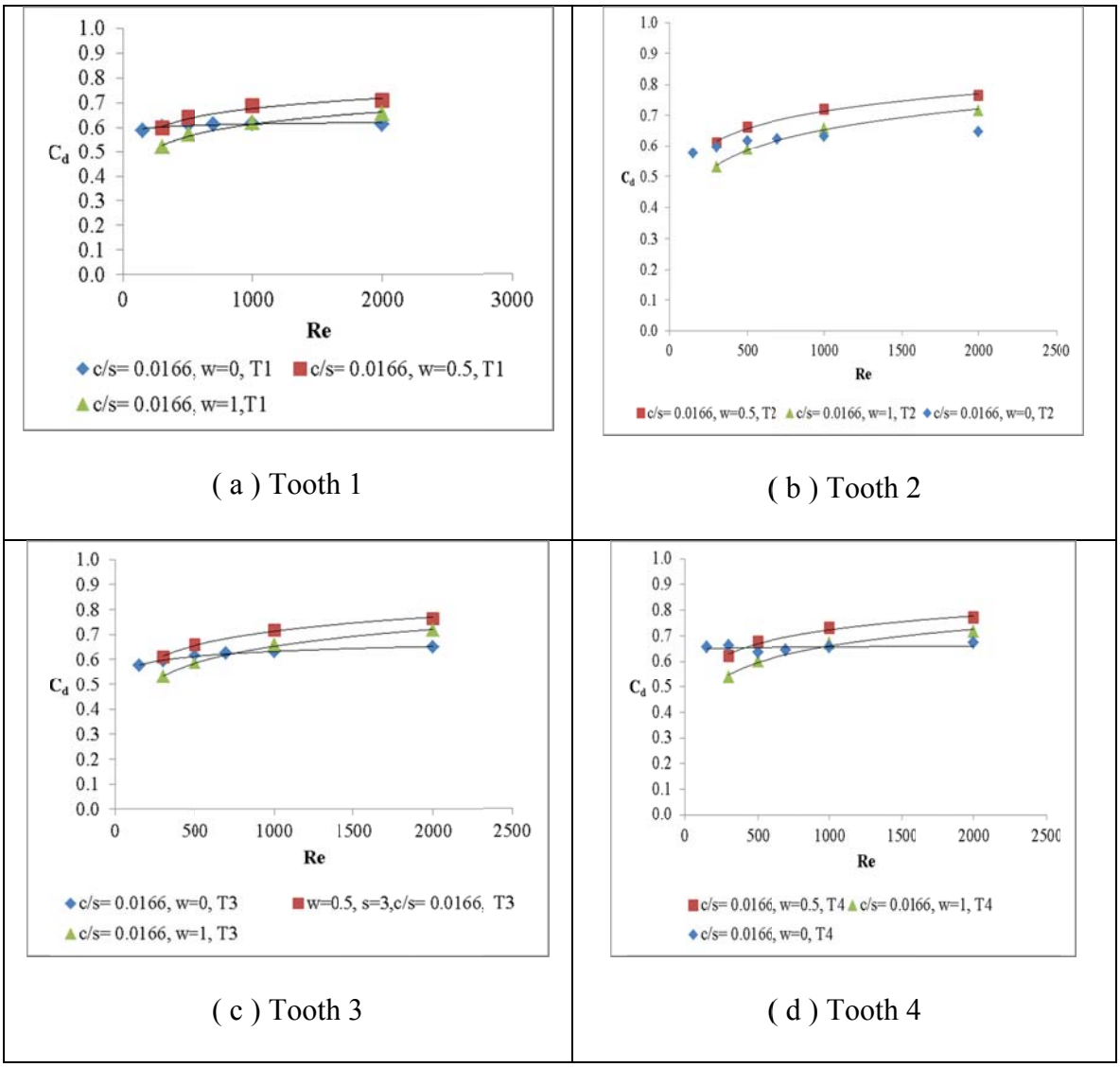

Fig. 4.17. Comparison of discharge coefficient variation with Re at different tooth locations for w=0, 0.5 & 1 mm (incompressible flow, right angle tooth, case 11, case 13, case 16).

For the compressible flow, a similar investigation is performed with the results presented in Fig. 4.18 and Fig. 4.19. It is found that for tooth shapes the higher tooth width produces a lower discharge coefficient at a given Reynolds number.

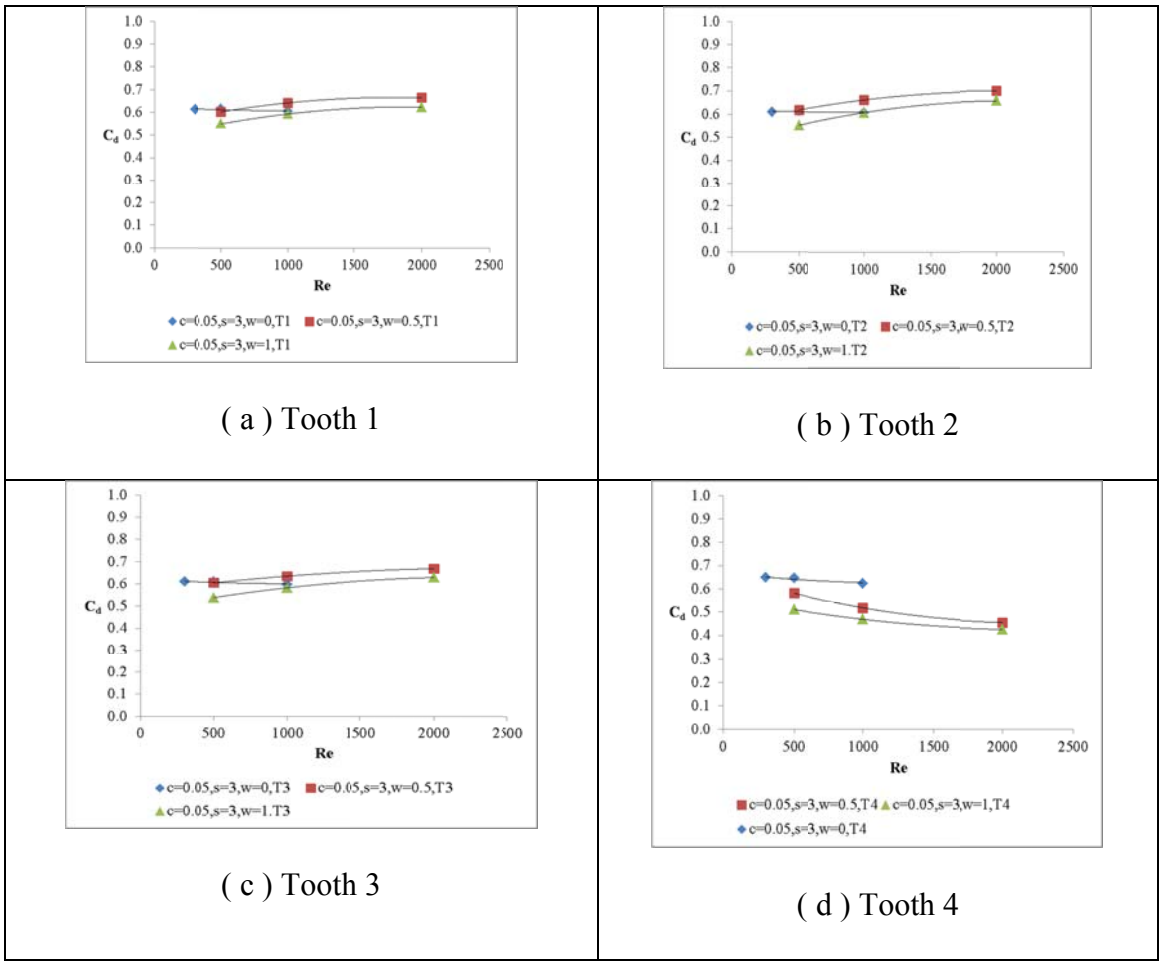

Fig. 4.18. Comparison of discharge coefficient variation with Re at different tooth location for w= 0, 1 & 0.5 mm (for compressible flow, isosceles triangle tooth, case 1, case 8, case 9).

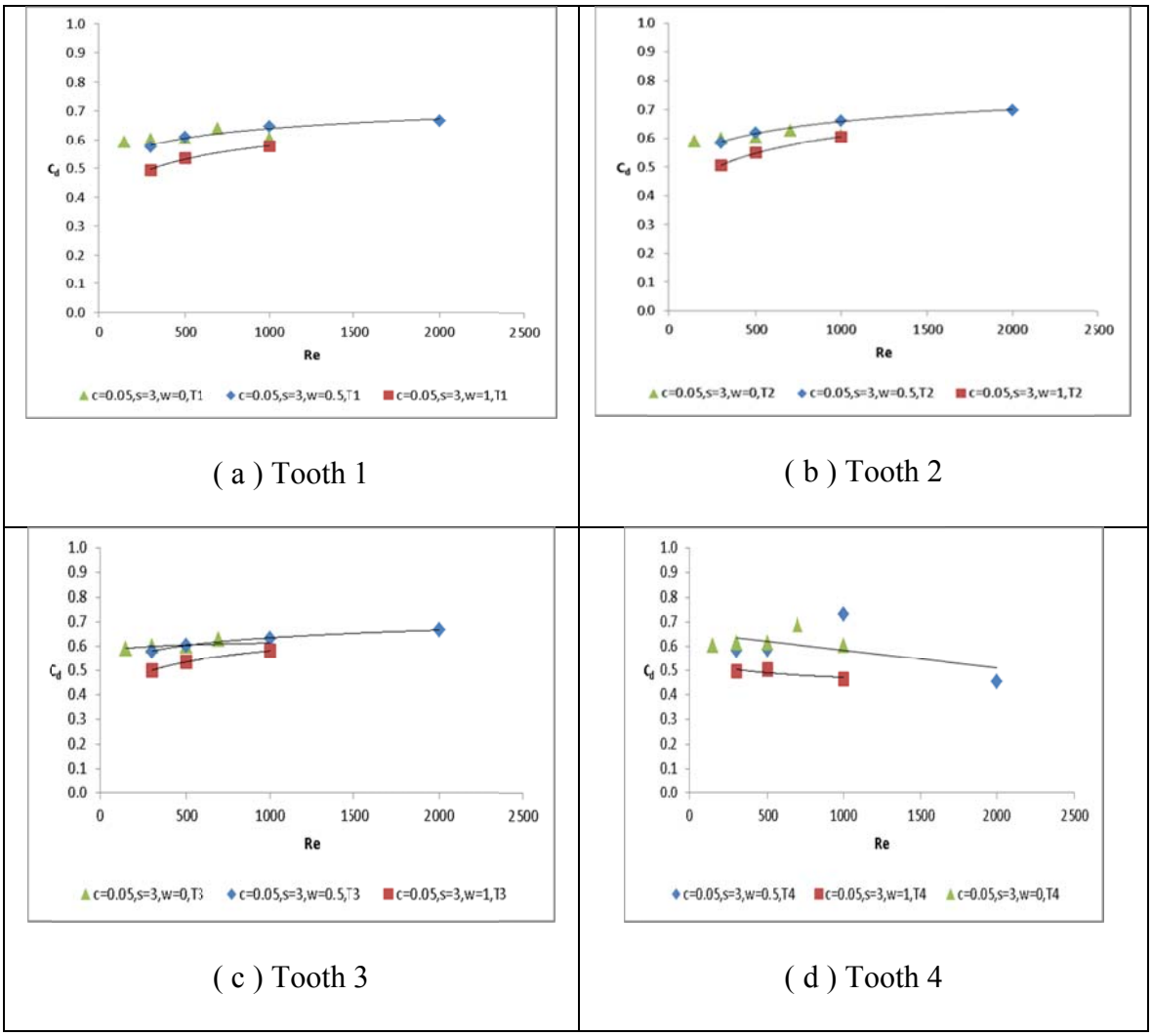

Fig. 4.19. Comparison of discharge coefficient variation with Re at different tooth location for w=1 & 0.5 (for compressible flow, right angle tooth, case 11, case 13, case 16).

Pressure distribution across the tooth for the different tooth widths shows in Fig. 4.20. In a laminar flow through a channel, the pressure drop increases for the higher channel length (tooth width). This result is shown in Fig. 4.20.

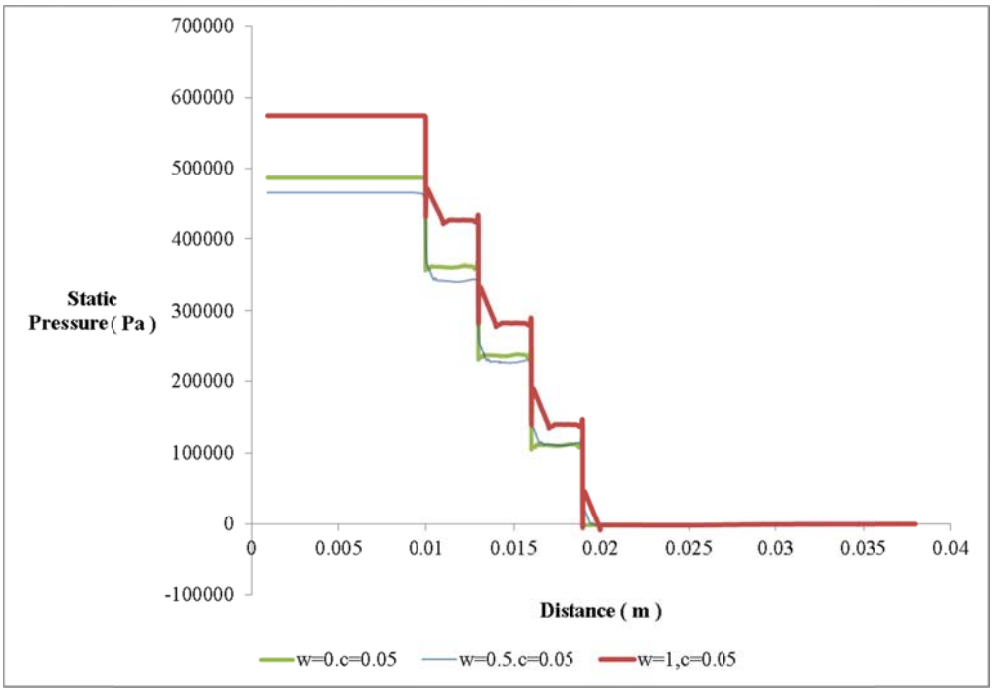

Fig. 4.20. Pressure drop along the length of seals with w = 0,0.5 & 1 mm, (for water, case 1, case 8, case 9 , Re 500).

4.3.4. Effect of Pitch

In order to examine the pitch effect simulations are performed for 3 different pitches, s =3, 4 and 5 mm. The results as seen in Fig. 4.21 show that at low Reynolds number the pitch has very less effect on the discharge coefficient, C_d. At the higher Reynolds number, Re = 2000, a 66% increase of the pitch caused a 6% reduction of the discharge coefficient. So it is evident from this figure that pitch has less effect on discharge coefficient than clearance. This conclusion is made for isosceles tooth shape and for

incompressible flow. Fig. 4.22 shows the variation of discharge coefficient with Re for different pitch. values. To understand the effect of pitch on the discharge coefficient it is very important to understand the flow pattern inside the each cavity and fluid flow under the tooth.

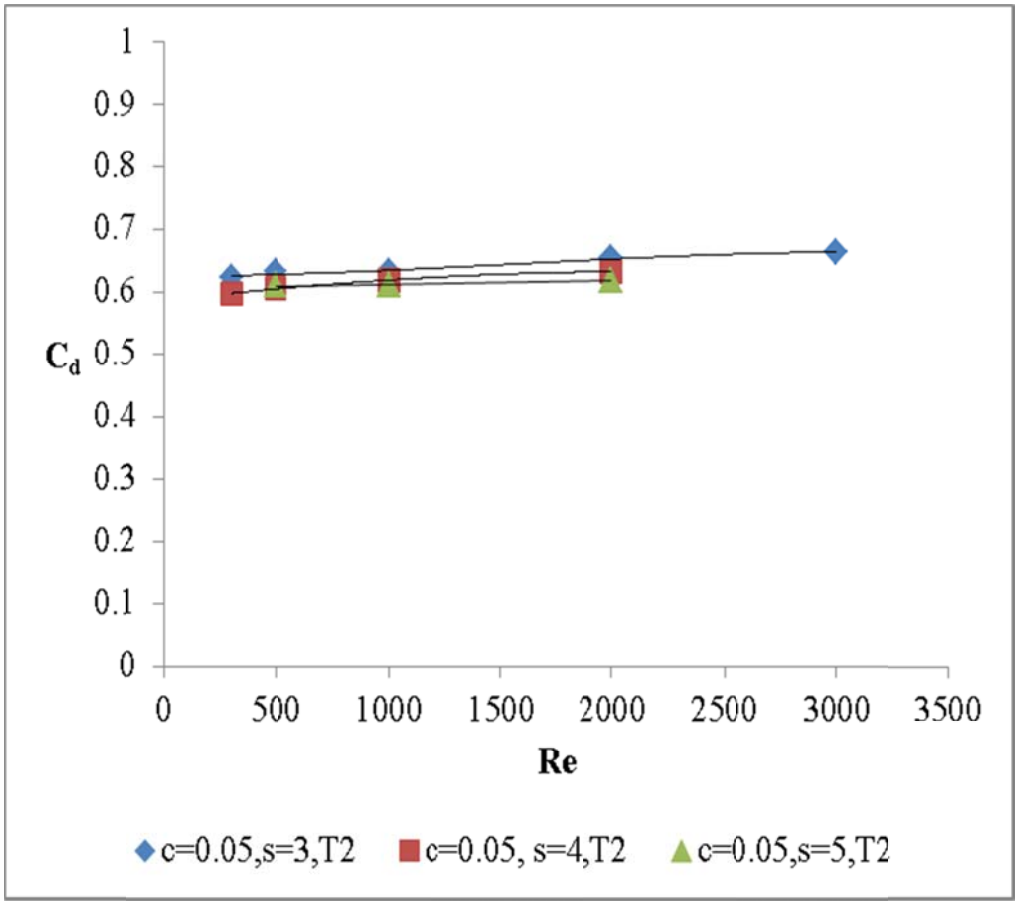

Fig. 4.21. Pitch effect on the C_d of second tooth (for incompressible flow, isosceles triangle tooth shape , case 1, case 7, and case 10).

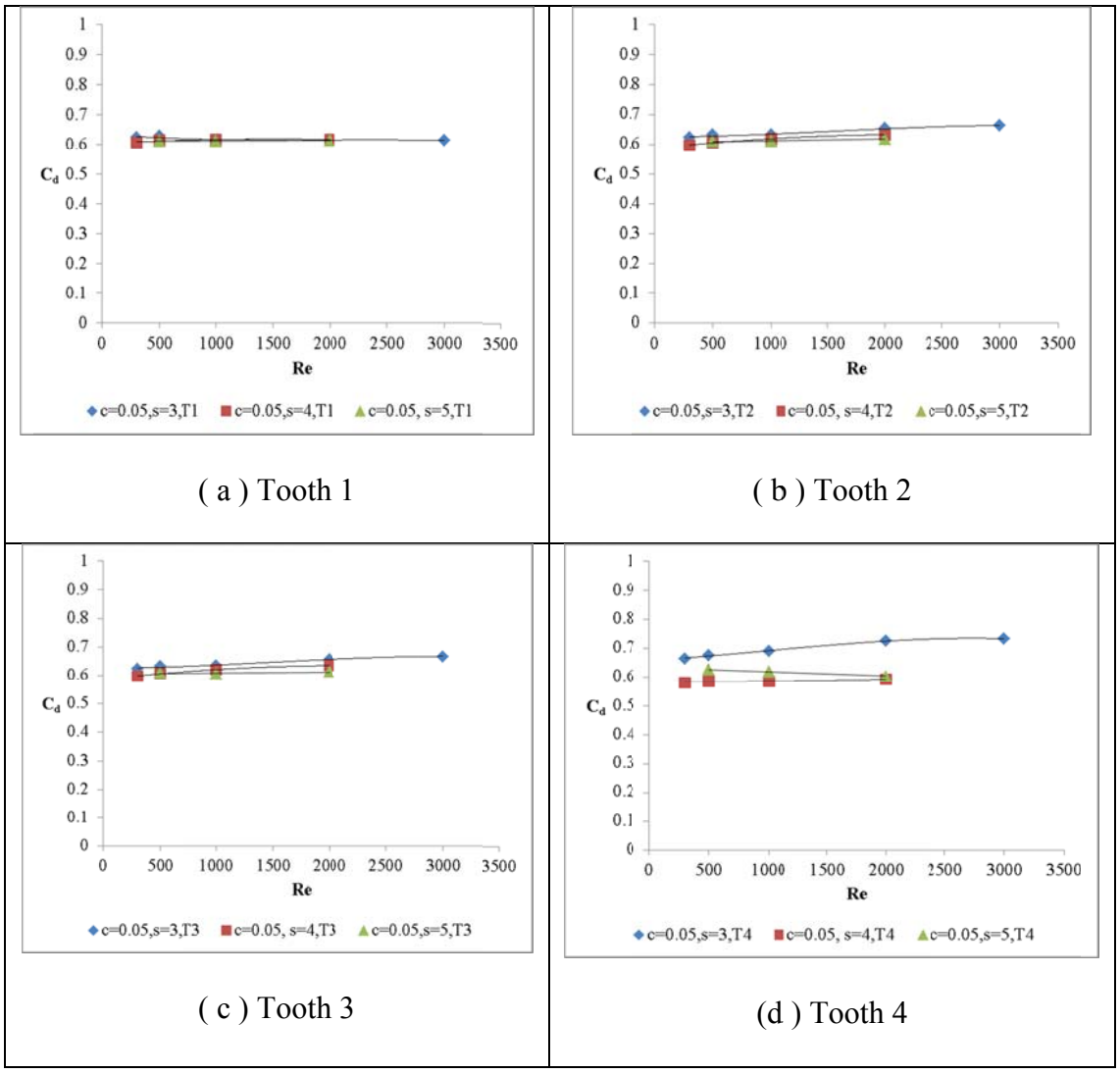

Fig. 4.22. Comparison of discharge coefficient variation with Re at different tooth location for s=3, 4, 5 mm (incompressible flow, isosceles triangle tooth, case 1, case 7 and case 10).

Fig. 4.23 shows the flow pattern in each of the cavities for the isosceles tooth shape seal for the pitch values, s=3 and 5 at Reynolds number 2000. Similar flow patterns are observed in each cavity for different pitch values.

In the section 3.3.4. , it is shown that higher pitch values produce lower carryover coefficients for a given Reynolds number. Higher pitch means a larger distance between two adjacent teeth and more cavity space. This increase in distance results in higher viscous resistance to the flow. Further, as the fluid flow moves under the tooth the pressure head is converted to kinetic energy head. This causes additional pressure loss downstream of the tooth. This is the physics which is causing reduction in the discharge coefficient for higher pitch values at given Reynolds number.

Fig. 4.24 shows the pressure losses between the adjacent teeth of the labyrinth seal for different pitch values s=3,4 and 5 mm. It is evident from the graph that at the higher pitch value, the pressure loss across each tooth is higher which results in lower discharge coefficients, C_d.

From the above discussion it can be concluded that higher pitch value produces lower discharge coefficient for incompressible flow at a given Reynolds number.

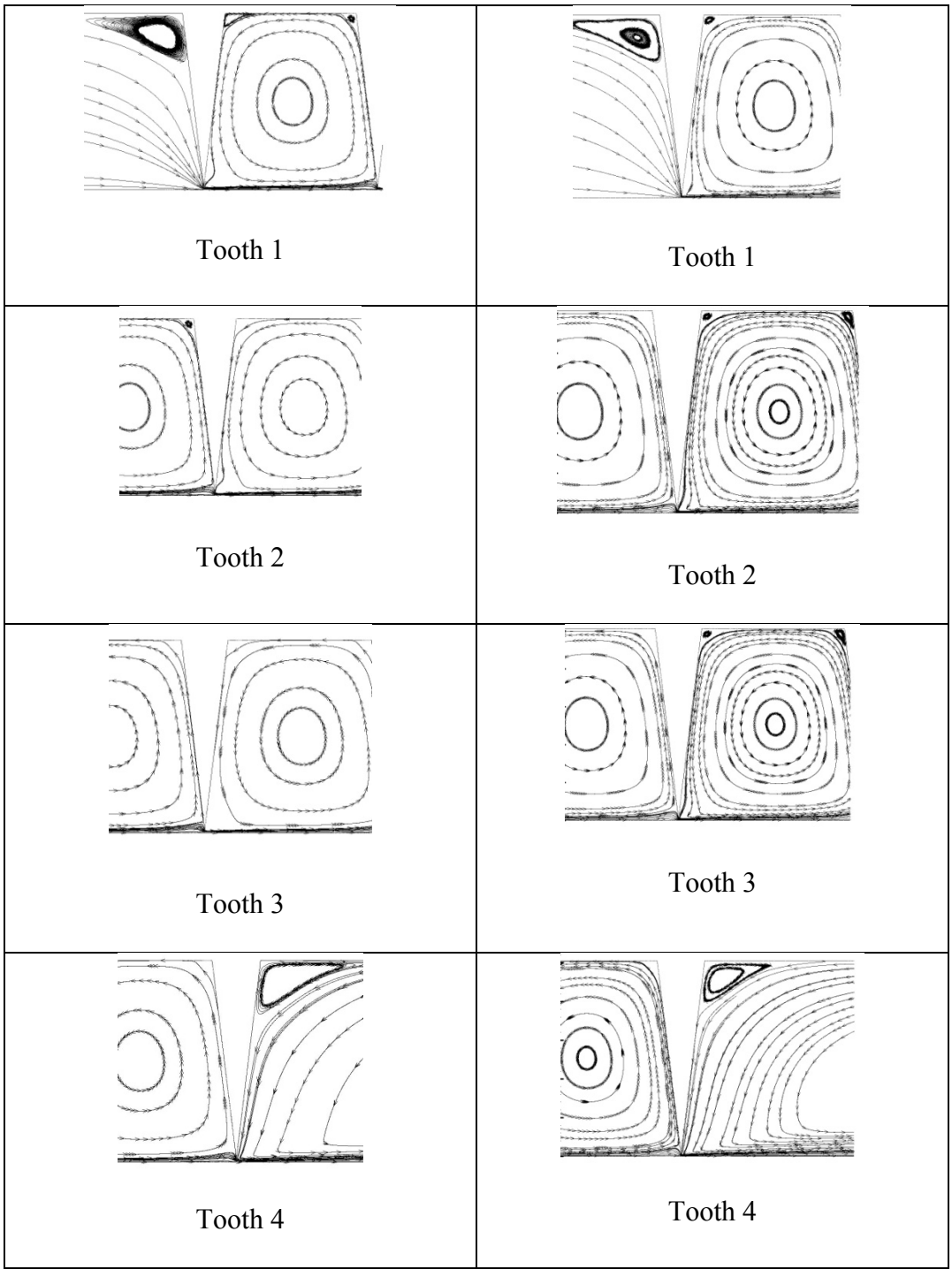

Fig. 4.23. Flow pattern in four teeth for different pitch values (1st column s=3, 2nd column s=5 , incompressible flow , Re 2000, c=0.05, B=7°).

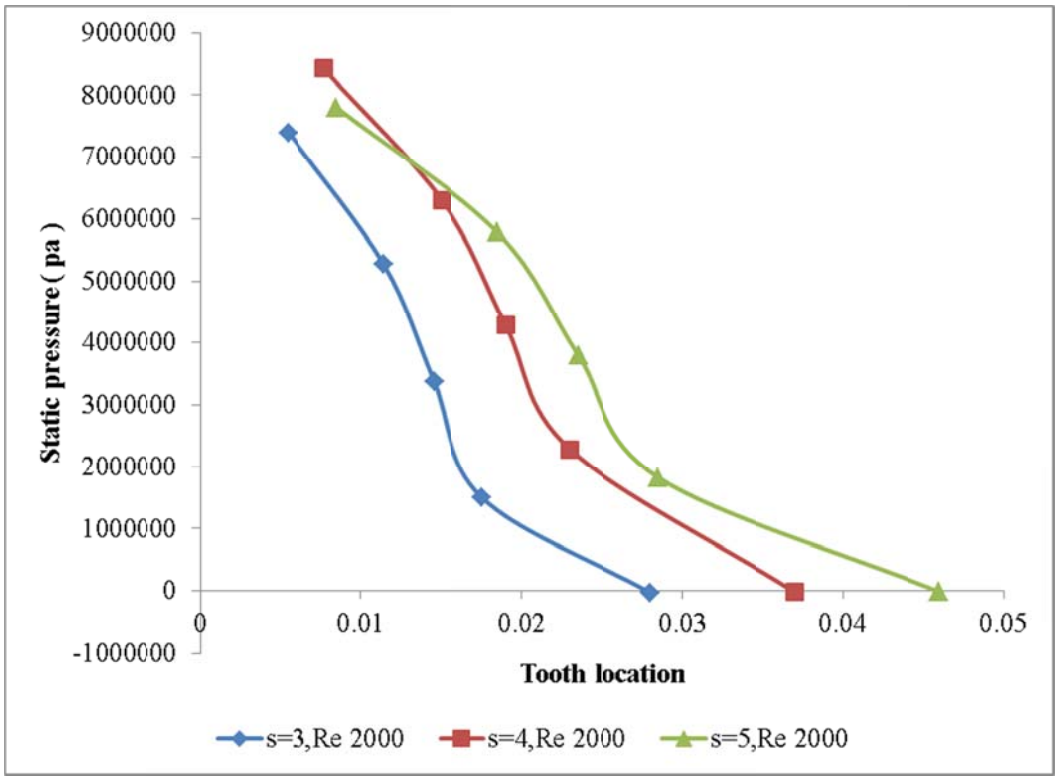

Fig. 4.24. Pressure drop across the tooth of the seal for different pitch values. (incompressible flow, case 1, case 4, case 10).

Fig. 4.25 shows the variation of the discharge coefficient with Re for two different pitches, s =3 and 4.at four tooth locations in the seal This plot is generated for the right angle tooth seal and for incompressible flow. The results in the plot show that at Re 2000, a 3.3% reduction in discharge coefficient is found for a 33% increase of the seal pitch. It can be concluded that the pitch has less (for 33% Δs, ΔC_d = 3%) effect on the discharge coefficient for a given Reynolds number.

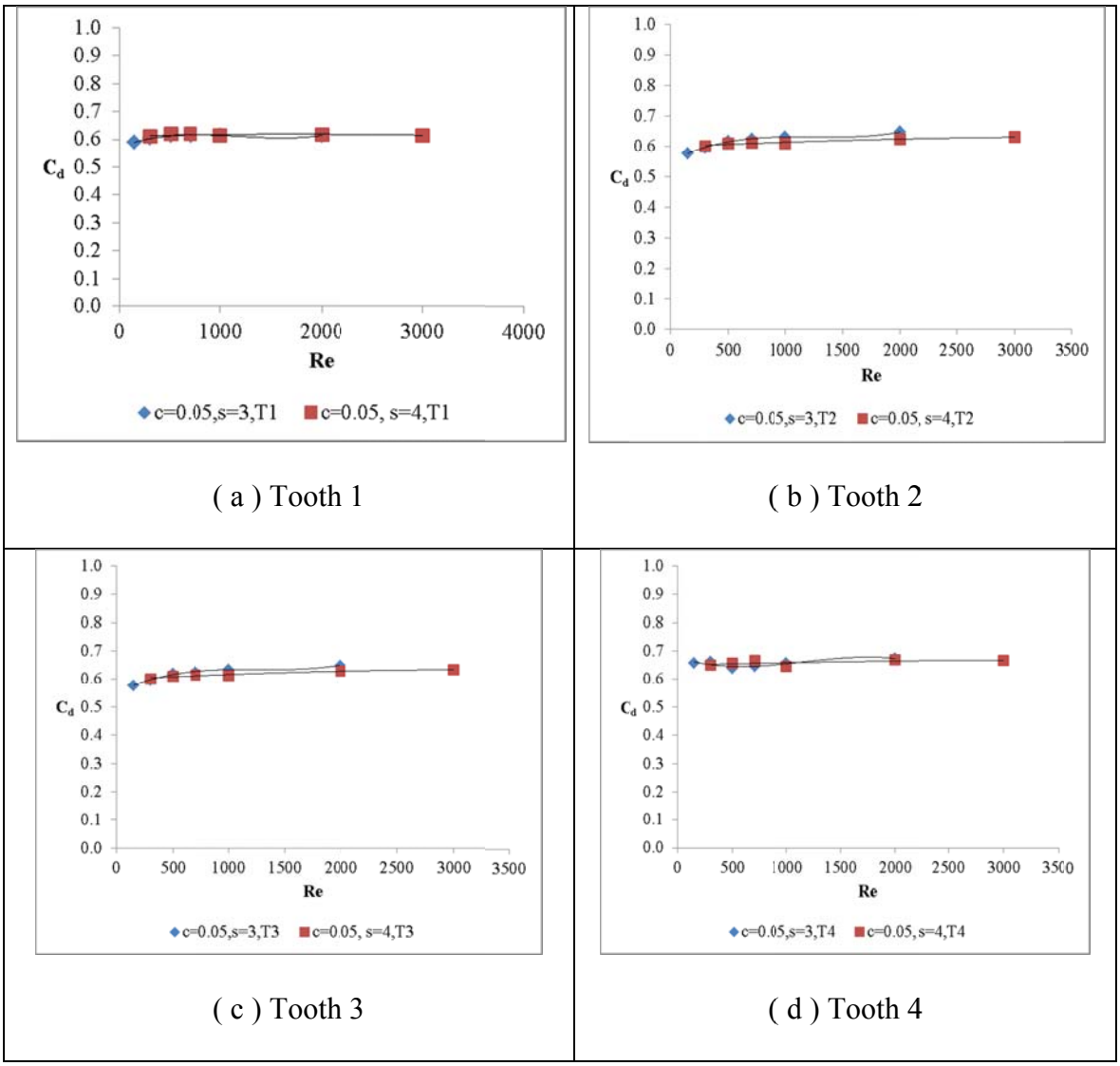

Fig. 4.25. Comparison of discharge coefficient variation with Re at different tooth location for s=3 and 4 mm (incompressible flow, right angle tooth , case 11 and 15).

For compressible flow , the effect of pitch on the C_d for the isosceles tooth shape seal is insignificant. This result is shown in Fig. 4.26.

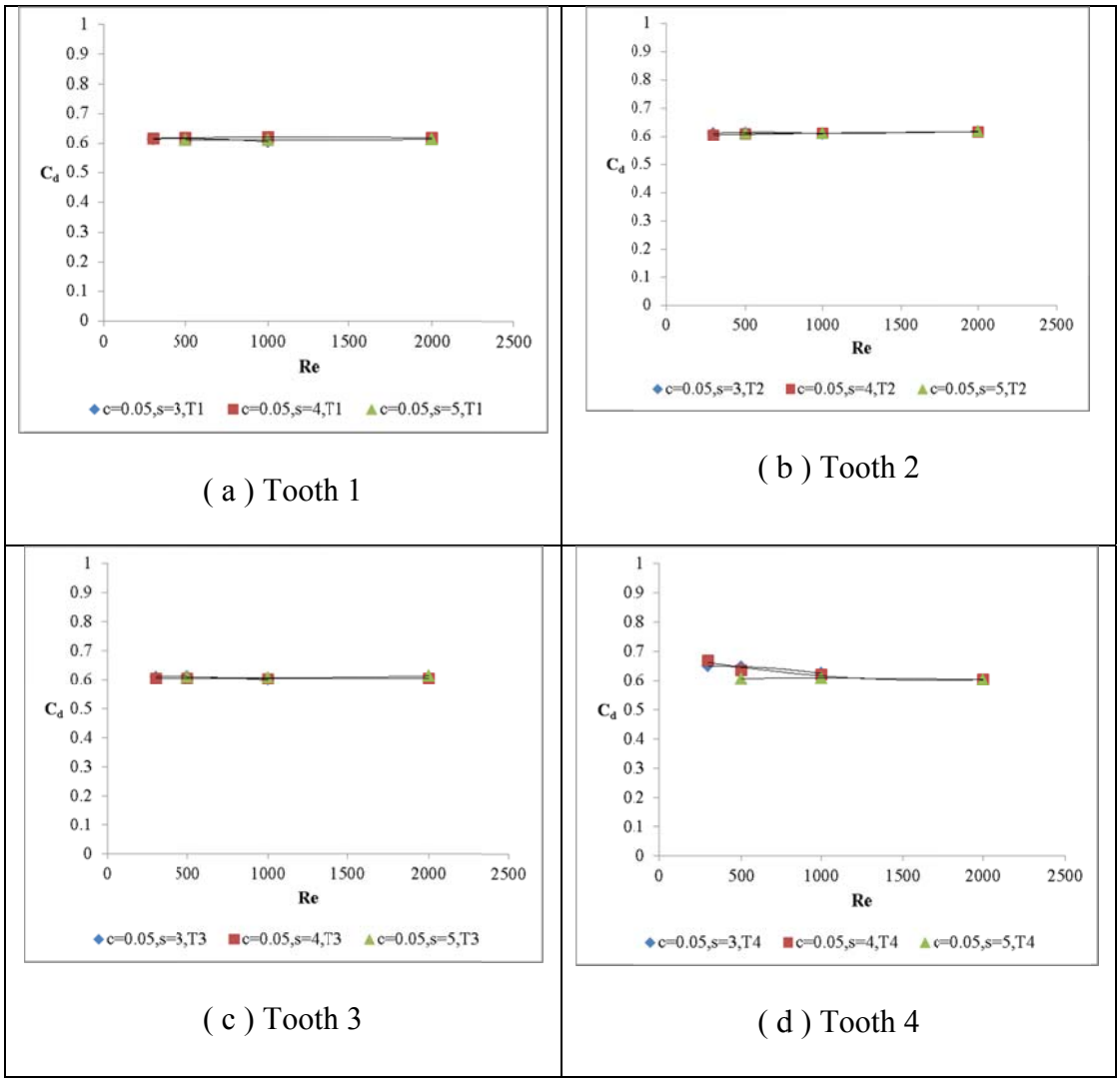

Fig. 4.26. Variation of Discharge coefficient at different tooth with Re for s=3, 4 and 5 (for compressible flow, isosceles tooth, case 1, case 7, case 10).

4.3.5. Effect of Tooth Angle

In the previous discussion in the section 3.3.5. , it is observed that higher upstream angle gives lower carryover coefficient for the isosceles triangle tooth shape for both compressible and incompressible flow. But it has no effect on the right angle shape tooth

due to unchanged upstream approach angle. In the case of the discharge coefficient, the upstream angle has marginal effect on the C_d for above two shapes for both compressible and incompressible flow. Above discussion results in Fig. 4.27, Fig. 4.28 , Fig. 4.29, and Fig. 4.30.

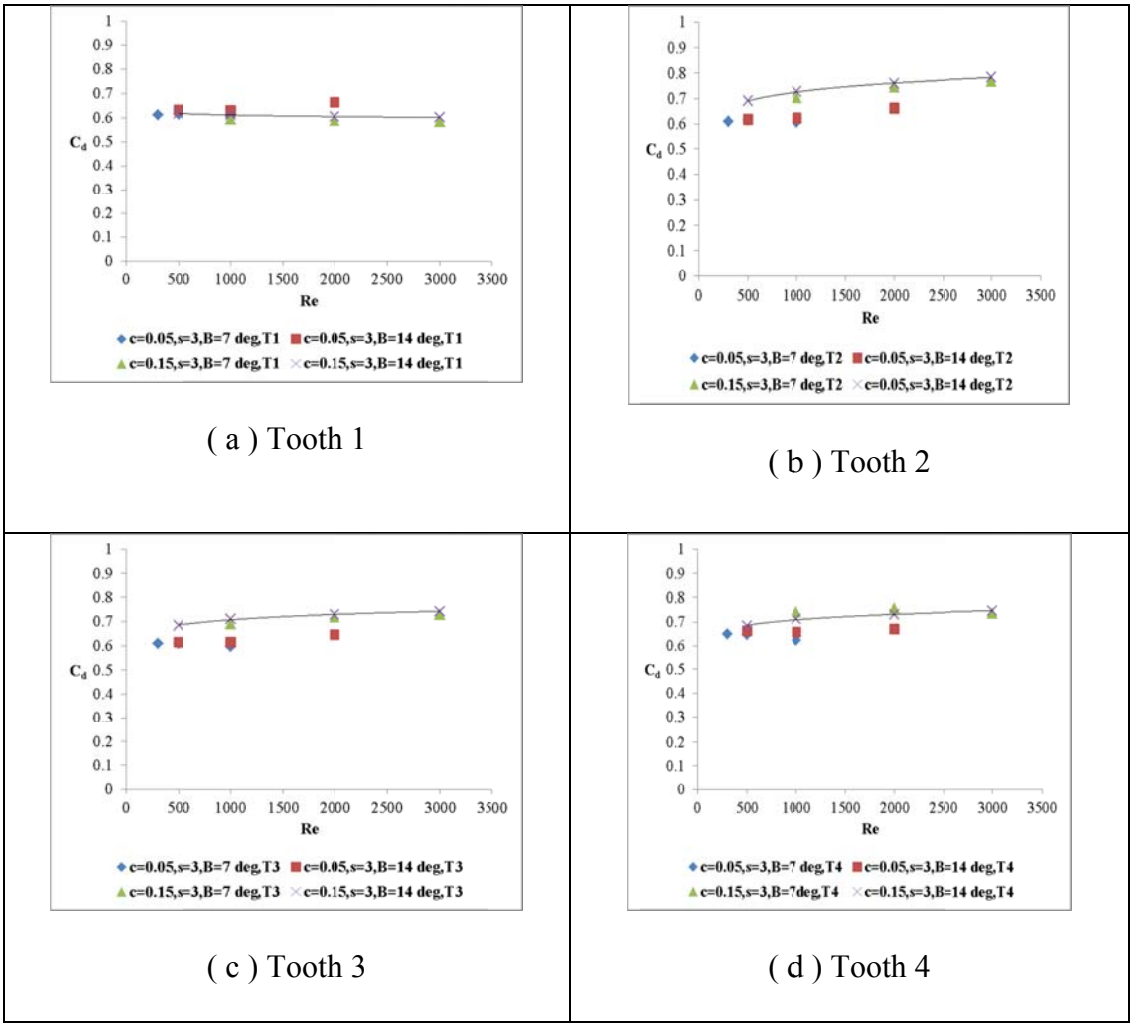

(a) Tooth 1

(b) Tooth 2

(c) Tooth 3

(d) Tooth 4

Fig. 4.27. Comparison of discharge coefficient with Re at different tooth location for B=7, 14 degree (compressible flow, isosceles triangle tooth, case 1, case 2).

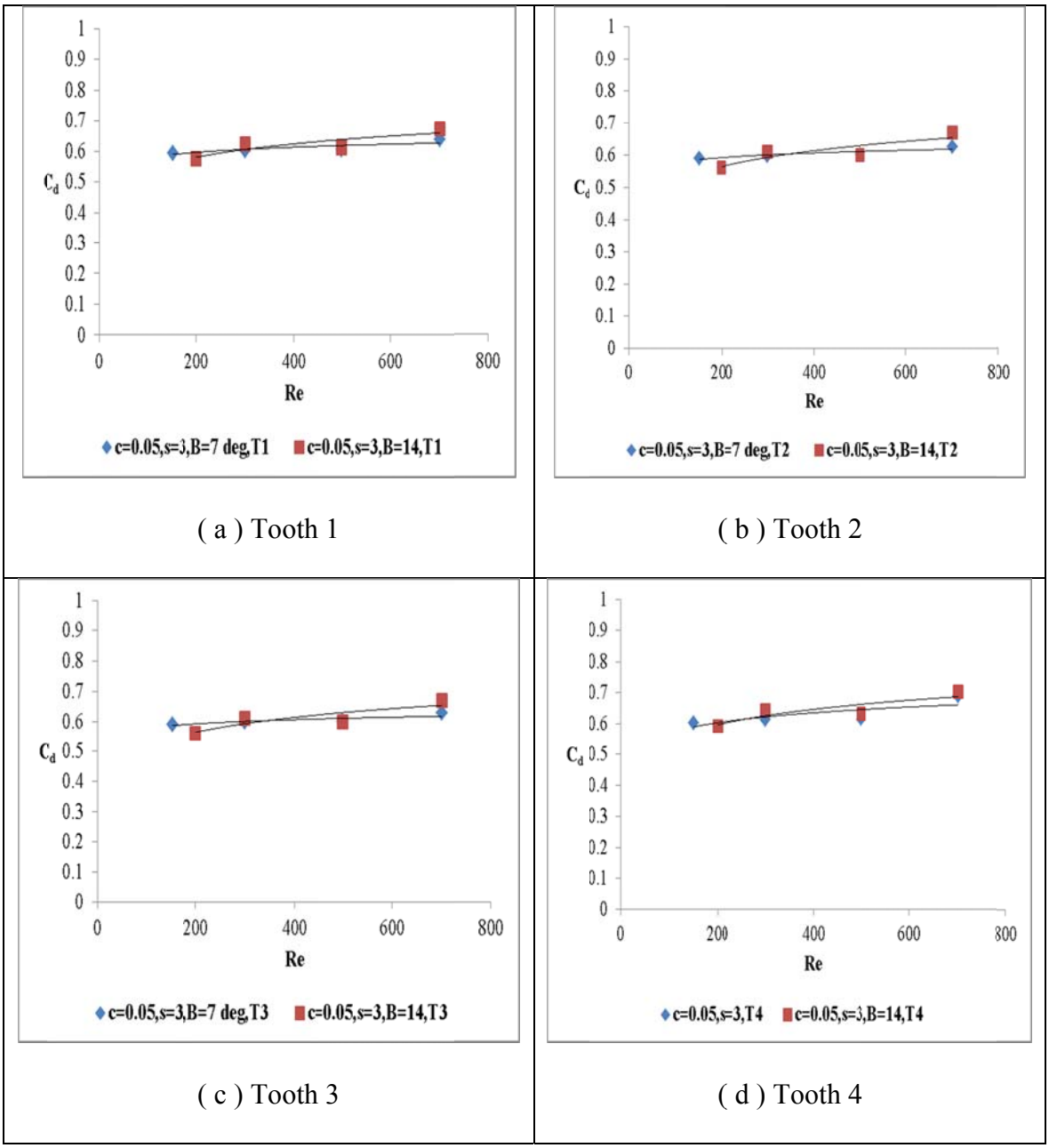

Fig. 4.28. Variation of discharge coefficient with Re for different B= 7,14 degree (compressible flow, right angle tooth, case 11, case 14).

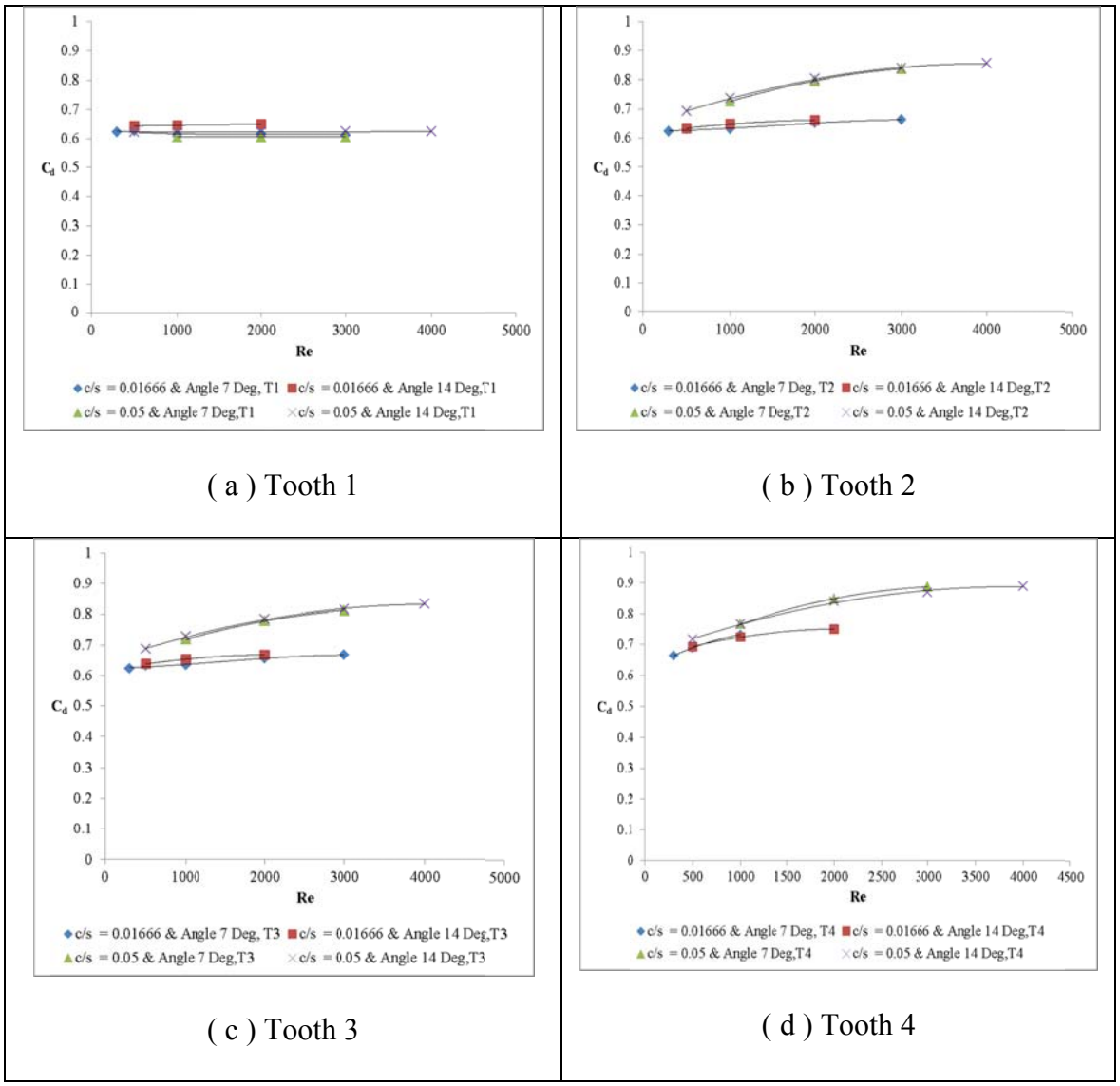

(a) Tooth 1

(b) Tooth 2

(c) Tooth 3

(d) Tooth 4

Fig. 4.29. Deviation of discharge coefficient with Re for different B = 7, 14 degree (for incompressible flow, isosceles triangle, case 1, case 2).

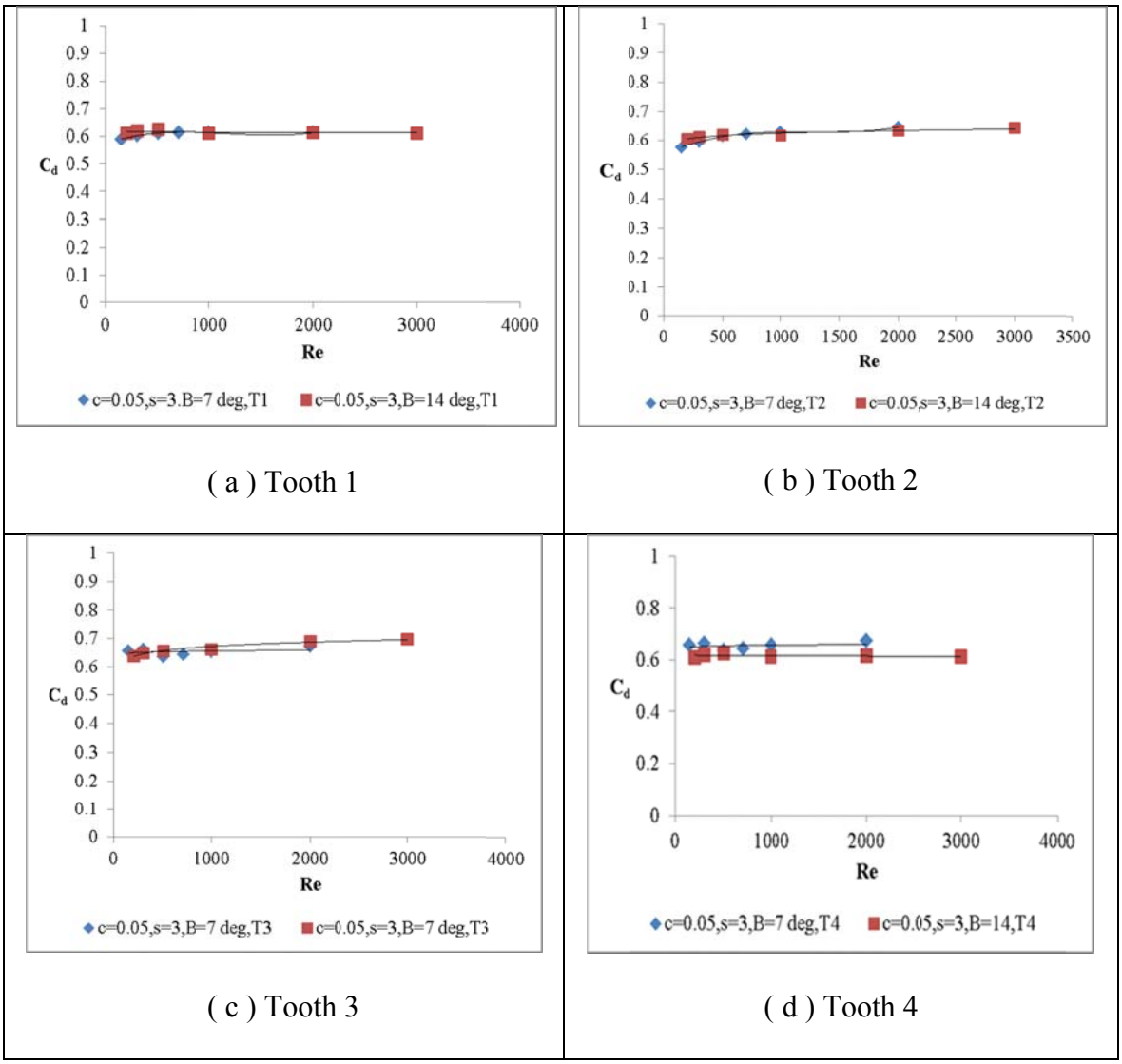

Fig. 4.30. Discharge coefficient variation with Re for different B = 7, 14 deg (for incompressible flow, right angle tooth, case 11, case 14)

It is observed from the Fig. 4.31 that at higher upstream angle, the pattern of vena contracta is similar compare to lower upstream angle. This similar vena contracta pattern is the reason which is making marginal impact of tooth angle on the C_d.

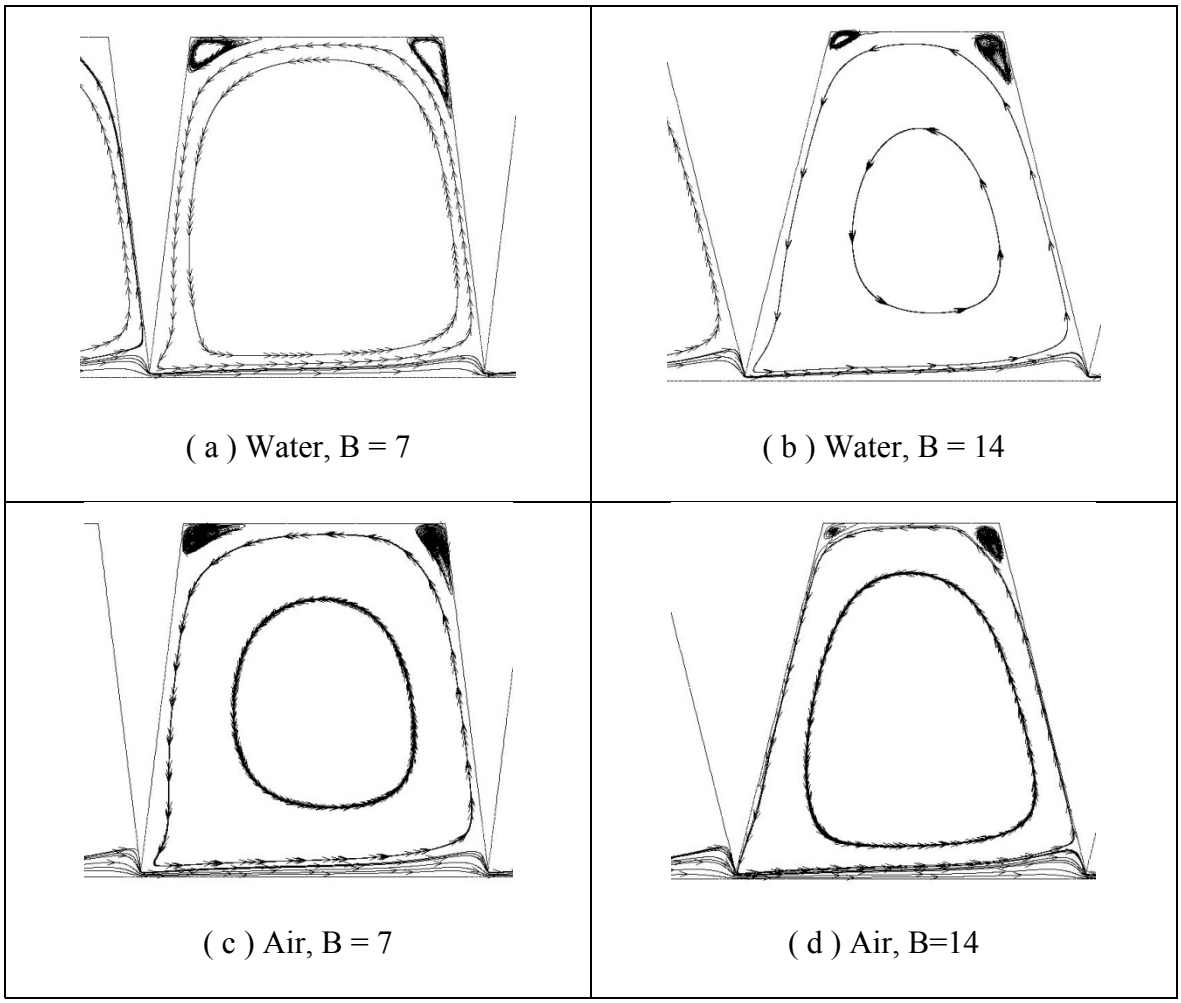

Fig. 4.31. Vena contracta effect for B = 7 and 14 deg (W_{sh} = 0, Re 500, cavity 2, isosceles tooth shape, case 1, case 2).

4.3.6. Effect of Shaft Speed

The CFD simulations using axisymmetric swirl are performed for different shaft RPS and Reynolds number. For all of the simulations, shaft speed, W_{sh}, is employed from 1000 -7000 RPS range. The effect of shaft speed on discharge coefficient is evaluated for fixed geometry including pitch, radial clearances, upstream angle, and tooth width. This investigation is performed for the isosceles triangle tooth shape seal for both compressible and incompressible flow. In this section the shaft speed effect is discussed for geometric parameters such as radial clearances, c, pitch, s, upstream angle, B and tooth width individually and the flow parameter Reynolds number. Previous studies [18] show that shaft rotation has a significant effect on discharge coefficient at low axial Reynolds number for rectangular straight through labyrinth seals.

4.3.6.1 Effect of Shaft Speed on C_d for Re

Form the result of the Fig. 4.32, it is found that at low Reynolds number (Re 500), the discharge coefficient , C_d reducing from 0.627 to 0.319 (49% reduction) as W_{sh} is increased from 0 to 7000 rps. As the Reynolds number increases the difference decreases to zero at Re 3000. So it can be concluded that the shaft speed effect is insignificant at higher Reynolds number. This plot only shows the effect on 1st tooth.. Fig. 4.32 and Fig. 4.33 show the influence of shaft speed, W_{sh}, on the discharge coefficient as a function of the Reynolds number. The effect of rotational speeds for all teeth is shown in Fig. 4.33.

At the lowest Reynolds number (Re = 500) and highest shaft speed (7000 RPS) a 46% reduction was obtained. Waschka et al. [18] obtained similar result for the straight through labyrinth seal for incompressible flow. The reason explained in his study that for pure laminar flows, axial and peripheral components are initially independent to each other but beyond a critical peripheral speed, the further augmentation in flow resistance which is causing the reduction of the discharge coefficient becomes insignificant. At higher rotational speeds and low Re, the swirl velocity dominates the flow field generating high centrifugal forces. This is one reason of the discharge coefficient reduction at high shaft speed.

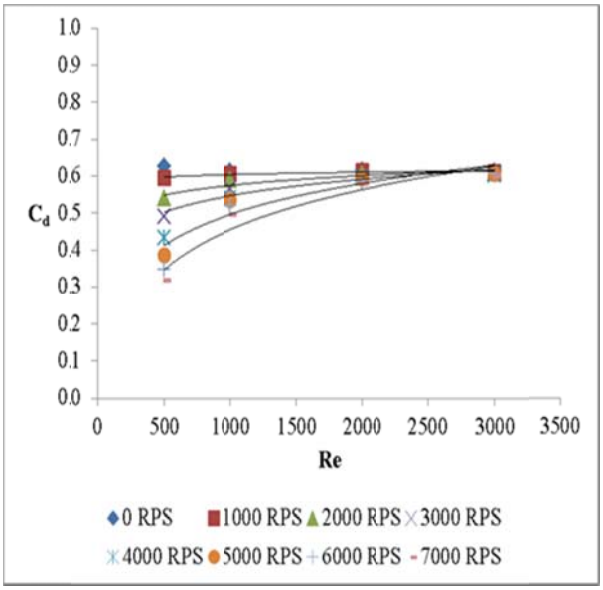

Fig. 4.32. Shaft speed effect on C_d with Re (incompressible flow, 1st tooth, isosceles , c=0.05, s=3, B=7°, case 1).

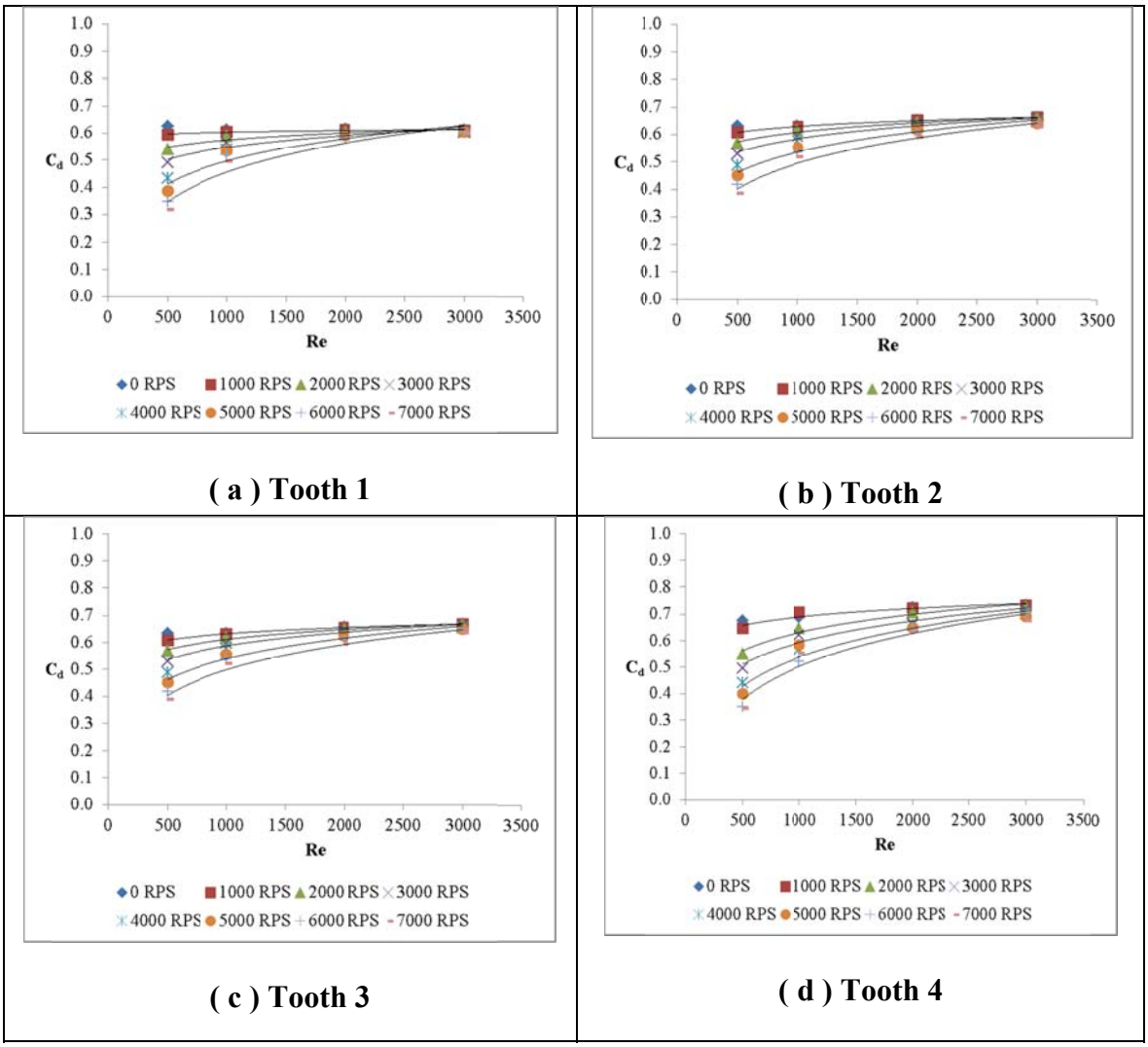

Fig. 4.33. Shaft rotation effect on the discharge coefficient with Re at different tooth locations (for incompressible flow, c=0.05, s=3, B=7, case1).

For the compressible flow, the effect of shaft speed on the discharge coefficient is insignificant. This result is shown in Fig. 4.34.

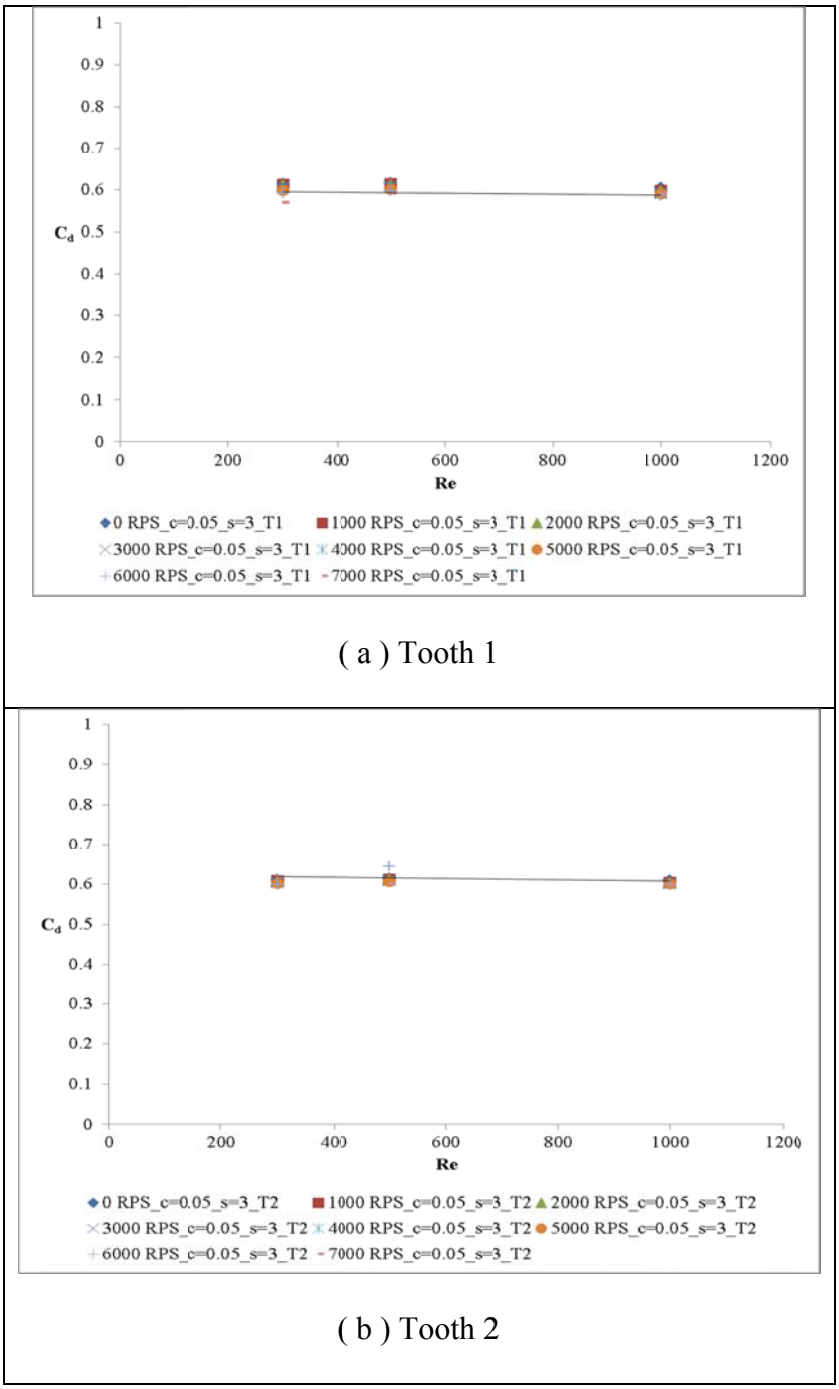

Fig. 4.34. Variation of discharge coefficient with Re for different W_{sh} (for compressible flow, case 1).

4.3.6.2 Effect of Shaft Speed on C_d for Different Clearances

Fig. 4.35 shows the influence of shaft speed, W_{sh}, on the discharge coefficient as a function of c. It is evident from the plot that shaft rotation has significant effect on discharge coefficient for different clearances. The result shows that at the highest clearance (c =0.2) and maximum rotational speed (W_{sh} = 7000 rps) , a 58% reduction in the discharge coefficient was obtained.

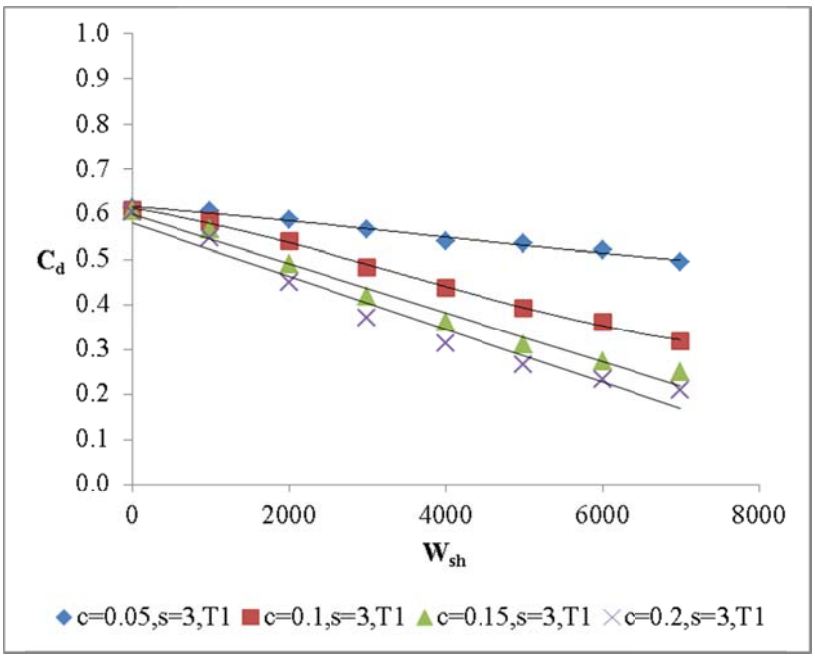

Fig. 4.35. Variation of discharge coefficient of seal with shaft speed for first tooth at different clearances (for incompressible flow , isosceles triangle tooth, Re 1000, case 1, case 3, case 4, case 6).

It is important to evaluate the effect on all of the teeth. For better visualization, the effect of shaft rotation for different clearances at different tooth locations is shown in the Fig. 4.36.

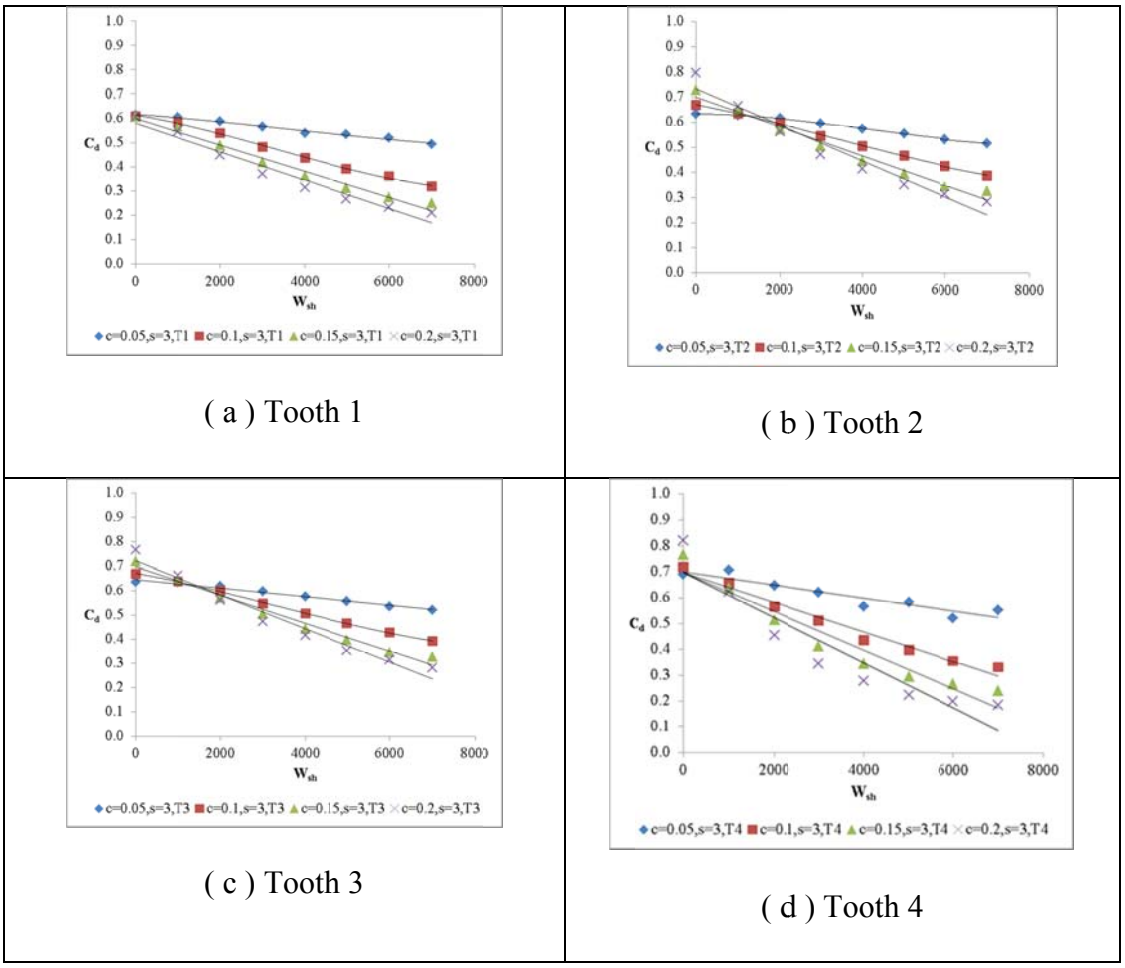

Fig. 4.36. Variation of discharge coefficient at different tooth location with W_{sh} (incompressible flow, Re 2000, case 1, case 3, case 4, case 6).

Fig. 4.37 illustrates a comparison between two clearances (c 0.05 and 0.15) that the Reynolds number at which the shaft speed effects stop, depends on the clearance. This is a very important findings. It is evident from the comparison that the limiting

Reynolds number seems to increase from 3000 to 10000 with increasing clearance from 0.05 to 0.15 mm.

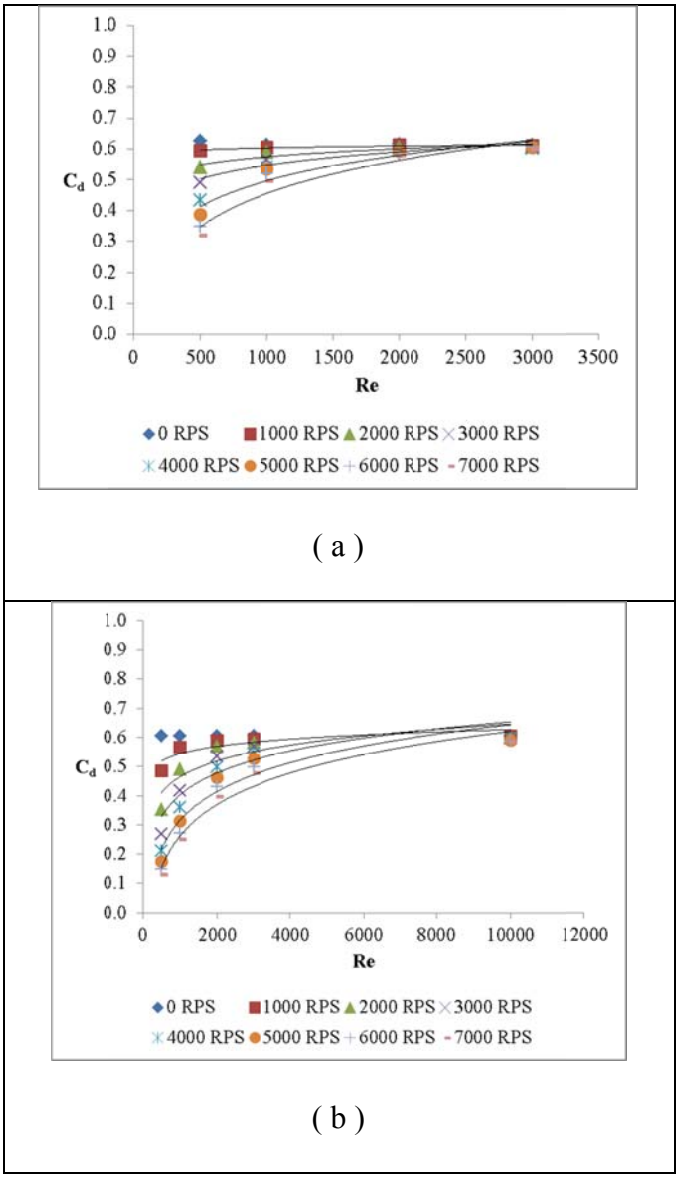

Fig. 4.37. Rotational speed as a function of Re (for incompressible flow, isosceles triangle tooth shape, (a) c=0.05, s=3 ; (b)c=0.15, s=3.

Fig. 4.38, Fig. 4.39, Fig. 4.40 and Fig. 4.41 are plotted to explain the combined effect of W_{sh}, c, Re on the discharge coefficient. Fig. 4.39, Fig. 4.40 and Fig. 4.41 shows the combined effect of W_{sh}, Re for a given clearance on the discharge coefficient of four teeth.. The results in Fig. 4.38 show that C_d decreases as Re decreases and W_{sh} increases. Again from same plot for c =0.15 mm, it is observed that C_d decreases more compare to 0.05 mm as W_{sh} increases. It is evident from the figure that shaft speed has a significant effect on the C_d for maximum shaft speed. For example, at c = 0.05 and Re 500, a 33% reduction of C_d with maximum speed was obtained. Also it is evident from the result that shaft speed has significant effect at low Reynolds number for all four tooth of the seal.

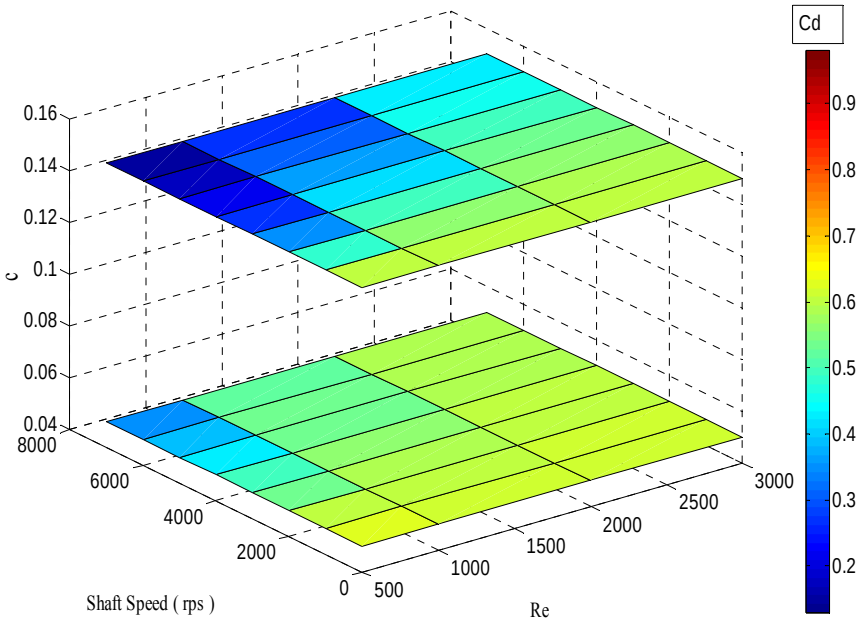

Fig. 4.38. Combined effect of Wsh, Re, c on discharge coefficient (for incompressible flow , 1st tooth, case 1, case 3).

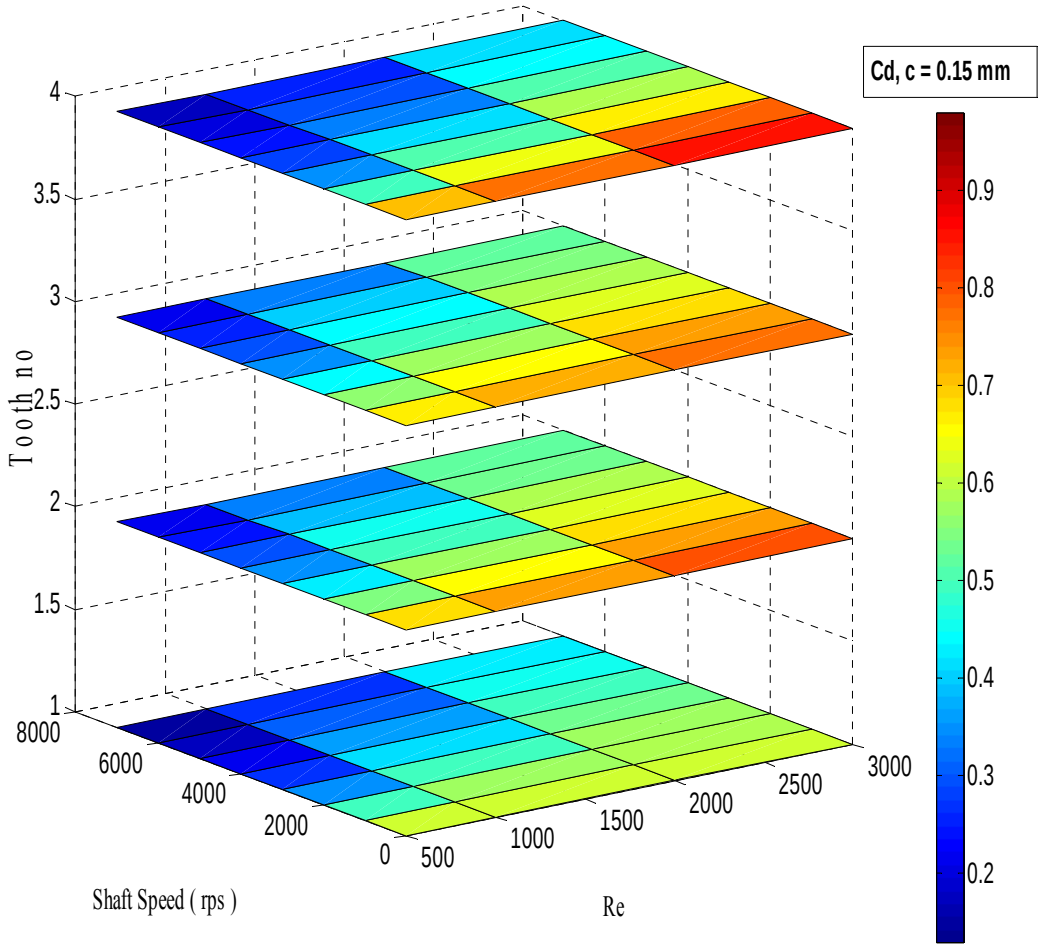

Fig. 4.39. Combined effect on the discharge coefficient (for incompressible, all teeth, c =0.15, s=3, case 4).

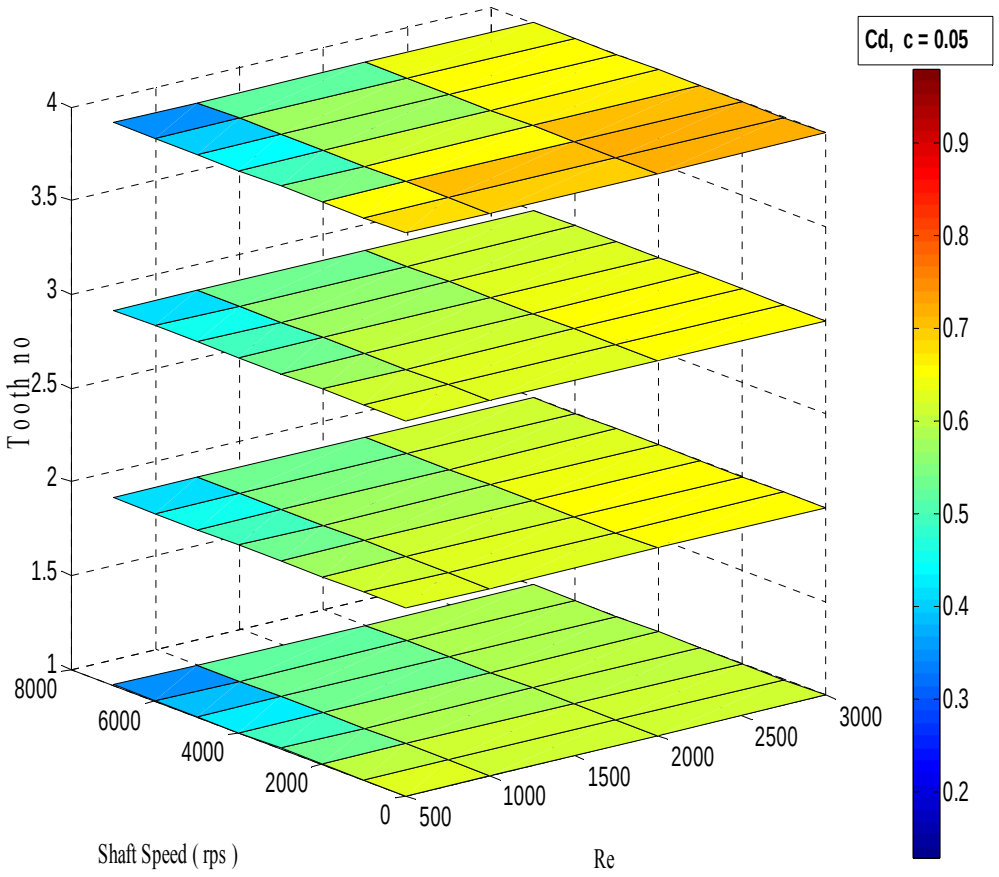

Fig. 4.40. Combined effect on the discharge coefficient (incompressible, all teeth, c= 0.05, s=3, case 1).

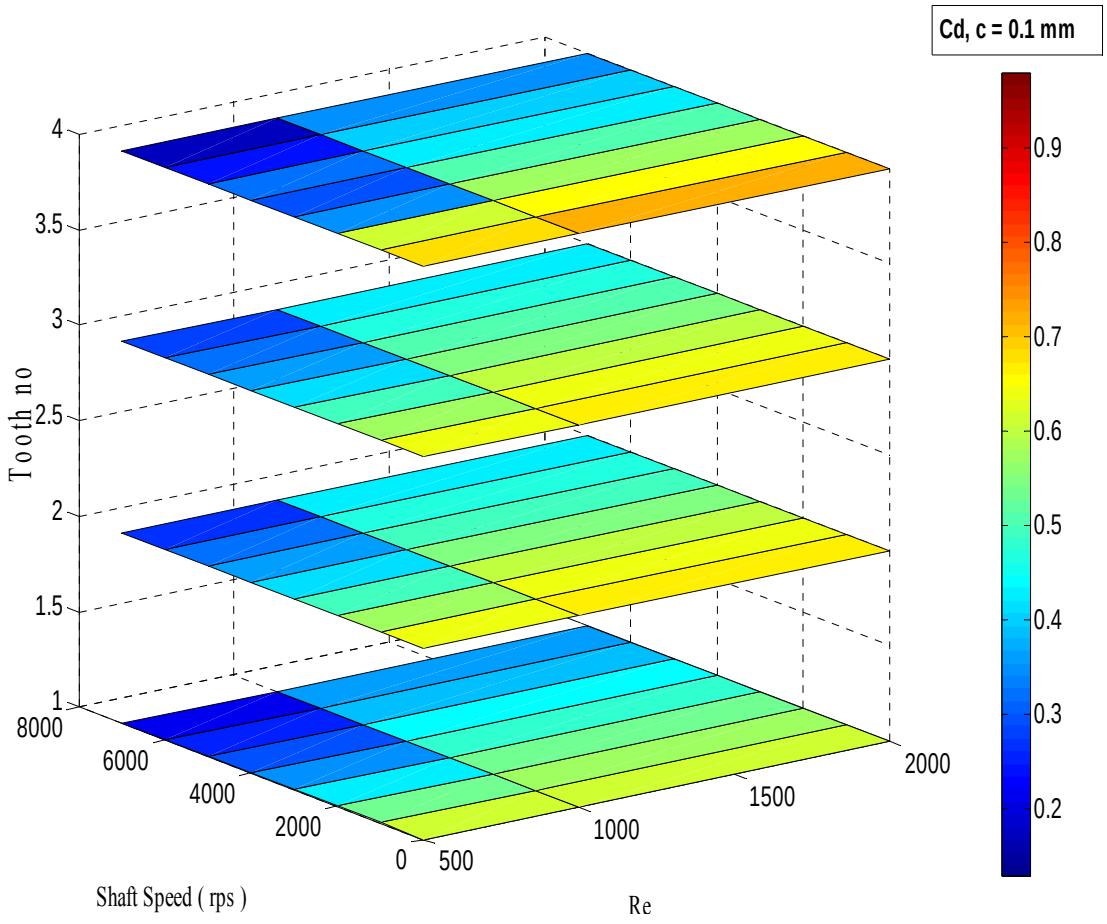

Fig. 4.41. Combined effect on the discharge coefficient (incompressible, all teeth, c= 0.1, s=3, case 3).

Fig. 4.42 shows that rotational speed effect as a function of clearance is insignificant. for the case of compressible flow.

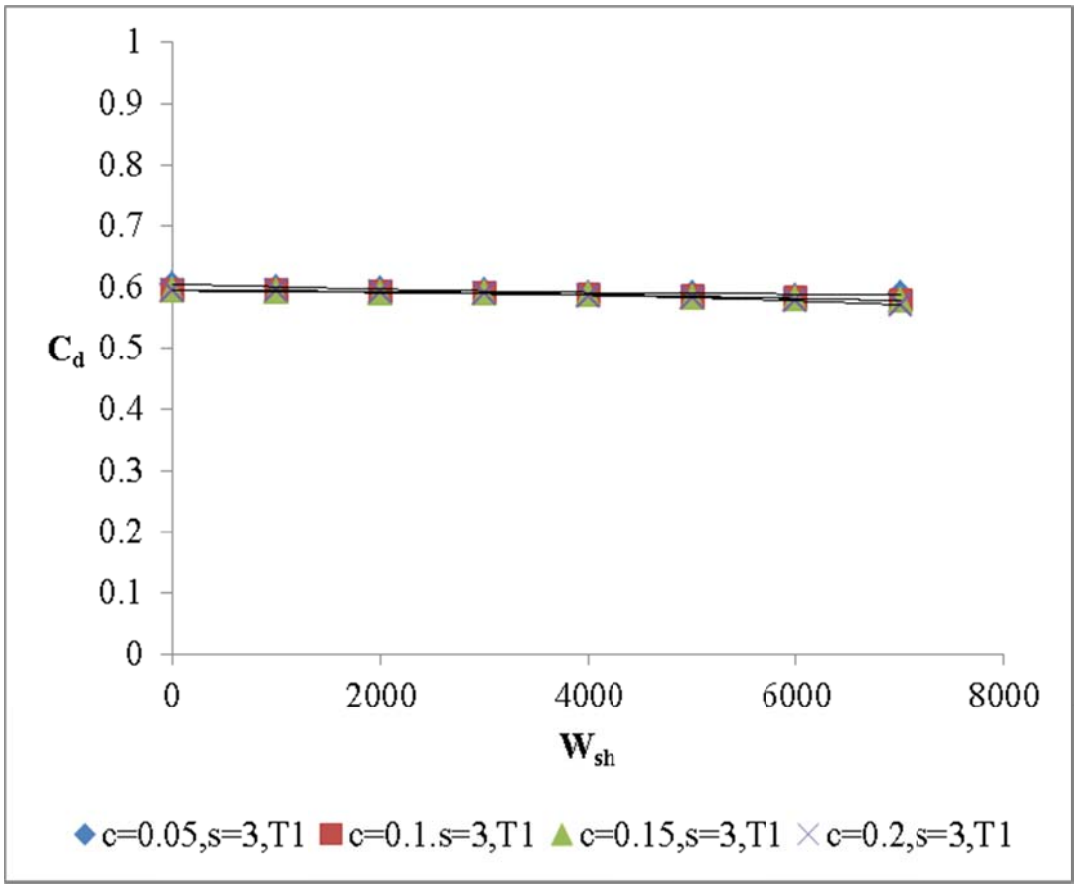

Fig. 4.42. Variation of discharge coefficient of seal with shaft speed for first tooth at different clearances (for compressible flow , isosceles triangle tooth, Re 1000, case 1, case 3, case 4, case 6).

From the combined effect plot it is observed that shaft rotation as a function clearance has insignificant effect on the discharge coefficient. The C_d distributions for all teeth are shown in Fig. 4.43 to Fig. 4.46.

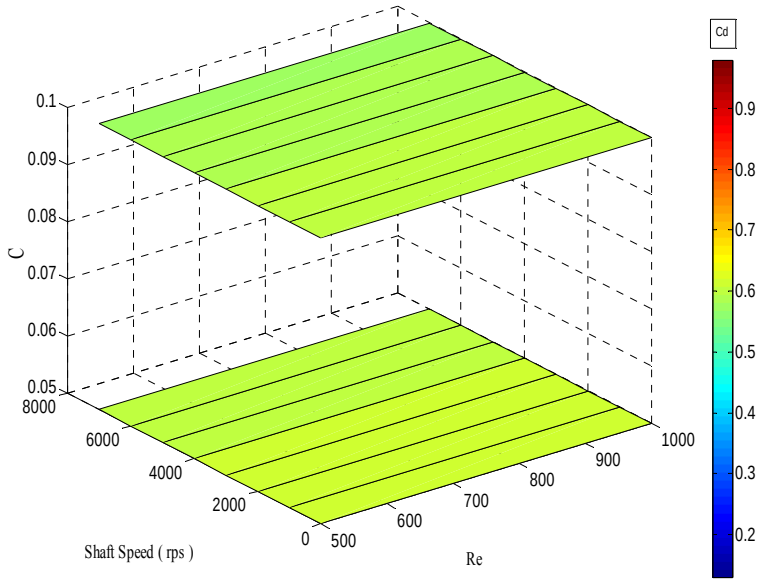

Fig. 4.43. Combined effect on the discharge coefficient (compressible flow, 1st tooth, case 1, case 3).

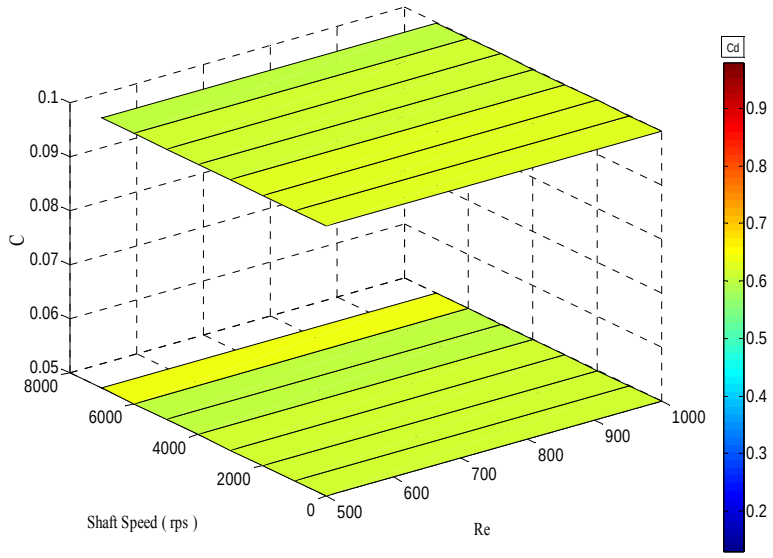

Fig. 4.44. Combined effect on the discharge coefficient (compressible flow, 2nd tooth, case 1, case 3)

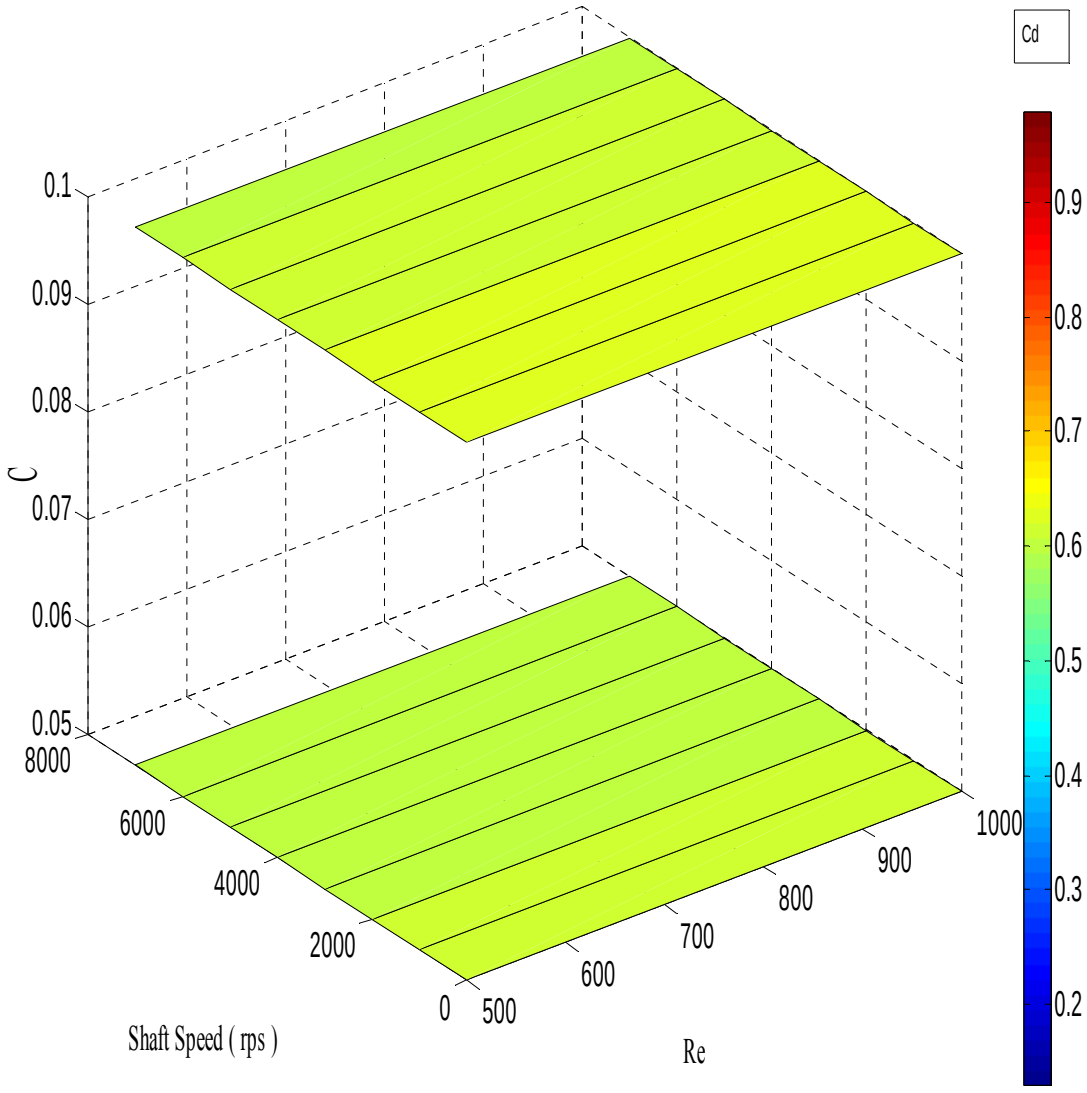

Fig. 4.45. Combined effect on the discharge coefficient (compressible flow, 3rd tooth, case 1, case 3).

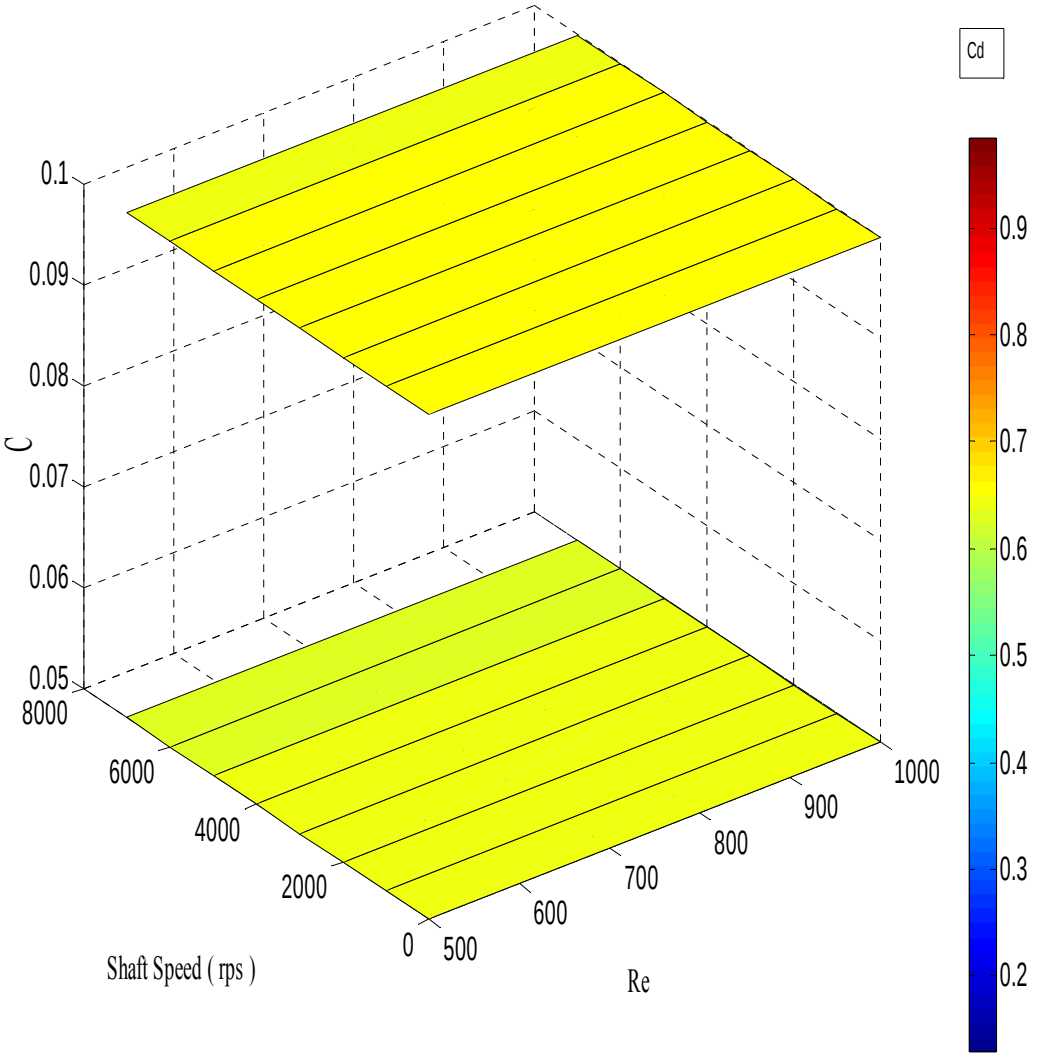

Fig. 4.46. Combined effect on the discharge coefficient (compressible flow, 4th tooth, case 1, case 3).

4.3.6.3 Effect of Shaft Speed on C_d for Tooth Width

Earlier in the section 4.3.3. it was shown that at zero shaft speed, the discharge coefficient is decreases with the increasing. tooth width for incompressible flow. Fig. 4.47 shows the shaft speed effect as a function of tooth width, w= 0, 0.5, and 1 mm. for Re 500,1000 and 2000.It is observed from the plot that at smallest Reynolds number (Re = 500) and higher shaft speed (W_{sh}=7000 rps) a 10% reduction in the discharge coefficient was obtained for the wider tooth. The shaft speed has less effect as a function of tooth width at high Reynolds number, Re 2000.

This result in Fig. 4.48 shows the combined effect of shaft rotation, w and Re on the C_d for incompressible flow. It is observed that shaft rotation has significant effect on wider tooth at low Reynolds number. So it can be concluded that for the laminar flow at high shaft speed wider tooth provides lower discharge coefficient. The physics behind this is that at low Reynolds number the peripheral momentum dominates the axial momentum which originates a secondary vortex in the cavity as a result additional flow resistance causing more pressure drop across the tooth.

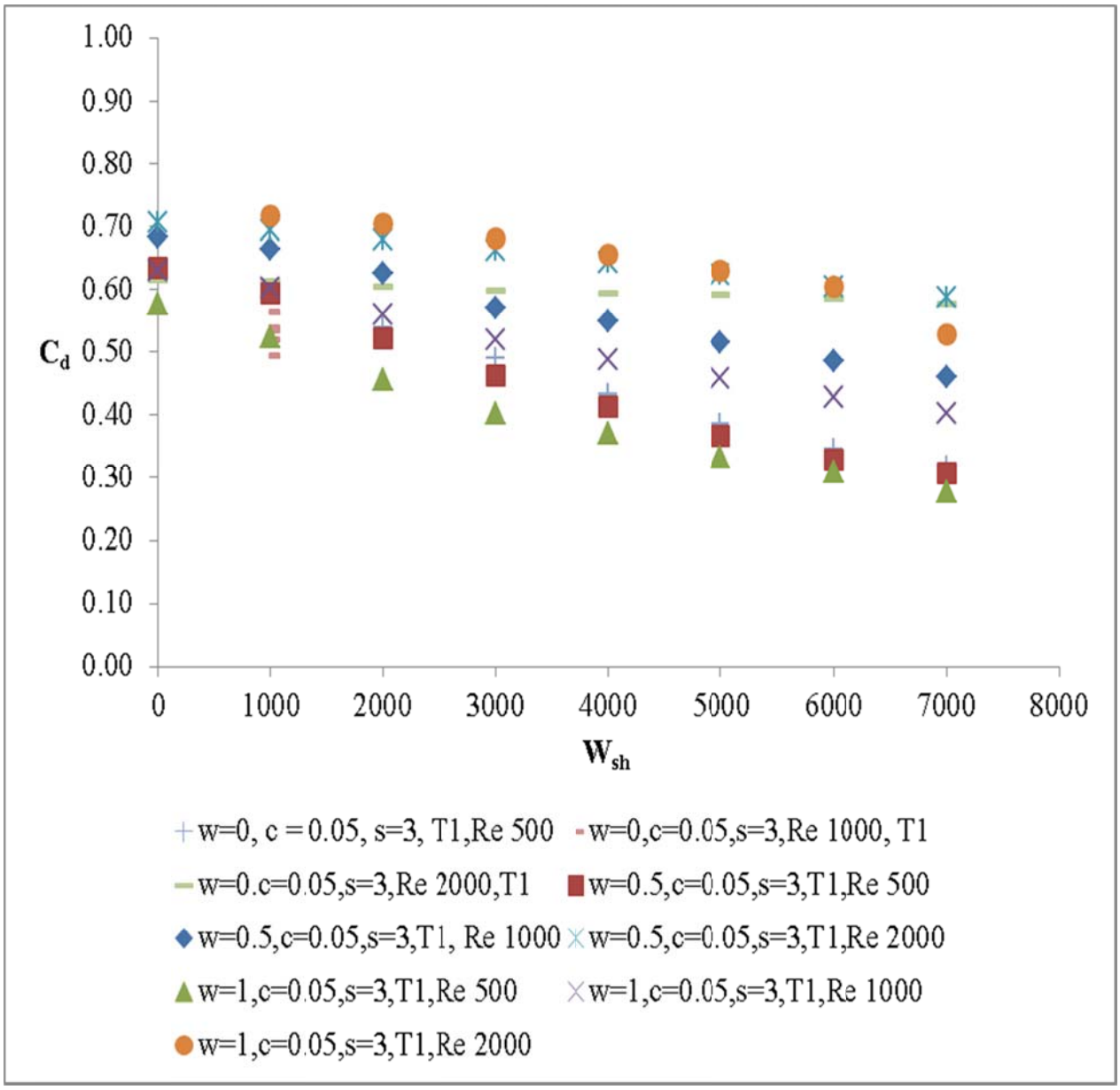

Fig. 4.47. Shaft speed effect as a function of tooth width (for incompressible flow, case 1, case 8, case 9).

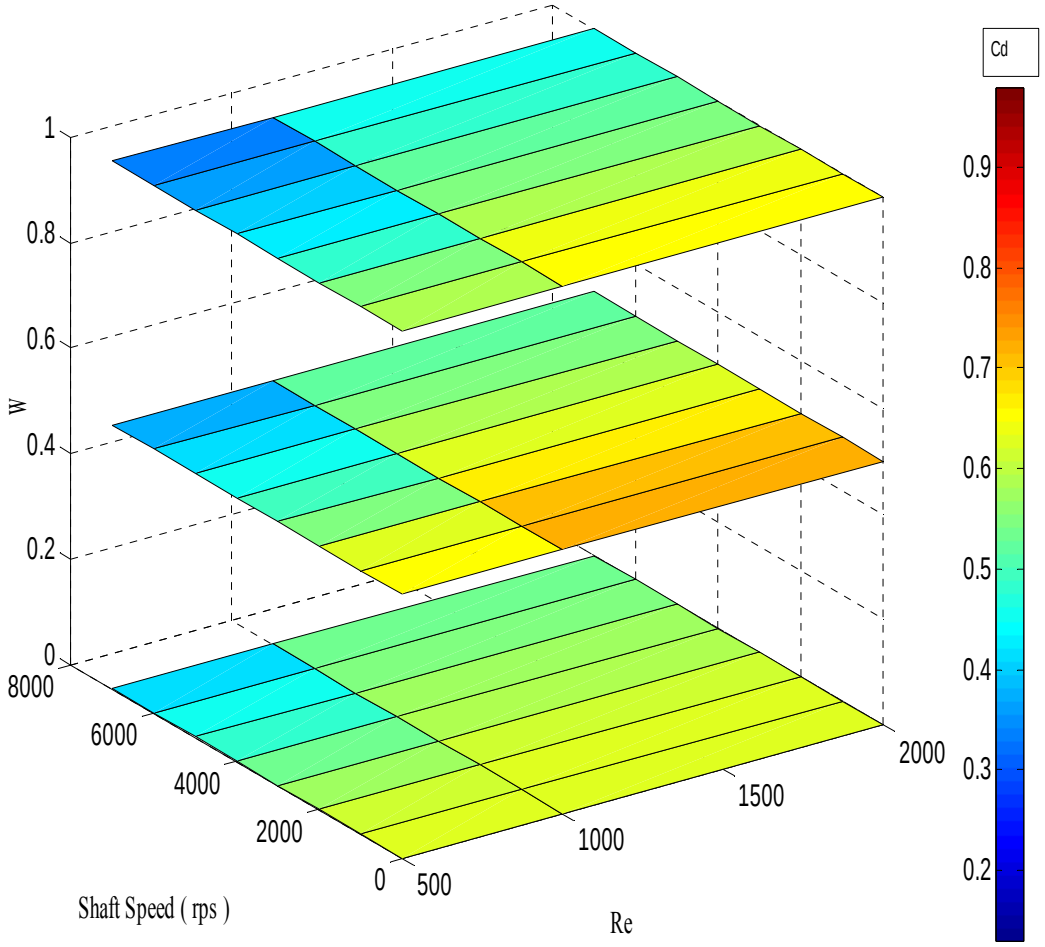

Fig. 4.48. Combined effect of W_{sh}, Re and w (for incompressible flow , 1st tooth, case 1, case 8).

Combined effect of Reynolds number, shaft speed on the discharge coefficient of four teeth for zero tooth width is shown in Fig. 4.49. A Similar plot is generated in Fig. 4.50 for tooth width of 1 mm for incompressible flow.

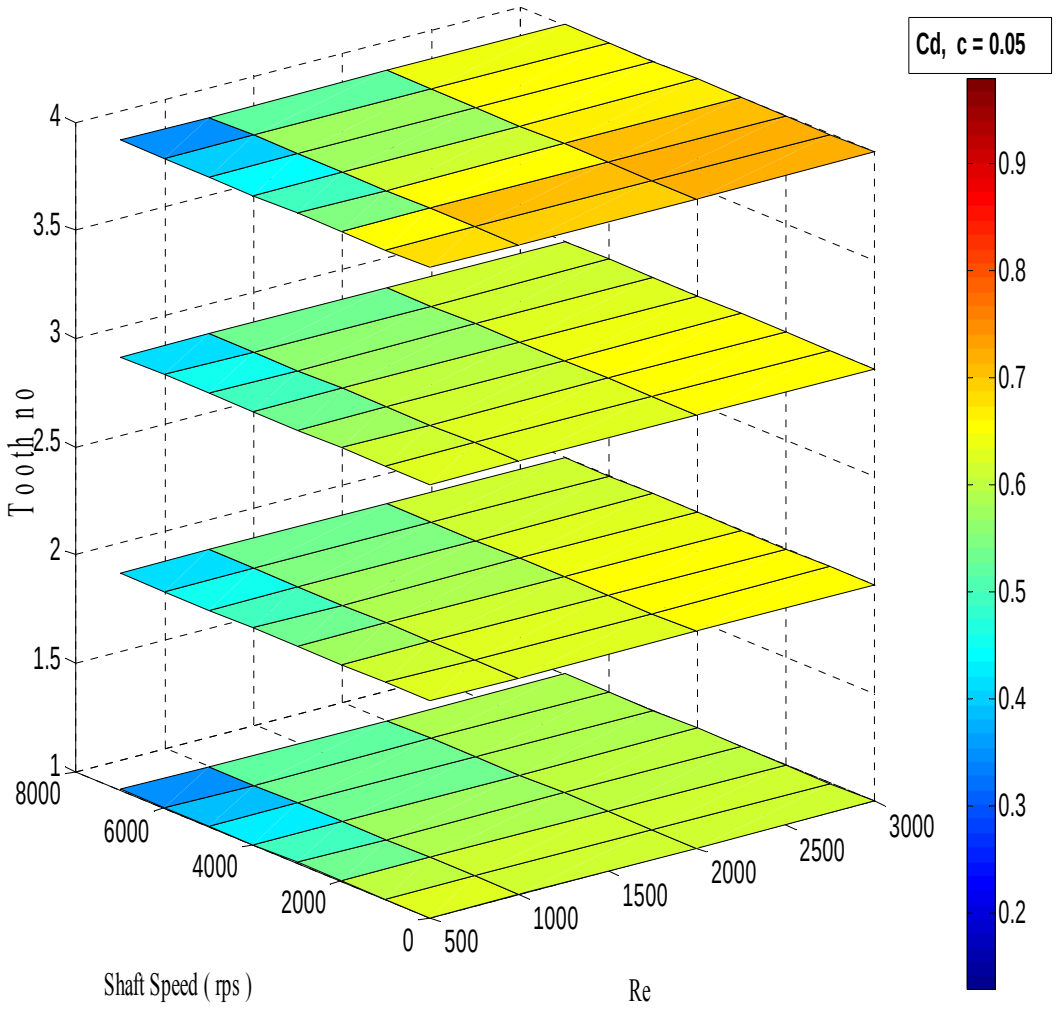

Fig. 4.49. Combined effect of W_{sh}, Re and w (for incompressible flow , w=0, 4 teeth , c=0.05, case 1).

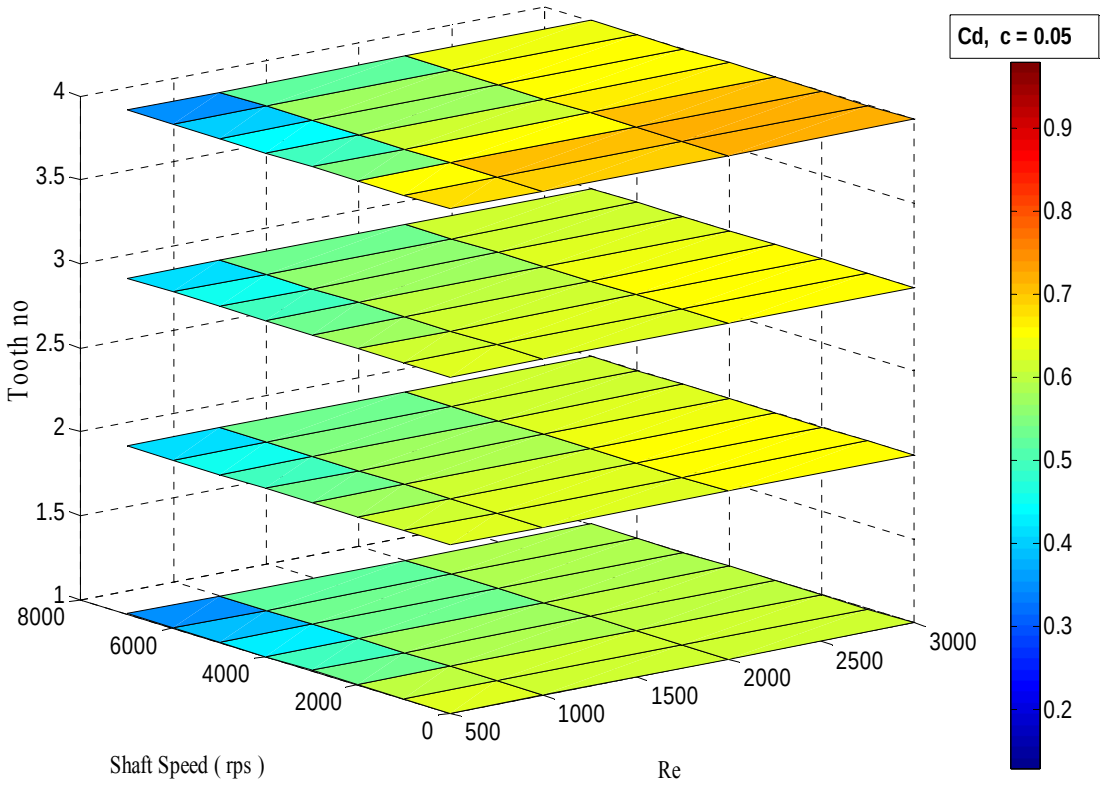

Fig. 4.50. Combined effect on the discharge coefficient (incompressible, w =1 mm, all teeth, c =0.05, case 8,).

Fig. 4.51 shows the effect of shaft rotation at different tooth locations for w= 0, 0.5 and 1 mm for low Reynolds number, Re 500. At all four teeth location the shaft speed effect seems consistent at Re 500. So it can be concluded that for the smallest Reynolds number, the discharge coefficient is decreasing for higher shaft speed at all teeth locations. For compressible flow it is observed that the smallest Reynolds number (Re = 500), the effect of shaft rotation is insignificant on the discharge coefficient For all of the teeth, this result is shown in Fig. 4.52.

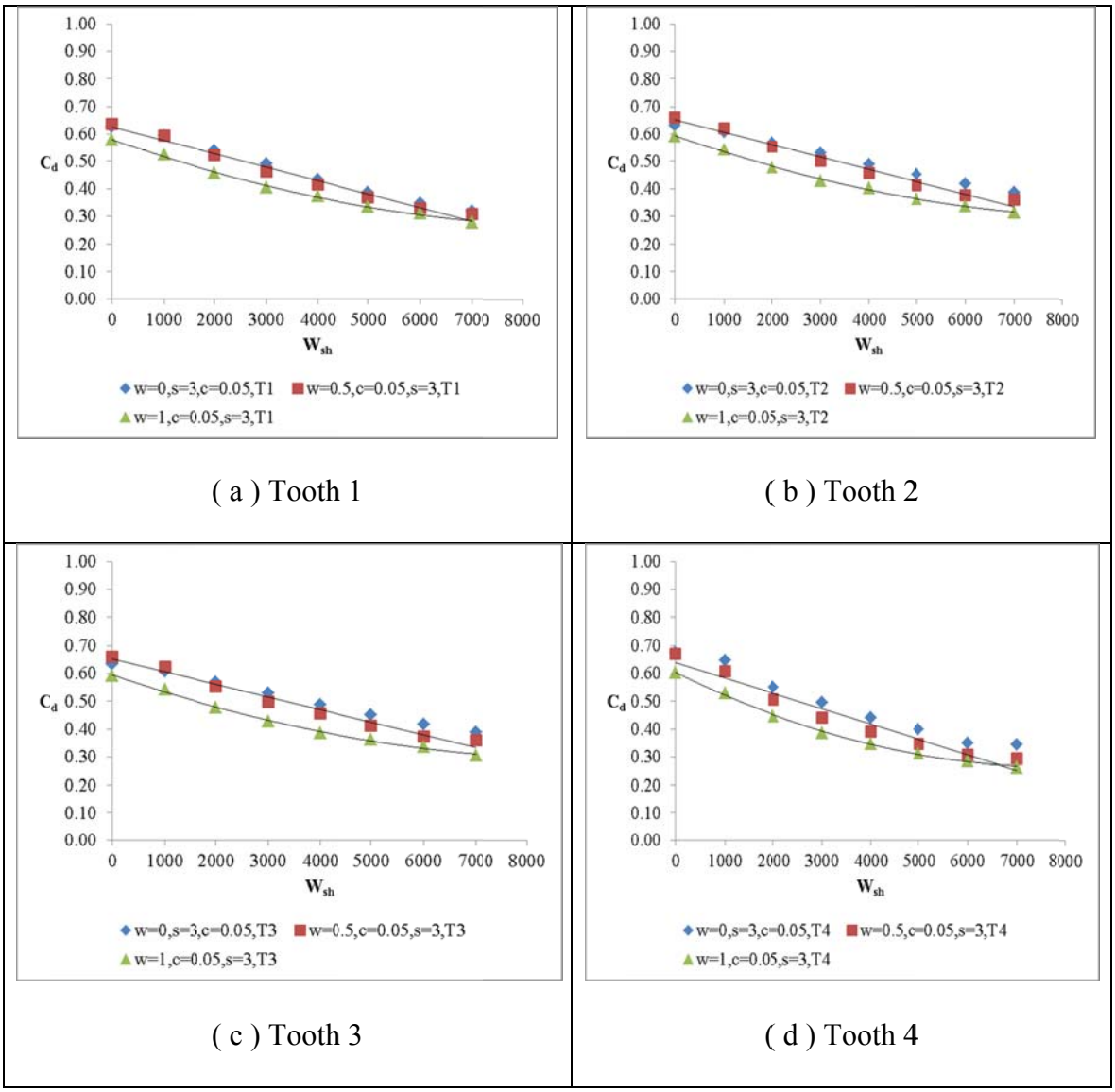

Fig. 4.51. Shaft speed effect at different tooth locations (for incompressible flow, Re 500, case 1, case 8, case 9).

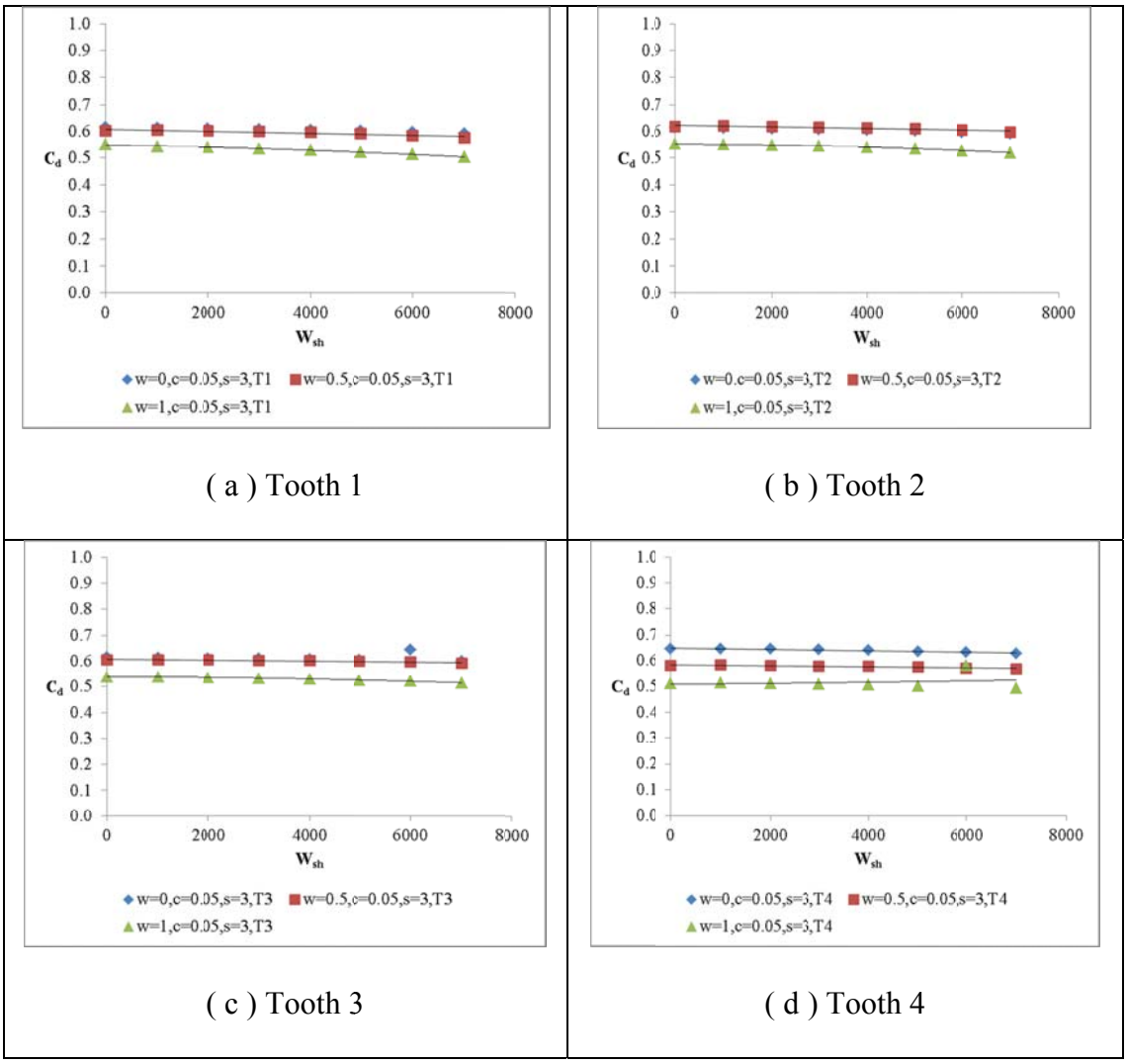

Fig. 4.52. Shaft speed effect at different tooth locations for tooth width (for compressible flow, Re 500, case 1, case 8, case 9).

It is found from the result that at zero shaft speed , wider tooth gives lower C_d compare to sharp tooth. The reason can be explained in terms of vena contracta effect shows in Fig. 4.53. For the zero width at minimum speed, there is more vena contracta effect compare to wider tooth. It is also observed that at maximum shaft speed, wider tooth has multiple region of flow separation and reattachment which is causing more

pressure drop. In another way this phenomenon can be explained by flow through channel. Higher channel length cause higher pressure drop for laminar flow.

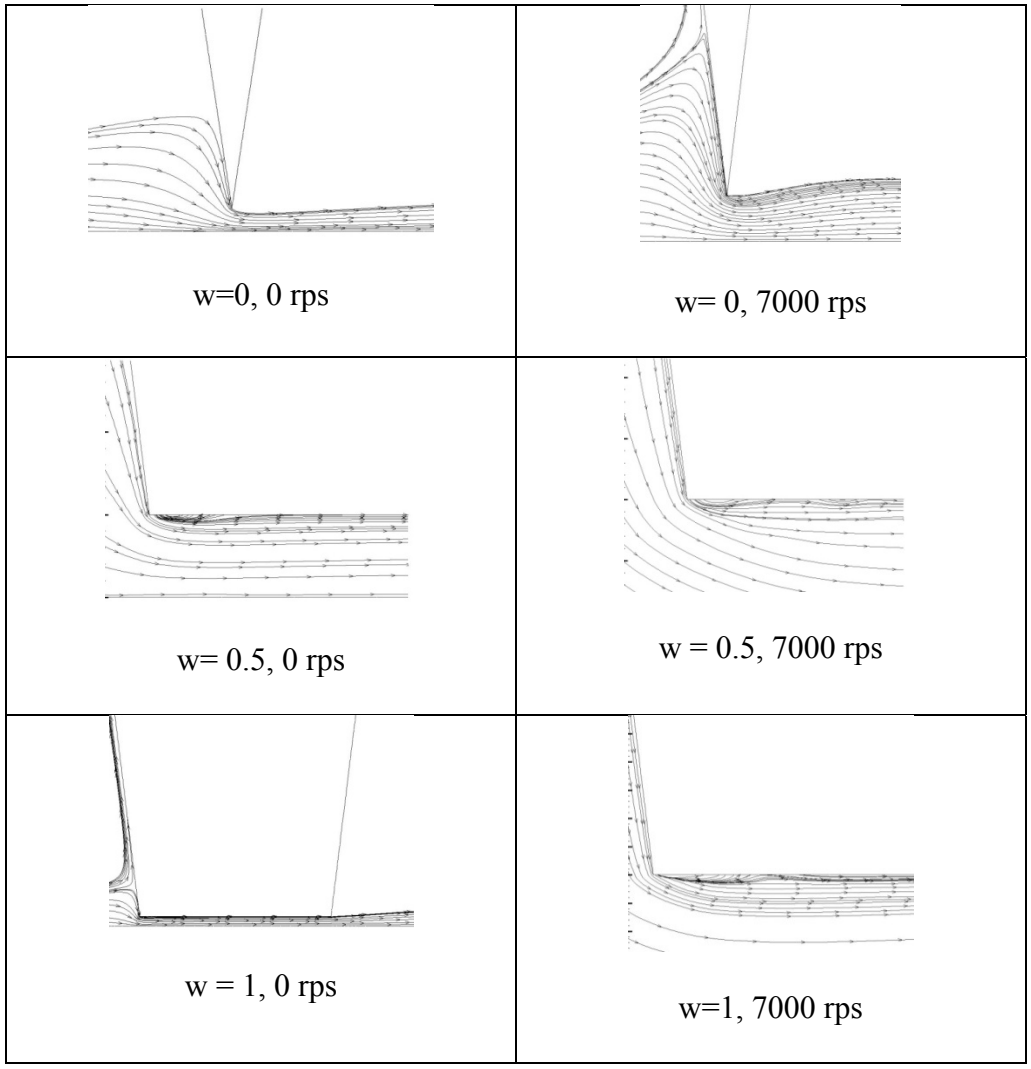

Fig. 4.53. Vena contracta effect for different tooth width (incompressible flow, Re 500, case 1, case 8, case 9).

4.3.6.4 Effect of Shaft Speed on C_d for Pitch

Dependence of shaft rotation effects as a function pitch is investigated in this study for two different pitch value, s=3 and 5 mm. Fig. 4.54 shows the shaft speed effect on all four teeth of the seal. It is observed from the plot that at higher pitch value (s =5) and maximum shaft speed, 7000 rps. 90% decrease of the discharge coefficient was obtained for 100% increase in Reynolds number.

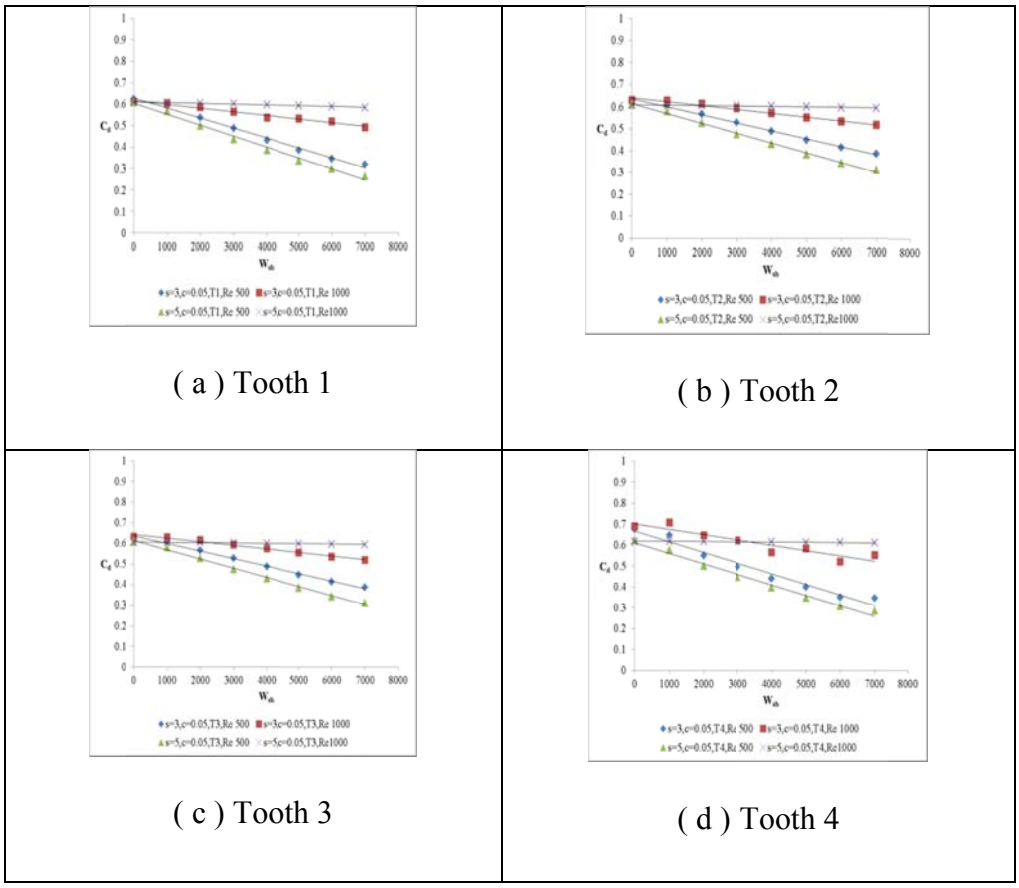

Fig. 4.54. Shaft speed as function of pitch (for incompressible flow, isosceles triangle shape tooth, case 1, case 5).

For the seal with higher pitch (s=5) and at higher shaft speed (Wsh) secondary vortices inception was noticed in the cavity. This secondary vortices is creating additional flow resistance due to the domination of swirl velocity. As a result discharge coefficient is decreasing. This result is shown in the Fig. 4.55.

.

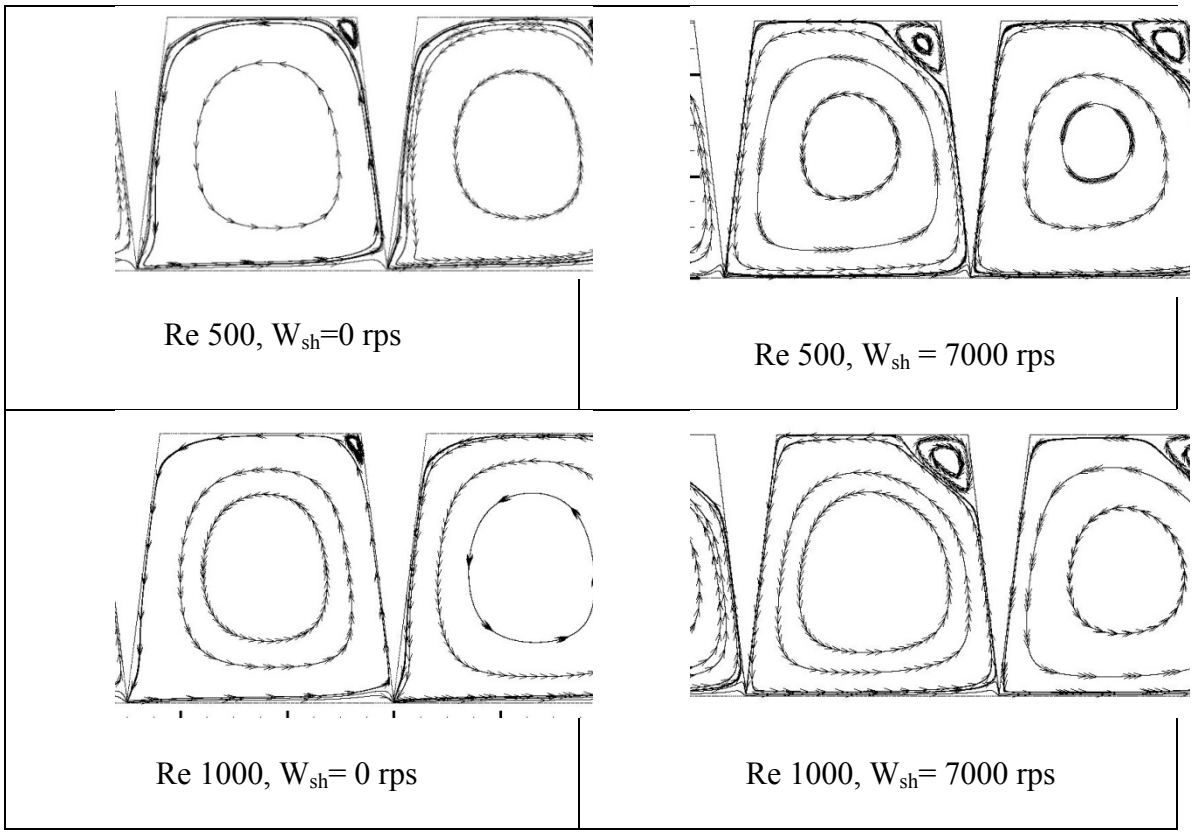

Fig. 4.55. Flow pattern in 1st and 2nd cavity for higher pith (incompressible flow, c=0.05, s=5, case 10).

Combined effects of the shaft speed, pitch and Reynolds number on the discharge coefficient is shown as a 3D plot in Fig. 4.56 to Fig. 4.59 for all four teeth. From the 3D plots, it is found that at higher shaft speed, higher pitch results lower discharge coefficient at small Reynolds number. This is true for all of the tooth in the seal. It is concluded that for this small Re range, C_d independent of Re and function of only W_{sh}

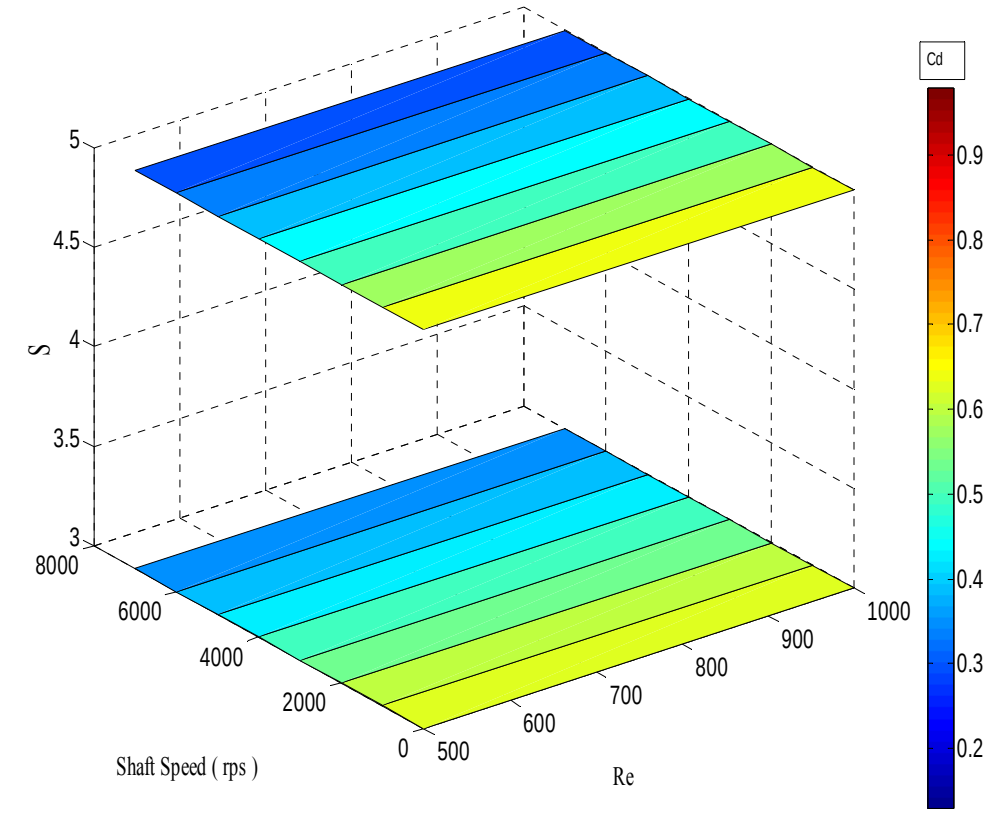

.

Fig. 4.56. Combined effect of Re, Wsh, on discharge coefficient of 1st tooth (for incompressible flow).

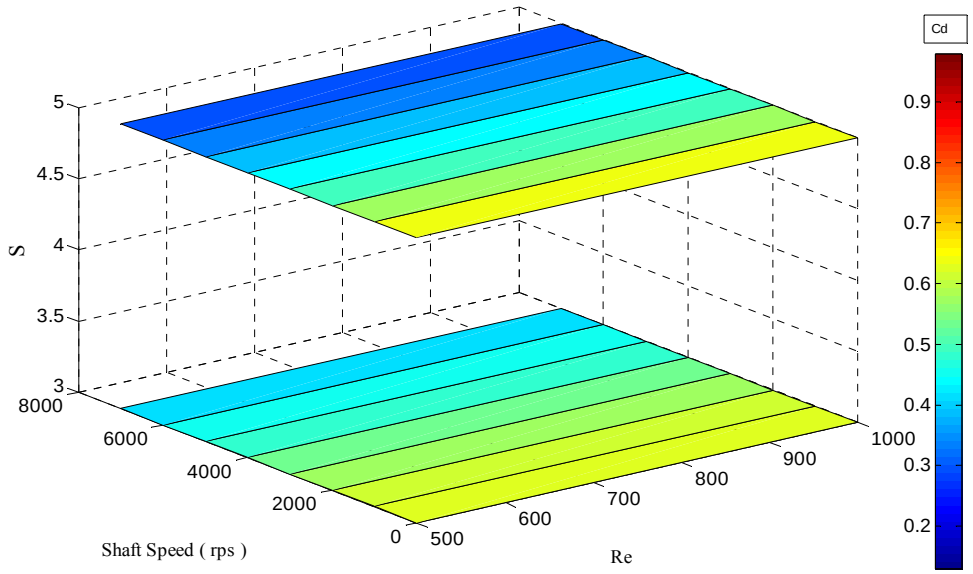

Fig. 4.57. Combined effect of Re, W_{sh}, on discharge coefficient of 2nd tooth (for incompressible flow).

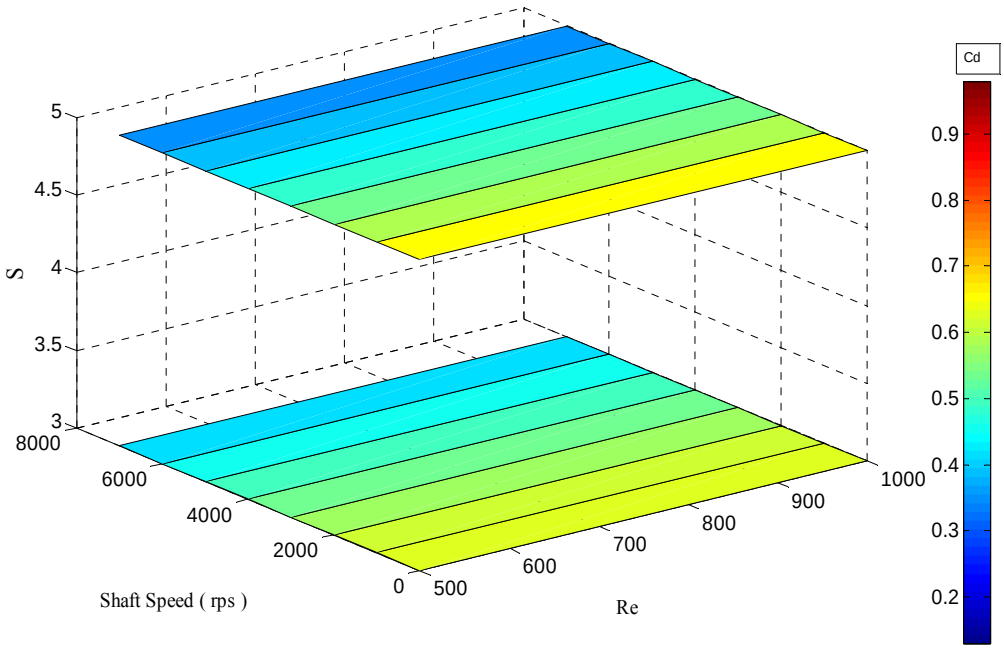

Fig. 4.58. Combined effect of Re, W_{sh}, on discharge coefficient of 3rd tooth (for incompressible flow).

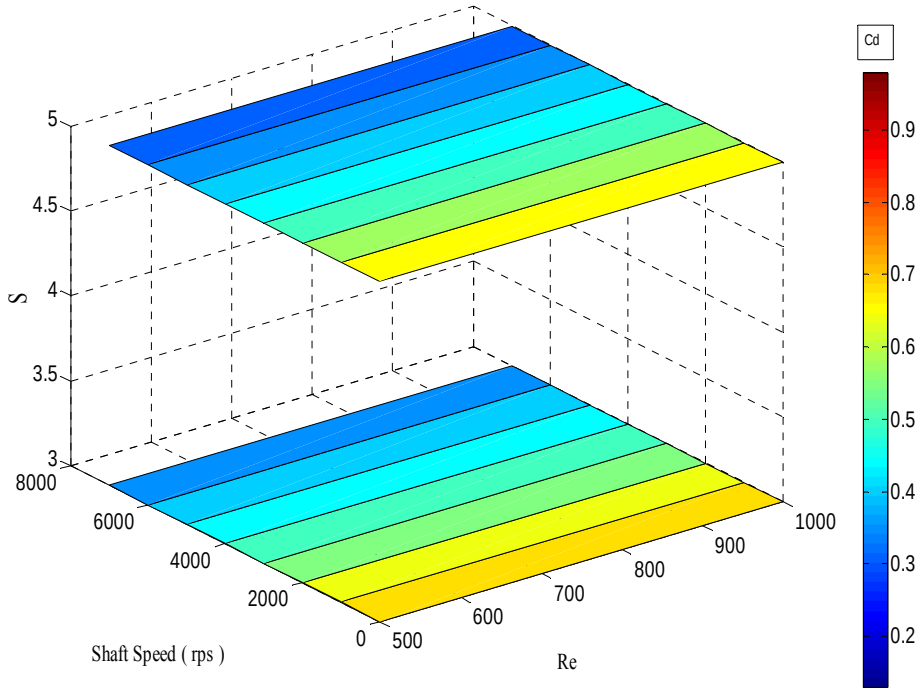

Fig. 4.59. Combined effect of Re, W_{sh}, on discharge coefficient of 4th tooth (for incompressible flow).

The combines effect of Reynolds number, pitch and shaft speed on the discharge coefficient are shown in Fig. 4.60 and Fig. 4.61 for compressible flow for first and second tooth respectively. It is evident from the figures that shat rotation has insignificant effect on the discharge coefficient.

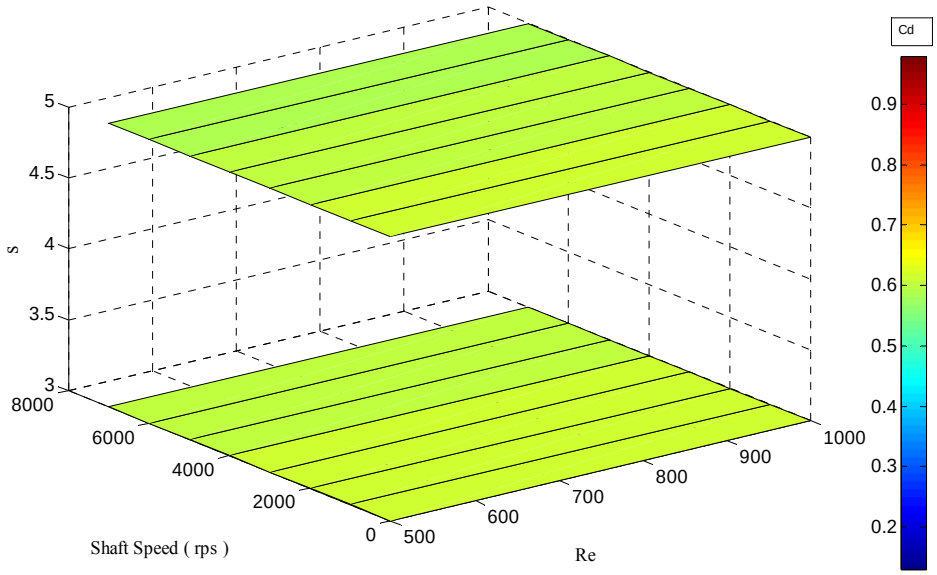

Fig. 4.60. Combined effect of Re, W_{sh}, on the discharge coefficient of 1st tooth (compressible flow).

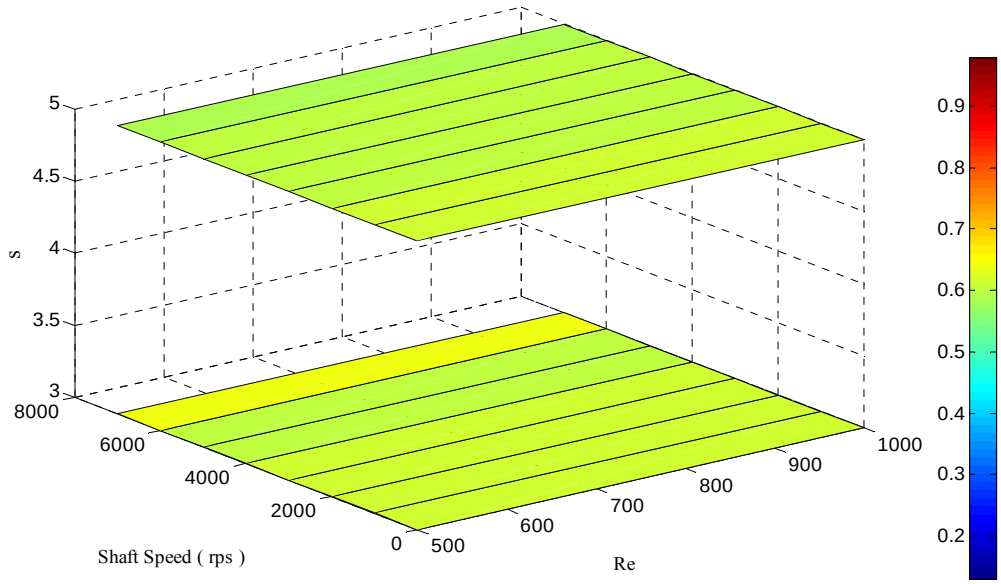

Fig. 4.61. Combined effect of Re, W_{sh}, on the discharge coefficient of 2nd tooth (compressible flow).

4.3.6.5 Effect of Shaft Speed on C_d for Tooth Angle

In previous discussion in section 4.3.5. it is observed that at zero shaft speed, the tooth angle has no effect on the discharge coefficient. In this section similar approach is followed to evaluate the effect of shaft speed as a function of upstream angle on the discharge coefficient. Fig. 4.62 shows that higher tooth angle results in low discharge coefficient.

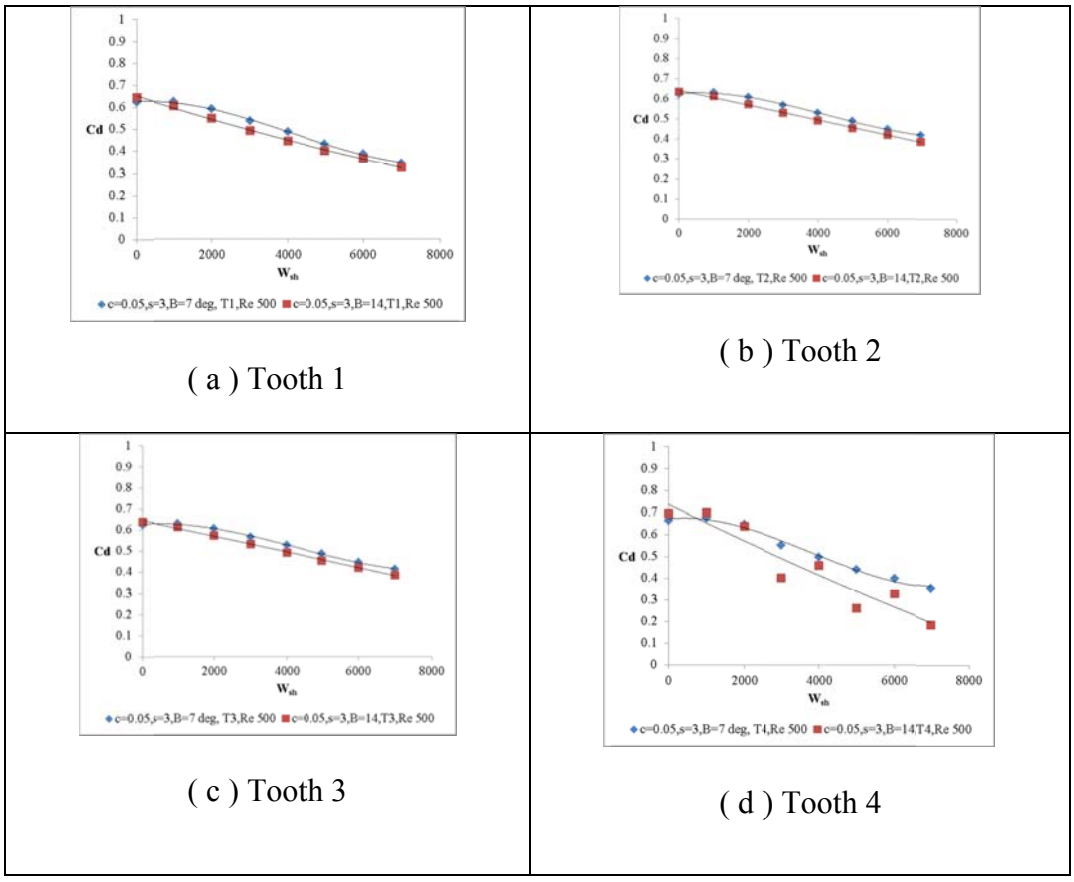

Fig. 4.62. Effect of W_{sh} as a function of B on the C_d (for incompressible flow, case 1, case 2).

It is also observed that 1st,2nd and 3rd tooth of the seal provides the similar effect on the $C_{d.}$ It is very important to understand flow pattern inside the cavity for two different cases of upstream angle. Flow pattern is the key physics to explain the variation of the discharge coefficient for different tooth angle. It is observed from the Fig. 4.63 that at $B=14^{\circ}$ and maximum shaft speed (7000 rps), secondary flow vortices inception is occurred at incompressible flow. This secondary recirculation zone is responsible for additional flow resistance and this additional resistance results in additional pressure drop which causes lower discharge coefficient.

For the lower tooth angle, it seems from the plot that there are no secondary recirculation zone. The absence of the secondary vortices resulting higher discharge coefficient compare to higher tooth angle.

Fig. 4.64 to Fig. 4.67 are plotted to show the combined effect of the $W_{sh,}$ Re, B on the discharge coefficient. From the 3D plots it is observed that at higher shaft speed, 1st and 4th tooth have more effect on the discharge coefficient at low Reynolds number compare to 2nd and 3rd. At the first tooth, higher upstream angle creates higher approach flow angle which gives higher vena contracta effect compare to intermediate teeth positions. It can be concluded that higher tooth angle has more effect on the C_d at low Reynolds number and maximum shaft speed.

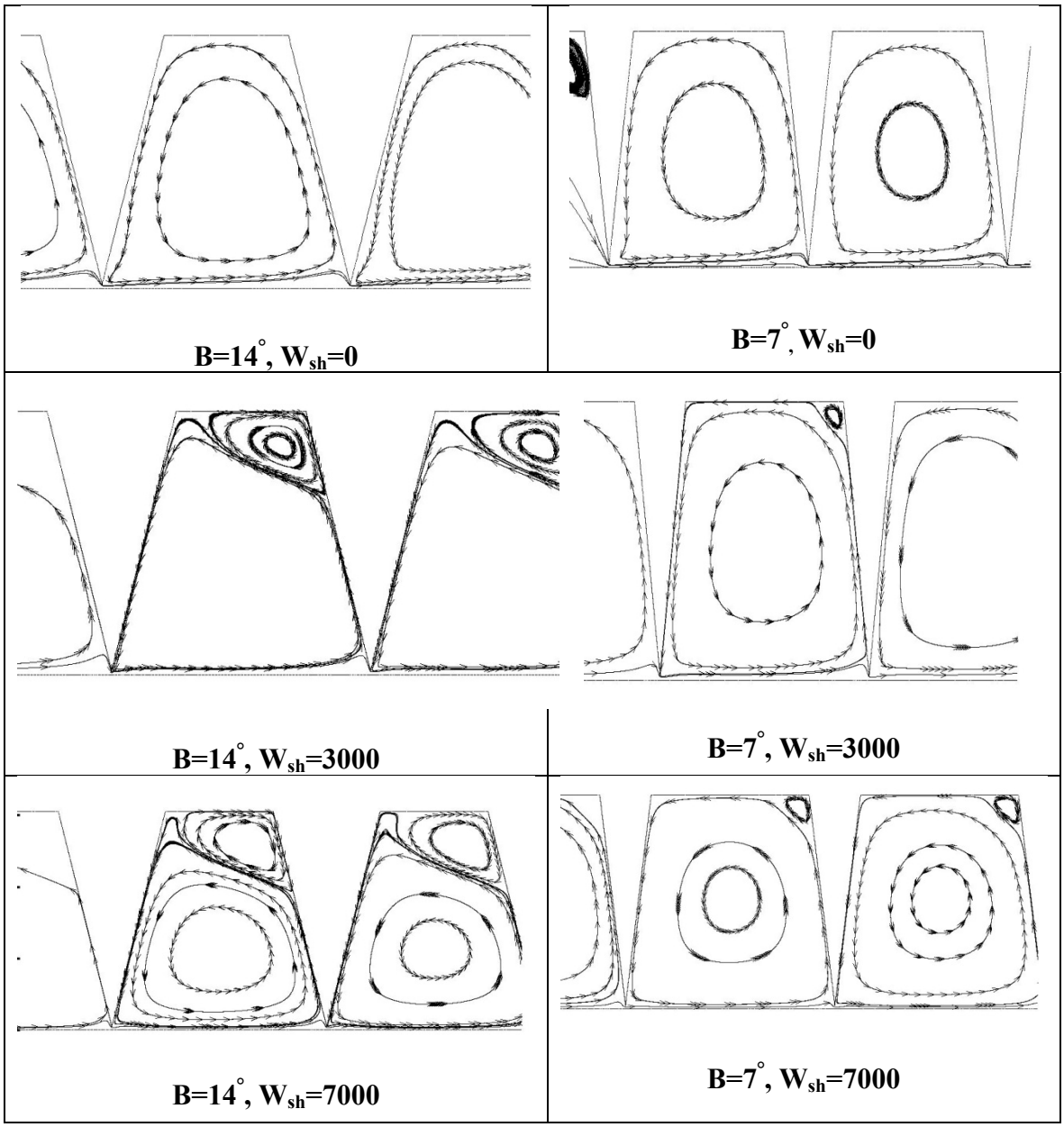

Fig. 4.63. Comparison of flow pattern between B=7° and 14° (for incompressible flow, case 1, case 2).

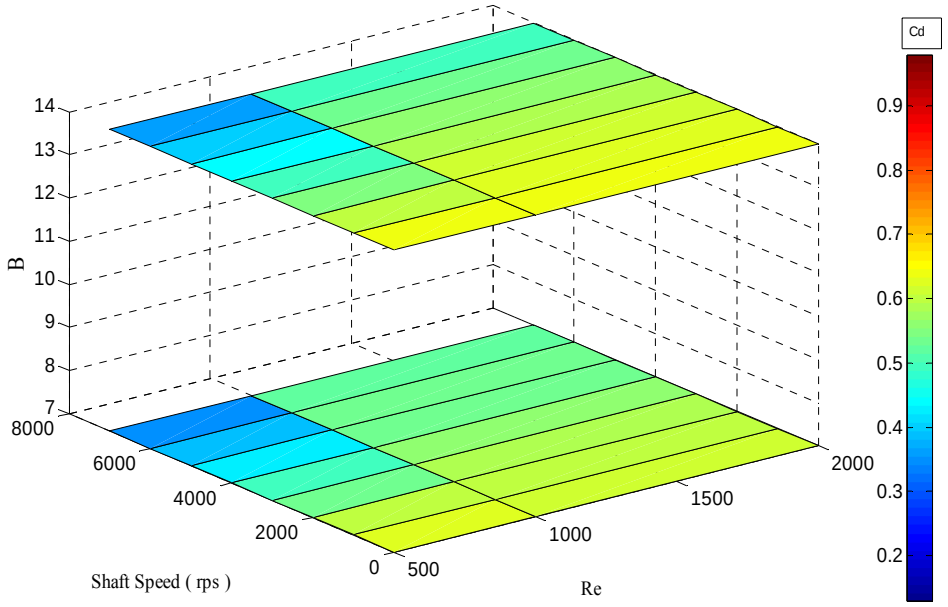

Fig. 4.64. Combined effect on 1st tooth (incompressible, case 1, case 2).

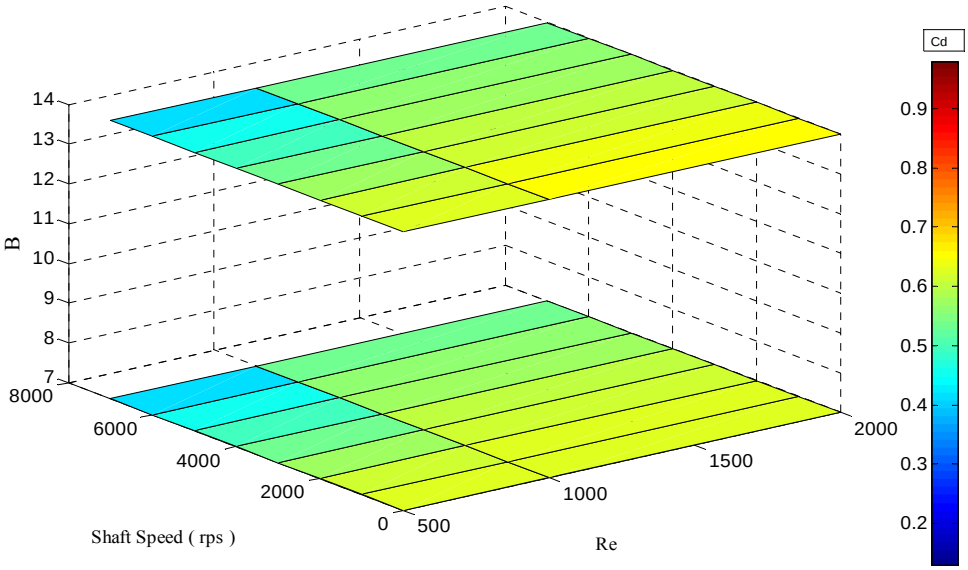

Fig. 4.65 Combined effect on 2nd tooth (incompressible, case 1, case 2).

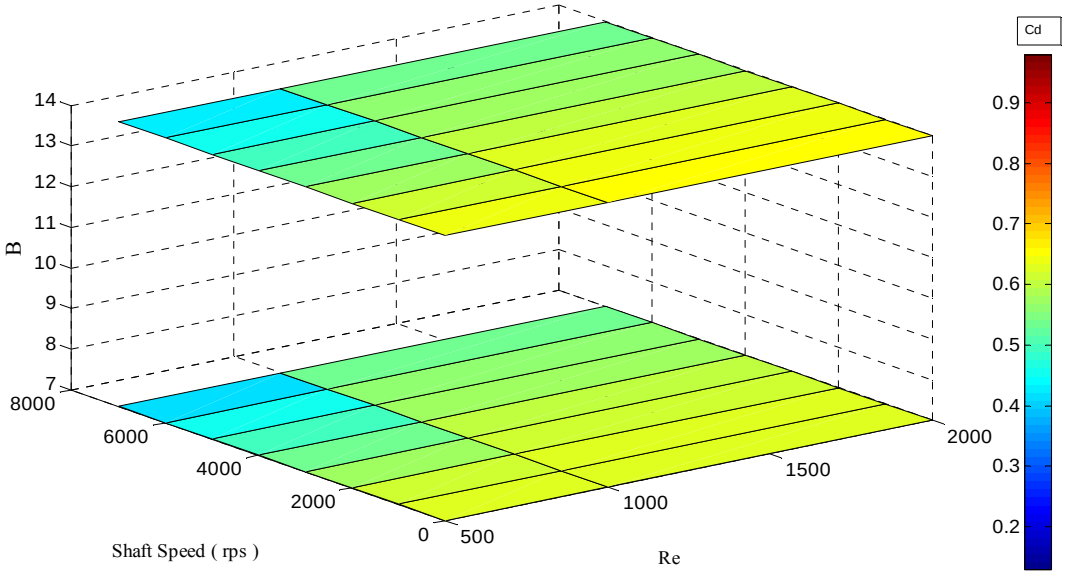

Fig. 4.66 Combined effect on 3rd tooth (incompressible flow).

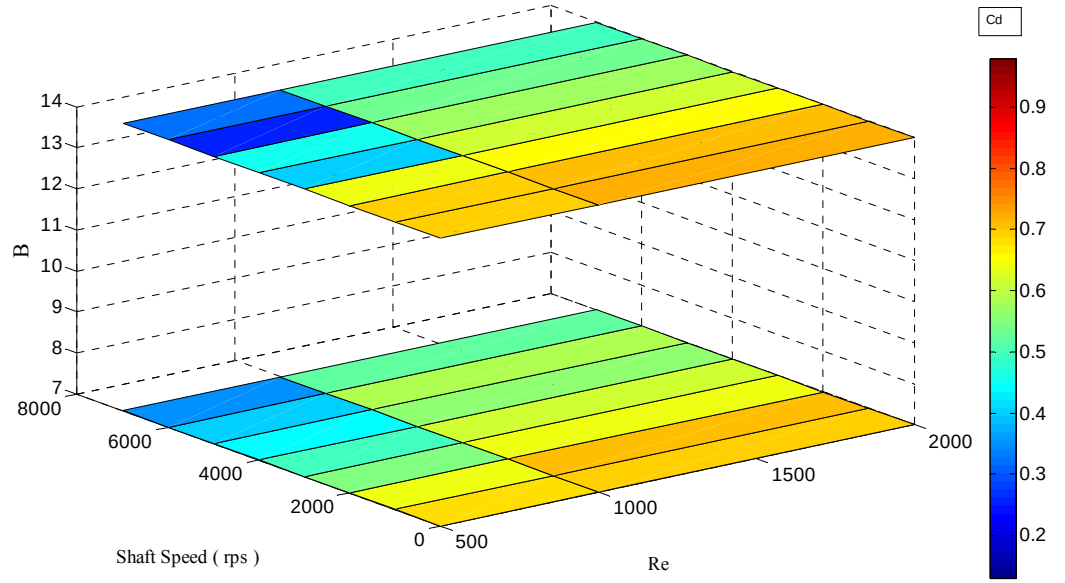

Fig. 4.67 Combined effect on 4th tooth (incompressible flow).

For the compressible flow this investigation is done for c =0.05 and Reynolds number, Re 500,1000 along with W_{sh}. Reynolds number of 500, 1000, 2000 are used with shaft speed to investigate the effect of upstream angle on the discharge coefficient. Fig. 4.68 show that tooth angle as a function of shaft speed has no effect on the C_d at low Reynolds number for compressible flow. It is observed from the Fig. 4.69 and Fig. 4.70 that tooth angle and shaft rotation have marginal effect on the discharge coefficient for compressible flow.

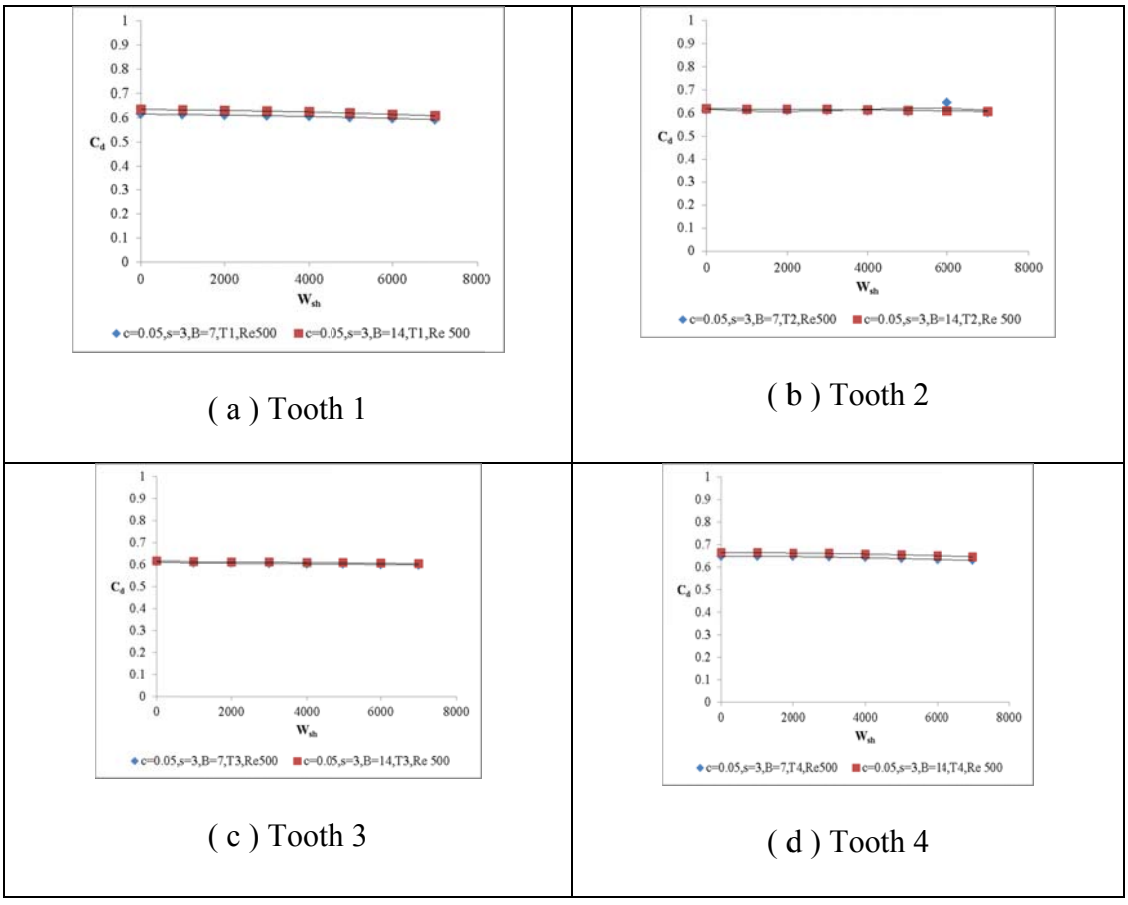

Fig. 4.68. Upstream and shaft rotation effect on C_d (compressible flow , case 1, case 2).

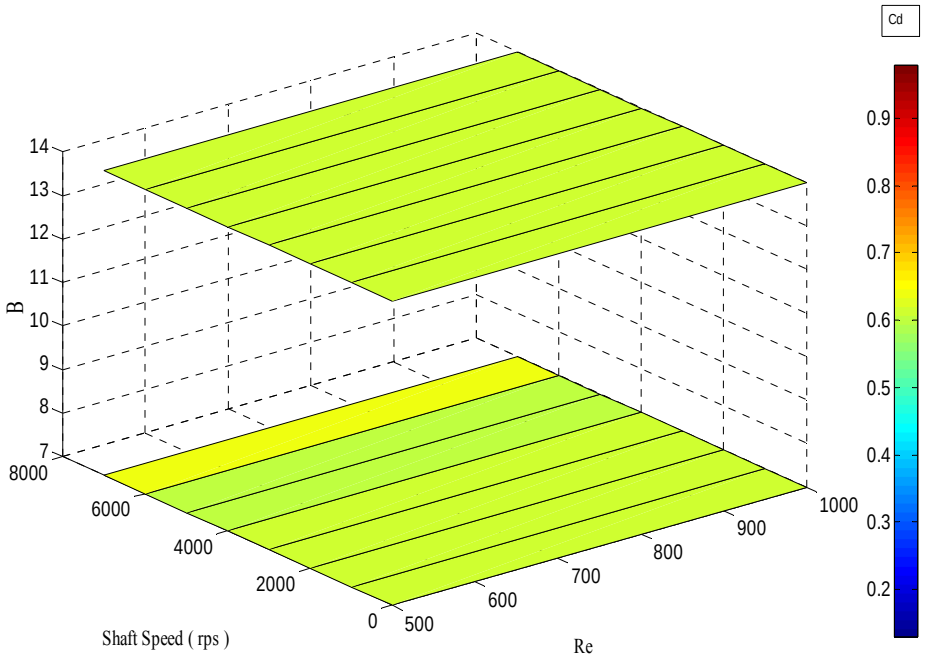

Fig. 4.69. Combined effect on 2nd tooth (Air , case 1, case 2)

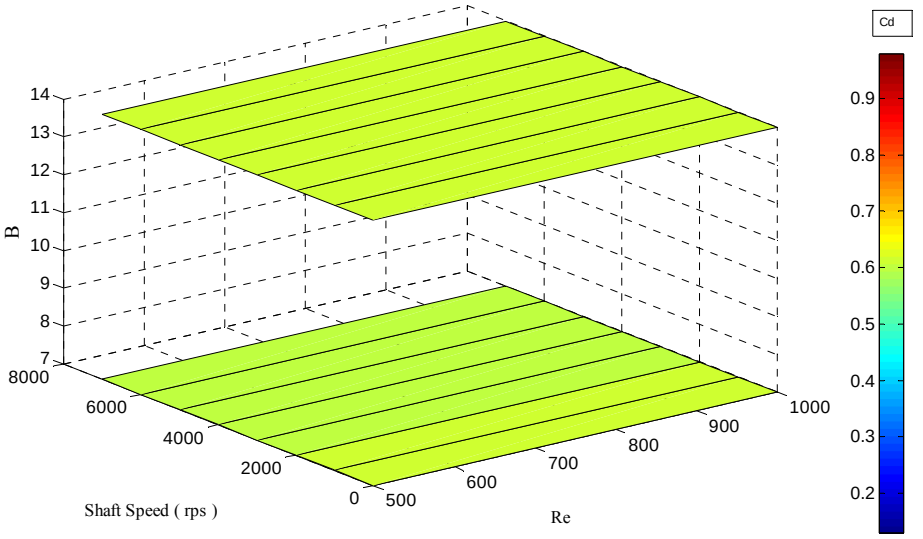

Fig. 4.70. Combined effect on 3rd tooth (Air , case 1, case 2).

5 EXPANSION FACTOR

5.1. Definition of Expansion Factor

Expansion factor is a dimensionless parameter which relates the carryover and discharge coefficient parameters of compressible and incompressible flow. In another way, the expansion factor is a measurement for compressibility effect on the carryover and discharge coefficient. The expansion factor can be utilized to visualize the compressibility effect by multiplying this factor with C_d or γ which are obtained from a incompressible flow simulation. Similar axisymmetric simulation is performed for different flow and seal geometry to evaluate the expansion factor.

5.2. Expansion Factor Calculation

Expansion factor is defined in this section as a function of pressure ratio, pr for a given Reynolds number. This pressure ratio is defined as follows:

$$pr = \frac{P_{out}}{P_{in}} \qquad (5\text{-}1)$$

where P_{in} and P_{out} are defined as the upstream and downstream pressure across the tooth for a given Reynolds number. This pressure ratio is obtained across the tooth of the seal for compressible flow (air).

So expansion factor is calculated on the basis of pressure ratio across the tooth of compressible flow. In this study the compressible flow is defined as the flow of air. In this section, φ_{γ} is defined as carryover coefficient expansion factor and φ_{cd} is defined as discharge coefficient expansion factor. Following two equations are used in the study to calculate the expansion factor for the carryover and discharge coefficient.

$$\varphi_{\gamma}^{\cdot} = \frac{\gamma_{air}}{\gamma_{water}} \qquad (5\text{-}2)$$

$$\varphi_{cd} = \frac{C_{d_{dir}}}{C_{d_{water}}} \qquad (5\text{-}3)$$

If the above ratio is 1 then it can be said that there is no effect for the compressibility. If the goes above 1 then it is understandable that air is leaking more than water for the seal at respective Reynolds number. And the last if goes below 1 then it means there is a effect of compressibility for a given Reynolds number.

5.3. Evaluation of Expansion Factor

Similar computational technique used for the carryover coefficient and discharge coefficient is applied to investigate the expansion factor. This evaluation is done for flow parameter like Reynolds number and seal geometric parameters such as clearance, tooth width, pitch and upstream angle.

5.3.1. Effect of Reynolds Number

The Effect of Reynolds number on the expansion factor is investigated for the instance of Re 300, 500 and 1000. The radial clearance, c =0.05 is considered for this study. Isosceles profile is evaluated in this study.

Fig. 5.1 and Fig. 5.2 shows the expansion factor distribution for four teeth as a function of pressure ratio, pr. It is observed from the figure that for all of the teeth, expansion factor is decreasing with increasing pressure ratio. Higher pressure ratio is obtained for higher Reynolds number. It can concluded from the plot that the expansion factor is decreasing with increasing pressure ratio.

It is also observed from the Fig. 5.1and Fig. 5.2 that expansion falls in a linear relationship with pressure ratio. So it can be concluded that expansion factor is a function of pressure ratio and Reynolds number.

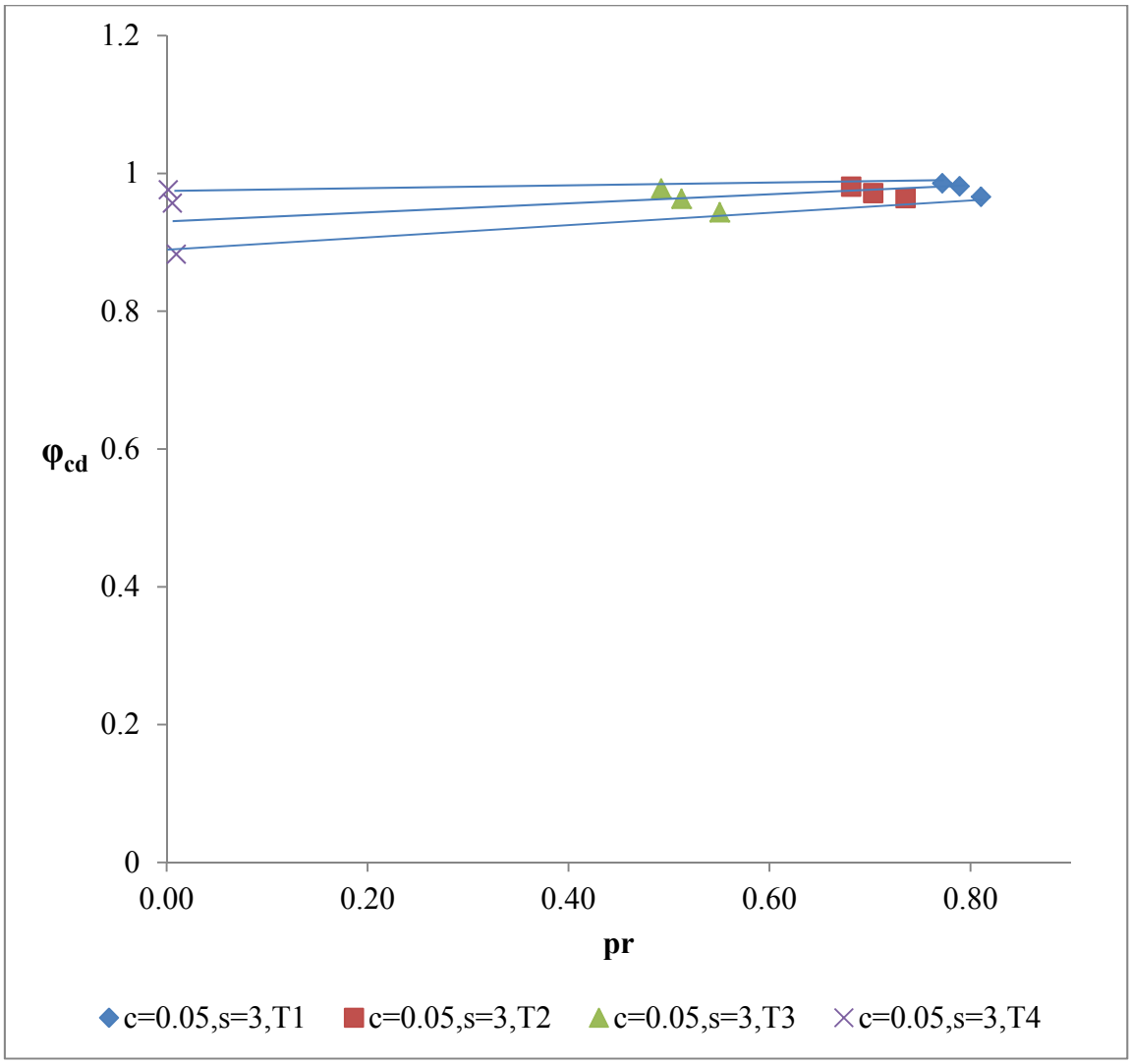

Fig. 5.1. Expansion factor as a function of pr for discharge coefficient (isosceles tooth , case 1, Re 300, 500 and 1000, W_{sh} = 0).

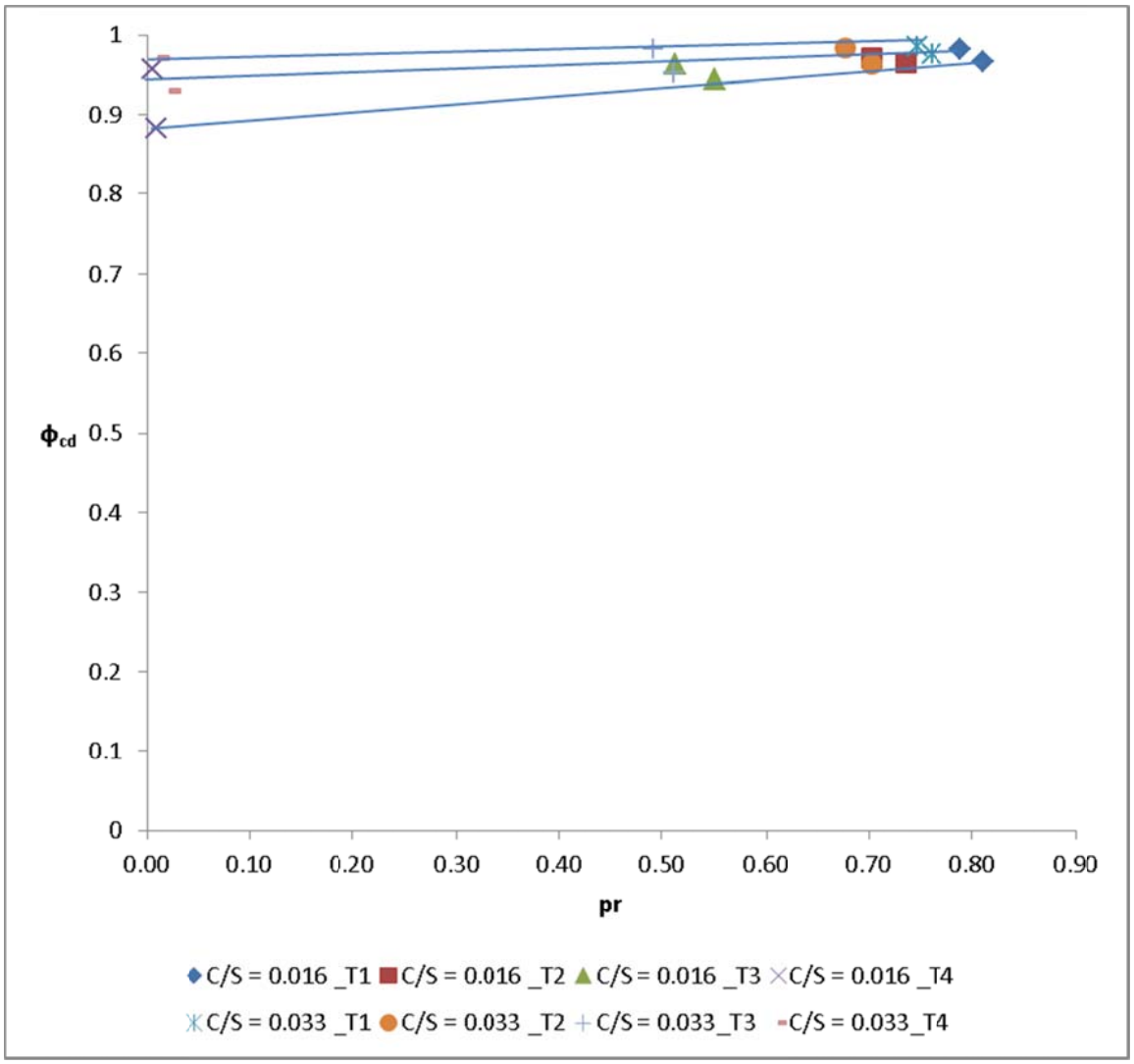

Fig. 5.2. Expansion factor as a function of pr (isosceles, case 1, case 3, Re 500 and 1000).

Fig. 5.3 shows that the effect of expansion factor (carryover coefficient) as a function of pressure ratio is insignificant for isosceles tooth shape seal. There is no compressibility effect. Also it is evident from the plot that carryover coefficient expansion factor is not a function of Reynolds number.

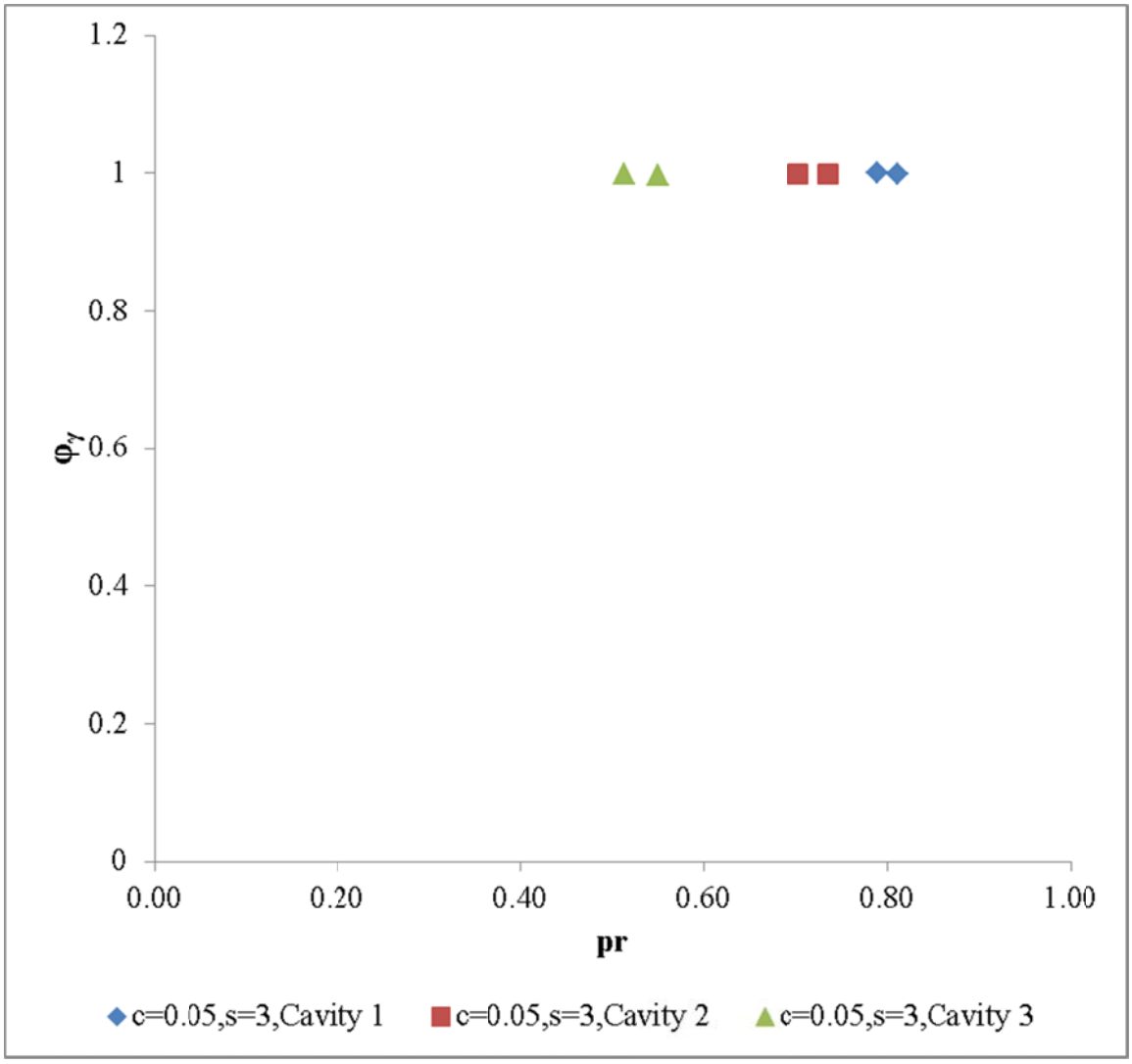

Fig. 5.3. Expansion factor as a function of pr for carryover coefficient (isosceles tooth, case 1).

5.3.2. Effect of Shaft Speed

The shaft rotation effect is investigated for isosceles triangle tooth shape labyrinth seal. axisymmetric simulation with moving boundary rotor wall condition is executed to evaluate the shaft speed, W_{sh}, effect on expansion factor for both carryover and discharge coefficient. This evaluation is done for geometric parameters such as clearance, tooth width and pitch. of the seal. The effect of shaft rotation as a function of clearance is evaluated for Re 500 ,1000 and c = 0.05,0.1. This investigation shows that at a given Reynolds number, Re 500 and maximum shaft speed (W_{sh}=7000), 78% increment in the expansion factor with 100% increment of clearance was obtained. This result is shown in the Fig. 5.4. This figure shows the effect of shaft rotation and Re on the expansion factor of all teeth.

It is evident from the above discussion that clearance has significant effect on the discharge coefficient expansion factor. At higher rotor speed, air is leaking more than water at higher clearance that which is found from above investigation.

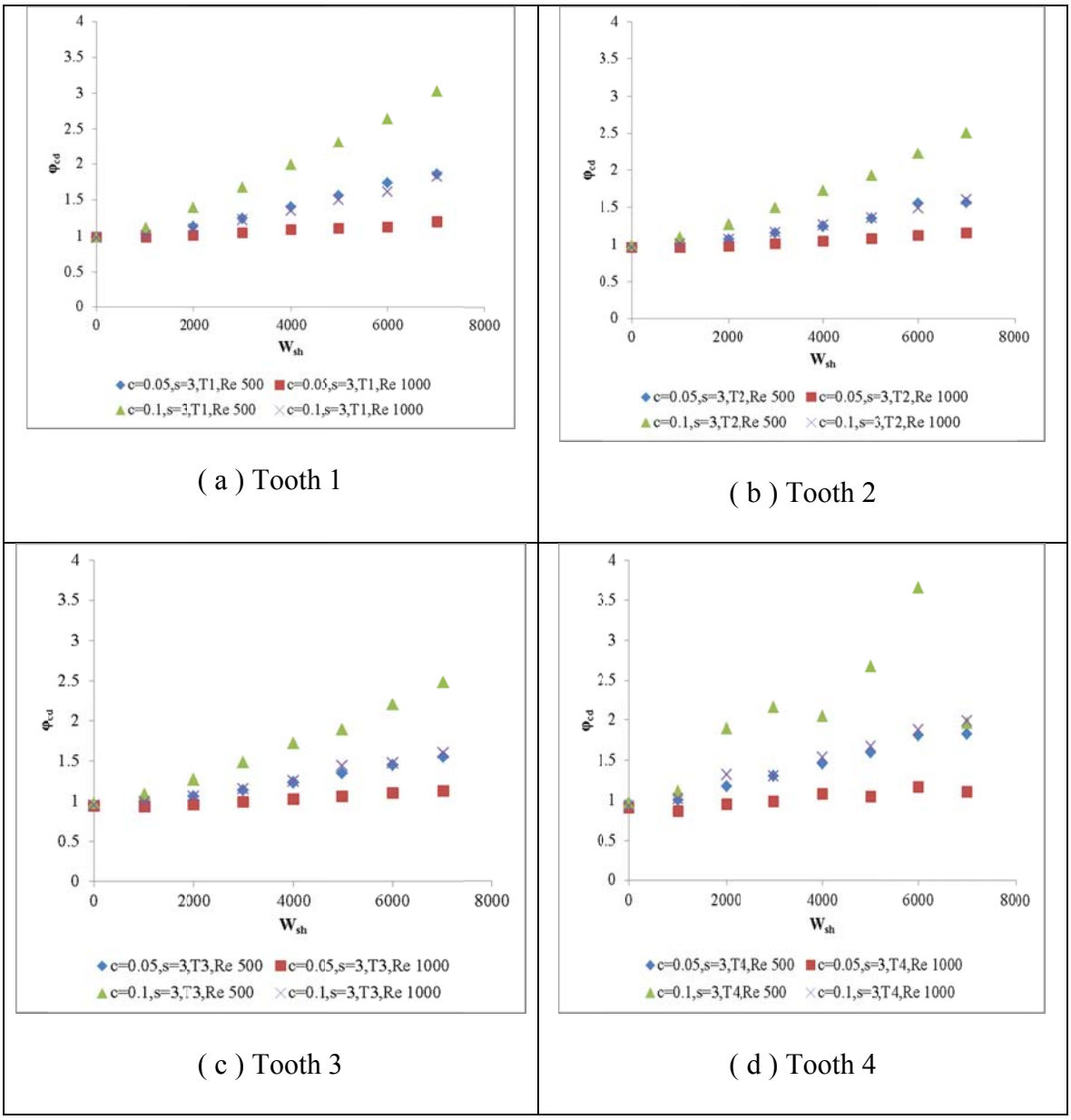

Fig. 5.4. Expansion factor effect as a function of clearance for discharge coefficient (all four teeth , case 1, case 3).

6 SUMMARY AND CONCLUSIONS

6.1. Carryover Coefficient

Carryover coefficient, γ, is a dimensionless parameter which explains the energy dissipation of the working fluid inside the cavity of the seal. It is calculated using two equations (3-1) and (3-2) based on Hodkinson's [10] definition. This coefficient was evaluated for different seal geometry (c, s, B, w) and flow parameters (Reynolds number, Re and shaft speed, W_{sh}). Evaluation of the carryover coefficient is conducted for both compressible and incompressible flow.

Evaluation based on seal geometric parameters is discussed in this section. It is found that the effect of tooth position on the carryover coefficient is insignificant. Clearance has major impact on the carryover coefficient among all parameters. To investigate the effect of clearance, rests of the parameters are kept constant. Clearance values of c = 0.05, 0.1, 0.15 and 0.2 mm are considered to evaluate the effect of the carryover coefficient at constant pitch, s=3 mm. It is found from the section 3.3.2. that higher clearance value produces higher carryover coefficient. At small clearance, c=0.05, the carryover coefficient value is found close to 1 which means better energy dissipation inside the cavity.

Evaluation of the tooth width is carried out for w =0, 0.5 and 1 mm. In this investigation the clearance and pitch values are kept constant (c=0.05, s=3). It is observed in section 3.3.3. that wider tooth provides higher carryover coefficient. Pitch

effect on the carryover coefficient is evaluated for s= 3, 4, 5 mm and the clearance value is kept constant value of c =0.05 mm. From the section 3.3.4. , it is found that large pitch value gives better energy dissipation inside the cavity. As a result, large seal provide low carryover coefficient. For the low pitch value, it is vice versa.

Evaluation of upstream angle effect on the carryover coefficient is discussed in section 3.3.5. It is found that upstream angle has significant impact on the carryover coefficient for both isosceles and right angle tooth. This evaluation is conducted for both compressible and incompressible flow. This effect was evaluated by varying B = 7 to 14 degree for constant clearance, c= 0.05 and pitch , s =3 mm. It can be concluded from the evaluation that higher tooth angle gives lower carryover coefficient.

Flow parameters have significant effect on the carryover coefficient. The carryover coefficient increases when the Reynolds number increases. It is observed that after certain Reynolds number the carryover coefficient increase is marginal due to the maximum pressure difference. Low carryover coefficient is observed at higher shaft speed compare to zero shaft speed.

6.2. Discharge Coefficient

The discharge coefficient, C_d, is a representation of seal overall efficiency in terms of pressure drop while the carryover coefficient shows the effectiveness of a seal cavity in terms of energy dissipation. In the entire study the discharge coefficient is calculated by using equation (4-1) in section 4.1.

Similar approach is applied as carryover coefficient to evaluate the discharge coefficient for seal geometric and flow parameters. It is found that small clearance, c, gives lower discharge coefficient. When clearance increases, accordingly the discharge coefficient is increases. For the carryover coefficient it is found that the tooth position has no effect. Tooth position has significant effect on the discharge coefficient for both compressible and incompressible flow. First tooth has no impact on the discharge coefficient as a function of clearance. But 2^{nd},3^{rd} and 4^{th} tooth have significant effect on the discharge coefficient.

In the earlier discussion in section 4.3.3. it is found that the wider tooth gives higher carryover coefficient. From the analysis it is found that wider tooth provides low discharge coefficient. Evaluation of pitch effect showed that higher pitch provides lower discharge coefficient for incompressible flow. This effect is not very significant compare to clearance. It is also observed that pitch variation has less effect on first tooth compare to 2^{nd}, 3rd and 4^{th} tooth. Pitch effect is insignificant for compressible flow.

Tooth angle evaluation shows that it has no effect on the discharge coefficient for both compressible and incompressible flow. This evaluation is done for both isosceles and right angle tooth shape labyrinth seal.

It is observed that flow parameters have significant effect on the discharge coefficient. The downstream teeth have more effect on the discharge coefficient compare to first tooth. The coefficient of discharge increase with the increase of Reynolds number This is observed for both compressible and incompressible flow. In the case of shaft speed, in overall it is found that the discharge coefficient is decrease as the shaft speed

increase. Also it is observed that at low Reynolds number, shaft speed effect is very significant compare to high Reynolds number. For the compressible flow, the shaft speed effect is insignificant on the discharge coefficient.

6.3. Expansion Factor

Expansion factor IS calculated for a given Reynolds number, shaft speed and tooth position. In this study the expansion is defined for discharge coefficient and carryover coefficient. These two expansion factor were calculated by using equation (5-2) and (5-3). It is observed that the tooth position has significant effect on the expansion factor. Downstream tooth in the seal has lower expansion factor compare to upstream tooth. This means more compressibility effect is observed at downstream tooth. From the evaluation, it is found that geometric and flow parameters have no impact on the carryover coefficient expansion factor. So it can be concluded that there is no compressibility effect on the carryover coefficient.

It is found that at small clearance, the expansion factor is decreases with increasing pressure ratio. But for the carryover coefficient expansion factor , the effect of clearance is found insignificant. There is no compressibility effect on the carry over coefficient for large clearances. It is found that shaft speed has significant effect on the expansion factor. The expansion factor increases when the shaft speed increases. Finally it is found that expansion factor is a function of pressure ratio and Reynolds number.

6.4. Evaluation Summary

The main objective of this study is to evaluate the effect of geometric and flow parameters on the discharge coefficient, C_d, carryover coefficient, γ, and expansion factor, φ. This evaluation is performed for both compressible and incompressible flow. Table 6.1 and Table 6.2 show the summary of the above mentioned evaluation for compressible and incompressible flow. In this entire research, evaluation of the triangular tooth on stator seal is conducted by using sixteen cases and these case details are given in seal geometries matrix.

Table 6.1. Evaluation summary (incompressible flow).

Increases	γ	C_d
c	Increases	increases
s	Decreases	decreases
w	Increases	decreases
B	Decreases	insignificant
Re	Increases	increases
W_{sh}	Decreases	decreases

Table 6.2. Evaluation summary (compressible flow).

Increases	γ	C_d
c	Increases	increases
s	Decreases	decreases
w	Increases	decreases
B	Decreases	insignificant
Re	increases	increases
W_{sh}	decreases	insignificant

So far based on the above evaluation, it was found that the clearance, c is the most important geometric parameter which affects the carryover and discharge coefficient most compare to other parameters. Pitch, p and width, w, are the next two parameters followed by clearance which affect the performance of the seal.

It was found that for a constant pitch value, when clearance decreases the carryover and discharge coefficient are decreasing. Again for constant clearance, the higher pitch value gives lower discharge and carryover coefficient. It is evident from the study that wider tooth gives lower discharge compare to thinner tooth. But for the carryover coefficient this result is found opposite.

Upstream angle has no effect on the discharge coefficient. But the carryover coefficient decreases when upstream angle increases. It was found that flow parameters have significant effect on the carryover and the discharge coefficient. When Reynolds

number increases both the carryover and discharge coefficient increases significantly. Shaft rotation has significant effect on the carryover and discharge coefficient. When shaft speed is increases both of the parameters are decreases. But for compressible flow, shaft speed has insignificant effect on the discharge coefficient.

So to design an ideal triangular tooth on stator seal it is very to make an optimization of clearance, pitch and tooth width. Based on 17 cases in this study, it was found that Case 8 is the best seal for both compressible and incompressible flow in terms low C_d (based on 1^{st} tooth) and γ. Case 8 showed the presence of secondary recirculation zone at low Reynolds number and high shaft speed This SRZ is the main reason for this case to be provide better sealing in terms of the carryover and discharge coefficient.

7 RECOMMENDED FUTURE WORK

The main objective of this study was to investigate the effects of flow and seal geometric parameters on the seal performance. Seal performance was evaluated based on three major parameters such as carryover coefficient, discharge coefficient and expansion factor. It was concluded that clearance, pitch and tooth width are the three major influential parameters among all geometric parameters which dominate the seal performance. This study was done for only triangular see through labyrinth seal. There are plenty of other seal geometry can be modeled for future work. In the following lists of paragraph, possible future research scopes are listed.

1. This whole study was investigated for the Newtonian fluid. In future it is recommended to evaluate the seal performance for non-newtonian fluid.
2. In this entire study shaft diameter of the rotor was kept constant. So there is a scope to study the evaluate the effect of shaft diameter on the seal performance
3. Two types of triangular teeth(isosceles, right angle) were investigated in this study. But for isosceles triangle tooth, shaft speed was introduced to evaluate the effect on the seal performance. In future study, right angle tooth shape can be investigated for high shaft speed effect to evaluate the discharge coefficient.
4. This investigation was executed for see through arrangement. So there is an opportunity in future to investigate the staggered arrangement.

5. It was found from the evaluation that for compressible flow, effect of shaft rotation is marginal on the discharge coefficient. In future this can be validated by using different Air model. In this study Air was modeled as an ideal gas.
6. It seems from current study that both flow and geometric parameters have no effect on the carryover expansion factor In this study outlet boundary condition was defined as 1 atm for all of the simulations. So it is highly recommended to run for different outlet pressure to validate the results of the carryover and discharge coefficient expansion factor.
7. The pitch over height ratio in this study was kept 1. So in future, there is a scope to vary this ratio to see the effect on the seal performance.

REFERENCES

[1] Gamal, A. M., 2007, "Leakage and Rotodynamic Effects of Pocket Damper Seals and See Through Labyrinth Seals,"Ph.D., Texas A&M University, College Station.

[2] Morrison, G. L., and Al-Ghasem, A., "Experimental and Computational Analysis of a Gas Compressor Windback Seal," Proc. 2007 ASME Turbo Expo, May 14, 2007 - May 17, 2007, American Society of Mechanical Engineers, pp. 1231-1247.

[3] Sneck, H. J., 1974, "Labyrinth Seal Literature Survey," J Lubric Tech-T Asme, **96**(4), pp. 579-582.

[4] C.A., P., 1938, "The Labyrinth Packing " Engineer, **165**(No. 4280), pp. 23-84.

[5] Becker, E., 1907, "Stromungsvergange in Ringformigen Spalten," V.D.I, **51**, pp. 1133-1141.

[6] Martin, H. M., 1908, "Labyrinth Packings," Engineer, **85**, pp. 35-38.

[7] Stodola, A., 1927, Steam and Gas Turbines, Mcgraw-Hill.

[8] Gercke, M. J., 1934, "Berechnung der Ausflussmengen von Labyrinth Dichtungen," Die Warme, **57**, pp. 413-417.

[9] Egli, A., 1935, "The Leakage of Steam through Labyrinth Seals," Trans. ASME, **57**, pp. 115-122.

[10] Hodkinson, B., 1939, "Estimation of the Leakage Through a Labyrinth Gland," ARCHIVE: Proceedings of the Institution of Mechanical Engineers 1847-1982 (vols 1-196), **141**(1939), pp. 283-288.

[11] Zabriskie, W., and Sternlicht, B., 1959, "Labyrinth-Seal Leakage Analysis," American Society of Mechanical Engineers -- Transactions Journal of Basic Engineering, **81, Series D**(3), pp. 332-336.

[12] Heffner, F. E., 1960, "General Method for Correlating Labyrinth-Seal Leak-Rate Data," American Society of Mechanical Engineers Transactions Journal of Basic Engineering, **82**(Ser D, 2), pp. 265-275.

[13] Prasad, B. V. S. S. S., Manavalan, V. S., and Rao, N. N., "Computational and Experimental Investigations of Straight-Through Labyrinth Seals," Proc. Proceedings of the 1997 International Gas Turbine & Aeroengine Congress & Exposition, June 2, 1997 - June 5, 1997, ASME, p. ASME.

[14] Rhode, D. L., and Hibbs, R. I., "Comparative Investigation of Corresponding Annular and Labyrinth Seal Flowfields," Proc. Preprint - American Society of Mechanical Engineers, June 4, 1989 - June 8, 1989, Publ by American Society of Mechanical Engineers (ASME), pp. GT195 197p-GT195 197p.

[15] Wittig, S. L. K., Doerr, L., and Kim, S., "Scaling Effects on Leakage Losses In Labyrinth Seals," Proc. 27th International Gas Turbine Conference and Exhibit., ASME, pp. ASME, Gas Turbine Div, New York, NY, USA.

[16] Willenborg, K., Kim, S., and Wittig, S., 2001, "Effects of Reynolds Number and Pressure Ratio on Leakage Loss and Heat Transfer in a Stepped Labyrinth Seal," Journal of Turbomachinery, **123**(4), pp. 815-822.

[17] Kmitir, K., Miyake, K., 1977, "Leakage Characteristics of Labyrinth Seals With High Rotating Speed " Tokyo Joint Gas Turbine Congress, Tokyo, Japan, **22-27**, pp. 378-380.

[18] Waschka, W., Wittig, S., and Kim, S., 1992, "Influence of High Rotational Speeds on The Heat Transfer And Discharge Coefficients In Labyrinth Seals," Journal of Turbomachinery, **114**(2), pp. 462-468.

[19] Zimmermann, H., and Wolff, K. H., "Air system correlations. Part 1: Labyrinth Seals," Proc. Proceedings of the 1998 International Gas Turbine & Aeroengine Congress & Exhibition, June 2, 1998 - June 5, 1998, ASME.

[20] Demko, J. A., Morrison, G. L., and Rhode, D. L., 1990, "Effect of Shaft Rotation on The Incompressible Flow In A Labyrinth Seal," Journal of Propulsion and Power, **6**(2), pp. 171-176.

[21] Suryanarayanan, S., 2009, "Labyrinth Seal Leakage Equation " Master's thesis, Texas A & M University, [College Station, Texas, Texas A&M University, 2010].

[22] Suryanarayanan, S., and Morrison, G. L., "Analysis of Flow Parameters Influencing Carry-Over Coefficient of Labyrinth Seals," Proc. 2009 ASME Turbo Expo, June 8, 2009 - June 12, 2009, American Society of Mechanical Engineers, pp. 1137-1145.

[23] Suryanarayanan, S., and Morrison, G. L., "Effect of Tooth Height, Tooth Width and Shaft Diameter on Carry-Over Coefficient of Labyrinth Seals," Proc. 2009 ASME Turbo Expo, June 8, 2009 - June 12, 2009, American Society of Mechanical Engineers, pp. 1147-1152.

[24] Inam, O., 2011, "Labyrinth Seal Leakage Analysis"," M.S. M.S. thesis, Texas A & M University, College Station.

[25] Pope, S. B., 2000, Turbulent Flows, Cambridge University Press, New Delhi, India.

APPENDIX A

STANDARD k-ϵ TURBULENCE MODEL

The k-ϵ model is the most popular model now a days to complete turbulence model. This model is used in commercial CFD packages to solve turbulence in the flow field. In this model two turbulence quantities (k and ϵ) are used to solve the model transport equations. A length scale ($L = k^{3/2}/\epsilon$), a time scale ($\tau = k/\epsilon$), a quantity of dimension ν_T (k^2/ϵ) can be formed from these two quantities. As a result two –equations model can be completed without flow dependent specification l_m (x). Along with turbulent viscosity hypothesis, the k-ϵ model consists of

1. Model transport equation for k

$$\frac{\overline{D}k}{\overline{D}t}^{\cdot} = \nabla.\left(\frac{\nu_T}{\sigma_k}\nabla k\right) + P - \epsilon \qquad \text{(A-1)}$$

2. The model transport equation for ϵ
3. Specification of the turbulent viscosity as

$$\nu_T^{\cdot} = C_\mu \frac{k^2}{\epsilon} \qquad \text{(A-2)}$$

where $C_\mu = 0.09$ is one of five model constant

In simple turbulent shear flow , the model yields [25]

$$\frac{|\langle uv\rangle|}{k} = \left(C_\mu \frac{P}{\epsilon}\right)^{1/2}{}^{\cdot} \qquad \text{(A-3)}$$

VITA

Hossain Ahmed Tanvir received his Bachelors of Science degree in Mechanical Engineering from Bangladesh University of Engineering and Technology, Dhaka, Bangladesh in November 2004. After that, he served three years in a pharmaceuticals process engineering field. He received his Master's degree in May 2012. His research interest includes aerodynamics of turbomachinery, computational fluid mechanics and labyrinth seal performance analysis.

Mr. Tanvir may be reached at Texas A&M University, Department of Mechanical Engineering, 3123 TAMU, College Station, TX 77843-3123. He can be reached by email at tanvir_ha@hotmail.com